GSFC S 480-128

Advanced Technology Microwave Sounder (ATMS)
Phase-A Feasibility Study Report

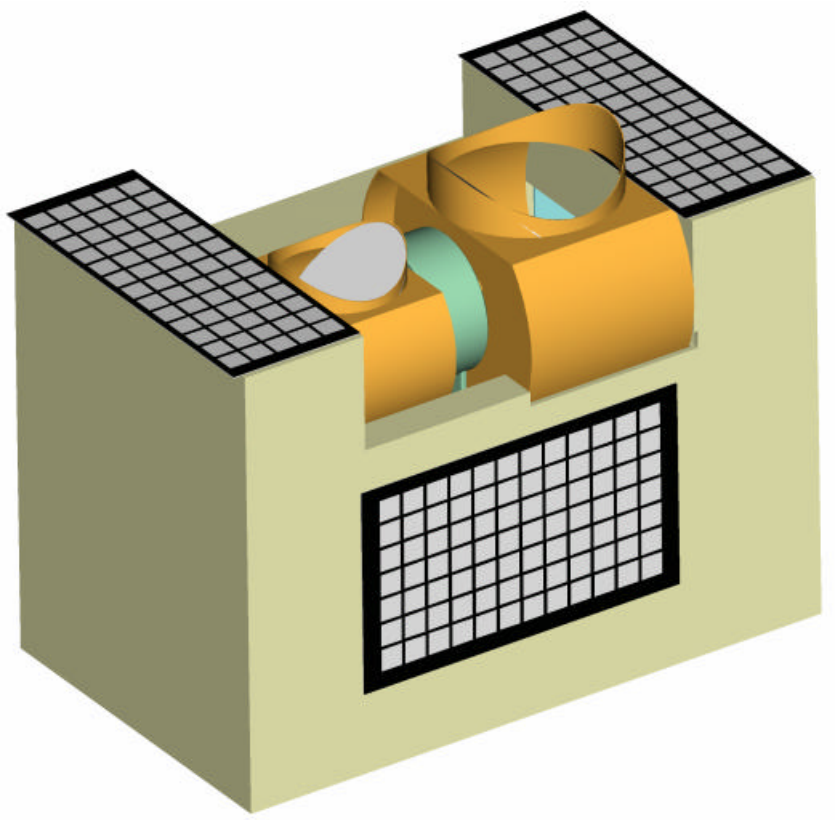

Prepared

by

NASA Goddard Space Flight Center
Flight Projects Directorate
Greenbelt, Maryland 20771

October 31, 1999

PREFACE

This report documents the results of the Advanced Technology Microwave Sounder (ATMS) instrument Phase-A Feasibility Study. The format and content for many of the subsections are the actual interim reports that were developed by team members as the study progressed.

Table of Contents

Tables

Illustrations

1.0 INTRODUCTION

A Feasibility Study was conducted within the Flight Projects Directorate at the Goddard Space Flight Center (GSFC) to develop an instrument concept for the Advanced Technology Microwave Sounder (ATMS). The ATMS is the microwave portion of a microwave/infrared-sounding suite used to measure global atmospheric temperature and moisture profiles. The ATMS serves both NASA research needs and National Polar-orbiting Operational Environmental Satellite System (NPOESS) operational measurement requirements.

1.1 BACKGROUND

The NASA Associate Administrator for Earth Science and the Director of the NPOESS Integrated Program Office (IPO) signed an Initial Implementation Agreement (IIA) in August 1998. The IIA committed NASA to the development of the ATMS and the IPO committed to the development of the complementary Cross–track Infrared Sounder (CrIS), which will be flown with the ATMS. NASA will conduct the procurement and oversee the production of the first ATMS instrument, which is scheduled to fly on the NPOESS Preparatory Program (NPP) in 2005. The contract will be transferred to the IPO for direct procurement of subsequent units to fly on the NPOESS platforms beginning approximately 2008.

1.2 STUDY OBJECTIVES

The ATMS Phase-A Study Plan required four key objectives for the Feasibility Study:

- Define the ATMS requirements that must meet both scientific and operational needs.
- Identify candidate technologies for incorporation into the ATMS and assess their readiness.
- Develop a strawman configuration for the ATMS instrument for use in instrument specification development and initial cost estimation.
- Prepare for the ATMS procurement.

Each objective was achieved during the study.

1.3 STUDY APPROACH

The GSFC Polar Operational Environmental Satellites (POES) Project initiated the Feasibility Study for the ATMS in November 1998. A study team was assembled with GSFC civil servants and support contractors, the IPO, Massachusetts Institute of Technology (MIT)/Lincoln Laboratory, and Jet Propulsion Laboratory (JPL) for technology support. A 5-month study schedule was prepared.

Attention focused first on requirements. The IPO provided information on its operational requirements, including a 7-year on-orbit lifetime. The IPO provided the resource goals for weight, power, data rate, and dimensions. The IPO stated that its science requirements were expressed as environmental data records and it wanted the same capability as the existing

Advanced Microwave Sounding Unit / Microwave Humidity Sounder (AMSU/MHS) instruments. The NASA Study Scientist prepared a set of suggested channels for the ATMS that consisted of comparable channels to the AMSU/MHS and two enhancement options for improved science.

Regular weekly meetings were held to review progress and present the results of studies and analyses throughout the study. The IPO attended all meetings and actively participated throughout the study. Trade studies were conducted to determine ATMS scan rates, scan patterns, including oversampling and beam widths. A workshop was held with JPL in December 1998 to discuss the latest NASA Code Y-funded microwave technology efforts. Preliminary interface meetings were held with NPP spacecraft representatives to explore spacecraft accommodation issues.

A conceptual design was developed to meet the requirements. Computer Aided Design (CAD) drawings were developed for different instrument configurations. In February 1999, a design review was conducted of a snap shot of the instrument concept development. An instrument reliability model was developed. Design trade studies were conducted, such as the use of analog vs. digital filters. The design was iterated to fit within the resource goals requested by the IPO. Very specific technology questions were sent to JPL to research. By the end of the study, the ATMS instrument concept evolved to the point that it fit the resource goals that were specified by the IPO.

The Study Team assessed ATMS channel selections in response to science feedback from NASA Headquarters. One of the options (for mesospheric channels) was dropped. The remaining channels were prioritized at a meeting of the IPO Sounder Operational Algorithm Team (SOAT). This permitted an improved reliability analysis that identified the needed level of redundancy and allowed the development of instrument descope options.

Cost estimates were developed and submitted to the NASA budget process. Procurement initiation was started. The ATMS Instrument Performance Specification was prepared and released to industry for comment. A Project Implementation Plan for ATMS was written.

This report summarizes the technical results of the ATMS Feasibility Study, which was completed in March 1999. More detailed information is in the Phase-A Study Plan, handouts from technical meetings, the ATMS Phase-A Informal Concept Review, the ATMS Instrument Performance Specification, the ATMS Project Implementation Plan, and the ATMS Cost Estimate.

2.0 SCIENCE AND OPERATIONAL REQUIREMENTS

ATMS requirements are broken into two categories: 1) Science Requirements and 2) Operational Requirements.

2.1 SCIENCE REQUIREMENTS

The majority of science requirements are taken directly from ATMS heritage Advanced Microwave Sounding Unit (AMSU)-A and Advanced Microwave Sounding Unit (AMSU)-B /Microwave Humidity Sounder (MHS)/ Humidity Sounder Brazil (HSB) instruments. The NASA Study Scientist and his science team made minor requirements changes in three areas:

- The number of channels and channel assignments.
- Static beam widths of the AMSU-A corresponding channels.
- Noise Equivalent Temperature Difference (NEΔT)s of the AMSU-A corresponding channels with changed beam widths to provide heritage proportional NEΔTs.

Polarization, center frequency stability, and calibration accuracy remained unchanged from the heritage requirements. Table 2-1 presents ATMS Channel Characteristic Requirements.

In order to give the ATMS contractor more design flexibility, without science degradation, Channels 18 through 22 upper/lower specifications were relaxed. This allows the builder to decide whether utilization of the upper band pass is necessary, as long as NEΔT is met. Similarly, the Channel 16 center-frequency specification is flexible to allow the builder the option of using one local oscillator for Channel 16 and Channels 17 through 22. The following subsections describe the key requirement differences between ATMS and the heritage instruments.

2.1.1 Channels

Table 2-1 presents each ATMS channel requirement. Channels 1 to 16 are found in the AMSU-A, while Channels 17 to 22 are found in the AMSU-B/MHS instruments. Channel 4 (51.76 GHz), Channel 19 (183.31 ± 4.5 GHz) and Channel 21 (183.31 ± 1.8 GHz) are added to the existing predecessor AMSU frequencies in order to fill the gaps between widely spaced channels.

Channels 17 through 22 were the least affected by changes from AMSU-B/MHS/HSB to ATMS (the same NE T, the same static beam width.). The differences are as follows. Channel 17, which used to be 150 GHz, was shifted to 166.31 GHz but still provides the same science. This change allowed a better grouping of water vapor channels for engineering implementation. Additionally, Channels 19 and 21 were added for better coverage of water vapor.

Channels 23 through 31 are new. These channels are considered an enhancement option to the basic Channels 1 through 22. The function of Channels 3 through 10 is similar to Channels 10 through 15, where both sets of channels are geared to characterize atmosphere between 700 mB to 80 mB. However, these new channel frequencies are better protected by Federal Radio

Frequency Management. Although frequency protection is not an issue right now, it is not guaranteed that Channels 10 through 15 will be uncorrupted during ATMS mission lifetime.

Table 2-1. ATMS Channel Characteristics

CHANNEL	CENTER FREQUENCY (GHz)	MAXIMUM BANDWIDTH (GHz)	CENTER FREQUENCY STABILITY (Mhz)	TEMPERATURE SENSITIVITY (K) NEΔT	CALIBRATION ACCURACY (K)	STATIC BEAM WIDTH ØB (degrees)	QUASI POLARIZATION	CHARACTERIZATION AT NADIR (REFERENCE ONLY)
1	23.8	0.27	10	0.9	2.0	5.2	QV	window-water vapor 100 mm
2	31.4	0.18	10	0.9	2.0	5.2	QV	window-water vapor 500 mm
3	50.3	0.18	10	1.20	1.5	2.2	QH	window-surface emissivity
4	51.76	0.40	5	0.75	1.5	2.2	QH	window-surface emissivity
5	52.8	0.40	5	0.75	1.5	2.2	QH	surface air
6	53.596 ±0.115	0.17	5	0.75	1.5	2.2	QH	4 km ~ 700 mb
7	54.40	0.40	5	0.75	1.5	2.2	QH	9 km ~ 400 mb
8	54.94	0.40	10	0.75	1.5	2.2	QH	11 km ~250 mb
9	55.50	0.33	10	0.75	1.5	2.2	QH	13 km ~ 180 mb
10	57.290344	0.33	.5	0.75	1.5	2.2	QH	17 km ~ 90 mb
11	57.290344 ±0.217	0.078	.5	1.20	1.5	2.2	QH	19 km ~ 50 mb
12	57.290344 ±0.32 22±0.048	0.036	1.2	1.20	1.5	2.2	QH	25 km ~ 25 mb
13	57.290344 ±0.3222 ±0.022	0.016	1.6	1.50	1.5	2.2	QH	29 km ~ 10 mb
14	57.290344 ±0.3222 ±0.010	0.008	.5	2.40	1.5	2.2	QH	32 km ~ 6 mb
15	57.29 ±0.3222 ±0.0045	0.003	.5	3.60	1.5	2.2	QH	37 km ~ 3 mb

Table 2-1. ATMS Channel Characteristics (continued)

CHANNEL	CENTER FREQUENCY (GHz)	MAXIMUM BAND WIDTH (GHz)	CENTER FREQUENCY STABILITY (Mhz)	TEMPERATURE SENSITIVITY (K) NEΔT	CALIBRATION ACCURACY (K)	STATIC BEAM WIDTH $\emptyset_B$ (degrees)	QUASI POLARIZATION	CHARACTERIZATION AT NADIR (REFERENCE ONLY)
16	87-91	2.0	200	.5	2.0	2.2	QV	window H_2O 150 mm
17	166.31	2.0	200	0.6	2.0	1.1	QH	H_2O 18 mm
18	183.31±7	2.0	100	0.8	2.0	1.1	QH	H_2O 8 mm
19	183.31±4.5	2.0	100	0.8	2.0	1.1	QH	H_2O 4.5 mm
20	183.31±3	1.0	50	0.8	2.0	1.1	QH	H_2O 2.5 mm
21	183.31±1.8	1.0	50	0.8	2.0	1.1	QH	H_2O 1.2 mm
22	183.31±1	0.5	30	0.9	2.0	1.1	QH	H_2O 0.5 mm
23	113.25	1.0	50	0.5	2.0	1.1	QV	window
24	115.25	1.0	50	0.5	2.0	1.1	QV	window
25	116.2	0.5	30	0.6	2.0	1.1	QV	window-H_2O vapor 60 mm
26	116.7	0.5	30	0.6	2.0	1.1	QV	Surface air
27	117.15	0.4	20	0.7	2.0	1.1	QV	700 mb
28	117.55	0.4	20	0.7	2.0	1.1	QV	400 mb
29	118.75±0.8	0.4	20	0.5	2.0	1.1	QV	250 mb
30	118.75 ±0.45	0.3	15	0.6	2.0	1.1	QV	180 mb
31	118.75 ±0.225	0.15	8	0.8	2.0	1.1	QV	80 mb

2.1.2 Static Beam Widths

In addition to the frequency changes described in previous sections, the scientists agreed to increase the size of the static beam width for Channel 1 and Channel 2 (23.8 and 31.4 GHz) from 3.3 degrees to 5.2 degrees. This will allow a smaller scan reflector and, therefore, a smaller, lighter weight and lower power instrument, since the reflector diameter is proportional to the beam width. A scientific rationale increased the size of the beam widths: Channels 1 and 2 provide very useful and unique information for water vapor on the surface. Because these channels are window channels, they are mainly used as flags to further process data; therefore, the size of their footprints is not critical.

The static beam width decreased to 2.2 degrees from the 3.3 degrees of the heritage AMSU Channels 3 through 16. This reflected another significant ATMS change that was adopted by the scientific community. They recognized that the optimum scan-rate for the new ATMS should be 8/3 seconds (the same as the predecessor AMSU-B/MHS) compared to 8 seconds for the predecessor AMSU-A instruments. The scientists believed that the 2.2-degree beam width represented better resolution. At the same time, the scan reflector size was kept as small as possible.

2.1.3 Noise Equivalent Temperature Requirements

Noise Equivalent Temperature Difference (NEΔT) requirements are changed for those channels that had their static beam width changed compared to the heritage AMSU-A instrument. The change is proportional to the changed static beam width and the new 8/3 scan rate. However, the ATMS NEΔT value is equal to the original heritage NEΔT value when a 3.3-degree beam width is reconstructed during ground data processing

An additional benefit of the reduction in beam width is that it allows scientists who are interested in special resolution to get better resolution than was available on AMSU-A. On the other hand, scientists who are interested in sounding can still reconstruct NEΔT during ground processing.

The requirement for 3.3 degrees reconstructed NEΔT was not changed from the AMSU-A requirement even though actual instrument performance exceeded requirements with a significant margin. Therefore, ATMS NEΔT performance with significant margin will not be guaranteed.

2.2 OPERATIONAL REQUIREMENTS

It is planned that ATMS will be integrated with both the NPOESS and the NPOESS Preparatory Program (NPP) spacecraft. However, all the operational requirements, interfaces, and spacecraft accommodation used as our study basis came from the NPOESS spacecraft. Since the NPOESS missions will be a.m. and p.m. missions, and NPP is an a.m. mission, accommodating NPOESS requirements guarantees compatibility with NPP. Additionally, both spacecraft are to have similar Power and Command and Data Handling (C&DH) distribution subsystems.

2.2.1 NPOESS and NPP Common Requirements

This section contains operational requirements and interfaces that are common to both the NPOESS program and the NPP platforms or satellites.

ATMS will operate in a near-polar, sun-synchronous orbit. The sun angle (defined as the angle between the satellite-to-sun line and the normal-to-the-orbital plane) may have any value. Therefore, the instrument must operate within specifications at all sun angles.

The ATMS will organize data in Consultative Committee for Space Data Systems (CCSDS) source packets and insert time, orbit, and position data received from the spacecraft. The time tag uniquely defines the start of each scan.

The total scan period including calibration targets will be 8/3 seconds. Scans will be orthogonal relative to the orbital velocity vector and counter-clockwise looking in the orbital velocity vector direction.

ATMS instrument constraints include: a mass of 88 kgs, average power consumption of 75 watts, a maximum data rate of 50 kbps, and dimensions of 70 cm (velocity direction) x 60 cm (nadir direction) x 40 cm (anti-solar direction).

2.2.2 NPOESS Preparatory Program (NPP) Platform

The NPOESS Preparatory Program (NPP) Platform will operate at an altitude of approximately 705 km with a morning nodal crossing time.

2.2.3 NPOESS Platform

The NPOESS Platform will operate at an altitude of 833 km. The ATMS will nominally fly on the afternoon satellite.

2.3 OPTIONS

2.3.1 Enhanced Science

The ATMS shall contain all 31 channels identified in Table 2-1.

2.3.2 Comparable Science

The ATMS shall contain Channels 1 through 22 as identified in Table 2-1.

2.3.3 Descope Option # 1

The ATMS shall contain Channels 1 through 15 and 17 through 22 as identified in Table 2-1.

2.3.4 Descope Option # 2

The ATMS shall contain Channels 3 through 15 and 17 through 22 as identified in Table 2-1.

3.0 TECHNOLOGY ASSESSMENT

The ATMS Phase-A Study Team investigated the possibility of using new technologies to enable the reduction of some key spacecraft budget parameters such as size, weight, and power. The study team recognized that ATMS would need to employ state-of-the-art technologies to meet the NPOESS-imposed ATMS envelope constraints. Collectively, the Study Team felt quantum gains would come from four major areas:

- Instrument collector antenna sizes would be reduced compared to the heritage AMSU-A instruments based on the Science Team's relaxation of the static beam width requirements.
- Low-Noise Amplifiers (LNAs) would allow direct detection for some channels, while reducing the quantity of local oscillator/mixer components for other channels. If required, packaging LNAs and local oscillator/mixers using either Monolithic Microwave Integrated Circuitry (MMIC) or Microwave Integrated Circuitry (MIC) techniques could further reduce size.
- Modern-day electronics employing microprocessor and programmable gate-array technology would greatly reduce electronic size in comparison to the 15-year-old discrete electronic designs of the heritage AMSU instruments.
- Channel narrow-band filtering could be accomplished digitally within the instrument microprocessor supported by limited integrated electronics, thereby eliminating the need for discrete components and improving filter shape and repeatability.

3.1 LOW-NOISE AMPLIFIERS

3.1.1 Low-Noise Amplifier Versus Mixer Assessment

The first stage of a total power receiver, the front-end, can be either a Low-Noise Amplifier (LNA) or a mixer. The selection depends on a number of factors including frequency of operation, required noise performance, and receiver side-band requirements. In order to assess the state-of-the-art of these devices, it was decided to contact and query various experts/institutions specializing in necessary device development. The result of these queries is summarized in Table 3-1, Summary of Existing AMSU Receiver NFs and Options for ATMS.

The first column lists the AMSU and HSB channel numbers. The second column aggregates these channels into broad frequency ranges/bands that also encompass the ATMS frequency ranges. The third column attempts to summarize the actual noise performance of AMSU and HSB receivers, although the HSB data was difficult to obtain and is questionable. This third column establishes a benchmark by which to measure the improvement that ATMS may provide.

The next five columns summarize the noise performance readily available from different technologies as reported by a recognized leading institution in that technology. All LNAs in this

Table 3-1. Summary of Existing AMSU Receiver NF and Options for ATMS

					OPTIONS FOR ATMS			
			AMSU-A & HSB	Ga As LNA	InP LNA, MMIC	InP LNA, MIC	Ga As Mixer	Ga As Mixer
	AMSU-A & HSB	Frequency Group	RCVR Performance	Miteq	TRW	NRAO	Millitech	Millitech
	Channel #	in GHz (1)	NF in dB (2)	NF in dB (3)	NF in dB (4)	NF in dB (5)	NF in dB (6)	NF in dB (7)
A2	1	23-32	3.5	3	N/A	1.5		4
	2							
	3							
	4							
	5							
	6							
A1	7							
	8	50-59	3.8	7	3	2.6		4
	9							
	10							
	11							
	12							
	13							
	14							
	15	86-92	6.5	N/A	4	3.4	5.5(4 for LNA)	4
	16	112-120	10	N/A	6	N/A	9-11,SSB	4
HSB	17							
	18	164-185	10	N/A	8	N/A	7.5-8.0	6.5
	19							

Notes:

(1) Frequency groups attempt to encompass both AMSU channels and suggested ATMS channels.

(2) From AMSU-A performance from AE-24869B, 30March1995; AMSU-B from MHS Receiver Spec, PC2240-A, Issue B.

(3) From Commercial Off-The-Shelf (COTS) catalog.

(4) From IMAS report (description of 183 performance is confusing). Note: LNAs are MMIC.

(5) From John Webber/NRAO. NFs are MAP LNA performance at room temp. Note: LNAs are MIC.

(6) From a conversation with Rich Chidester, who designed W-band mixer for AMSU-B.

(7) From a Communique from Aerojet Corporation: NFs are Double Side Board, (DSB).

summary have power gains of at least 20 dB. This value is generally recognized as high enough to render any second stage contribution essentially negligible.

A Miteq company representative supplied the information in Table 3-1for the Gallium Arsenide (GaAs) LNA column. These LNAs use MIC technology and GaAs Field Effect Transistors (FETs). The 3-dB Noise Figure (NF) for the 23-32 GHz frequency range is virtually a catalog value or Commercial Off-The-Shelf (COTS) value. (Figure 3-1 and Table 3-2 show a suitable COTS LNA for this application.) In Table 3-1 the 7-dB noise figure for the 50-59 GHz range would require development. For frequencies higher than 60 GHz, the noise performance of these techniques is not competitive.

FEATURES:

- Ultralow Noise Figures From 2.5
- Excellent Phase and Group Delay
- Miniaturized for Coax or Microstrip Interface
- WR28 and Drop-in Version Available
- Military Temperature Range Applications

Figure 3-1. COTS 23 – 32 GHz Amplifier

While the next two columns in Table 3-1 address InP LNAs, but the first column implementation addresses Microwave Monolithic Integrated Circuitry (MMIC) and while the second addresses Microwave Integrated Circuitry (MIC).

In MMIC technology, all the components, such as the transistors, capacitors and resistors, are fabricated and positioned photo-lithographically. An advantage is that many identical circuits can be produced at one time, which can yield cost savings if many units are needed. A disadvantage is that "manual fine-tuning" to counteract manufacturing tolerances and optimize performance is not possible.

In MIC technology, all the components are positioned and connected by hand, so that the component tolerances can be compensated and optimum performance can be achieved. But such hand-tuning is very expensive. In addition, the lead length/bonding wire length required for connections limits the application of this technique to frequencies of 90 GHz and below.

The experts in this field believe that although better noise performance can be achieved using MIC today, the next year or two will bring advances in MMIC techniques that will narrow or eliminate this gap.

Table 3-2. Low-Noise Amplifiers: 26 to 40 GHz

SPECIFICATION PARAMETERS*	JS4D-26004000-25-8P JS4-26004000-25-8P	JS3D-26004000-30-8P JS3-26004000-30-8P
Frequency	26 – 40	26 – 40
Gain	26	18
Gain flatness	±2.5	±2.5
Noise figure	2.5	3
Input/output VSWR	2:1	2:1
Phase linearity Per GHz over complete band	±5	±5
Phase linearity over full band	±10	±10
Unit-to-unit phase tracking	±20	±20
Group delay	±50	+50
Output power at 1 dB compression	8	8
Output IP3	19	19
Output IP2	40	40
Input power (CW max. survival)	20	20
DC power supply: +12 to +20 volts	200	150
* Electrical parameters are specified at +23deg C		

Source: Miteq Company, http://www.miteq.com/micro/amps/jsamps/ln26402.htm

The source for the information in the InP LNA MMIC column is TRW corporation. The noise figures for the various frequency bands are laboratory measurements. The source for the information in the InP LNA MIC column is the National Radio Astronomy Observatory (NRAO) in Charlottesville, VA. This is the institution that designed and manufactured the LNAs (a quantity of 40 units) to be flown on the Microwave Anisotropy Probe (MAP). This column is provided for reference only, since there is little likelihood that NRAO would become a supplier of LNAs for ATMS.

The final two columns address GaAs mixers. The NF values in the first mixer column were provided during a brief telephone conversation with Millitech corporation. The NF values in the final column were extracted from an informative communiqué provided by Aerojet corporation, which is included as Appendix B.

Using the information in Table 3-1, a selection of the most appropriate technology, in terms of noise performance, has been made by frequency group. Accurate cost estimates are expensive to obtain and are only mentioned on for the highest frequency group.

For 23-32 GHz, the Miteq company's GaAs LNAs are the obvious practical choice, although the NRAO InP LNAs can provide substantially better noise figure.

For the rest of the frequency groups, it appears to be a contest between InP MMIC LNAs and GaAs planar diode mixers.

For 50-59 GHz, there is a noise figure advantage to using the TRW InP LNAs instead of the Aerojet corporation's GaAs mixers. These LNAs utilized in the receiver configuration described in subsection 5.3.3 of this report may be the best compromise between pushing technology and restraining costs.

For 86-92 GHz, the noise performance of the two prime candidates is the same; this allows costs to be the deciding factor.

For the last two frequency groups, 112-120 GHz and 164-185 GHz, the noise performance definitely favors the mixer approach. Rough, informal cost estimates provided by both TRW and Aerojet also substantially favor the mixer approach.

Finally, calculations were made to predict the NEΔT of the baseline ATMS channels, using these low-noise receiver components and the receiver configurations discussed in subsection 5.3.3 of this report. The results are shown in Table 3-3, Predicted NEΔT for ATMS Baseline Channels. These results demonstrate that the ATMS requirements can indeed be met.

3.1.2 Low-Noise Amplifier Survey

The team developed a set of questions to help further quantify the current design maturity and cost of the LNAs. We divided the ATMS channels into five logical frequency ranges and chartered JPL and queried industry to assess LNA technology and maturity for 22-33 GHz, 50-59 GHz, 89 GHz 112-120 GHz**,** and 166-185 GHz frequency ranges. Responses to requests in three areas were solicited:

- *Maturity*

  For each of the frequency ranges, indicate the state of available hardware maturity. Bear in mind that to be viable for the ATMS program, the LNA must be mature by 2001. If available as a Commercial Off-The-Shelf (COTS) product, indicate suppliers and provide hardware specification data sheets. If not available as COTS, assess when the component(s) will be mature enough to be used for flight.

Table 3-3. Predicted NEDT for ATMS Baseline Channels

ATMS REQUIREMENTS						ATMS PERFORMANCE			
					AMSU			EFFECTIVE	
CHAN #	CENTER	MAX RF BW/BAND	NEdT	AVAILABLE	IF OR PREDET BW	RCVR CONFIG	RECEIVER NFs	IF OR PREDET BW	NEdT
	FREQUENCY in GHZ	in MHZ	in K	RF BANDS	in MHz		in dB [1]	in MHz	in K [2]
1	23.8	270	0.9	1	135	direct detect	3	270	0.32
2	31.4	180	0.9	1	90	direct detect	3	180	0.39
3	50.3	180	1.2	1	90	LNA w SSB mixing	3	180	0.39
4	51.76	400	0.75	1	--	LNA w SSB mixing	3	400	0.26
5	52.8	400	0.75	1	200	LNA w SSB mixing	3	400	0.26
6	53.596+/-.115	170	0.75	2	170	LNA w SSB mixing	3	2 X 170	0.28
7	54.4	400	0.75	1	200	LNA w SSB mixing	3	400	0.26
8	54.94	400	0.75	1	200	LNA w SSB mixing	3	400	0.26
9	55.5	330	0.75	1	165	LNA w SSB mixing	3	330	0.29
10	57.2903	330	0.75	1	165	LNA w DSB mixing	3	165	0.41
11	57.2903+/-.217	78	1.2	2	78	LNA w DSB mixing	3	78	0.59
12	57.2903+/-.322+/-.048	36	1.2	4	36	LNA w DSB mixing	3	2 X 36	0.62
13	57.2903+/-.322+/-.022	16	1.8	4	16	LNA w DSB mixing	3	2 X 16	0.93
14	57.2903+/-.322+/-.010	8	2.4	4	8	LNA w DSB mixing	3	2 X 8	1.31
15	57.2903+/-.322+/-.004	3	3.6	4	3	LNA w DSB mixing	3	2 X 3	2.15
16	89	6000	1.5	1	3000	DSB mixing	4	3000	0.12
17	166.31	4000	0.6	1	2000	DSB mixing	6.5	2000	0.27
18	183.31 +/- 7	2000	0.8	2	2000	DSB mixing	6.5	2000	0.27
19	183.31 +/- 4.5	2000	0.8	2	2000	DSB mixing	6.5	2000	0.27
20	183.31 +/- 3	1000	0.8	2	1000	DSB mixing	6.5	1000	0.38
21	183.31 +/- 1.8	1000	0.8	2	1000	DSB mixing	6.5	1000	0.38
22	183.31 +/- 1	500	0.9	2	500	DSB mixing	6.5	500	0.54

NOTES:

[1] Assumes choice of LNAs and mixers discussed in section 4.4

[2] Assumes RF losses (ahead of rcvr) = 1 dB, Tscene = 255 K, tau = 18 msec, total power configuration

- *Engineering Parameters*

  Provide engineering parameters for each frequency range depicting the current and expected noise figures, overall gain, plus gain / frequency stability as a function of a 7- to 8-year life requirement. Address availability to acquire each component as a class "s" component.

- *Cost*

  Indicate the current year cost and delivery lead-time to procure COTS-available devices. For non-COTS devices, indicate development and recurring cost-plus-time duration for both development and recurring phases.

Table 3-4 and Table 3-5, respectively, provide Sanders/Lockheed Martin company and TRW industry responses to our query for LNA status and maturity.

3.1.3 Low-Noise Amplifier Summary

The team concluded that LNA technology was at hand for the first three frequency ranges and it would probably be available for the 112-120 GHz and 166-185 GHz frequency ranges early in the year 2001. This conclusion was based on the JPL inputs, our industry queries, and industry responses. Cost would determine which of the two technologies the ATMS contractor would use. The team also recognized that weight, power, and envelope size of either technology was approximately the same so the ATMS strawman was design using LNA technology recognizing that it probably represented the worst case from a cost point of view.

3.2 AVAILABLE MONOLITHIC MICROWAVE INTEGRATED CIRCUIT RECEIVERS

Monolithic Microwave Integrated Circuits (MMIC) are used for building smaller, lighter, and less power consuming microwave receivers. These characteristics make a MMIC implemented receiver an excellent candidate for reducing the size of the ATMS radiometer receivers. MMIC circuits are fabricated using Gallium Arsenide (GaAs) or Indium Phosphide (InP) semiconductor processes for different frequency uses. MMIC radiometer receivers are built around the IC substrate with associated interface circuitry either inside or outside the shell. Packaging is an integral part of the design of a MMIC receiver.

Table 3-4. Sanders Low-Noise Amplifier (LNA) Assessment

	COTS					Development			Engineering Parameters							
Frequency Range (GHz)	COTS Y/N	Suppliers	Purchase Lead Time (Months)	Unit Cost K$	"S" Upgrade K$	Development Time (Months)	Non-Recurring K$	Recurring K$	Substrate Material	Noise Figure dB	Gain dB	# of Stages	Gain vs. Temp dB/DegC	Size L-W-H (cm)	Mass Kg	Power Watts
22-33	Y	Sanders	6	30	10				0.15 um GaAs PHEMT	3	25	3	0.045	2x2x1	50 gms	30 mW
	Y	Sanders	6	30	10				0.1 um InP HEMT	2	30	3	0.030	2x2x1	50 gms	15 mW
	Y	Sanders	6	30	10				0.1 um InP HEMT	2	35	3	0.030	2x2x1	50 gms	30 mW
50-59	N	Sanders				9	250		0.15 um GaAs PHEMT	4	25	4	0.060	2x2x1	50 gms	60 mW
	N	Sanders				9	250		0.1 um InP HEMT	3	23	3	0.030	2x2x1	50 gms	25 mW
50-56, 57-63 GHz (see note)	Y	LM-CPC	6	30	10				0.15 um PHEMT, 0.1 um InP HEMT	3	20	3	0.032	7.0 x 3.8 x 2.2	160 gms (see note)	320 mW (see note)
89	N	Sanders							0.1 um GaAs PHEMT	6	18	4	0.060	2x2x1	50 gms	100 mW
	N	Sanders				9	250		0.1 um InP HEMT	4	17	3	0.030	2x2x1	50 gms	25 mW
112-120	N	Sanders				9	250		0.1 um InP HEMT	5	15	3	0.030	2x2x1	50 gms	20 mW
	Y	Sanders	6	30	10				0.1 um InP HEMT	6	21	6	0.060	2x2x1	50 gms	40 mW
166-185	N	Sanders				9	250		0.1 um InP HEMT	8	16	4	0.040	2x2x1	50 gms	25 mW

Assumptions:

1. Quantities > 100
2. Low DC power assumes low RF output power: < 0 dBm up to 90 GHz
   < - 5 dBm above 90 GHz
3. No DC-DC converter included in mass or DC power estimates
4. Size assumes single MMIC packaged in aluminum housing

50-63 GHz LNA Notes:

V-Band flight LNA design exists from DMSP Program
All mass/size data includes I/O isolators, W/R-15 transitions LNA mounting & DC voltage regulation circuitry
P/N = 23002699P1 & P2
Units can be tuned to specific bandwidths as required
Unit operates from +8 VDC supply (single voltage); DC power can be reduced to 160 mW with elimination of regulator
All data based on measured flight hardware
V-Band Flight LNA/Downconverters exist and are available as COTS

90595-01

Table 3-5. TRW Low-Noise Amplifier (LNA) Assessment

	COTS					Development			Engineering Parameters							
Frequency Range (GHz)	COTS Y/N	Suppliers	Purchase Lead Time (Months)	Unit Cost K$	"S" Upgrade K$	Development Time (Months)	Non-Recurring K$	Recurring K$	Substrate Material	Noise Figure dB	Gain dB	Gain Stability dB	Gain vs. Temp dB/DegC	Size L-W-H (cm)	Mass Kg	Power Watts
26-32	N	TRW							GaAs	3	23			5x2.5x2.5		0.25
26-32	N	TRW							InP	3	30			5x2.5x2.5		
50-59	N	TRW							InP	3.8	18			5x2.5x2.5		0.063
77-105	N	TRW							InP	3.5	21			1.5x2x2		0.021
112-120	N	TRW							InP	4.8	14			1.5x2x2		0.03
165-192	N	TRW							InP	9	11			1.5x2x2		0.132

90595-02

3.2.1 Direct Determination Radiometer

Figure 3-2 is a sample of the year 2000 JPL/JASON oceanography mission's18-GHz direct-detect radiometer. The upper half of circuit inside the enclosure is the actual MMIC circuit with a detector diode. The bottom half is the detector amplifier and voltage to frequency converter. The enclosure size is 10cm x 7.6cm x 5cm, mass 0.4 kg, power consumption of <=1 watt.

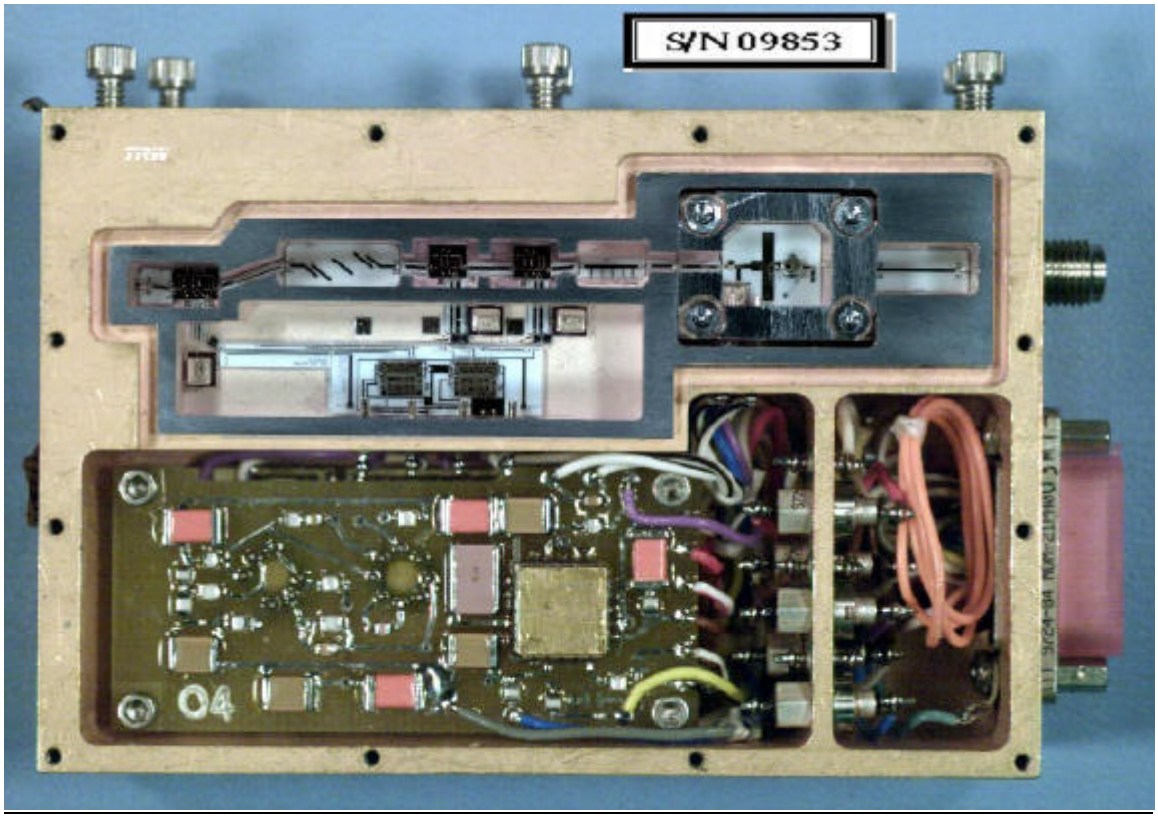

Figure 3-2. JPL/JASON 18-GHz MMIC Radiometer

3.2.2 Down Converter Radiometer

Figure 3-3 illustrates a prototype of a 118-GHz down-converter radiometer receiver developed by the (IMAS) program. The IMAS program developed MMIC receiver technology for uses in the range from 118 to 183 GHz, which are frequencies of interest to microwave sounding radiometers. This particular receiver is built with InP technology using modular Low-Noise Amplifiers (LNAs), developed within IMAS, mounted onto the InP substrate. A well-shaped machined overlay (top half) is mounted over the MMIC substrate to provide good wave-guide characteristics at this frequency and prevent reflections along the signal path.

The Local Oscillator (LO) mixer for this implementation is external. This particular MMIC implementation uses a series of LNAs (produced by TRW), providing a Noise Figure (NF) ~6dB at 118 GHz. Other LNAs produced by this manufacturer are being built for frequencies in excess of 183 GHz, exhibiting a NF of ~7db at 183 GHz.

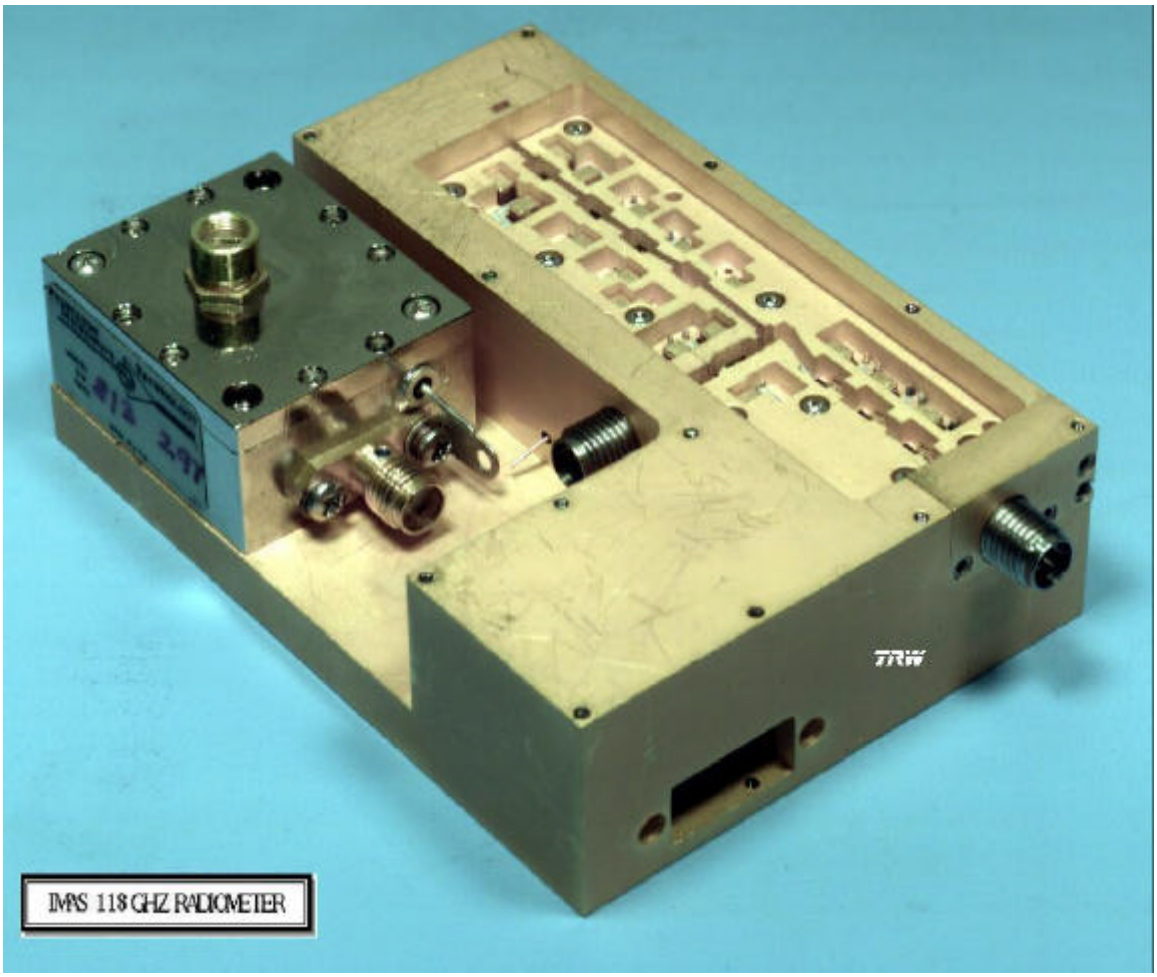

Figure 3-3. IMAS 118-GHz Radiometer

3.2.3 Summary

The Study Team recognized the high-density packaging advantages of the MMICs, but decided to evaluate whether packaging the ATMS using discrete components was possible for our strawman design, as this represented our worst case scenario. The discrete approach was recognized to impose less development time and less program risk while being much less expensive.

4.0 ANALYSIS AND TRADE STUDIES

4.1 ATMS SCAN PATTERN

4.1.1 Introduction

The scan pattern is an important design variable for enabling the ATMS to meet its radiometric requirements. ATMS must provide the functionality of AMSU-A1 and -A2 (AMSU-A) as well as that of AMSU-B in the microwave portion IR/microwave sounder suite. This portion works with the Cross-track Infrared Sounder (CrIS), the Infrared Atmospheric Sounding Interferometer (IASI), or Atmospheric Infrared Sounder (AIRS).. The functions previously packaged in the three AMSU-A/AMSU-B instrument modules with four scanners must fit into one module approximately the size of AMSU-A1. Minimizing differences between scanners presents an opportunity to reduce the cost.

Historically, the HIRS/MSU and later the AMSU suite have had a scan pattern that leaves significant sounding gaps near the equator extending to ±30 degrees in latitude. This can easily be corrected in the ATMS (and companion IR sounders) to provide better temperature and moisture data for weather prediction in equatorial regions, which includes the Southern United States.

Subsection 4.1.2 describes the current AMSU scan strategy; 4.1.3, ATMS design options; 4.1.4, calibration issues; 4.1.5, the mapping of the AMSU-A or ATMS beam to possible IR sensor measurements; and 4.1.6, the removal of near-equator coverage gaps. Appendix A presents a treatise of temperature errors introduced by microwave vs. IR instrument spot size differences.

4.1.2 AMSU Scan Patterns

Figures 4-1 and 4-2 show the existing AMSU-A/AMSU-B timing and scan patterns. Note that the AMSU-A utilizes an 8-second scan period with a step and settle scan across the Earth scene while the AMSU-B utilizes an 8/3-second scan period with a constant speed scan across the Earth scene.

In Figure 4-1, a possible constant speed scan option for AMSU-A (not used) is shown for comparison. It illustrates the reduced time available for integration over the Earth scene. The constant speed scan is attractive from the standpoint of simplifying the mechanism and reducing momentum changes. But, it substantially reduces available integration time for Earth scenes and calibration views since much of the time is spent in transitions between measurements. For the constant speed scan case, the Earth-viewing fraction is about 28 % of the scan vs. 75 % for AMSU-A and 62% for AMSU-B.

Figure 4-3 shows a comparison of the AMSU-A and AMSU-B beam patterns (footprints) on the Earth near nadir. AMSU-A operates with a step-scan across track. With the 3.3-degree beam size and the 8-second scan period, the beam footprints are non-overlapping across track and along track. The AMSU-B uses a constant speed scan across the Earth scene. With its 1.1 degree beam size and 8/3-second scan period, the fields-of-view of the beams are elliptical and overlapped across track but non-overlapping along track (~16 km along track, ~32 km across track). This is

shown to the right as a comparison of the actual AMSU-B fields-of-view along with the "artistic liberty" used to simplify the illustration.

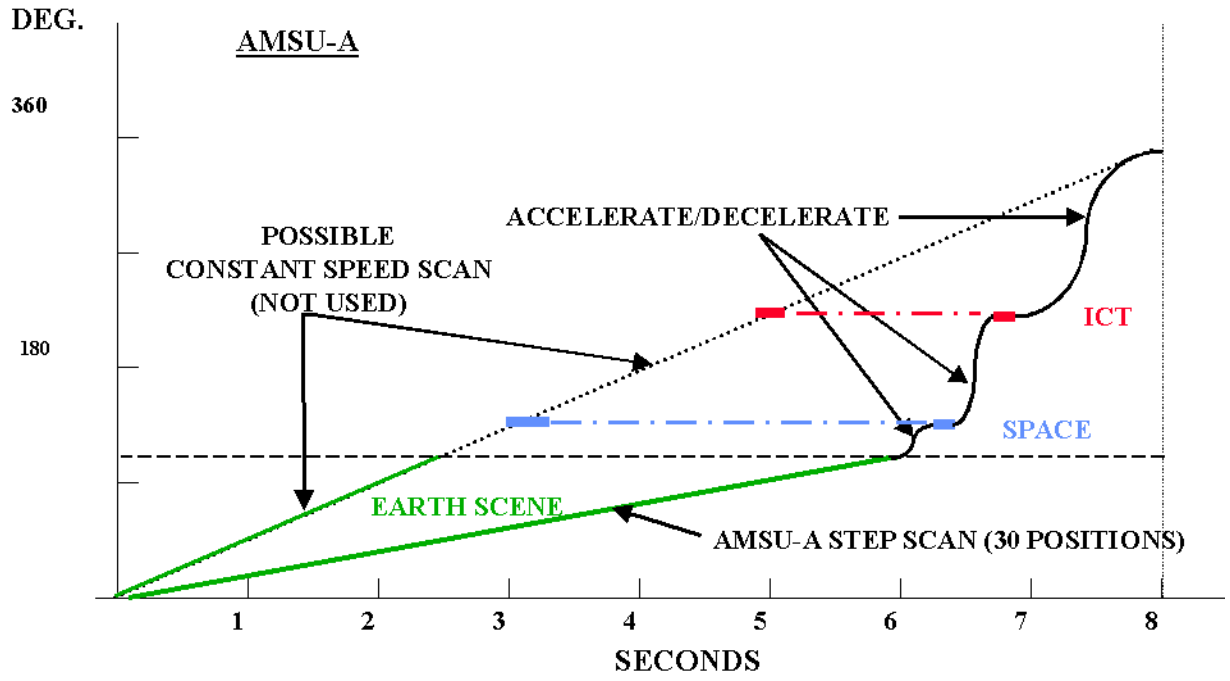

Figure 4-1. AMSU-A Scan Pattern Timing
Note step scan vs. continuous scan considerations.

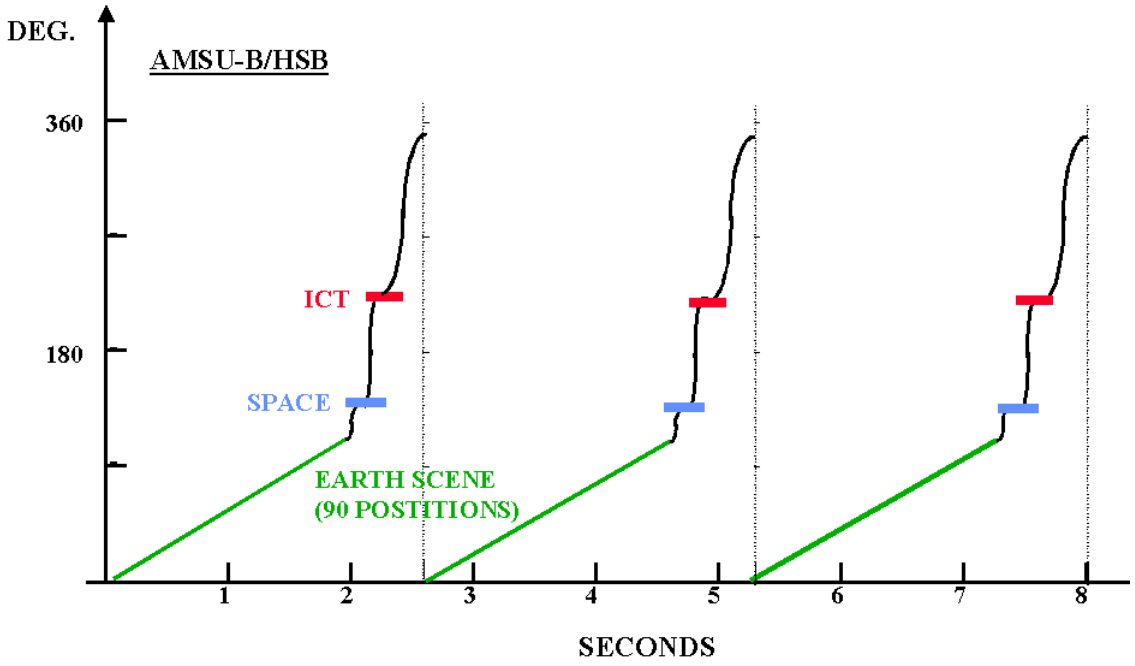

Figure 4-2. AMSU-B/HSB Scan Pattern Timing

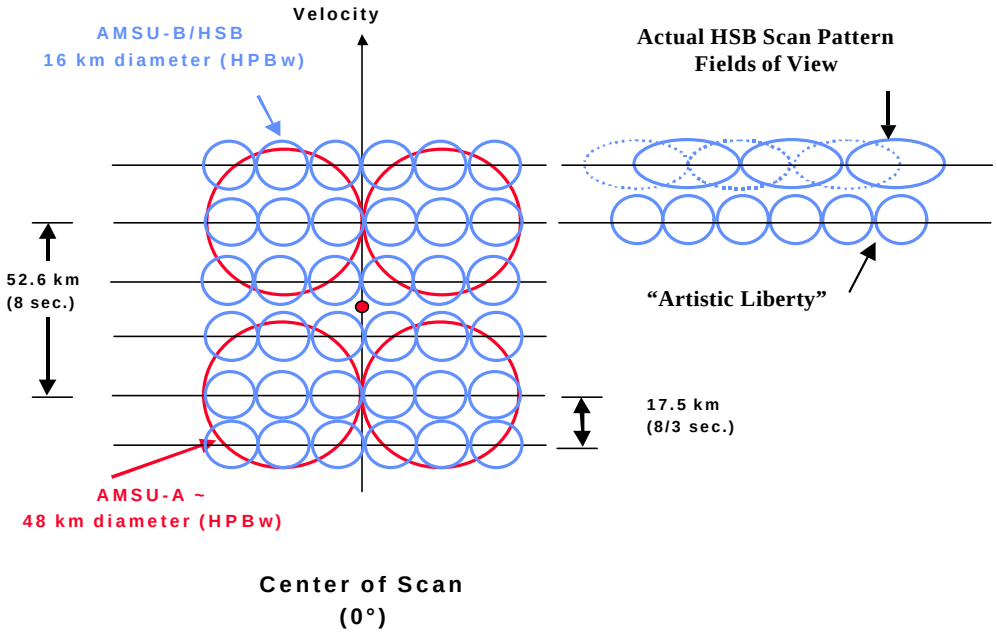

Figure 4-3. AMSU-A and AMSU-B Beam Patterns Near Nadir

4.1.3 ATMS Scan Pattern Options

Both the AMSU-A and AMSU-B scan patterns under-sample, in a Nyquist sampling sense (a spacing of less than half a beam width), the temperature and humidity scene information. Errors in knowledge of the scene temperature can be reduced significantly by using a beam narrower than 3.3 degrees and a scan pattern that samples the scene at a spacing of less than one beam width. Sources of error in the microwave measurements are discussed in more detail in Appendix A, Scan Options.

During the ATMS study, a number of scan pattern options were examined. A summary of options is presented in Table 4-1, including the existing AMSU-A/AMSU-B scanning patterns shown in the first two lines.

To meet the requirement of providing microwave sounding data to work with a variety of IR scan patterns, good accuracy in interpolating microwave data to determine the position of the IR beams is required. This is particularly important for the AMSU-A temperature measurements. Options, such as ATMS-5 (see Table 4-1), were examined that provided half beam width sampling (or better) for all the beams. For ATMS-5, AMSU-A and AMSU-B beams can both be synthesized from the measurements from each channel to construct the respective AMSU/AMSU-B beam at desired positions and retain the AMSU-A/AMSU-B NEΔTs.

Table 4-1. AMSU and ATMS Scan Pattern Options

Configuration	Period s.	8/N N	Earth Fraction	Earth s.	Cal/Rtn ms.	Cold ms.	ICT ms.	Rtn (Non Cal) ms.	Earth Scene deg	Earth Views	Step+ Integ ms.
AMSU-A	8.00	1.0	0.750	6.00	2000.0	330	330	1340.0	99.0	30	200.00
AMSU-B (HSB)	2.67	3.0	0.610	1.63	1040.0	72	72	896.0	99.0	90	18.07
AMSU-B'	2.67	3.0	0.750	2.00	666.7	72	72	522.7	99.0	90	22.22
ATMS Nominal	**2.67**	**3.0**	**0.650**	**1.73**	**933.3**	**110**	**110**	**713.3**	**105.6**	**96**	**18.06**
ATMS-5	1.33	6.0	0.675	0.90	433.3	55	55	323.3	105.6	192	4.69
ATMS-6	1.60	5.0	0.675	1.08	520.0	0	132	388.0	105.6	192	5.63

Notes: 1) B14ATMS-6 eliminates one acceleration/deceleration in the Cal/Rtn period:
shown for ICT but the Cal alternates between Cold and ICT on alternate scans.
2) Some power savings should result - not considered in this model.
3) ATMS-6 option: along track is slightly below Nyquist sampling.

The penalty of half beam width sampling for the AMSU-B channels is a higher data rate, some additional scan power, and some design effort to scan at twice the current AMSU-B rate. The ATMS Study Team elected only to scan at the AMSU-B, 8/3-second rate, which provides half beam width spaced samples for the AMSU-A temperature channels and uses the existing sampling strategy for the AMSU-B channels. The data rate required for this option is a modest increase over the AMSU-A/AMSU-B ~ 8 kbps to ~20 kbps for ATMS. The "ATMS Nominal" design shown in Table 4-1 does not penalize Earth-scene integration time or unduly impact scan motor power relative to how this was accomplished for the heritage AMSU-B. The ATMS Nominal design is discussed in detail in this section and in the Appendix A.

The ~20-cm-diameter apertures that can be accommodated in the ATMS envelope result in beam widths of approximately 2.2 degrees in the 50-GHz band. Beam widths at 23.8 and 31.4 GHz are ~ 5.2 and 4.0 degrees, respectively, due to the limited aperture size. The 50-GHz beams could be "spoiled" to provide 3.3-degree beams. But, using the 2.2-degree beams at 50 GHz provides an opportunity for a better temperature measurement resolution as well as only requiring one scan rate (8/3 second). The ATMS study recommends that both the 23.8- and 31.4-GHz beams have a 5.2-degree beam width to permit comparison of the moisture information from these channels. These are over-sampled in a Nyquist sense both across track and along track. Some resolution improvement is possible in the sounding data, using the over-sampled spatial data and simple weighting algorithms as discussed in subsections 4.1.3.1 and 4.1.3.2 and in Appendix A.

4.1.3.1 AMSU-A, ATMS Equivalence

Figure 4-4 shows the ATMS nominal design with 2.2 degree beams for the 50-GHz AMSU-A channels, 1.1 degree beams for the AMSU-B channels and the IR beams for a notional CrIS or AIRS at nadir. Equivalent noise performance and beam width to AMSU-A can be achieved by taking a weighted sum of the nine ATMS beams lying in the footprint of the AMSU-A beam; see Appendix A.

The AMSU-A provides 165 ms of integration time for the 3.3 degree beam and the ATMS nominal design provides ~18 ms of integration time for each 2.2 degree beam. Since the ATMS

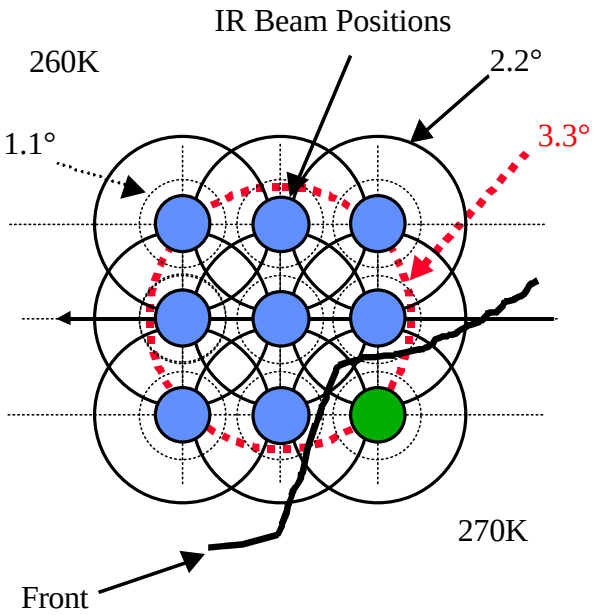

Figure 4-4. AMSU-A, AMSU-B, ATMS, and IR Sounder Beam Positions Shown on a Hypothetical Temperature Field Near a Weather Front

integration time is approximately 1/9 of AMSU-A, equation A11 in Appendix A shows the resulting NEΔT of each ATMS beam is three times larger for each of the nine measurements. Since the nine ATMS beams are non-overlapping in time, they are statistically independent. A beam formed by averaging the nine temperature measurements has a NEΔT that is reduced by three from that of the individual measurements or is equivalent to the AMSU-A NEΔT.

Figure 4-5 shows the shape of this synthesized or constructed beam footprint that meets the AMSU-A beam width specification of 3.3 degrees ±10% (3.36 degrees along and across track, 3.54 degrees on the diagonal). If a circular 3.3-degree beam is desired, a weighted average of ATMS beams must be calculated and there is a ~6 % increase in NEΔT over the equally weighted case. See the Appendix A for a detailed discussion.

4.1.3.2 ATMS Provides Better Knowledge of the Temperature Field

Figure 4-4 also shows a temperature field at the position of the ATMS and IR beams that as might be found near a weather front or land-sea boundary. The temperature as seen by the 3.3-degree AMSU-A beam would be an average of the nine regions or ~261.1 K.

A typical AMSU-A channel might have a NEΔT of 0.25 K so the nine ATMS measurements would have a NEΔT of 0.75 K each. If the average temperature of the scene from the AMSU-A was used by the IR, there would be a considerable error at the lower right position, which is at 270 K vs. 261.1 K ({8*260 K + 270 K }/9) for the average. At this lower right position, the raw ATMS measurement with an NEΔT ~0.75 K is considerably better than the temperature average from the 3.3 degree beam and provides additional insight about the temperature field.

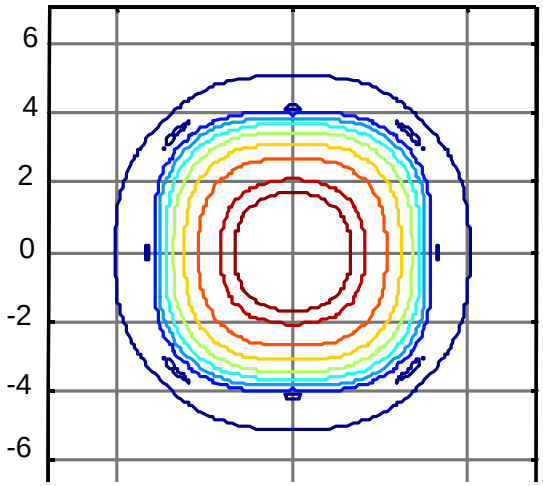

Figure 4-5. Synthesized 3.3-Degree Beam

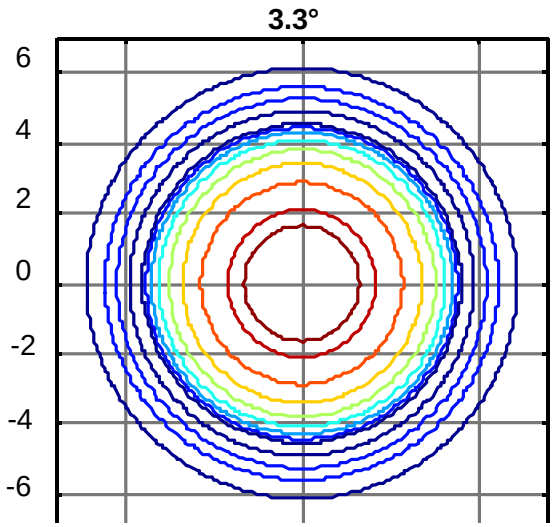

Figure 4-6. AMSU-A 3.3-Degree Beam

Figure 4-5 represents a synthesized 3.3-degree beam from averaging nine 2.2-degree ATMS beams. The synthesized beam is within the 10% beam width tolerance allowed for AMSU-A beams. Figure 4-6 represents the heritage AMSU-A 3.3-degree beam. The inner contour presented in Figures 4-5 and 4-6 is -3 dB relative to the peak of the beam, next in order is -5, -10, -15, -20, -25, -30, -35, -40 dB.

4.1.4 Calibration Target Options

The existing AMSU-A/AMSU-B scan patterns collect data at both the space view and Internal Calibration Target (ICT) on each scan. The ground processing uses a running average over ~5 AMSU-A scans to reduce the errors of the calibration measurements since the gain of the receivers do not vary significantly over a ~40-second interval. The calibration time per scan for ATMS must be justified based on the gain stability of the system.

With the proposed ATMS 8/3-second scan rate for all channels, a reduction in scan power and momentum is possible. This can happen by alternating the calibration scene each rotation and dwelling twice as long on each to retain the same amount of calibration accuracy over the running average. The space view and ICT can be arranged or built for use over as much as 5 to 20 degrees of the scan rotation. Additional measurements of each could also be taken “on the fly” on the scans where a target dwell is skipped.

4.1.5 ATMS Operation with IR Sounders

Figure 4-7 shows the scan patterns of several IR sounders that may be used with the ATMS microwave sounder. The CrIS is planned for the NPOESS satellites. Its field-of-view pattern may rotate with scan position as it moves off from nadir as shown in Figure 4-7 (CrIS). The IASI will be flown with ATMS on the (METOP) satellites. The AIRS will be flown on the EOS-PM satellite. Both the IASI and AIRS scan patterns remain constant with scan position.

To best initialize the IR retrievals of temperature and water vapor, a microwave beam that has a beam width close to that of the IR beam and is located near the center of the IR beam is desired. This situation is best approximated by the ATMS beams (2.2 degree beam width) whose measurements are closely spaced. As shown in Appendix A, it is possible to interpolate between microwave measurements to accurately estimate the temperature at the location of the IR beam if the microwave measurements are spaced by approximately one-half beam width.

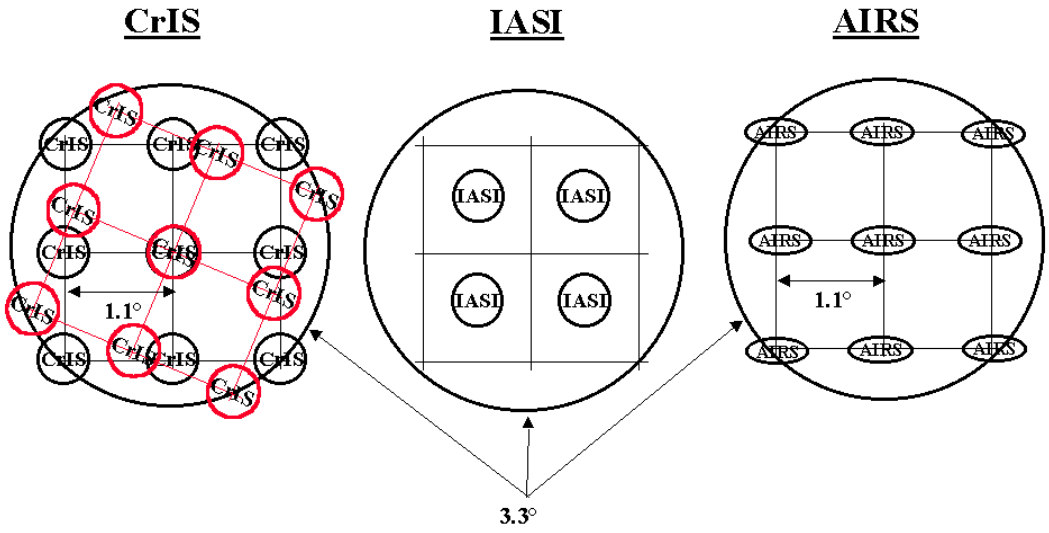

Figure 4-7. IR Sounder Measurement Footprints Compared to AMSU-A 3.3-Degree Beam

4.1.6 Scan Coverage Gaps at the Equator

A historical accident in a previous redesign of the TIROS/POES satellite constellation led to the existing coverage gaps at the equator that are illustrated in Figure 4-8. The original satellite constellation was operated at a higher altitude. When the spacecraft bus was changed to utilize the (DMSP) bus technology, the HIRS instrument's scan coverage was not increased from ~99 to ~104.6 degrees to eliminate gaps in coverage in the equatorial region. Present and future improvements in understanding of IR and microwave soundings should allow data at these slightly wider scan angles to be used.

A consequence of the gaps is that sounding coverage for numerical weather prediction programs is missing in about 25% of the equatorial region. These regions of missing data extend into the Southern part of the United States and lead to significant gaps in coverage of severe storm fronts that spawn tornadoes. These breaks in the measurements of the strength and progress of hurricanes reduce the forecasting accuracy of landfall and can lead to wider areas of evacuation. Reducing the discontinuities, benefits the continental United States middle latitudes as it extends the areas of overlap of the coverage swaths and provides additional updates on adjacent orbits.

The equatorial gaps can be eliminated by an additional ~3 degrees of scan coverage on each side of the swath. This can be accommodated by either a slightly faster retrace time (used in Table 4-1), by a 10% reduction in integration time for the Earth-scene measurements or a combination of

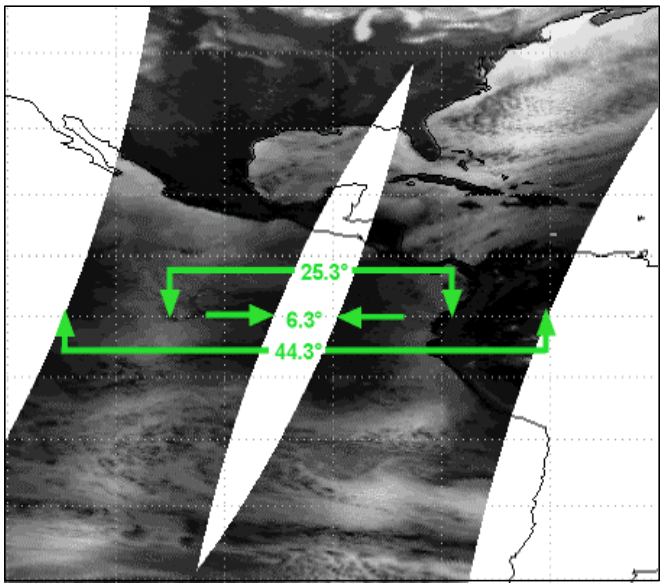

Figure 4-8. Equatorial Coverage Gaps for AMSU

Note: Gaps cover about 25% of area at the equator.

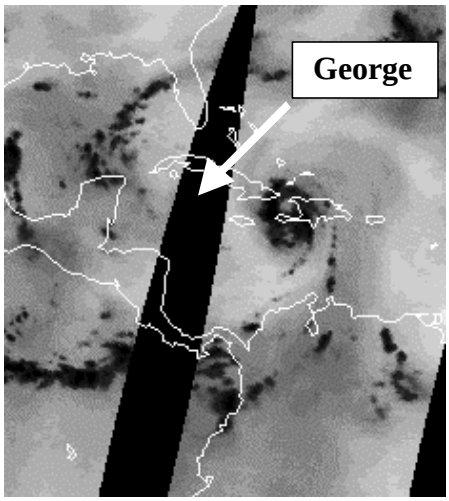

Figure 4-9. Gap Near Hurricane Georges

Note: The size of the data gap in Figure 4-8 is comparable to Hurricane Georges gap as it approached Florida on 9/23/98.

both. In any case, the cost is insignificant if done from the inception of the ATMS design. Comparable scan coverage should also be provided on the companion IR sounder.

4.1.7 Summary

The study team including the NASA Study Scientist, his science team, and the IPO Sounder Operational Science Team concluded that the ATMS should have a 8/3 second scan period, the same as the heritage AMSU-B. Similarly, the Earth-scan field-of-view should be 106.6 degrees, in order to eliminate gaps at the equator.

4.2 Analog Versus Digital Narrow-Band Filtering

4.2.1 Narrow-Band Analog Filters

The narrowest heritage AMSU-A channels are 11 through 14. These exhibit pass bands of 36 mhz, 16-mhz, 8-mhz and 3-mhz at U-band (57.290 GHz). The receiver approach for these channels was to down-convert the U-band signals to an Intermediate Frequency (IF) of approximately 300-mhz, where channel filtering was provided by Surface Acoustic Wave (SAW) devices. At this IF frequency, the narrowest bandwidth is 1% of the center frequency, which is well within the capability of SAW filters. However, SAW filters have very high insertion loss, and they are high in cost. Therefore, an investigation into alternatives appeared desirable and was performed.

The result of the investigation into narrow-band analog filters for ATMS is shown in Table 4-1. To fairly compare the various technologies, an attempt was made to standardize or "normalize" the bandwidth and number of sections. The bandwidth was chosen at 3-mhz, because this is the narrowest bandwidth (Channel 15) required by ATMS science. Five sections were chosen, because this amount will provide the Shape Factor (skirt selectivity) of 1.3 required by the AMSU specification. Unfortunately, the Multi-Mix example could not be "normalized" because pertinent performance data was not available.

The "Filter Center Frequencies" listed for each technology example were derived by taking into account the minimum bandwidth and minimum center frequency obtainable in each technology. They are all suitable as IF frequencies. But it should be noted that in order to obtain a 3-mhz bandwidth, both the ceramic technology and the mini-cavity technology have been pushed to the lowest limit of both their available bandwidth range and their available center frequency range. Generally, operating at or near device limits does not constitute a conservative approach.

The "Insertion Loss" column shows the large SAW loss. Fortunately, losses can be compensated by relatively cheap and stable IF gain.

The "Size" column shows that all the technologies require approximately the same volume.

The "Temperature Stability" column shows that all technologies provide temperature performance that either equals/exceeds SAW performance, which has been adequate for the heritage AMSU-A.

Therefore, it would appear that there are alternatives to SAW filters for the narrow-band channels of ATMS. The final choice will be strongly influenced by cost considerations.

Table 4-2. Narrow-Band Analog Filter Options

ATMS-FILTER-TRADE-2.XLS										
maruschak										
16-Apr-99										
	Filter	Filter	Min Obtainable	Filter	Min Obtainable	Insertion				
Technology	Bandwidth	Center Freq	Center Freq	Bandwidth as	Bandwidth as	Loss	Number of	Size	Temp Stability	Miscellaneous
	in MHz	in MHz	in MHz	% of Ctr Freq	% of Ctr Freq	in dB	Sections (1)	in inches	over -5 to 35C	
SAW (2)	3	317.7	20	0.9	0.5	29	5	1.6x1.4x.6	<0.4 MHZ	mfr is Phonon
Ceramic	3	300	300	1	1	4	5	1.7x1.5x.4	<0.1MHz	mfr is Integrated
									(5 ppm/C)	Microwave
Mini-cavity	3	200	200	1.5	1.5	13	5	2.4x.7x.4	<0.2MHz	COTS; mfr is Reactel
									(24 ppm/C)	
Multi-Mix (3)	2.7	1000	500	0.27	0.2	7	2	1x.3x.3	similar to SAW	new technology;
										mfr is Merrimac
Lumped (4)	3	150	3	2	2	10	5	1x.5x.4	<0.2MHz	COTS; mfr is Reactel

Notes:

(1) Approximately five sections needed to provide the Shape Factor (selectivity) of 1.3 required by the AMSU specification.

(2) Characteristics from the specification for AMSU Channel 14.

(3) Trademark of Merrimac Industries, new multi-layer, three-dimensional technique with potential for low cost.

(4) Reactel's "Micro-Mini" series.

4.2.2 Narrow-Band Digital Filters

Digital filter technology has been utilized in spacecraft for many years. As the state-of-the art in high-speed, low-power Analog-to-Digital (A/D) converters and low-cost digital logic has increased, the sample rate, which can be supported in flight instruments, has drastically increased. For example, 80-million-samples-per-second (msps) Complementary Metal Oxide Semiconductor (CMOS) A/D converters have been tested for space use. Additionally, 1-GHz, Positive Emitter Coupled Logic (PECL) A/D converters have also been shown to be acceptable for some flight environments. Digital filters offer unit-to-unit repeatability unobtainable with traditional analog filters. Additional advantages of digital filters include increased reliability and low recurring costs. Using a common A/D converter also enhances channel-to-channel repeatability and stability. Power and the additional complexity of the digital design will make digital filtering impractical for signals over a critical sample rate. For this implementation, a maximum sample rate of 64 msps was established, because it has been demonstrated for prior flight applications. Channels 12-15 are candidates for digital filtering using this criterion.

Digital filters for Channels 12-15 would require about five A/D converters and 12 ACTEL Company FPGAs. A system of this size would require approximately 16 watts at 5.0V. At this time, the power required is too high to allow digital filtering to be competitive with traditional analog methods. As technology advances and the supply voltage required for high-speed A/D converetors and digital logic is reduced, the digital filter input power is reduced.

Some options do exist for implementing the narrow-band filters in novel ways. The first option involves implementing an A/D and Finite Impulse Response (FIR) / Fast Fourier Transform (FFT) in Ultra Low Power (ULP) technology. This would drastically reduce the power required and increase the maximum sample rate of the system. The second option involves implementing the narrow-band filters using Micro Electro Mechanical Systems (MEMS) technology. The third option requires researching algorithms that filter or FFT the data with 3-5 variable level quantified data. This would allow a drastically simplified A/D and FIR chain. Unfortunately, the optimum quantification levels are dependent on the input data amplitude. This makes the determination of the power in each channel a closed-loop process, which increases the real-time data analysis requirements for the instrument.

4.2.3 Summary

Some form of mechanical filter is the correct answer for the ATMS instrument. Digital filters should probably not be used for the next-generation instrument. MEMS filters, however, may be a real option to replace the SAW filters used in the AMSU instruments.

5.0 STRAWMAN INSTRUMENT DESIGN

5.1 INTRODUCTION

Our methodology for the design detail was to develop an ATMS strawman instrument that met all 31-channel enhancement option requirements as defined in Table 2-1. Once detailed and finalized for the 31-channel configuration, the strawman design was then modified. This occurred through a series of reductions to account for the three options that required fewer channels, namely 22 for Comparable Science, 21 for Descope Option #1, and 19 for Descope Option #2, respectively.

The Study Team used a modular design approach for the development of the strawman design. The ATMS was broken into major subsystems and each was independently developed based on stated and derived subsystem requirements. The subsystems were then integrated into a strawman ATMS system and reiterated for the final product. This design approach allowed for maximum parallel efforts; this accounted for the amount of detail the Team was able to incorporate in a 5-month study period.

Our first instrument concept was 100% redundant with the front-end antenna subsystem. It contained a single dual-winding motor and in-line optics; it was packaged in a 110-cm x 40-cm x 40-cm envelope. This iteration was used to evaluate and help the team to understand the various subsystem interdependencies. Figure 5-1 depicts this first iteration.

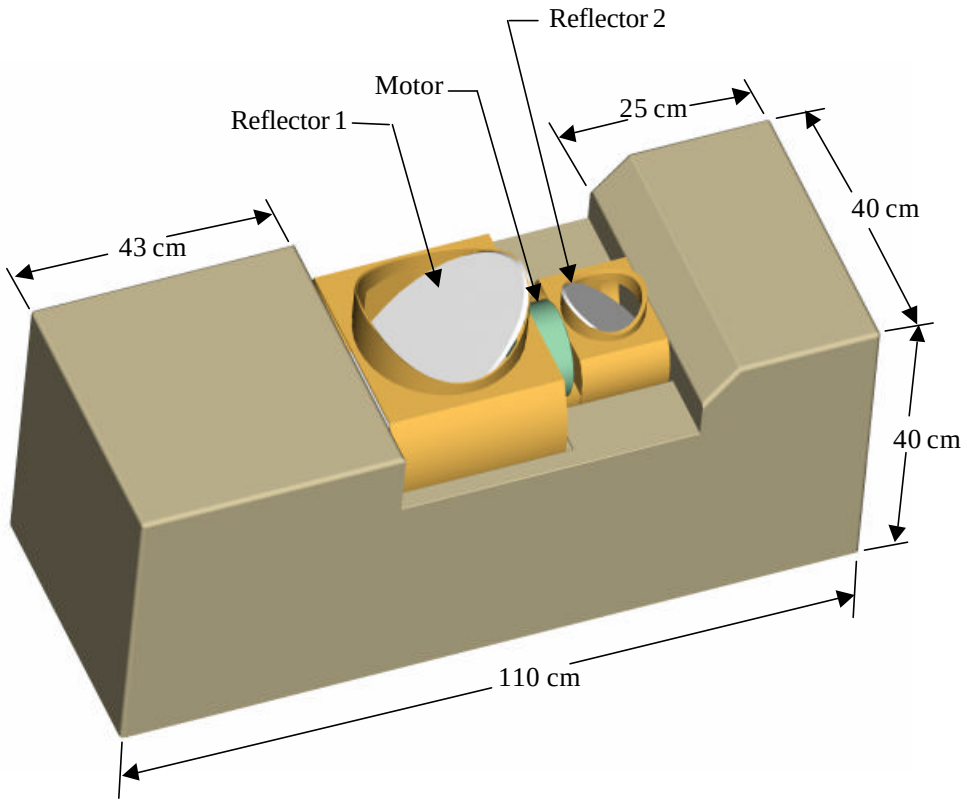

Figure 5-1 . In-Line Optics Configuration

Figure 5-2 shows our second packaging concept that used two motors positioned (offset) much like the heritage AMSU A1. This offsetting of the high-and-low frequency reflectors allowed the optics to be positioned within the 0.7-meter envelope without using folding optics. This iteration, while meeting the packaging requirements, pushed the weight and power resource requirements.

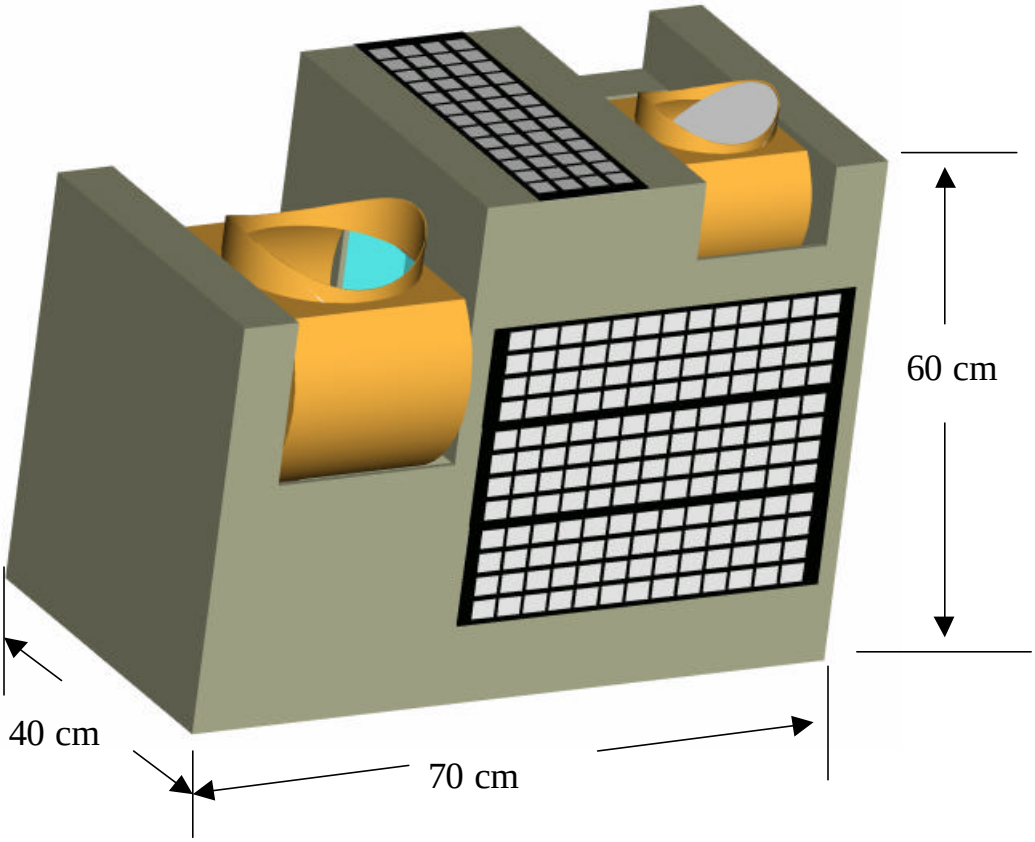

Figure 5-2. Offset Optics Configuration

Figure 5-3 is a snap shot of the final design that was weight optimized, had redundancy only as required, and used a single motor. In order to meet the required ATMS envelope constraints, the final optimal configuration also employed a folding mirror in the 23-, 32- and 50- to 59-GHz channels.

The first iteration design detail was given to the team's reliability engineer who performed a series of "what if" analyses to determine reliability and life values for various redundant configurations. With the help of the NASA scientist, channel lifetime priorities were established and through judicious use of the reliability model the new iterated design eliminated receiver redundancy needs for all receiver channels except 3 through 15. All remaining subsystems, e.g., digital electronics, motor drivers, power supplies were redundant.

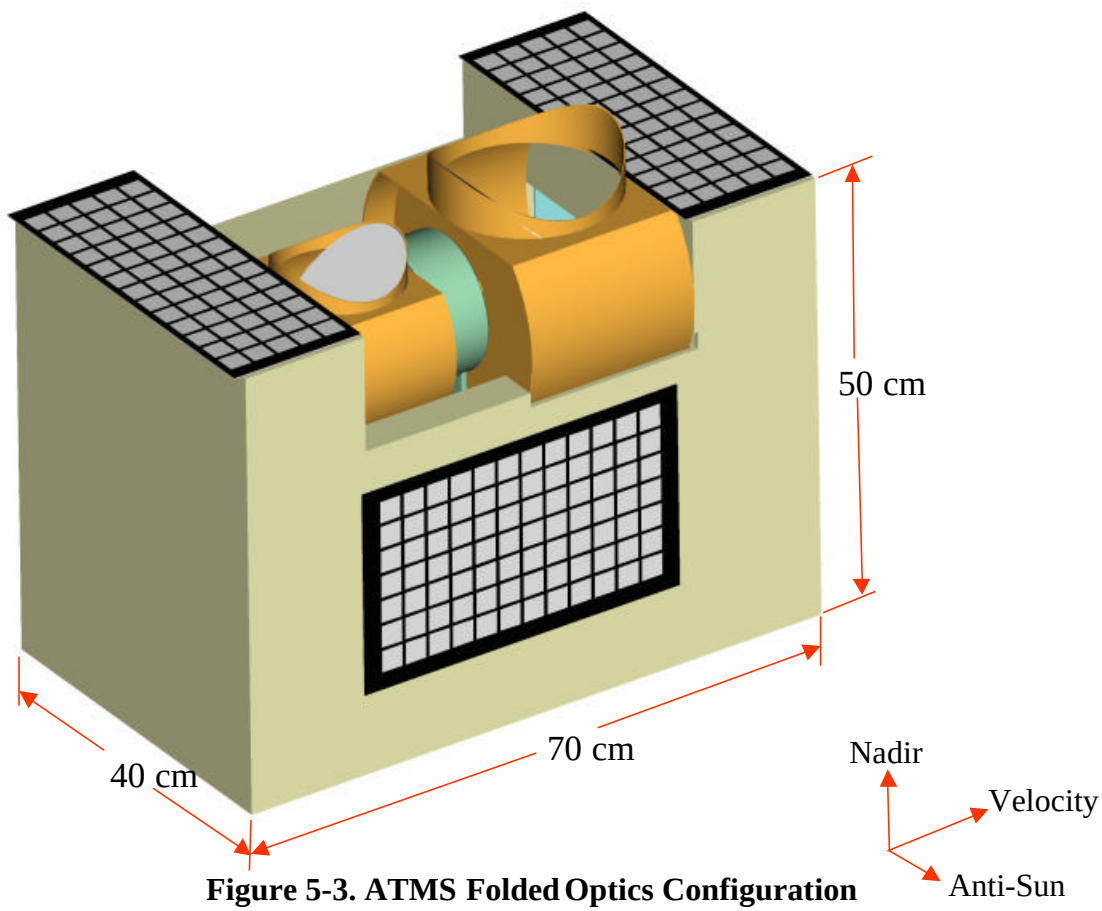

Figure 5-3. ATMS Folded Optics Configuration

The remainder of Section 5 provides the details for each subsystem design concept. They are ordered in a layout fashion that emulates the flow of the microwave through the instrument. Section 5.2 presents the three optical concepts. Section 5.3 shows the redundant and non-redundant receivers including analog amplifiers and RF detectors. Section 5.4 presents the digital electronics including analog to digital conversions, telemetry, multiplexing and motor servo controllers. Section 5.5 provides details for the power supply including schema for redundancy switch-over. Section 5.6 defines the packaging/mechanical layouts and defines how the resource database was developed. Section 5.7 presents the thermal design concept. Section 5.8 details the reliability analysis.

5.2 ANTENNA (OPTICAL) SUBSYSTEM

5.2.1 Design Requirements

The RF design requirements for the antennas are described in this section. The mechanical scanning of the antennas and the calibration loads viewed by the antennas are treated in another section of the report. The RF design of the antenna is described in subsection, 5.2.2.

5.2.1.1 Frequency Channels

The thirty-one frequency channels for the ATMS instrument are shown in Table 2-1. The bandwidths, antenna half-power beam widths, and linear polarization states for the thirty-one channels are also contained in Table 2-1. The partition of these frequency channels between the two antenna apertures is described in the Receiver Design Section 5.3.

5.2.1.2 Beam Widths

The antenna half power beam widths are shown in Table 2-1. Channels 1 and 2 have 5.2-degree beam widths while channels 3-16 have 2.2-degree beam widths. The remaining channels 17-31 have 1.1 degree beam widths. The beam widths shall not vary more than +/- 10% over the values in Table 2-1.

5.2.1.3 Polarization

All channels have either horizontal or vertical linear polarization. The polarization state for each channel is shown in Table 2-1. Vertical polarization is defined as the polarization perpendicular to the satellite ground track while horizontal polarization is defined as the satellite polarization parallel to the ground track (for the nadir-pointing beam). The polarizations are not constant with scan angle since the feed horns are fixed and the reflectors mechanically rotate. Then, as the reflector antenna moves, the polarization+ state rotates.

5.2.1.4 Beam Efficiency

The beam efficiency of the antenna shall be greater than 95% in order to ensure good radiometric sensitivity. The beam efficiency is defined as the ratio of the main lobe principal polarization energy to all of the energy (principal and cross polarization) contained in the full radiation pattern. Since the antenna patterns often do not have sharp null depths for the main beam, the null beam width is defined as 2.5 times the half-power beam width for this definition of beam efficiency.

5.2.1.5 Beam Alignment

The beam centers of all channels shall be coincident in time and space. The maximum variation of the beam widths shall not exceed +/- 0.1 degrees.

5.2.1.6 Pointing Accuracy

The pointing accuracy of the antenna beams shall be less than 0.1 of the beam width and the pointing knowledge shall be less than 0.01 of the beam widths shown in Table 2-1.

5.2.1.7 Cross Polarization

The cross polarization is not specified, but it is implied in the definition of the principal polarization beam efficiency described. A high value of beam efficiency requires low cross polarization levels.

5.2.2 Components

5.2.2.1 Offset Reflector Geometry

The concept for the development of the offset parabolic reflector is shown in Figure 5-4. The parent reflector Figure 5-4(A), is a symmetric parabola with a focal point shown at a distance F from the vertex. If a portion of the symmetric parent parabola is removed, then the offset geometry shown in Figure 5-4 (B) results. The feed horn located at the focal point F is now

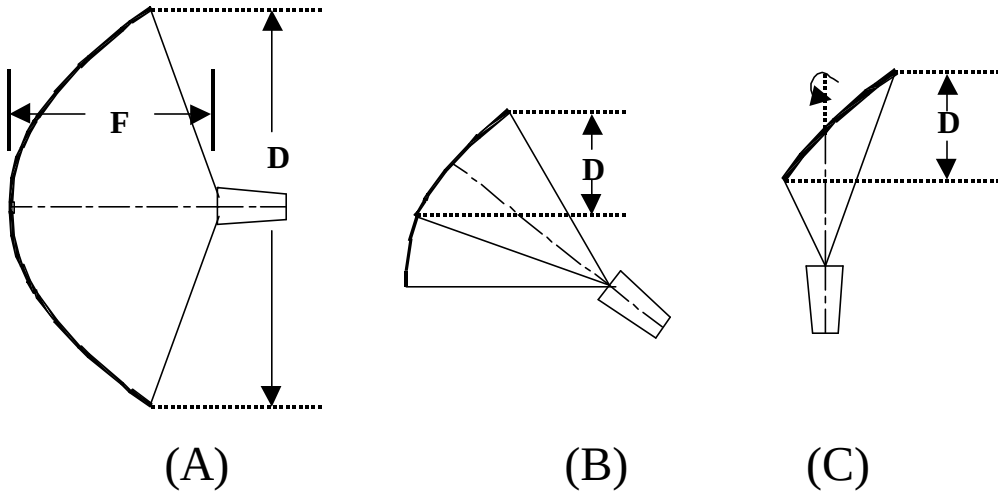

Figure 5-4. Offset Parabolic Reflector Geometry

tilted with respect to the focal line to illuminate the off set section. If the feed horn is now rotated a full 90 degrees with respect to the focal line, the compact reflector geometry of Figure 5.4 (C) results. If this reflector is now rotated about this 90-degree feed axis, with the feed horn fixed in its location, the antenna pattern of the reflector will rotate giving mechanical beam scanning. Since the feed horn polarization is fixed with respect to the rotating reflector, the electric field polarization vector will rotate with the reflector motion. This compact antenna configuration was used for the AMSU-A and –B instruments and the technique will be used for the ATMS antennas.

Figures 5.5 and 5.6 show the cross sectional views of the two ATMS antenna apertures. The projected aperture diameters are 19 and 15 cm, respectively. Nominal distance from the edge of the reflector where the parabola focuses is 15.2 cm for the 19-cm reflector and 10 cm for the 13-cm reflector. This is the exact location where the feed horn must be located. The focal length/ diameter parent ratios are the same for both apertures. The path lengths from the focal point to

the upper and lower edges of the reflector aperture are unequal as can be seen in the Figures 5-5 and 5-6. This asymmetry causes the illumination from the feed horn to be unequal at the aperture edges resulting in some asymmetry in the side-lobe structure of the reflector antenna patterns. The amplitude from the horn at the reflector edges is highly tapered (for good beam efficiency). Therefore, the asymmetry of the reflector illumination does not cause severe radiation pattern asymmetry. The reflector edge illumination is typically 15-20 dB below the reflector center region illumination. This high edge taper prevents spillover radiation around the reflector edges that would contribute to low-beam efficiency.

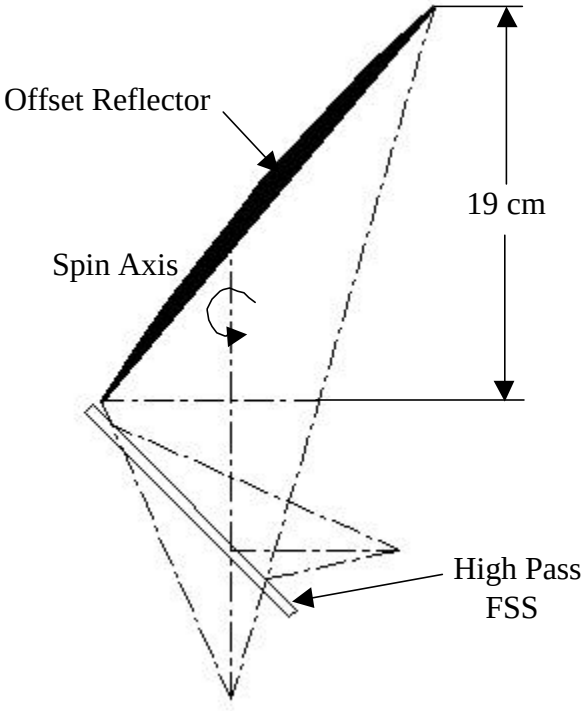

Figure 5-5. Cross Section of the 19-cm Aperture

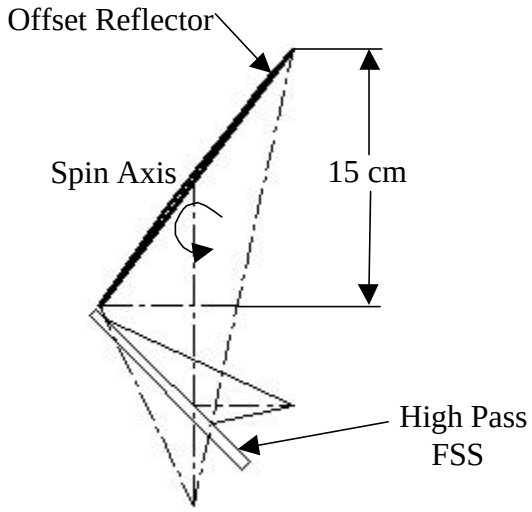

Figure 5-6. Cross Section of the 15-cm Aperture

5.2.2.2 Frequency Selective Surface

Figures 5-5 and 5-6 also show the addition of conducting diagonal flat plates. A conducting flat-plate reflector would cause the relocation of the focal point to the location shown in Figures 5-5 and 5-6. This new focal point is then 90 degrees displaced from the original focal point and energy reflected from the diagonal plate will focus to this new location. If the conducting diagonal flat plate is now replaced with a surface that is sensitive to frequency, a Frequency Selective Surface (FSS) can be implemented that will allow the use of both foci. This is dependent upon the frequencies that are transmitted through the plate and the frequencies reflected by the plate. There are two basic types of FSSs: the high- and the low-pass filters. The definition is self explanatory, i.e., high frequencies pass through the plate and low frequencies are reflected off the plate for the high-pass FSS. One implementation of a high-pass filter is a

conducting plate with circular holes as illustrated in the Figure. 5-7. This array of circular holes can be considered as circular wave-guides, which reflect energy that is below the wave-guide cutoff frequency of the holes and pass frequencies that are above the wave-guide cutoff frequency. The lowest mode that will propagate through the circular wave-guides is related to the diameter of the holes by the expression for the cutoff wavelength of the circular wave-guide.

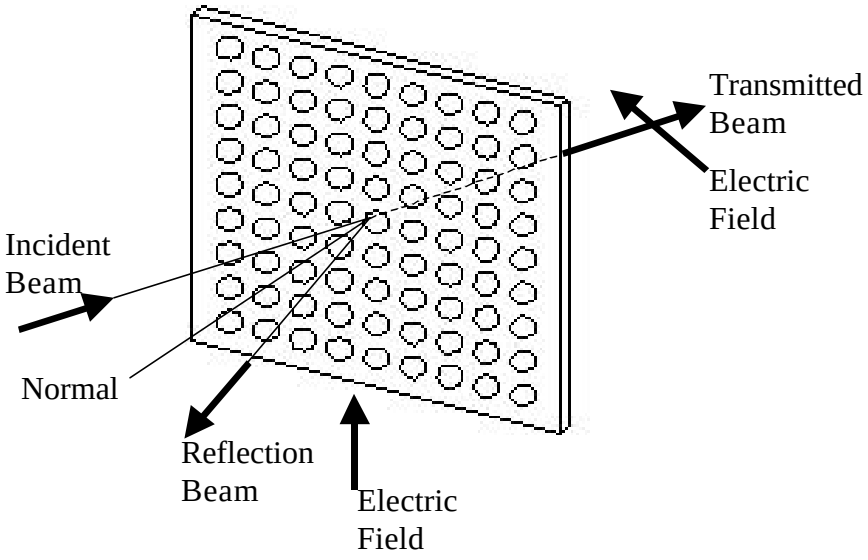

Figure 5-7. FSS Frequency Splitter

5.2.2.3 Surface Accuracy

The surface accuracy of the reflector antenna can be related to the loss of RF energy due to scattering by the surface roughness. The loss is important for radiometric applications where the energy scattering due to surface roughness contributes to the noise temperature and the sensitivity of the system. The highest frequency channel of the ATMS instrument determines the surface accuracy requirement of the 12.7-cm diameter reflector. Radiometric applications require rms surface accuracy of $1/100^{th}$ of the wavelength at the highest frequency (183.3-GHz channel). Similarly, for the 19-cm reflector, the surface accuracy requirement would be $1/100^{th}$ of the 57-GHz channel.

5.2.2.4 Constant Beam Width Radiation Patterns

The requirement for constant half-power beam width for all of the frequency channels is presented here. For a given fixed-aperture size and an operating frequency bandwidth, the radiation pattern beam width will normally narrow as the frequency is increased. This pattern narrowing with increasing frequency results from the relationship between the aperture diameter, the operating frequency and the radiation pattern beam width. If the ratio of the aperture diameter to the wavelength is fixed over the operating bandwidth, then a constant beam width radiation

pattern will result. A requirement for constant beam width over frequency then requires the effective aperture distribution to reduce as the frequency is increased. The parabolic reflector illumination from the horn feed must then satisfy a condition: the illumination taper over the aperture must result in a reduced illumination diameter as the frequency is increased so that the ratio of aperture effective diameter to the wavelength is fixed. The design of the feed horns is driven by this requirement to achieve constant beam widths of 5.2, 2.2, and 1.1 degrees over the frequency channels of ATMS as shown in Table 5-1. Four feed horn antennas are used in the design to satisfy the requirements for constant multiple beam widths. Table 5-1 gives the frequency channel assignments for each feed horn antenna. Table 5-1 shows that the RF bandwidths of the feed horns 1 and 3 are greater than 20%, while the RF bandwidths of horns 2 and 4 are 15%.

5.2.2.5 Horn Antenna Feeds

As discussed in the preceding subsection 5.2.2.4, the aperture illumination from the feed horn must change as frequency is increased in order to satisfy the constant beam width requirement. The feed horn must then illuminate a smaller portion of the parabolic aperture as frequency is increased to satisfy the requirement that the ratio of the aperture diameter to the wavelength is a constant over the operating bandwidth. The requirement on the feed horn radiation pattern is then to narrow its beam width in a fixed proportion with frequency to give a constant beam width from the reflector over the channel bandwidths. The illumination taper of the parabolic reflector from the feed horn is -20 dB at the upper and lower edges of the reflector geometry illustrated in Figure 5-4 (C).

The corrugated feed horn is used as a feed for offset parabolic antennas, because it has the properties of symmetric principal polarization beams, low cross polarization levels, and broad impedance and radiation pattern bandwidth. The four feed horns for the two apertures have bandwidths given by Table 5-1. Feed horns 1 and 2 are in the 12.7-cm aperture and feed horns 3 and 4 are in the 19-cm aperture. Horn 1 covers Channels 1 and 2, while horn 2 covers Channels 3 through 15. Feed horn 3 covers Channels 16 and 23-31, while feed horn 4 covers Channels 17-22. These feed horn designs also have the requirement for the generation of constant half-power beam widths from the parabola over all frequency channels listed in Table 2-1.

Table 5-1. Feed Horn Bandwidths

Horn	Lower Frequency	Center Frequency	Upper Frequency	% Bandwidth	Polarization
NO. (CHAN)	GHz	GHz	GHz		
1 (CHI 1-2)	23.67	27.578	31.49	28.37	QV
2 (CHI 3-15)	50.21	54.4	58.59	15.4	QH
3 CHI 16, 23-31	88	103.88	119.75	30.57	QV
4 (CHI 17-22)	164.31	177.81	191.31	15.18	QH

5.2.2.6 Reflector to Feed Horn Locations.

Figures 5-8 and 5-9 present the optical designs for the low- and high-frequency reflectors. Dimensions are presented to locate each component for nominal focus. Figure 5-9 presents the 12- to 31-GHz and 50- to 58-GHz feed horns and their required positions relative to the 19-cm low-frequency reflector's focus location. A high-pass FSS is used to separate the two frequency channels.

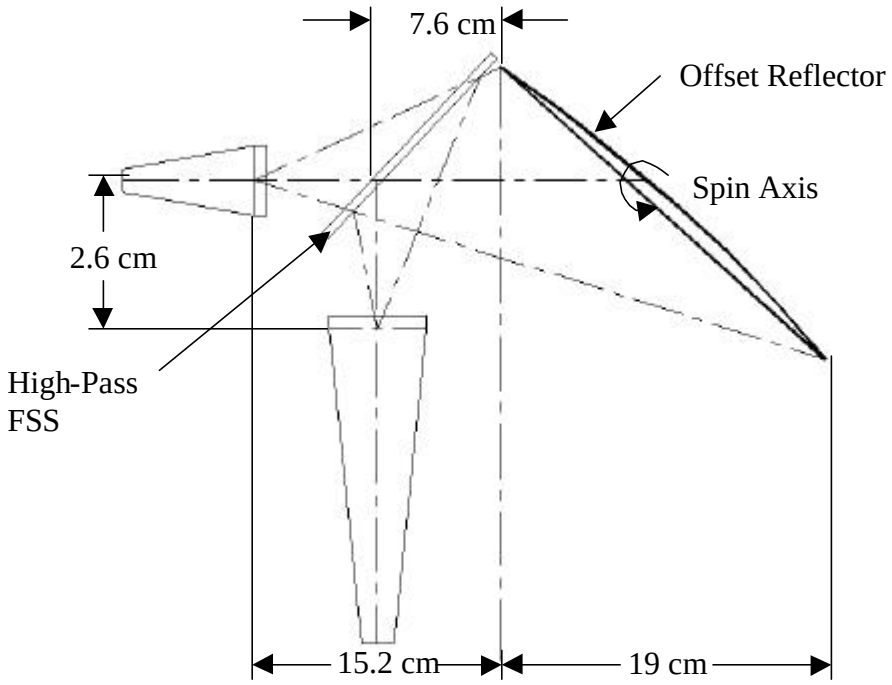

Figure 5-8. Cross Section of the Low-Frequency Reflector

Figure 5-9 presents the 160- to 183-GHz and 88- to 119-GHz feed horns and their required positions relative to the 12.7-cm high-frequency reflector's focus location. A high-pass FSS is used to separate the two frequency channels.

5.2.3 DESIGN DESCRIPTION

5.2.3.1 In-Line Optics

Figure 5-10 depicts the inline optics orientation that was developed as part of the first strawman iteration. It features a common motor on which both the high- and low-frequency reflector rotate in unison. The overall length of this configuration is 78 cm compared to a requirement of 70 cm . Component locations relative to each other were in accordance with the requirements of Figures 5-8 and 5-9. While this design exceeded the required envelope, it was useful for understanding component placement sensitivities.

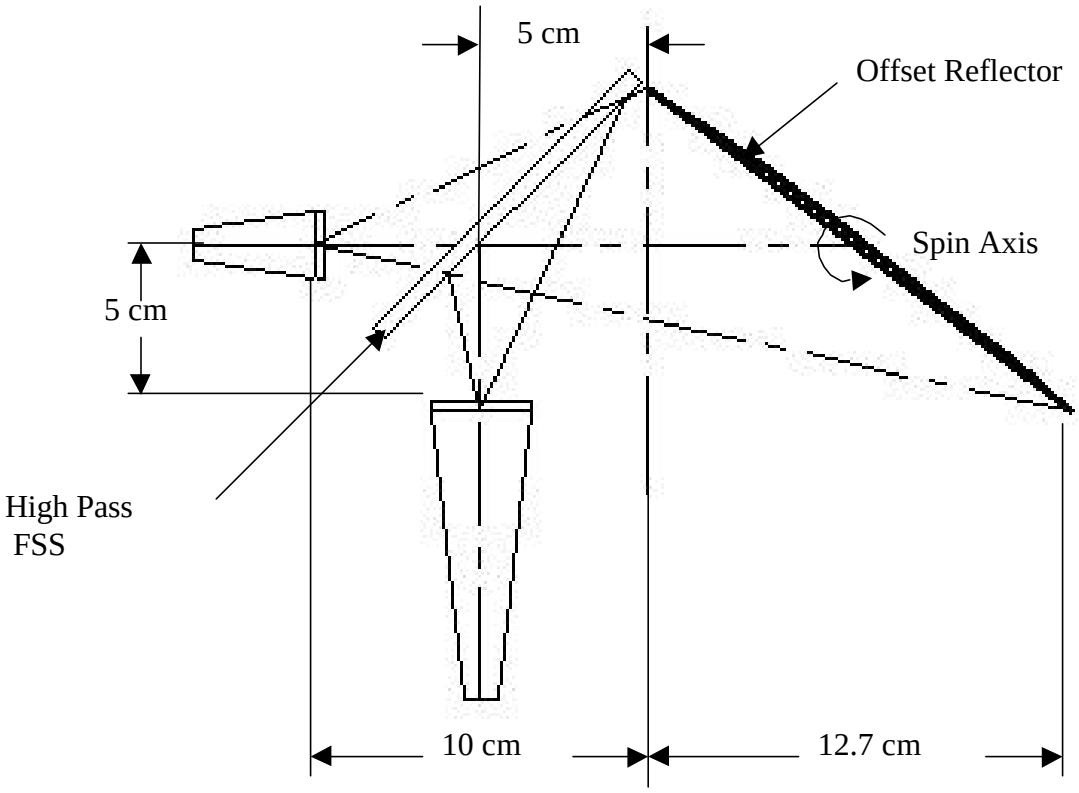

Figure 5-9. Cross Section of the High-Frequency Reflector

The 19-cm diameter aperture, which is shown in the left portion of the Figure 5-10, consists of an offset section of a primary parabolic reflector, a frequency-selective surface secondary mirror, and two corrugated feed horns. The 19-cm aperture accommodates frequencies from 23.8 to 57.3 GHz, Channels 1-15. The 12.7-cm diameter aperture shown on the right side of Figure 5-11 consists of an offset parabolic reflector, a frequency-selective secondary mirror, and two corrugated feed horn antennas. This 12.7-cm aperture accommodates frequencies from 89 GHz to 183.3 GHz, Channels 16-31. The frequency-selective surfaces allow frequency filtering in both apertures so that the 31 channels are partitioned between the four feed horns. The frequency channels assigned to each of the four horns are shown in Table 5-1. The percent bandwidth required for each horn is also shown in the Table 5-1. The greatest RF bandwidths are for horns 1 and 3. The center frequencies for the horns shown in Table 5-1 are used for the required pass-bands of the individual horns and are not ATMS frequency channels. Horns 1 and 3 are vertical polarization while horns 2 and 4 are horizontal polarization. Horns 1 and 2 are in the 19-cm aperture and horns 3 and 4 are in the 5-inch aperture.

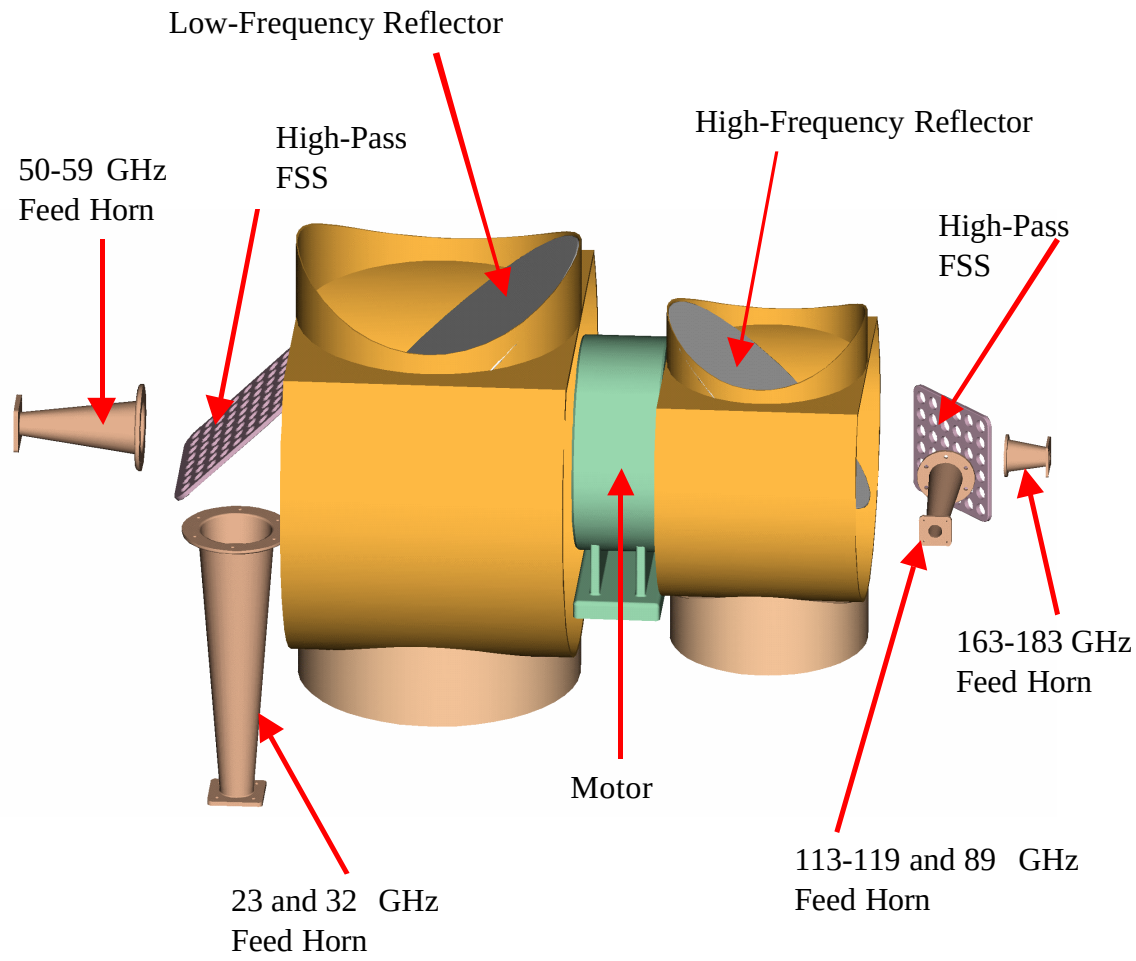

Figure 5-10. In-Line Optics Design

5.2.3.2 Offset Optics

Figure 5-11 shows the second strawman design iteration that offsets the high- and low-frequency optics relative to each other. In this iteration, the low-frequency feed horn/receiver shelf is out of plane with the high-frequency feed horn/receiver shelf. This arrangement of the optics, which is very similar to that used in the heritage AMSU-A1 design, allows the optics to be housed within the 0.7m envelope requirement. This concept requires an individual motor for each rotating reflector.

Component placement and frequency parameters for the high 12.7-cm and low 19-cm optics are identical to that as used in the inline design. The use of two motors pushes the overall power budget and complicates the scanner electronics because of the synchronization needs.

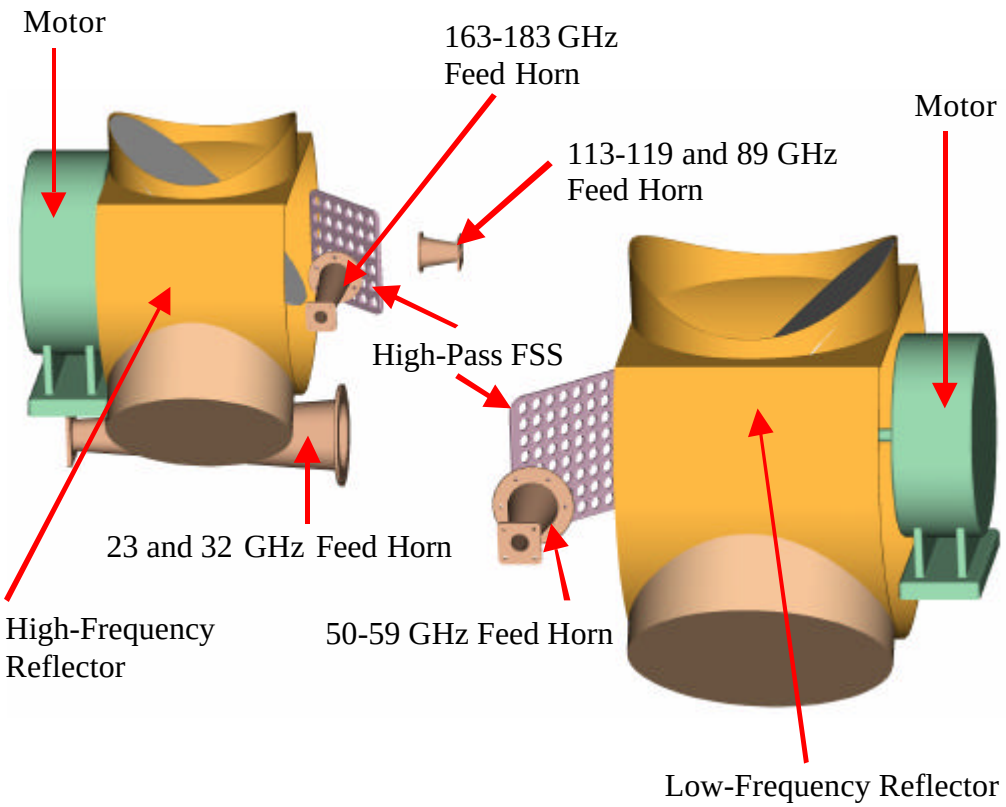

Figure 5-11. Offset Optics Design

5.2.3.3 Folded Optics

The final compact iteration, see Figure 5-12, was identical to the inline design except a tertiary folding mirror was added to fold the focal length of the 19-cm reflector. This configuration again permitted the antennas that consist of two reflector apertures to be driven by a common-shaft drive motor. This single-drive-motor concept, met the ATMS packaging requirements. The use of a folding mirror to compact the packaging is analogous to the design used in the heritage AMSU-A2 instruments.

5.2.4 Trade Options Considered

The trade options considered included the use of a curved secondary mirror to replace the flat-plate frequency-selective-surfaces. Wire grid polarizers to replace the frequency-selective-surfaces were also considered. Both approaches are described in subsections 5.2.4.2.

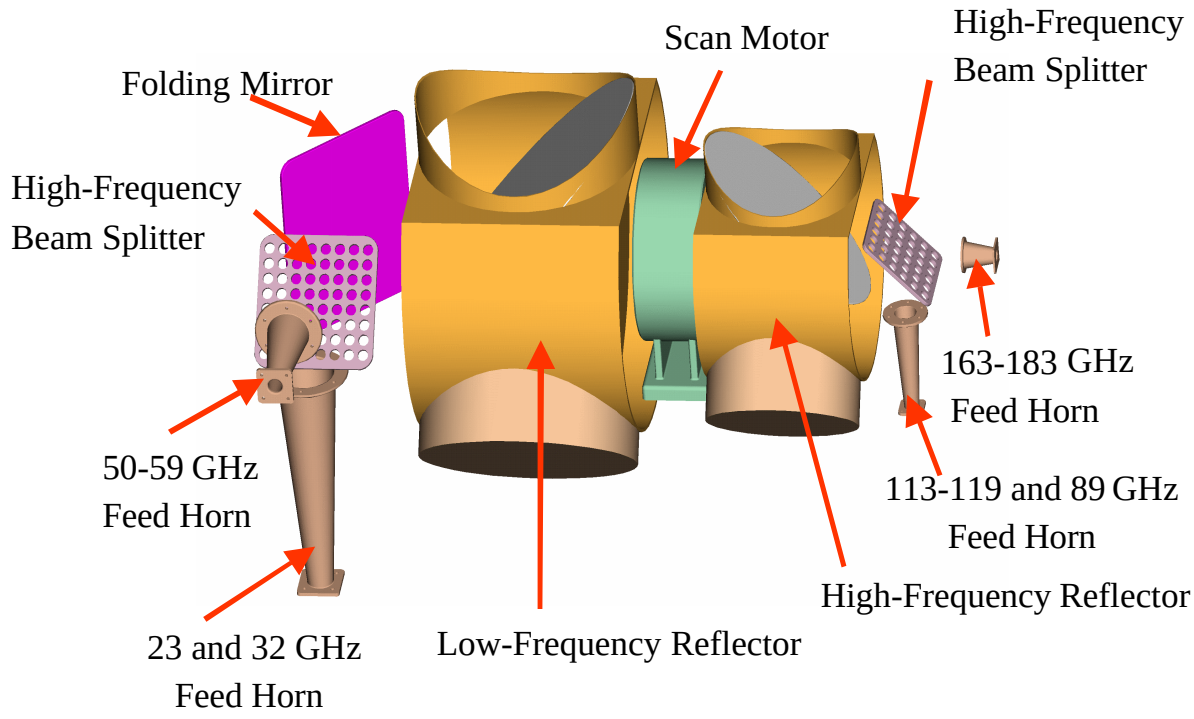

Figure 5-12. Folded Optics Design

5.2.4.1 Secondary Mirror

Hyperbolic mirrors may replace the flat-plate secondary reflectors. The hyperbolic reflectors would be frequency-selective-surfaces also, but the angle of incidence could be reduced from the flat-plate case. This would allow improved performance of the surface for both transmission and reflection bandwidths of the illumination from the two feed horns.

5.2.4.2 Wire Grids

The use of wire grid polarizers to replace the frequency-selective-surfaces was a tradeoff consideration. Table 5-1 shows that the polarization of Channels 1 and 2 are vertically polarized while channels 3-16 are horizontally polarized. Horn 1 could then be vertically polarized and horn 2 could be horizontally polarized. A linearly polarized grid could then replace the frequency-selective-surface in the 19-cm aperture. The grid would consist of parallel wires aligned to pass the perpendicular polarization and reflect the polarization parallel to the wires. A wire grid implementation for channel separation is shown in Figure 5-13. This figure shows the polarization of Channels 1 and 2 passing through the grid perpendicular to the wires while Channels 3-16 are reflected by the grid. A similar arrangement would apply to a wire grid polarizer for horns 3 and 4 in the other aperture. The wire grid polarizers can be designed for good performance with insertion losses for the transmission of 0.2 dB or less. The technology is well developed and much information is available for the polarizer performance versus bandwidth and angle of incidence.

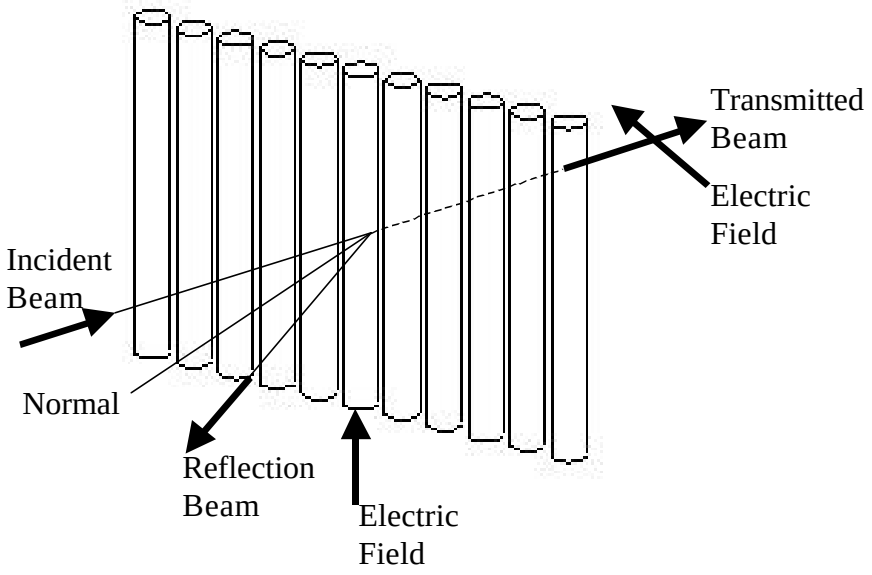

Figure 5-13. Wire Grid Polarizer

5.2.5 Effects Of Baseline And Descope Options

The enhanced instrument has been described in the previous sections. If the 118-GHz channels are removed, then the baseline system that is equivalent to the AMSU-A will result. The changes for the baseline system would be a reduced bandwidth for corrugated horn 3, which contains the 118-GHz channels.

If the ATMS is descoped further to Descope Option #1 so that 89-GHz channel is removed, then the design would eliminate feed horn 3 altogether leaving only feed horn 4 in the 5-inch aperture. This descope option would result in a much simpler design for the 5-inch aperture antenna with no frequency selective sub-reflector.

If the instrument is descoped further to Descope Option #2, so that only the 50- and 183- GHz channels remain, then one of the two apertures could be eliminated completely. A single aperture with the 183-GHz channels and the 50-GHz channels would comprise the full descope design.

5.2.6 Performance Characterization, Error Budget, and Modeling

The performance characterization is based upon geometrical designs for the aperture layouts. Diffraction programs would be required as a second step in the design procedure to determine the radiation patterns of the reflectors and the corrugated feed horn patterns. Beam efficiency could be determined from numerical integration of the patterns. The fundamental designs are based upon formulas for half-power beam widths, and Gaussian optics formulas for the designs. These formulas provide sound design information for the preliminary antenna design.

5.2.7 Issues and Risks

The bandwidths of the horn antennas and the requirement for constant fixed-pattern beam widths over all of the frequency channels are difficult design problems. The use of frequency-selective-surfaces for the secondary reflectors also has to be investigated for the flatness of the frequency pass-bands of the surfaces for the large surface incidence angles.

5.2.8 Summary

The ATMS strawman optical layout challenge was driven by the requirement to fit it within a 70-cm envelope. Two separate configurations were developed that met this requirement. The offset optics oriented the high- and low-frequency reflectors out-of-plane with each other, so that the low-frequency feed horn would was nested beneath the high-frequency reflector. This concept required two antenna reflector drive motors. The second concept used a folding mirror to fold the low-frequency reflector image, similar to the heritage AMSU-A2 design. This configuration used a single drive motor with a common shaft to rotate both antennas simultaneously.

5.3 RECEIVERS

5.3.1 Design Description

Based on our initial trades and the availability of Low Noise Amplifiers (LNAs), LNA technology was used throughout. Feed horn and channel splitting was iterated with the antenna design until optimum channel/feed horn pairing was accomplished. Other arrangements of feed horns and channels may be possible, but the one depicted in this section was selected for our strawman design to study packaging feasibility and costing.

The designs shown are notional for several of the receivers. Local Oscillator (LO) frequencies need to be selected consistent with filter implementation needs to prevent spurious responses and noise from the unwanted side bands. Possible sharing of LOs between receivers may be possible, e.g., for Channel 16 and Channels 17-22. Issues of gain stability were not addressed but need to be consistent with the calibration requirements of a total power radiometer.

Subsections 5.3.2, 5.3.3, and 5.3.4 discuss the final RF receiver design after reliability was assessed (see Section 5.8) and unnecessary redundancy was eliminated. Subsection 5.3.5 discusses the availability of components that are used in the RF receiver. Subsection 5.3.6 presents the impacts of implementing the options. Subsection 5.3.7 provides a summary of the receiver design as compared to the heritage AMSUs receivers.

5.3.2 Receiver Configurations for ATMS Channels 1 and 2

Our technology assessment showed that low-noise, high-gain GaAs amplifiers operating in the 20-to 32-GHz frequency range are readily available as “off-the-shelf” flight-proven components. Their availability warranted that the Channel 1 and 2 receiver designs use direct detection for signal rectification. Direct detection simplified the Channel 1 and 2 receivers, because the local oscillators and two mixers were no longer required and, therefore, were eliminated.

Figure 5-14 shows our first iteration direct detection implementation for ATMS Channels 1 and 2. Because low-noise amplifiers (LNAs) are extremely broadband, channel separation, via a power splitter, was accomplished after the LNA. Separating the channels before the LNA would have introduced a loss that would increase the noise temperature. This design requires the 23.8-GHz channel to have a 1% bandwidth filter and the 31.4-GHz channel to have a 0.6% bandwidth. These are narrow but feasible. Suitable square law devices are available for detectors.

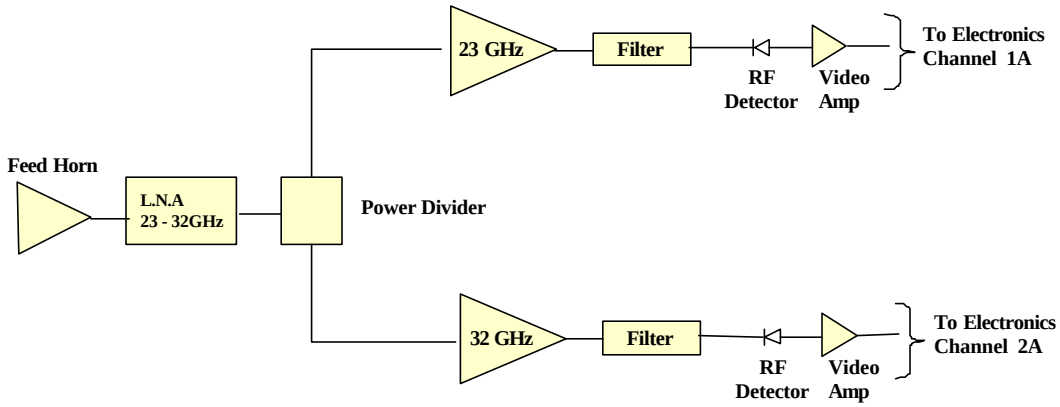

Figure 5-14. First Iteration Channels 1 and 2 Receiver Schematic

An alternate front-end configuration is shown in Figure 5-15. A low-loss frequency diplexer similar to that used in the AMSU-A2 is used to split the feed horn output to an LNA for each channel. This removes the LNA as a single-point failure between the two channels and reduces the LNA percentage bandwidth required from 28% to about 1%; this may allow equal or improved noise performance. Such a design is also less susceptible to Radio Frequency Interference (RFI) from out-of-band signals since the LNA bandwidth is reduced from ~7.8 GHz to ~200 mhz.

Power frequency splitters (frequency multiplexers) could be used in the implementation shown in Figure 5-14.

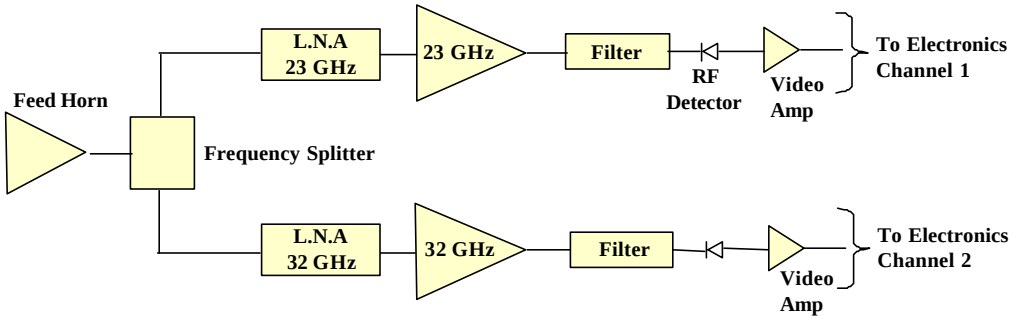

Figure 5-15. RF Receiver Schematic for Channels 1 and 2 with Frequency Splitter

5.3.3 Receiver Configuration for ATMS Channels 3-15

Figure 5-16 shows the first iteration for the Channel 3-15 receivers. This time, as a result of the available technology, off-the-shelf wide-band InP LNAs are implemented. Redundancy switching of the local oscillator might be implemented by a switch, as shown, or with a power divider. The latter approach requires slightly more RF power from the LO source.

The advantage of this configuration compared to similar heritage channels in the AMSU-A instrument was the elimination of nine mixer/IF amplifier front ends and their corresponding local oscillators with corresponding savings in volume, weight, and power. This design requires a more complicated IF section, while still allowing net savings.

This receiver design employs Single Side Band (SSB) down conversion of 13 channels compared to the Double Side Band (DSB) down conversion of single channels in the heritage AMSU-A receivers. The DSB operation of the heritage AMSU-A required folding of the two side bands into one IF band using half the available pre-detection bandwidth. The ATMS design allows use of the full channel bandwidth for the predilection filter. Therefore, no noise degradation occurred with respect to the DSB that was part of the heritage AMSU-A design.

Using the LNA for the first stage in place of the mixer/IF amplifiers has two significant advantages. First, the LNA sets the system noise temperature and, thus, creates better results than mixer/IF amplifier front-ends can provide. Second, eliminating several local oscillators reduces the receiver volume, weight, and power.

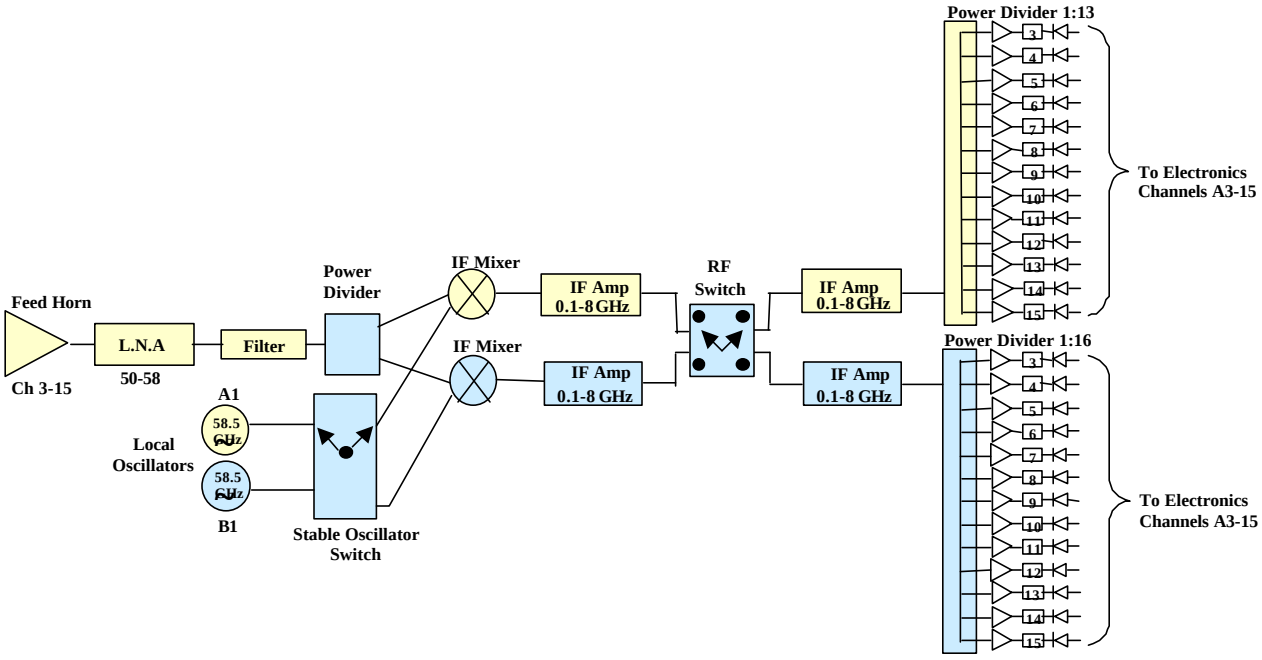

Figure 5-16. ATMS RF Receiver Schematics for Channels 3-15

5.3.4 Receiver Configuration for ATMS Channels 16, 17-22, and 23-31

Feed horn bandwidth requirements suggested the arrangement of channels shown in Figure 5-17. Channels 16 and 23-31 share one feed horn and Channels 17-22 share a second.

For Channels 16 and 23-31, the output of the feed horn might be split with a frequency diplexer. For Channel 16, adequate channel bandwidth and noise temperature is available to meet NEΔT requirements by any of several approaches. Channel 16 could be implemented by a DSB mixer/IF amplifier, direct detection, or by an LNA followed by an appropriate mixer/local oscillator, filter, and detector. Cost and component performance will determine the choice.

Channels 23-31 can be implemented in a manner similar to Channels 3-15 with the mixer LO on either the high or low side consistent with filter realization requirements to eliminate noise contributions from the unwanted side band. Opportunities may exist in the ATMS to share a given local oscillator frequency in more than one receiver to reduce cost and provide opportunities for fault tolerance or redundancy.

Channels 17-22 might use an LNA front-end; however, the survey showed that LNA technology for this band is currently in preliminary development. This technology may not be mature and available by the year 2001 in order to be base-lined for the ATMS. It is likely that ATMS may have to rely on a high-performance second harmonic mixer as a receiver front-end for these channels. Appendix A discusses mixer technology employing planar gas diodes and second harmonic mixing to simplify local oscillator design.

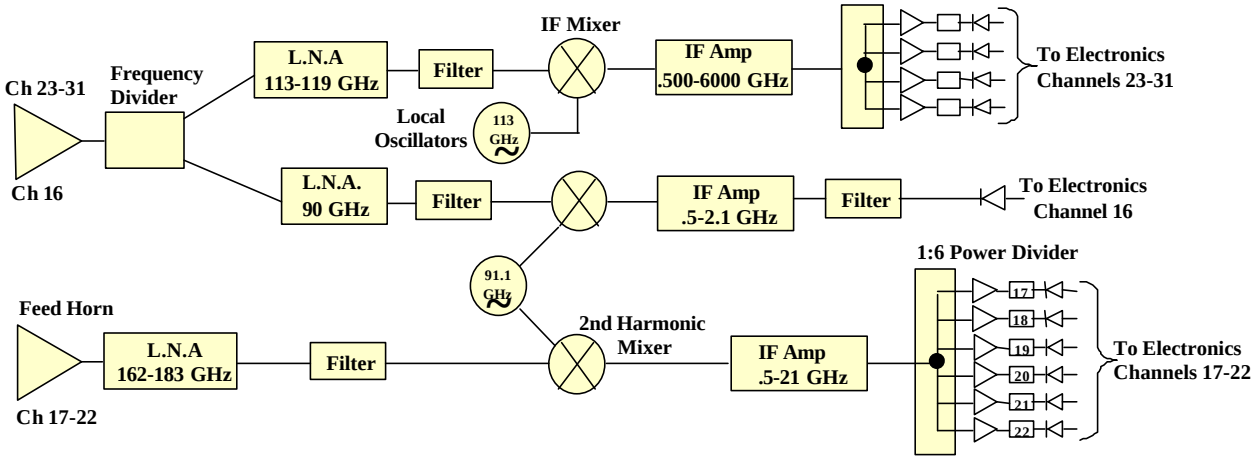

Figure 5-17. ATMS RF Receiver Schematics for Channels 16, 17-22, and 23-31

5.3.5 Component Availability

This subsection summarizes the availability of critical components in the receiver at the time of the ATMS study strawman design. Although a highly redundant version of the receivers was investigated, making the LNAs redundant with switches and their impact on reliability and noise performance appears unproductive at this time. Figure 5-18 shows component availability for Channels 1 and 2. In the Figures 5-18 through 5-20, a color code is used to summarize status:

Green = available
Yellow = has been available from select vendors
Red = selective vendors have the capability to develop as custom components

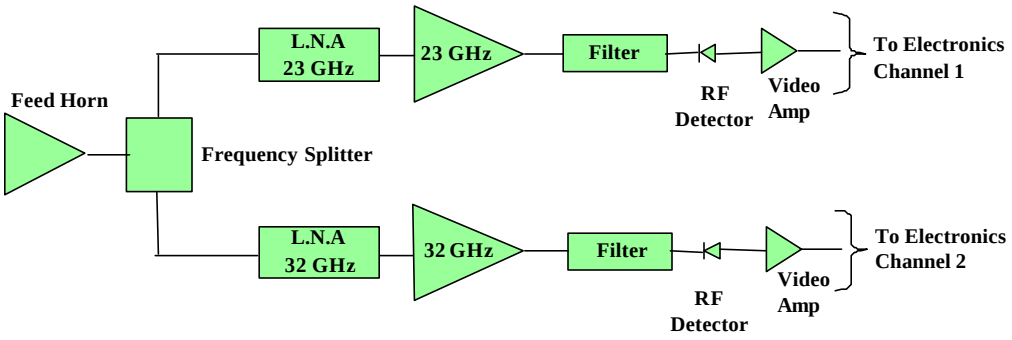

Figure 5-18. ATMS Component Availability for Channels 1 and 2

Figure 5-19 shows component status for Channels 3-15. The design shown is notional for the Channel 3-15 receiver. LO frequencies need to be selected consistent with filter implementation needs and possible sharing of LOs between receivers. Channels 3-15 use readily available component technology except the 0.1-8-GHz IF amplifiers that may be difficult to obtain. (A change in the LO frequency would alleviate this problem.)

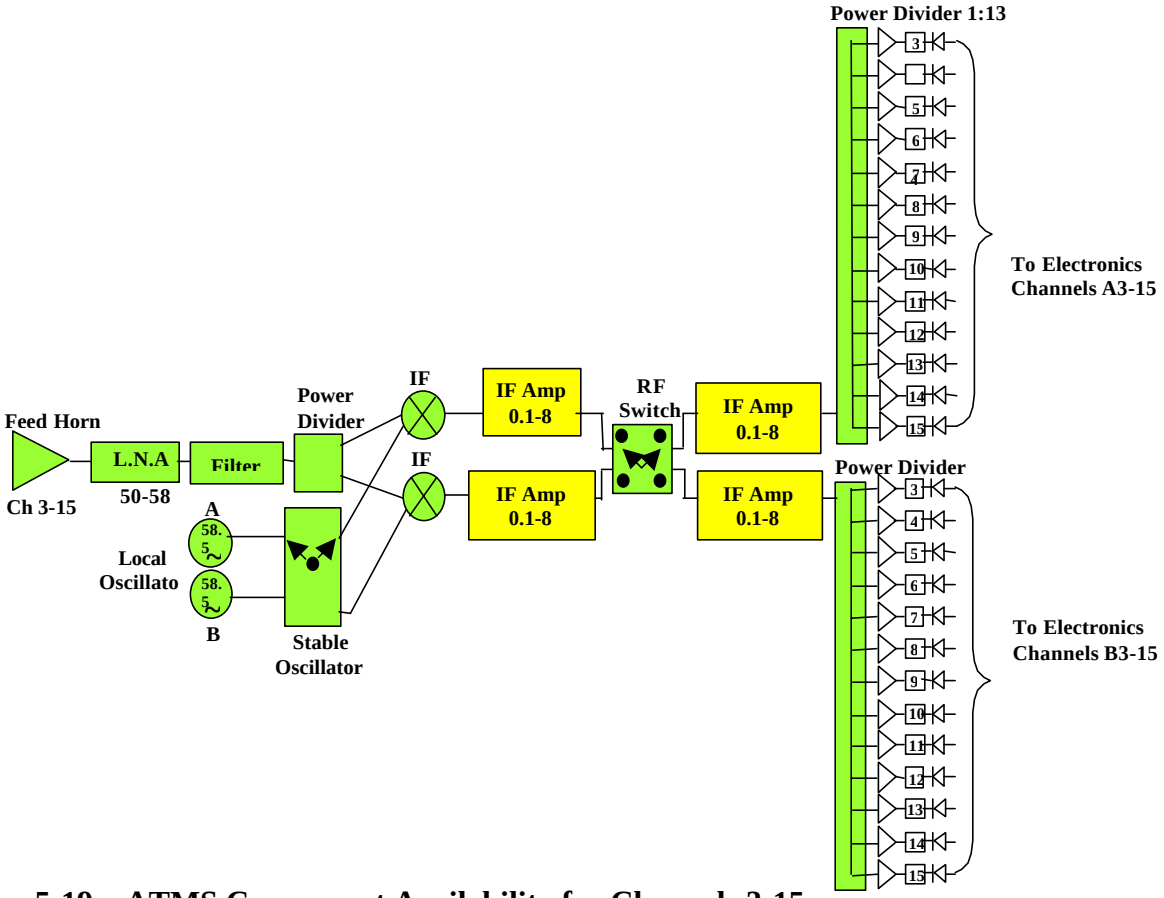

Figure 5-19. ATMS Component Availability for Channels 3-15

5.3.6 Options

Figure 5-20 shows the status of components for Channels 16-31. Within the Channels 16-31 receiver, the feed horn, frequency divider, 113- to 119-GHz LNA, and 162- to 183- GHz LNA are all custom components with the 162-183 LNA yet in preliminary development. The 89-GHz LNA is available from more than one vendor but is still a custom component at this time. The remaining components in these channels are readily available.

Because the ATMS strawman design was based on the 31-channel enhanced instrument option receiver, configurations for the remaining three options were accomplished by deleting all non-shared components that were integral with the deleted channels. Shared components that remained were simplified, because they no longer served dual purposes.

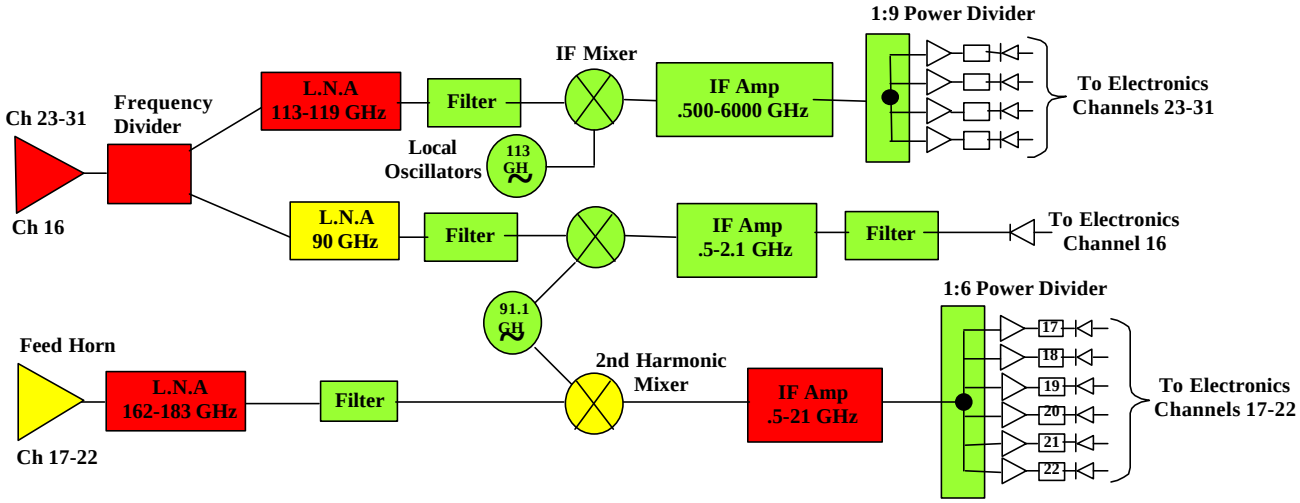

Figure 5-20. ATMS Component Availability for Channels 16, 17-22, and 23-31

5.3.7 Summary

The final ATMS strawman design was similar to the heritage AMSU instruments in that the receiver channel separation originated largely in the antenna/optics. Channel polarization requirements have considered multiplexing using wire grid polarizers for design simplicity. Unlike the heritage instruments, LNAs appear feasible for setting the system noise temperature up through the 118-GHz band and providing equivalent or better performance. Without redundancy, this design used only three oscillator types compared to 13 required in the heritage AMSU instruments. This resulted in greater reliability, considerable volume, and power savings.

5.4 Digital Electronics

5.4.1 Overview

The ATMS instrument digital electronics acquires and processes science data from the 31-channel radiometer system. The electronics formats the data and delivers the data to the

spacecraft (S/C) interface using a dual redundant MIL-STD-1553 interface. Additionally, the electronics controls and synchronizes data collection and antenna mirror motion with a time mark supplied over the MIL-STD-1553 interface. Figure 5-21 provides a block diagram of the overall digital electronics architecture. The electronics monitors the high-accuracy temperature sensors that are used to calibrate the radiometer. The design drivers established at the beginning of the study included minimizing the electronic size, mass, power, and cost. State-of-the-art flight components and electronic fabrication processes are baselined for the digital electronics. Components and designs used in this study support long ground storage and 7-10 years of on-orbit operation. The digital electronics concept is contained in a single enclosure measuring 20 cm x 20 cm x 5 cm. The total mass of the electronics was estimated to be about 0.5 kg. The size and mass for a brushless motor driver are estimated at 10 cm x 10 cm x 5 cm and 0.25 kg, respectively. The estimates are based on the NASA/Goddard Space Flight Center (GSFC) in-house SMEX reaction wheel driver electronics. In all cases, parametric requirements comparisons were made between circuits meeting the general requirements; detailed designs were not executed.

The implementation selected incorporated:

- MIL-STD-1553 interface based on the UTMC SUMMIT chip.
- UTMC 16-bit micro-Controller ram and Harris ROM.
- Redundant analog input system for platinum wire resistors with 50 inputs each.
- Redundant housekeeping analog inputs 16 channels each.
- Redundant analog input system with inputs for 31 radiometer channels each.
- Tachometer and angle sensor input electronic for the antenna platform.
- Optional digital interface for digitally processed channels

The parts list and practices of in-house GSFC projects were reviewed and specific implementations were baselined to allow size, mass, and power to be determined. The missions included the GSFC in-house SMEX and the MIDEX MAP. The baseline design incorporated high-density QFP, LCC, surface mount components, and Field Programmable Gate Array (FPGA) devices to reduce size and mass. Aluminum heat sinks were used for mechanical and thermal reasons. Each heat sink has two PWB assemblies attached with a thermally conductive adhesive. The ACTEL Company 14100A FPGA was used as a baseline for costing and sizing purposes.

5.4.2 Spacecraft Interface

The MIL-STD-1553 for this study was based on a SUMMIT MIL-STD-1553 bus chip, two transformers, and two shared memory SRAM chips. The SUMMIT chip also requires two initialization ROM chips, which were assumed to be part of the micro-controller interface. The micro-controller baselines a UTMC 16- Million-Instructions-Per-Second (MIPS) micro-controller with two EEPROM chips and two SRAM chips. The micro-controller interfaces to the MIL-STS-1553, PRT electronics A and B, science processing unit A and B, and the motor control unit. Each of these interfaces is via a FPGA bus-type interface.

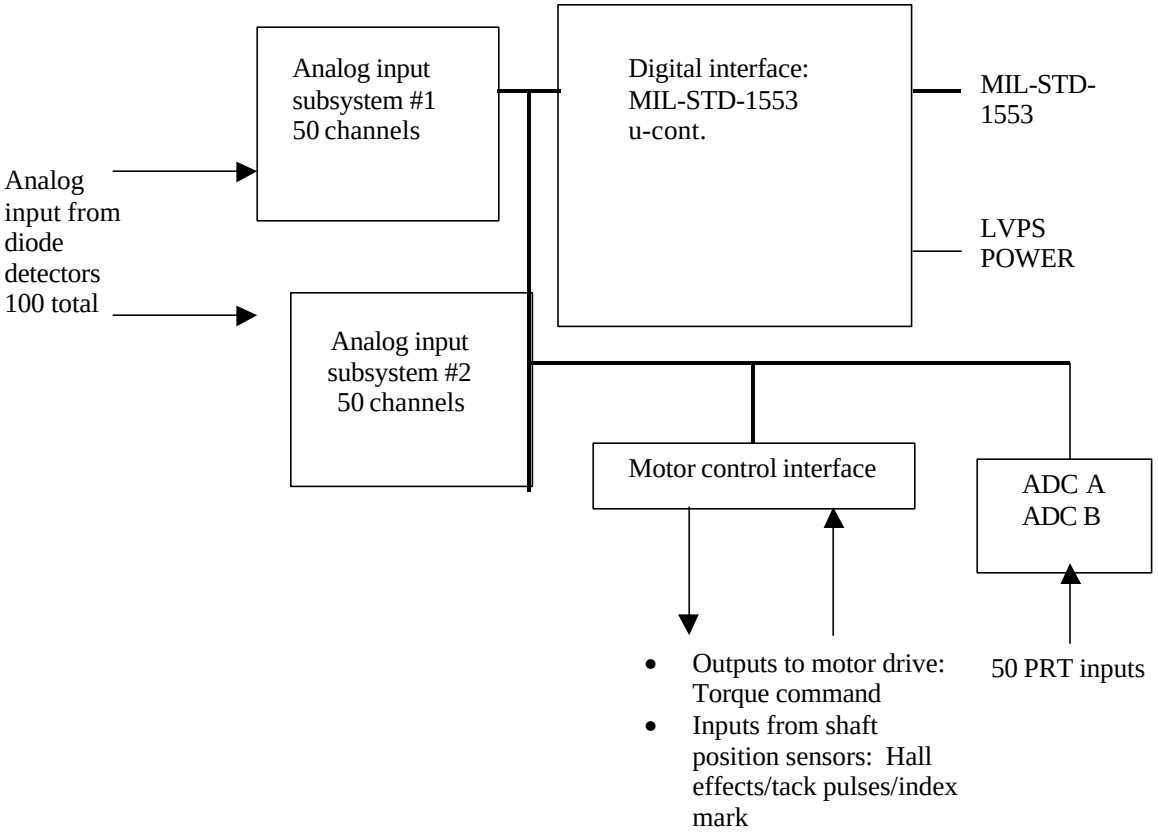

Figure 5-21. Digital Electronics for ATMS

All of the chips in this design are available in high-reliability versions with the exception of the monolithic 16-bit Analog-to-Digital Converter (ADC). The 16-bit ADC will require special radiation testing and screening. It was assumed that standard high-reliability FPGAs would be used for this instrument. These parts may require lot level radiation testing. Further, a shielding analysis may need to be performed to ensure that the FPGAs will survive the radiation environment.

5.4.3 Manufacturing/Assembly Techniques

State-of-the-art NASA-certified surface mount fabrication techniques, which include LCC chips, were assumed for this study. It was assumed that all board assemblies would consist of two single-sided boards glued to a planar metal heat sink. The planar heat sink is the main structural support for the two single-sided electronic cards as well as the heat sink for the electrical components on the circuit card assemblies. Parametric analysis was performed based on using data from the GSFC in-house SMEX program. Specific data and parametric comparisons were made with circuits in the SMEX and SMEX-Lite C&DH, Attitude Control System (ACS), and power systems. The electronics used in these missions use state-of-the-art surface mount and LCC fabrication practices.

The manufacturing approach utilizes:

- High-density manufacturing techniques.
- Flat-packs, LCC, quad flat packs, and surface mount discrete parts.
- Two single-sided boards mounted to an aluminum heat sink.
- Heat sinks mounted in card guides or mounted directly to chassis.
- Aluminum cover for EMI control.
- Special NASA-certification required for surface mount fabrication.

The electronics are organized into logical assemblies: digital interface, analog house keeping, motor control, and analog integrator board (if required). An optional digital filter unit was considered for several narrow-band channels. The digital filter module includes several 80-million-sample-per-second A/D converters to digitize down-converted and Nyquist-filtered IF signals with a maximum bandwidth of 35-mhz. This digitized data is then presented to several chips express laser programmable gate arrays. These arrays performed FIR filter operations, squaring, and accumulation. The outputs would be sent via a multiplexed digital bus to the digital interface unit. Digital filters have the advantage of repeatability and stability. Their main disadvantage is the limited flight heritage of high-speed A/D converters and the need to re-think the filter specifications for the digital implementation. The existing filter specifications were developed for SAW filter banks. The digital filters are more repeatable than the SAW filter banks, but the steep cut-off slopes and band-reject characteristics of the SAW filters would be very costly to reproduce. New frequency response curves for the digital filters need to be developed that take advantage of the stability and repeatability of the digital filters while relaxing the band-stop and cut-off slope requirements currently assumed. The digital filter approach is not practical without implementing new frequency response curves, which minimize the number of FIR poles or eigen function multiplications required to implement a particular digital filter bank.

5.4.4 Digital Interfaces

The baseline digital interface electronic unit includes a MIL-STD-1553 interface that supports Consultative Committee for Space Data Systems (CCSDS) packets. Figure 5-22 details the digital interface. All science, and housekeeping telemetry and commands are supported using this interface. This interface is also used for time synchronization, which is used to synchronize data collection and scan platform motion with a common time reference. Timing accuracy obtained with this method is dependent on the MIL-STD-1553 bus controller. Some missions currently flying have demonstrated a +/- 3-msec timing synchronization capability using a MIL-STD-1553 interface. The digital interface includes a MIL-STD-1553 interface chip and a simple 16-bit, 16-mhz micro-controller. The digital interface is a single string system utilizing the highest reliability parts available and a simple design. Circuits of this type and complexity have demonstrated on orbit reliabilities, which exceed this mission's requirements. The single string data interface significantly reduces the cost and complexity of the instrument by removing the requirement for cross strapping of the digital interface. The micro-controller controls data collection, processing, and scan platform control. The digital interface controls instrument functions:

- Instrument data collection from science and housekeeping ADC units.
- Scan motor control based on information provided by motor control FPGA.
- Synchronization of scan operations with science ADC operation.

The ATMS processor software can be loaded via the MIL-STD-1553 or a RS422 test interface. On-orbit software changes are possible. The ATMS processor will enable low-level testing and debugging capability of all ATMS instrument components. This will minimize the cost of instrument integration and test. A low-cost micro-controller was selected to reduce cost and complexity. Many other processors could be utilized, including digital signal processors such as the LMS 21020.

5.4.5 Analog Interfaces

The science analog inputs consist of input conditioning filters or integrators. One filter or integrator is required for each channel. Figure 5-23 depicts the analog interface. Thirty-one channels of science data are assumed. Redundancy for a second set of 31 channels would be accomplished by duplicating the depicted circuits. Each set of 31 channels has a 16-bit single chip ADC, eight eight-channel multiplexer chips, an integrator/filter bank, and an FPGA to control the MUX and ADC. Surface mount components are assumed for all sizing and costing purposes. Future trades between the integrator and filter solution could be performed. The integrator solution requires more and larger parts, while the filter approach requires more samples and averaging by the micro-controller. The 16-bit analog-to-digital converter has .015 microsecond conversion time. A FPGA state is included to control and synchronize the data collection with the scan platform and external time signals. Each ADC unit interfaces with the micro-controller. A data buffer is included in the FPGA to reduce micro-controller software.

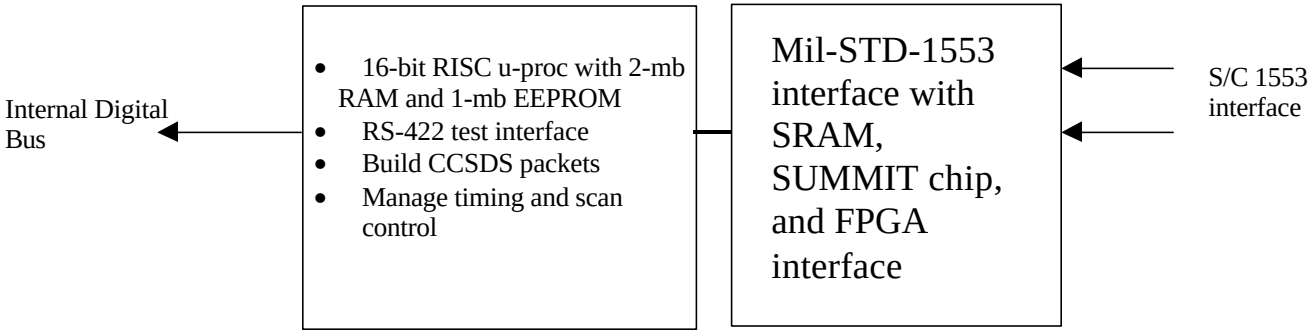

Figure 5-22. Digital Interface

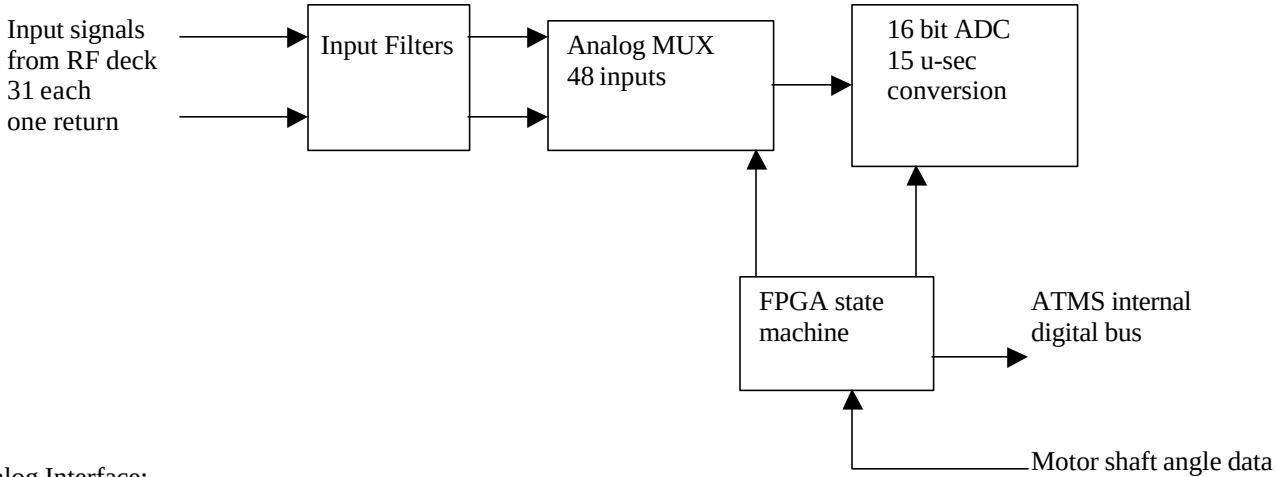

Analog Interface:

- Two units provided for redundancy.
- ADC and MUX are controlled by FPGA state machine.
- Data buffer allows ADC operation without micro-controller activity.
- All channels will be sampled for 90 Earth-scan positions every 8/3 seconds.
- All channels will be sampled at cold space and at hot load every 8/3 seconds.
- Scale factors bandwidth and number of samples per data point are TBD.
- ADC conversion time is less than 0.015 micro-seconds.
- A side and B side ADC units are not cross-strapped.
- Analog FPGA monitors shaft angle data from motor interface.

Figure 5-23. Analog Interface

timing requirements and software overhead. The ADC state machine has access to the scan platform angle from the Scan platform FPGA. Three requirements were considered when selecting this architecture:

- All channels will be sampled for 90 Earth-scan positions every 8/3 seconds.
- All channels will be sampled at cold space and at hot load every 8/3 seconds.
- ADC conversion time will be less than 0.015 microseconds.

5.4.6 Motor Control Electronics

A motor control unit is included in the electronics. Figure 5-24 depicts the Digital Motor Drive electronics. A brushless motor control was assumed. A separate digital tachometer (TAC) with index pulse is assumed to exist. The motor control included a torque command DAC for motor torque. It also includes a FPGA for tachometer processing. The FPGA interfaces to the micro-controller, which computes the motor torque commands. Velocity loop closure could also be included in the FPGA if required.

The digital motor control unit contains a FPGA, which monitors the scan angle and scan rate. The FPGA accepts Hall effect inputs, TAC pulses, and index pulses; it also derives scan angle and scan rate. This information is provided to the micro-controller. The FPGA also includes a DAC interface to command the torque to the scan platform. The micro-controller and FPGA can accomplish feedback control. Implementing complex scan control methodologies in software may require replacing the micro-controller with a digital signal processor. The scan angle is digitally encoded and provided to the Science ADC subsystem for data collection synchronization. The baseline control concept includes controlling and synchronizing the scan platform relative to the externally provided time reference and then synchronizing the ADC sampling to the actual shaft angle.

5.4.7 Analog Telemetry

The platinum resistance temperature (PRT) monitors are required to monitor the temperature of the receiver components and the calibration targets. Figure 5-25 depicts the analog telemetry concept. These temperatures are critical to the operation of the instrument. Ninety-six channels of PRT processing are provided with two independent 48-channel PRT electronic units. Each unit contains 50 op-amp circuits (one for each PRT), a current source, and 12 eight-channel chips. The temperature circuits are controlled by the micro-controller directly. The housekeeping ADC conversion is included with the PRT temperature monitors and adds two eight-channel multiplexer chips to each PRT electronic unit. A 12-bit analog-to-digital converter with 15- microsecond conversion time was assumed. A FPGA state machine is included to control and collect the temperature data. This circuitry also provides housekeeping data collection for the rest of the instrument. A data buffer is included in the FPGA to reduce micro-controller software timing requirements.

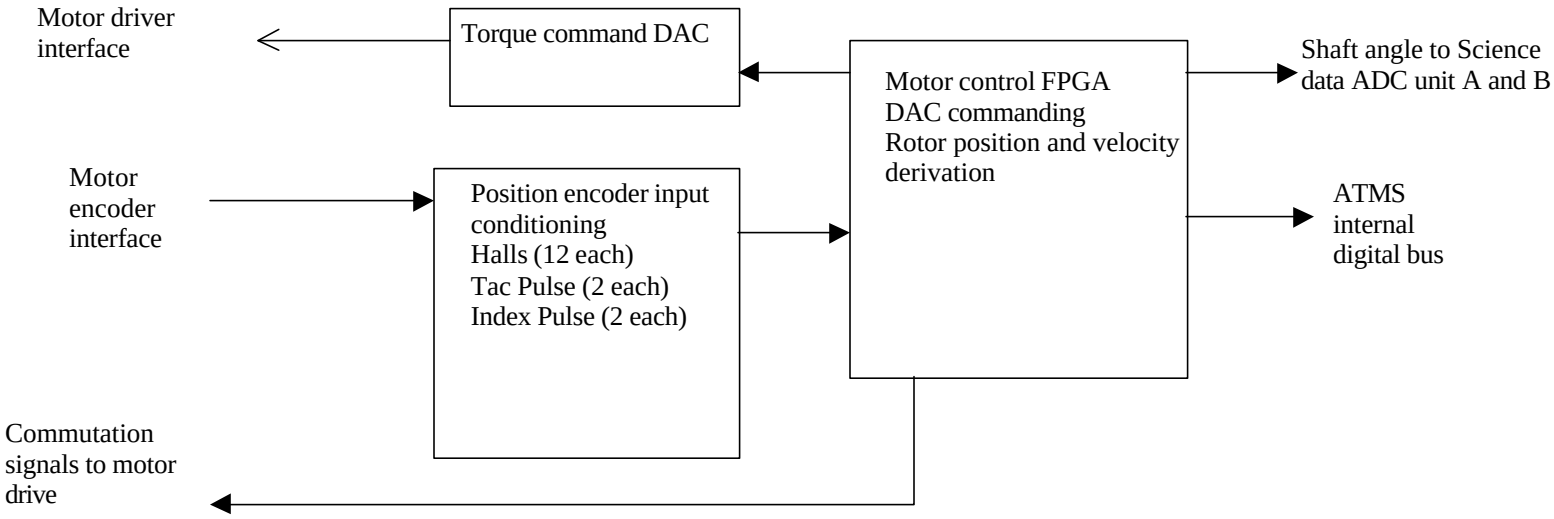

Motor control digital electronics include:

- Interface circuitry for Hall sensors, Tac Pulses, and Index Pulse (high-resolution optical encoder assumed).
- Direct feedback provided to ADC unit.
- ADC conversions triggered at proper angle.
- DAC provided for current/torque command to motor driver.
- Active deceleration may require additional interfaces to Motor control FPGA for SWAP detect.

Figure 5-24. Digital Motor Interface

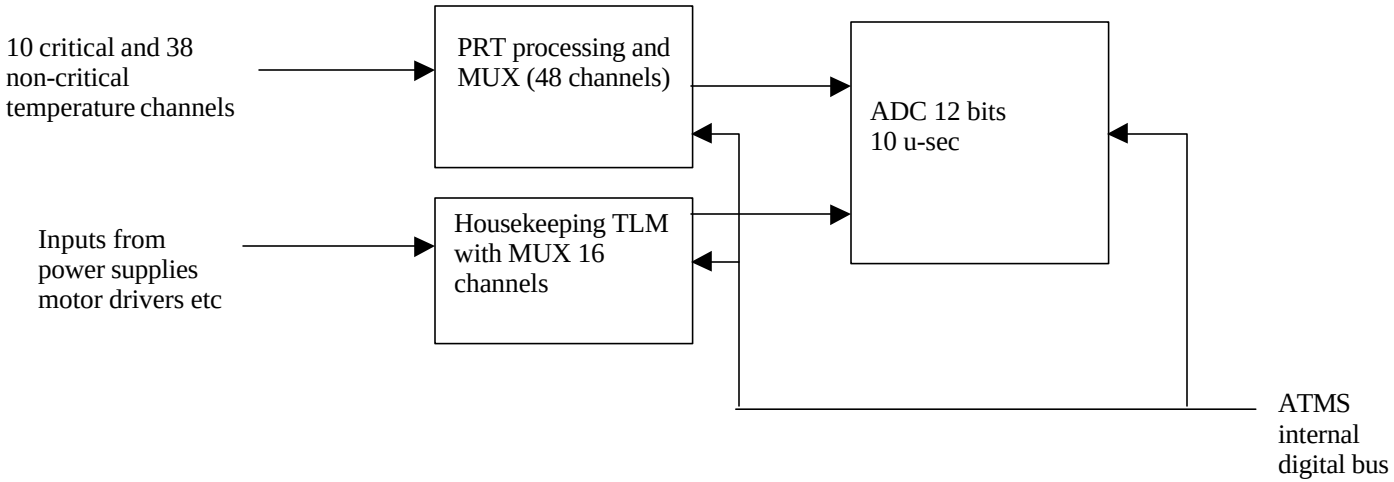

PRT temperature sensor processing and housekeeping ADC:

- 48 PRT signals conditioned on A side, additional 50 PRT channels on B side.
- Housekeeping telemetry provided for power supplies, motor drive, etc.
- Micro-controller controls housekeeping ADC and MUX operation.

Figure 5-25. Temperature Monitoring and Analog Housekeeping Redundant

5.5 POWER SUPPLY

5.5.1 Design Requirements

The design of ATMS allows the power supply requirements to be very similar to those of the AMSU-A instrument. The main difference in the power supply for ATMS is the requirement that the power supply be totally redundant to meet reliability requirements. Additional redundancy of selected instrument functions further suggests the desirability of accommodating the limited redundancy within the instrument by switching power from each of these supplies between redundant portions of the instrument. All basic spacecraft interface functional requirements will remain the same with the exception of the need for additional interfaces to support redundancy. The Electromagnetic Interference (EMI) requirements will remain the same as AMSU-A including the stringent radiated emissions requirement for the Search and Rescue Package. The power supply must meet instrument specifications when powered from a TIROS-type spacecraft power bus (28 +/- 3 volts). The power supply power switching stages must be capable of being synchronized to the instrument data system clock. Low noise and tight regulation are required and should be accomplished by use of multiple isolated outputs with selected usage of internal linear post regulators as were used with AMSU-A.

5.5.2 Design Description

The size and weight of the ATMS power supply subsystem is driven by the requirement for redundant power supplies. This requirement more than doubles the size and weight since redundancy implementation must include not only the equivalent of two power converter assemblies but also relays with command, telemetry, and internal power converter functions. The relays are required to totally disconnect the redundant supply from the instrument electronics (see subsection 5.5.3, Trade Options Considered). Operation of the relays requires two additional independent power converters for redundancy. In addition, the suggested design proposes relays to provide switching of power between redundant functions within the instrument itself when a failure occurs within the instrument, but it is not desired to switch to the redundant power converter assembly.

There are selected sections of the ATMS Instrument where redundant electronic circuits have been utilized to enhance reliability. This redundancy is found in the following circuits:

- The signal processing electronics has an A/B redundancy for the Analog ADC MUX, the HK ADC MUX, the scan mechanism electronics, and the 1553 transformer.
- The critical instrument channels (Channels 3 to 15) are redundant in both the amplifier sections and the local oscillator section.

Several assumptions have been made with respect to redundancy implementation and power distribution system design:

- The microwave amplifier power for each group of channels requires only a single power supply voltage. Based on this assumption there will be one output for each of three groups: Channels 1 and 2, Channels 3 to 15, and Channels 16 to 31. Since Channels 3 to

15 have redundancy, the power for Channels 3 to 15 will have relay switching to switch the power supply output to the redundant circuitry if necessary. The redundancy switching of Channels 3 to 15 will allow any combination of either the A-1 and B-1 LNA to be used with any combination of the A-2 and B-2 LNA by switching the relays accordingly.

- Each local oscillator will have a separate single output voltage for its power. The power supply output for Channels 3 to 15 will be switched from one local oscillator to another if there is a failure of the primary oscillator. This switching is independent of the configuration of the A-1, A-2, B-1, and B-2 configuration for the LANs. The block diagram of the implementation of both the power supply redundancy and the implementation of redundancy within the instrument is shown in Figure 5-26. Figure 5-27 shows all redundancy for the ATMS power supply assembly.

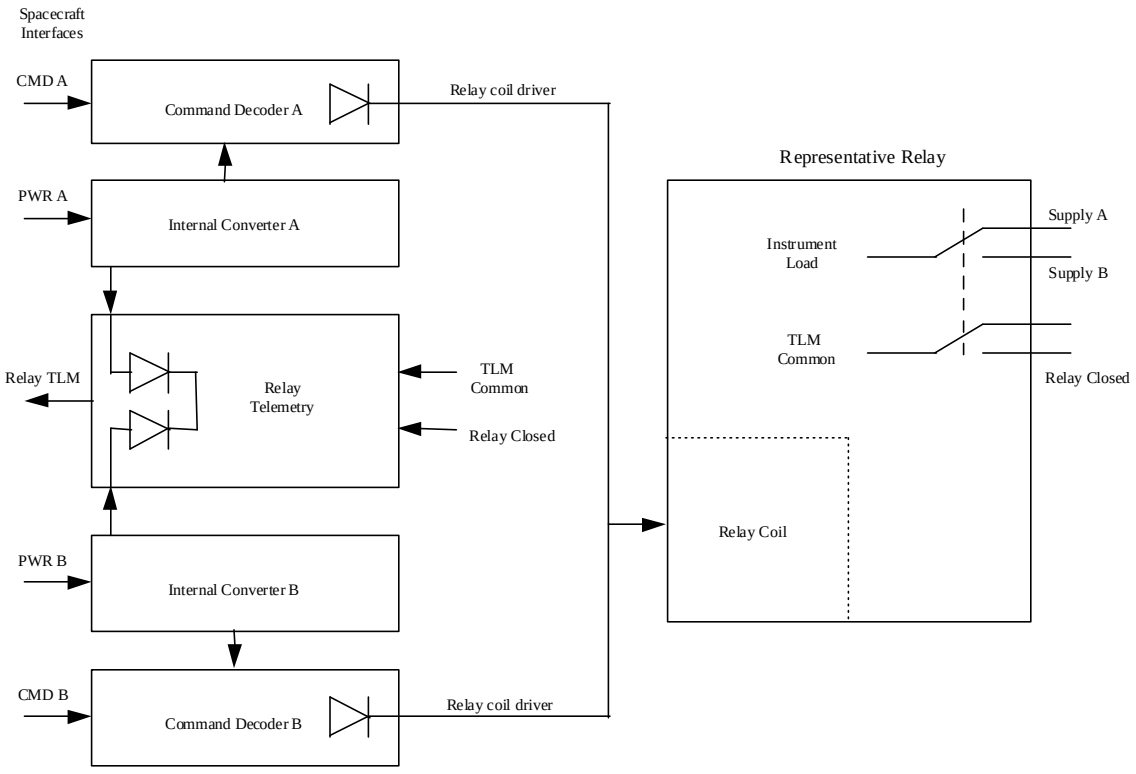

Figure 5-26. Diagram of Relay Switching for Power Supply Redundancy

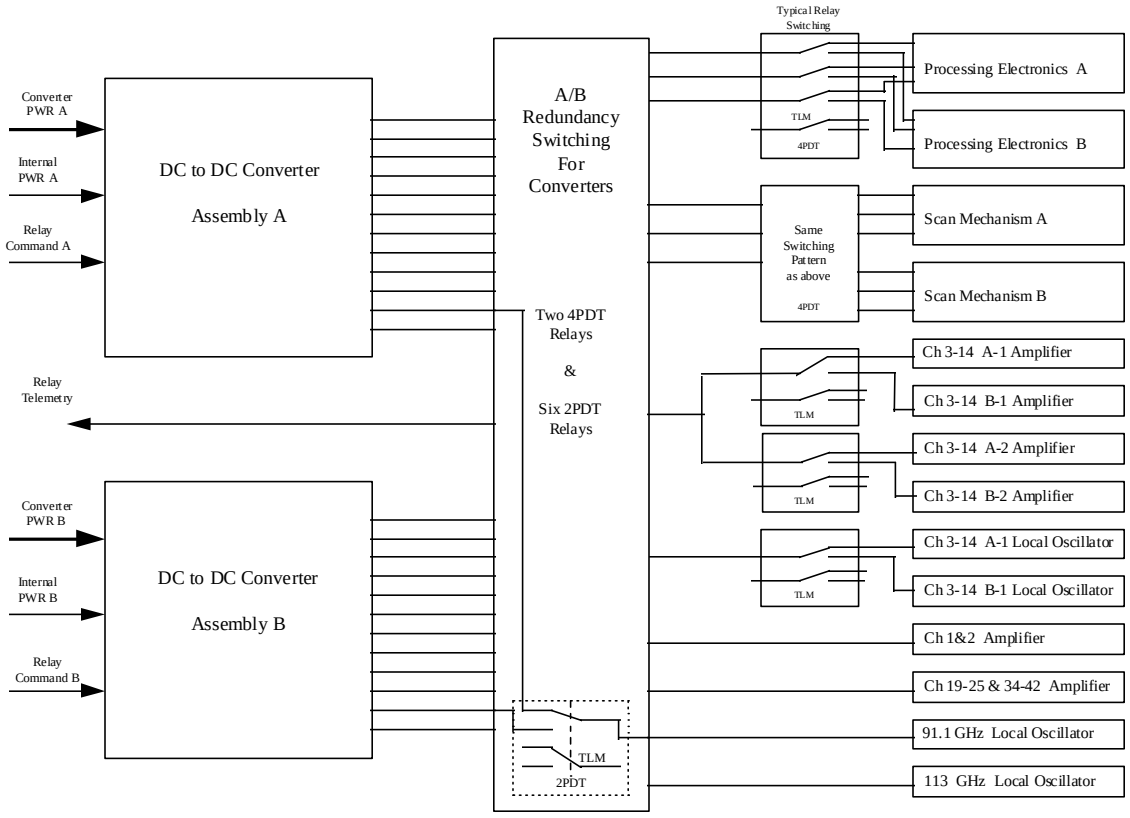

Figure 5-27. Block Diagram of ATMS Power Supply Assembly Showing All Redundancy

The actual converter design that is utilized within the ATMS supply should be patterned after the AMSU-A design. A detailed block diagram of the AMSU-A design is shown in Figure 5-28. The ATMS design assumes only 12 isolated outputs for each converter assembly. This has been taken into account in projecting the size and weight of ATMS by reductions proportional to the reduced number of outputs. ATMS will require only three of the four pulse width modulator (PWM) assemblies used on AMSU-A.

The resources required to implement the entire ATMS power supply based on utilization of the AMSU-A approach and incorporating redundancy are itemized below. The design of the power supply will be based on the combination of the three block diagrams presented above. A summary of the resources required are included in Table 5-2.

The projected efficiency of the power supply will range from 65 to 72 percent depending on how many of the 12 outputs require linear post regulators. A figure of 68 percent should be used for power allocation numbers. An additional power of 2 watts will be required when it is desired to re-configure the redundancy relays and to read relay telemetry. This power comes from a separate power feed that is controlled by the spacecraft.

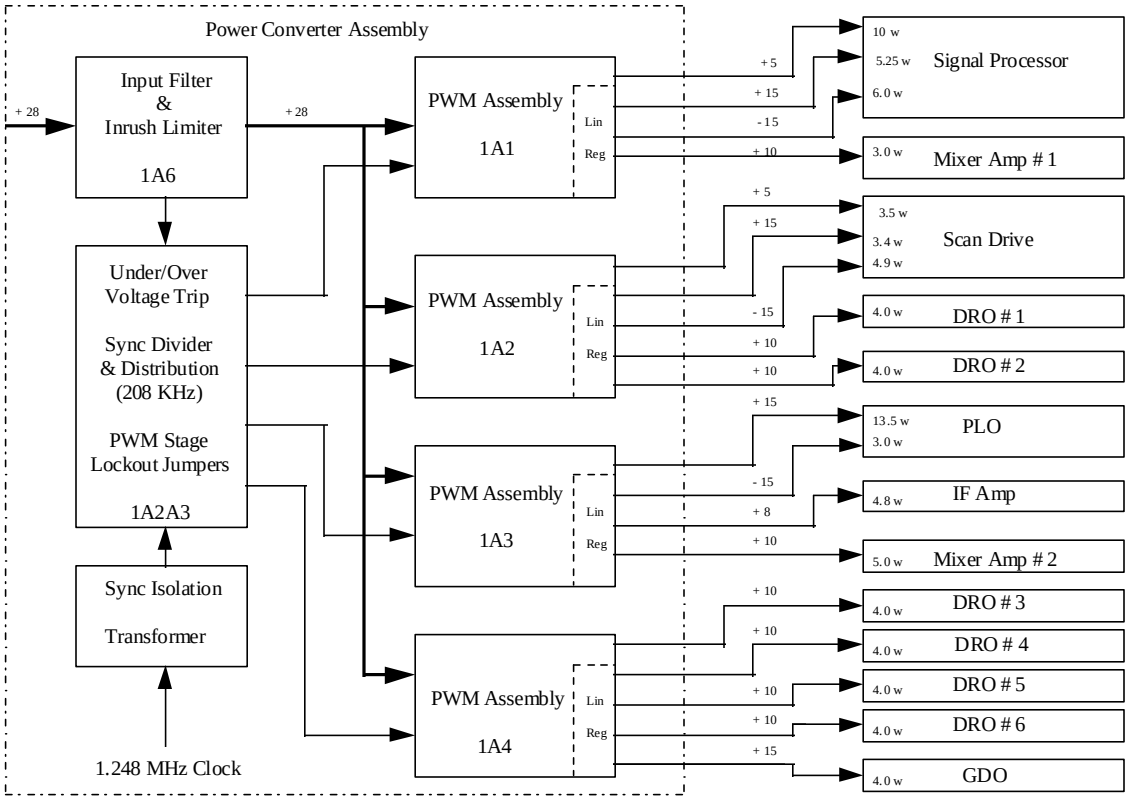

Figure 5-28. AMSU-A1 Power Converter Block Diagram

Table 5-2. DC Converter Estimated Size and Mass

DC to DC Converter A	21 x 11.5 x 6 cm	1.9 kg
DC to DC Converter B	21 x 11.5 x 6 cm	1.9 kg
Converter A and Command Decoder A	21 x 11.5 x 3 cm	0.8 kg
Internal Converter B and Command Decoder B	21 x 11.5 x 3 cm	0.8 kg
Relays, relay telemetry, and connector & harness wiring	21 x 10 x 9 cm	2.4 kg
Totals	21 x 33 x 9 cm*	7.8 kg

* Assumes that the internal converter and command decoder cards are mounted on top of each of the corresponding DC-to-DC Converters. It is assumed the relay telemetry will be incorporated on the relay card. The relay cards and interconnect harnessing plus the external box connectors will be a section located between the two converters.

5.5.3 Trade Options Considered

The objective of the trade study was to determine the power converter design approach that would yield the best compromise of performance, small size, light weight, high efficiency, and lowest costs for repetitive builds. The trade options section also contains a discussion of the implementation of redundant power supplies.

5.5.3.1 Technology Options

Power supply designs based on AMSU-A and AMSU-B heritage along with designs utilizing off-the-shelf hybrid converters were considered. A summary of the features and the advantages and disadvantages of each follows.

- *AMSU-A Power Supply Design*

  The AMSU-A supply is 25.5 cm x 11 cm x 5.7 cm in size (volume of 1,600 cubic cm) and provides around 50 watts of output power at an efficiency of about 65 percent. The supply provides 18 isolated outputs with 14 of the 18 outputs having added linear post regulators for better regulation and lower noise. This supply weighs 2 kg. The small size and light weight are achieved by dividing the loads among four smaller power switching stages to take advantage of smaller parts with a more distributed power dissipation to achieve better packaging efficiency. The small size of this supply is also achieved by the use of custom hybrid circuits for the power stage control and for the linear post regulators.

  Advantages: Smallest size, lightest weight, high-radiation tolerance, best output regulation and noise performance.

  Disadvantages: Lowest efficiency (could be made to equal other designs if linear regulators removed), limited selection of manufacturers due to use of custom hybrids.

- *AMSU-B Power Supply Design*

  The AMSU-B supply uses a buck pre-regulator to regulate the spacecraft bus input voltage to a push/pull switching stage. This switching stage drives a transformer that provides eight isolated outputs. The 5-volt processor electronics output is used for feedback regulation. The only outputs that have linear post regulators are the video amplifier +/- 15 volt. This supply is 20.6 cm x 12 cm x 19.2 cm (volume of 4,750 cubic cm) and weighs 4 kg. The supply provides an output of 61 watts at 72 percent efficiency. This supply operates from a more tightly regulated spacecraft bus (28 +/- 0.56 volts) than the AMSU-A (28 +/- 3 volts). This supply is more efficient than the AMSU-A supply, because it provides less regulation on the outputs by not utilizing as many post regulators.

  Advantages: High efficiency, high radiation tolerance.

Disadvantages: Large volume, heavy weight, number of outputs limited by transformer design, requires larger volume for the 12 outputs needed for ATMS.

- *Power Supply Design Using Off-the-Shelf Hybrid Converters*

  A baseline design using a hybrid converter configuration was developed to determine the comparison with the AMSU-A1 design to show the advantages and disadvantages. The baseline design provides 18 isolated outputs but groups multiple outputs on the same hybrid, where possible, when those outputs feed the same load function. Some of the hybrids are single outputs and some are dual outputs. Triple output hybrids were not considered, because the outputs generally share the same power return. This design required four dual output hybrids and 11 single output hybrids. The hybrid converters require auxiliary circuitry to meet all the ATMS requirements. This circuitry includes input power filter, inrush limiter, output common mode filters, and a synchronization driver circuit. The initial concept evaluated assumes that all converters are mounted in a single assembly to replicate the AMSU-A package. When all the items needed to make up the supply were considered, this power supply was estimated to be 25.5 cm x 10 cm x 8.9 cm with a volume of 2,270 cubic cm and to weigh 2.8 kg. It should be noted that this supply does not have the degree of regulation and noise performance possessed by the AMSU-A supplies, because no linear regulators are used as post regulators to enhance performance. They could be added at an even greater increase in size and weight, and decrease in efficiency. Special production runs will be required for the hybrids to obtain non-standard output voltages and to adjust switching frequency to allow synchronization.

  Advantages: High efficiency (about 73 percent), off-the-shelf availability for the converter module only (will require minor modification), converter hybrid available as standard QML part, slightly lower cost.

  Disadvantages: Larger volume than AMSU-A supply, only single-stage regulation with higher noise, standard hybrids available only with limited output voltages requiring either higher power supply dissipation or slight modification, requires even larger volume supply if radiation requirements exceed 25 Kilo-RAD (KRAD), may require slight modification of switching frequency to synchronize to data system clock frequency, dual output hybrids have limited minimum and maximum loading constraints on each output, manufacturers periodically have production run problems that translate to lower reliability.

If the hybrids are utilized as distributed converters where the converters are mounted on the same circuit board with the instrument load, then three items become considerations:

- The output common mode filter chokes will probably become the driving factor that establishes the maximum component height on the instrument circuits. This will increase package size for these circuits.
- This would still require a separate power supply box to provide a central input filter, inrush limiter, and synchronization driver and distribution wiring.

- This would put the noisy power converter on the same board and in proximity with sensitive circuitry.

Conclusion: The best power supply design selection appears to be a design patterned after the AMSU-A supply. It is possible to increase the power supply efficiency by eliminating linear post regulators where not required.

5.5.3.2 Redundancy Implementation

There are three ways redundancy could be implemented within the power supply:

- *Directly Parallel the Converter Outputs with only One Converter Powered at a Time*

  This approach may not always be possible depending on the power supply output power circuit design. This approach is also not usually acceptable; if a converter output stage develops a short, this short will also short the redundant converter output and defeat the redundancy attempt.

- *Diode-Or the Power Supply Outputs*

  This has the disadvantage that the actual power supply output voltage is one diode drop lower than the converter-regulated output. This diode adds more power supply dissipation, thus, reducing the overall efficiency. This diode is outside the converter regulation loop and, therefore, the power supply output is subject to variations due to current and temperature effects on the forward voltage drop of the diode. The specifications for AMSU-A make this approach unable to provide acceptable regulation for many of the instrument loads.

- *Relay Switching of Power Supply Outputs*

  This technique groups the outputs for each instrument load on a relay and uses the relay to switch the load from one power supply to another. In the case of the ATMS design, this would require 13 relays. In addition, it would require redundant auxiliary converters to power the control and relay driver circuits. Usually a requirement for a digital telemetry circuits is to provide relay status. If this type of redundancy is to be implemented, it is best implemented by having power converter assemblies, all relays, and other circuitry in one box. This minimizes connectors and external harnessing and has the additional benefit of not introducing electrical noise.

The use of redundant power supplies implies that there will be at least two separate spacecraft power feeds (four for the relay switching approach). The power feeds will be individually commandable from the spacecraft. Implementation of redundancy will require a larger volume than the AMSU-A supply, especially for the relay switching approach. None of the AMSU or the MHS Instruments has redundant power supplies.

5.5.3.3 Effects of Baseline and Descope Options

The ATMS instrument has been designed with four levels of science capability. The levels are listed in Table 5-3. The capability levels will not affect the size and weight of the power supply design since the power level changes are not extreme and the number of outputs required do not change. The main effect will be in the dissipation levels and heat transfer.

Table 5-3. DC Converter Power Requirements

	Output PWR	Dissipation	Input PWR
Enhanced Science	57.2 w	26.9 w	84.1 w
Comparable Science	49.8 w	23.4 w	73.2 w
Descope Option #1	46.9 w	22.1 w	69.0 w
Descope Option #2	41.9 w	19.7 w	61.6 w

Note: The listed power values in Table 5-3 are higher than those presented in the database in Section 6, because they are calculated at a very conservative 68 % efficiency instead of pushing the state-of-art at 75 % efficiency, the rate which was used in the database calculations.

5.5.4 Summary

The main difference between the ATMS power supply and the AMSU heritage supplies is the need to provide redundancy. This drives the need for more spacecraft interfaces for both command and telemetry, and for power. The preferred design approach relies on having a manufacturer that can provide custom hybrid designs that will significantly reduce size and weight. Only one output voltage was assumed to be needed for the amplifiers for each group of channels. If the number of needed outputs increases, the power supply size and weight will increase. There are no technology-related issues.

This report was not completed in time to make the database freeze for sizing and cost profiling the final ATMS iteration; two inconsistencies are noted:

- The DC converter efficiency of 68% is conservative and would cause the final power draw of the ATMS to be approximately 7 additional watts compared to the 75% efficiency used for the database calculations.

- The weight and volume will increase by 3.4 kg and 4.237 cubic cm. These increases are mainly due to our not allowing “real estate” for the redundancy switching circuits.

Neither of the database adjustments is anticipated to alter the design or cost as presented, because they are absorbed within the margin factors.

5.6 PACKAGING/MECHANICAL

5.6.1 Design Description

Design of packaging was accomplished on a subsystem-by-subsystem basis. An Excel database was developed that detailed individual discrete components resource requirements. Each component was characterized by name, size, (length x width x height), mass, volume, and power requirements. The database was configured in a logical flow starting with the reflectors and common subsystems, i.e., the power supplies and motor /drivers, and proceeding through to the four individual receivers. Section 6.0 provides database details for the final ATMS strawman instrument iteration. A combination of engineering experience, AMSU-A actual piece part characteristics, and catalog listings were used to quantify database attributes for each component. Figures 5-29 and 5-30 present typical components and Tables 5-4 and 5-5 show database parameters.

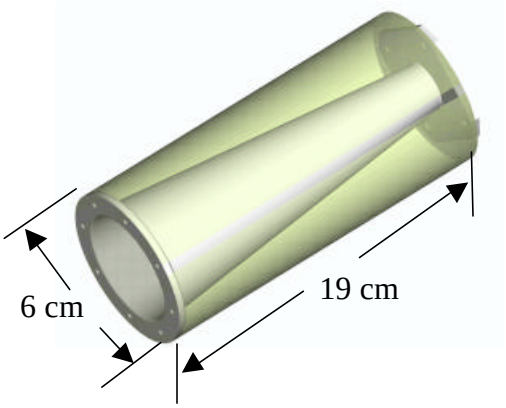

Figure 5-29. Feed Horn

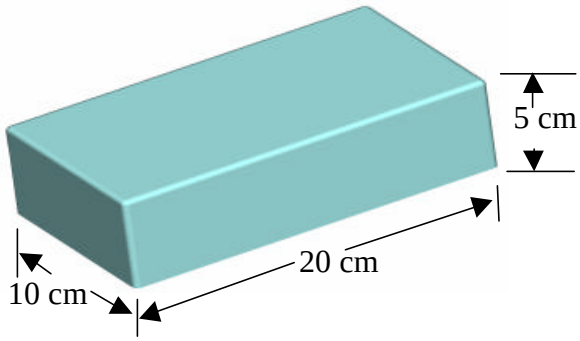

Figure 5-30. D/C Converter

Computer Aided Design (CAD) was utilized to develop component and subsystem packaging layouts. Discrete parts were drawn to scale and the incorporated in the layout architecture according to their use and subsystem location.

Table 5-4. Feed Horn Database

COMPONENT	Freq	Size			Mass	PWR	VOL
		L	W	H			
	GHz	cm	cm	cm	gms	Watts	cm^3
Beam Splitter		20	20	1	500		400
FeedHorn		19	6Dia	2	150		537

Table 5-5. D/C Converter Database

COMPONENT	Freq	Size				Ribs	Mass	PWR	VOL
		L	W	H	Skin	Fill			
	GHz	cm	cm	cm	cm	%	gms	Watts	cm^3
D/C Converter		20	10	5			2200	15	1000
D/C Converter		20	10	5			2200		1000

The optical components and receiver feed horn placement were in accordance with the dimension requirements identified in Section 5.2.2, Components. Placement was critical with respect to centerlines and distances from component to component. Layouts were developed and iterated for one and two motor designs and for folded and non-folded optics.

Receiver shelf designs, similar to the original AMSU-As, were developed to hold the optical and receiver components in place. The shelves were attached to the housing and individual receiver components that populated each shelf. The shelves were laid out according to the schematics identified in the Receivers Section 5.3, and physical sizes defined in the database. Low-frequency channel separation was accomplished by placing all 50- to 59-GHz components on one side of the shelf and all 23- to 32-GHz components on the other side of the shelf. Figure 5-31 shows the receiver shelves with embedded feed horns and motor mount layout for the final design configuration.

Receiver shelf outputs were routed to the power splitter; these were located on the post amplifier/detector “video” boards. “Video” board analog channel outputs were then routed to the digital electronics via RF cabling.

Our layouts and part spacing locations allowed for the use of wave guide connections for frequencies above 35 GHz and semi-rigid coax for all frequencies below 35 GHz. Figure 5-32 shows a typical “video” amplifier/detector board layout.

After the optics and receiver shelves detailed were completed, then the electronic boards, motor drivers, and the power supplies were located within the remaining housing envelope. All large power dissipaters, like the power supplies were mounted to the anti-sun side of the housing for ease of heat rejection. Figure 5-33 depicts component placement for the final design iteration.

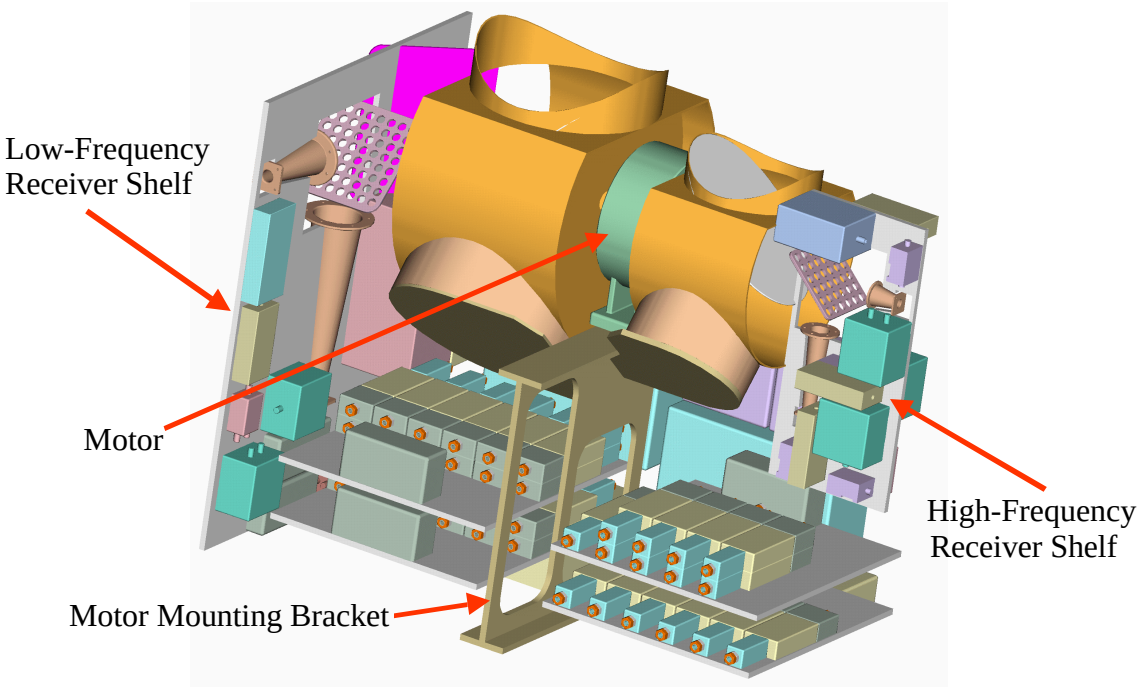

Figure 5-31. Receiver Shelves and Motor Mount

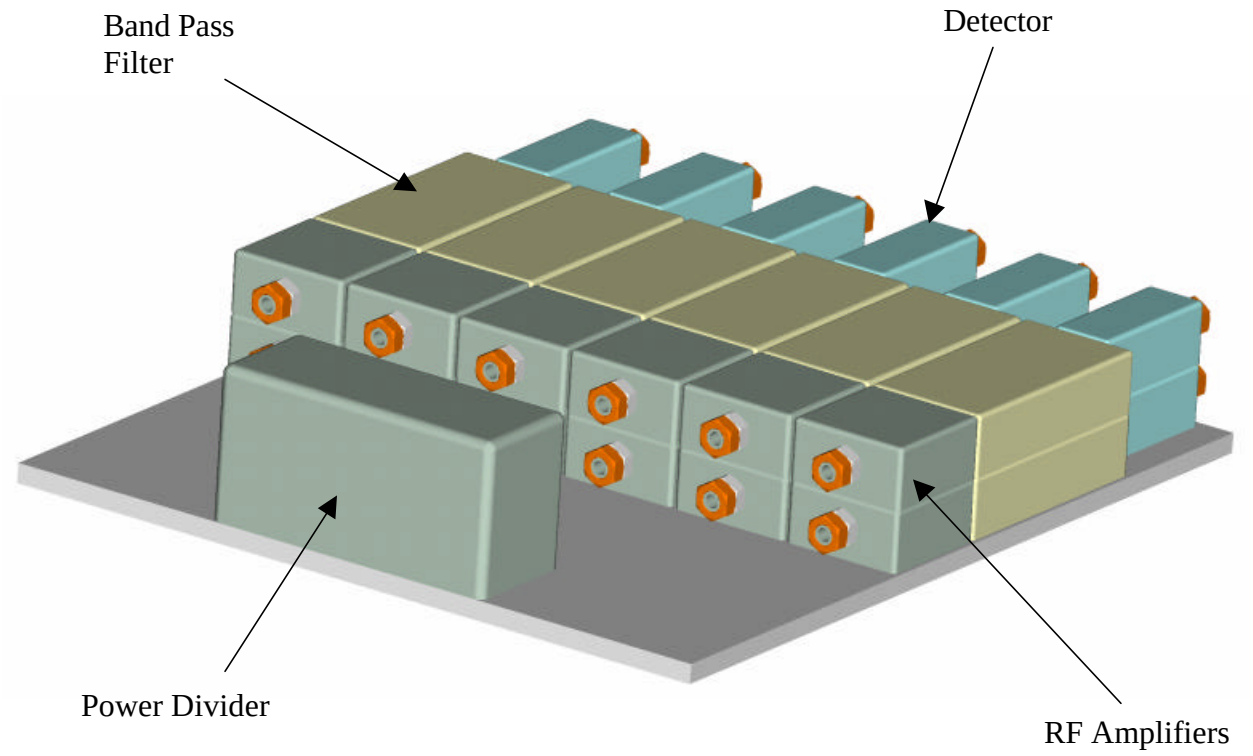

Figure 5-32. Typical Video Board Layout

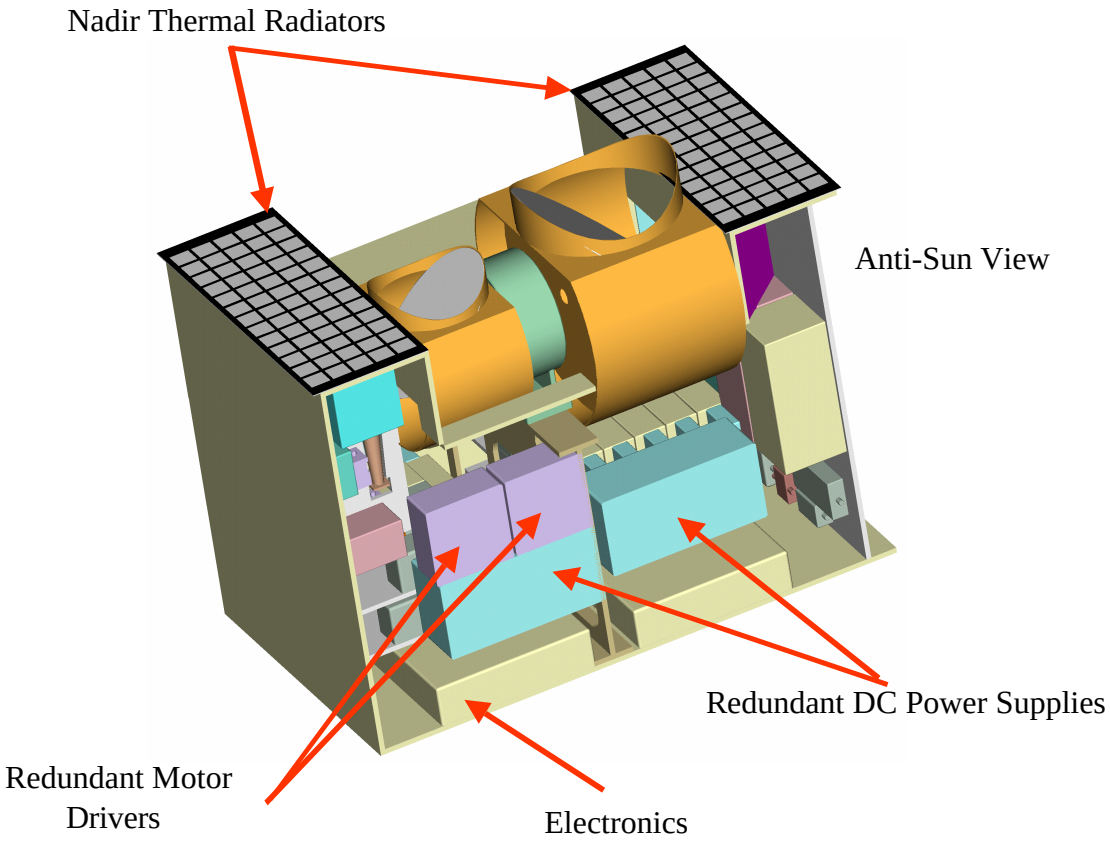

Figure 5-33. Location of High-Power Dissipaters

5.6.2 Structure Details

While not specifically detailed in the CAD models, a conservative approach was used to allow for structural integrity. Heavy mass was used for structural elements in the database. The housing was segregated into eleven discrete panels. They ranged from a baseplate to side panels and included the receiver shelves and motor mount. Each panel was sized, and a thickness and percentage of ribbing was estimated depending on the envisioned load requirements. Lastly, the mass of each panel was calculated using aluminum equivalent density at 1.5 gms/cm^3.

Structural integrity was assured, as the thickness of all key-supporting panels was either 1- or 2-cm thick. Ribs were envisioned to allow for weight-to-strength optimization when needed. Defining sufficient weight and volume for each panel assured structural integrity in the final design.

5.6.3 Final Package Sizing

During the study effort three different CAD packaging configurations were iterated. Our first package was 110 cm x 40 cm x 40 cm. It contained a common double-shafted motor that rotated both the high- and low-frequency antennas simultaneously. The optics were in line and all components were redundant with the exception of motor, antennas, feed horns, and the first stage of amplification (usually an LNA). This configuration was not acceptable because it did not meet the envelope constraints. However, because it was the simplest and most straightforward design it was used as a benchmark for understanding the technical challenges of packaging in the confined 70-cm x 60-cm x 40-cm envelope.

The second iteration used independent drive motors that were offset in the housing, similar to the AMSU-A1 design, in order to allow the optics to still remain inline. This configuration was still redundant, it was housed in the required 60-cm x 60-cm x 70-cm envelope, but it exceeded the weight and power requirements.

The final iteration used the single scan motor, employed a folding optical element in the low-frequency 23-GHz and 32-GHz bands, and eliminated some of the receiver redundancy as dictated by the reliability model and the Science Team's priorities. Even after folding the optics, this configuration was tight in the 70-cm velocity envelope direction. However, additional margin could be gained in the 70-cm direction by redesigning the optics to a slightly lower F/D ratio number. The strawman design used the same F/D ratio number as the Heritage AMSUs. This package was 70 cm x 50 cm x 40 cm and met all the interface requirements with a 10-cm height margin.

5.6.4 Density Packing Factor

The density-packing factor was used as a figure of merit to demonstrate the required volume of all the included ATMS parts when rationed to the allowable volume. Engineering experience indicated that a packing factor of 0.6 or less does not require heroic efforts to fit all the parts in the allowable package volume. As can be seen from the database summary, the envisioned comparable ATMS instrument had a packing factor of only .477 using a 70-cm x 50-cm x 40-cm envelope for the final design iteration. This would compare to a .298-packing factor using the IPO 70-cm x 60-cm x 40-cm requirement.

5.6.5 Summary

The ATMS instrument can be packaged into the required envelope. More than one configuration is possible depending on redundancy, the number of motors, and optical design details.

5.7 THERMAL DESIGN

5.7.1 Design Considerations

Thermal design for the ATMS is straightforward. The instrument uses 66 to 76 watts depending on which option is chosen. This means that the thermal subsystem must radiate 72 watts (worst case) to space allowing for 4 watts to be radiated from the scan cavities and 0 watts to the spacecraft. Assuming the instrument receivers and electronics needed to maintain a temperature of about 15-20°C, radiators could be used on the NADIR and anti-sun envelope surfaces to reject the 72 watts. Figure 5-34 shows nominal heat rejection at 20°C would be 150 watts/m^2 from NADIR and 285 watts/m^2 when facing anti-sun.

5.7.2 Design Concept

The final 70-cm x 50-cm x 40-cm envelope had .4 meter x .1m x 2 = .080m^2 available on NADIR view and a minimum of .7 meter x .5 meter = .35m^2 available on the anti-sun view for radiation of the ATMS heat. This equates to a capability of radiating 12 watts from NADIR and 100 watts from the anti-sun panels. When packaging the ATMS components, most of the power subsystems, like the motor controllers and the DC converters, were mounted directly to the anti-sun panel. Thermal control would only require proper radiator sizing and panel thickness control to control gradients. Prudent design of the receiver shelves would allow heat to either be radiated or conducted to either radiator. Figure 5-35 shows how the radiators might be proportioned assuming 12 watts were to be radiated to NADIR.

5.7.3 Summary

Design of the ATMS thermal system presents no significant problems or challenges. Using only the anti-sun view or a combination of anti-sun and NADIR views to radiate the ATMS 70 plus watts is benign.

5.8 ATMS RELIABILITY

5.8.1 Introduction

A reliability analysis was performed on the conceptual ATMS design to determine what level of reliability could be expected and also to evaluate design alternatives. Reliability Block Diagrams (RBD)s were developed from the functional schematic drawings and success/failure criteria, and a mathematical model was derived. Failure rate data needed to exercise the model was based partly on AMSU-A failure rate data contained in Aerojet Corporation's report 9831C, *Meteorological Satellites (METSAT) and Earth Observing System (EOS) Advanced Microwave Sounding Unit-A (AMSU-A) Reliability Prediction Report, dated March 1996.* Other sources of data include MIL-HDBK-217 and the MIDEX MAP Project reliability analysis.

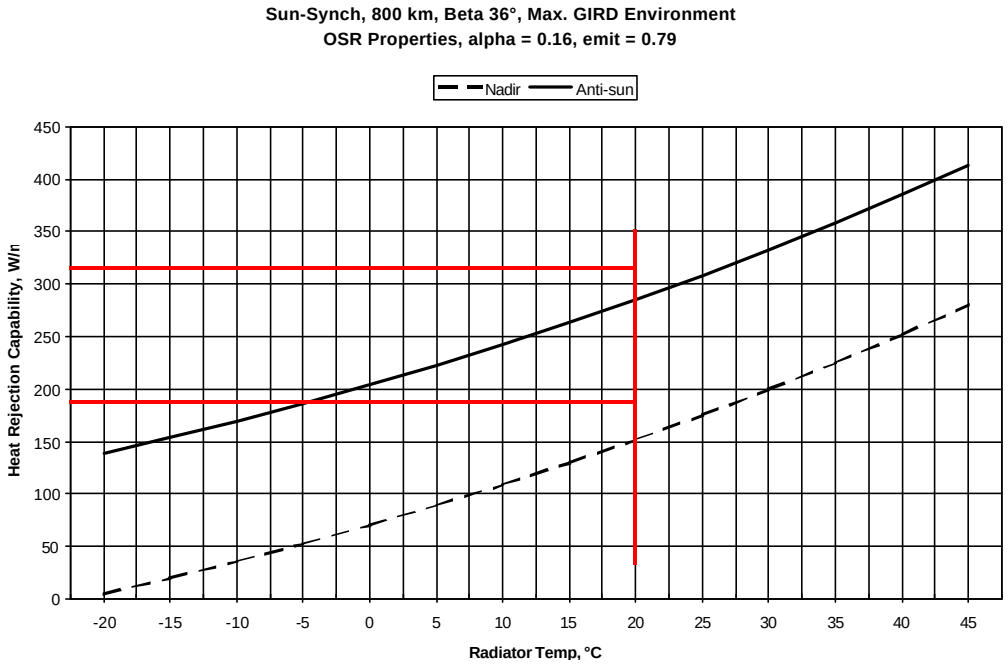

Figure 5-34. Theoretical Heat Rejection Capabilities

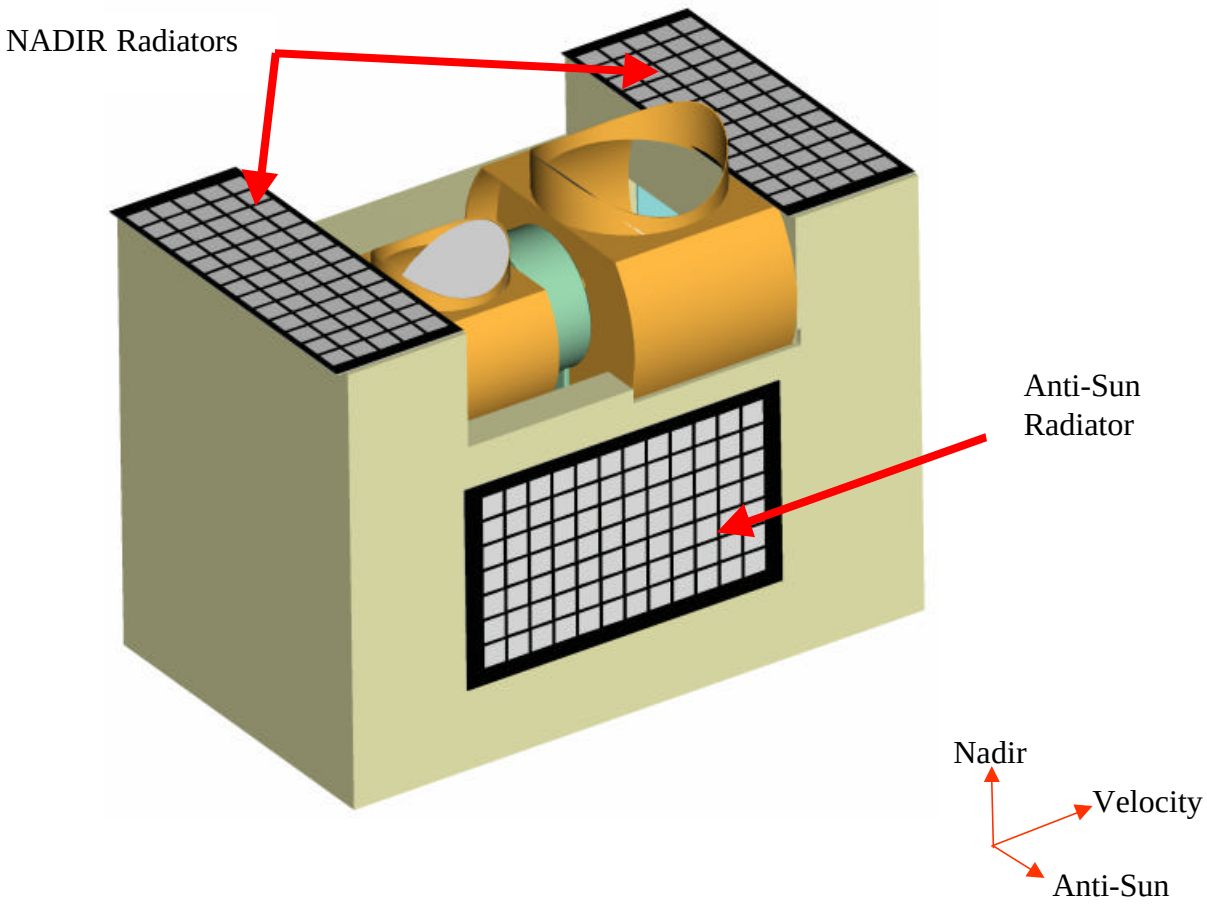

Figure 5-35. Advanced Technology Microwave Sounder

5.8.2 Priorities

Priority 1 and Priority 2 channels are the baseline channels in this study. Priority 3, 4, and 5 channels are referred to as optional.

Priority 1: Channels 3-15.

Only the loss of Channels 8 and 9 would require a new launch to replace an operational ATMS. However, Channels 13–15 are not considered mission critical as they are somewhat redundant with CrIS capabilities, but are included with Channels 3-12, because they are trivial to implement.

Priority 2: Channels 17-22 (166-GHz and 183-GHz window water vapor channels).

Priority 3: Channels 1 and 2 (23.8-GHz and 31.4-GHz window water vapor channels), and Channel 16 (89-GHz window water vapor channel).

Priority 4: Channels 23-31 (118-GHz oxygen channels).

While there are good reasons to have all the listed channels, they are not of equal priority. Baseline Channels 3-12 are mission critical and are Priority 1. Baseline Channels 17-22, which are important for humidity sounding, especially under overcast conditions are Priority 2. Optional Channels 1 and 2 are Priority 3, being quite desirable but not mission critical, closely followed by Baseline Channel 16, given a Priority 3.1. Baseline. Optional Channels 23-31 are Priority 4 as they provide enhanced science.

5.8.3 Results

The results of the analysis are shown among the following figures and tables.

Figures 5-49, 5-51, and 5-53 show the RBDs for Data Channels 1 through 31. Figure 5-55 shows the RBD for the signal processing function. These RBDs reflect the designs shown in the ATMS functional schematics. It should be noted that the DC torque motors are shown as a single element, however, redundant windings are considered in the actual calculations and plots shown in the accompanying plots and tables. The signal processing function is also shown as a single block for clarity, although there is significant redundancy as shown in Figure 5-55.

Figure 5-49 is the RBD for ATMS channels 1 and 2. Both channels and one of two power supplies are required for success. The channels are shown in a parallel configuration, however, the 2/2 notation, which means two of two required for success, defaults to a serial configuration mathematically. Table 5-6 details the failure rate data and resulting reliability calculations for Channels 1 and 2, while Figure 5-50 plots the reliability as a function of redundancy

Figure 5-51 is the RBD for ATMS channels 3 to 15. Groups A and B show fully redundant sets of data channels. Subgroups A1 and B1 are shown with thirteen of thirteen channels required for

success, however, actual success criteria will probably allow for the loss of one, two, or more channels as long as Channels 6 and 7 are not among the failed channels. Table 5-7 details the failure rate data and resulting reliability calculations for Channels 3-15, while Figure 5-52 plots the reliability as a function of redundancy.

Figure 5-53 is the RBD for ATMS Channels 16, 17 to 22, and 23 to 31. For purposes of this analysis, all channels are needed for success, however, in reality, certain channel failures may be acceptable. Table 5-8 details the failure rate data and resulting reliability calculations for Channels 16-22 and 23-31, while Figure 5-54 plots the reliability as a function of redundancy.

Figure 5-55 shows the RBD for the ATMS signal processing function.

5.8.4 Summary

In order to meet a .86 reliability at the end of 7 years, Channels 3-15 need to be 100% redundant end to end. All other channels can be single ended in the receivers and 100% redundant for the remainder of the circuitry in order to meet their .76 reliability at the end of 7 years. This equates to the dc converter, motor drivers, and signal processor subsystems all being 100% redundant in support of meeting the .86 Channels 3-15 and .76 Channels 1-2 and 16-31 end-of-life 7-year reliability requirements.

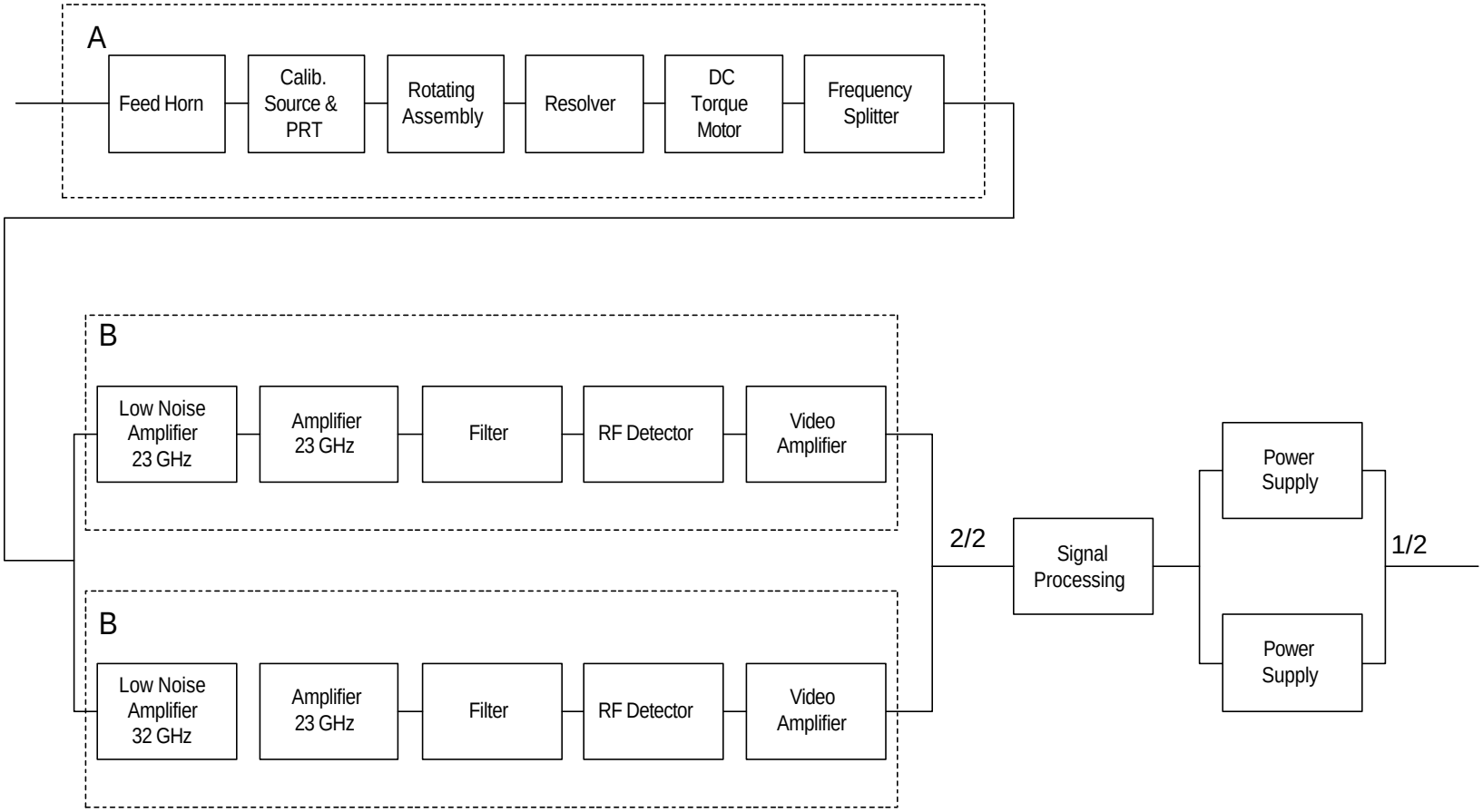

Figure 5-49. ATMS Channels 1 and 2 Reliability Block Diagram

Table 5-6. Channels 1 and 2 Failure Rates and Reliability Calculations

**Equivalent Mission Time = 61320		Ground Time =7008							
Component	F/R x10-6	1	2	3	4	5	6	7	Ground
Feed Horn	0.001	0.999984	0.999975	0.999967	0.999958	0.999949	0.999940	0.999932	0.999993
Calibration Source & PRT	0.008	0.999874	0.999804	0.999734	0.999664	0.999594	0.999524	0.999454	0.999944
Rotating Assembly	0.15	0.997638	0.996328	0.995019	0.993713	0.992408	0.991105	0.989803	0.998949
Resolver	0.00713	0.999888	0.999825	0.999763	0.999700	0.999638	0.999575	0.999513	0.999950
Dual Winding DC Torque Motor	0.15735	0.997522	0.996148	0.994776	0.993406	0.992037	0.990671	0.989306	0.998898
Single Winding DC Torque Motor	0.2098	0.996697	0.994867	0.993041	0.991217	0.989397	0.987580	0.985767	0.998531
Frequency Splitter	0.0175	0.999724	0.999571	0.999418	0.999264	0.999111	0.998958	0.998805	0.999877
RF Switch	0.02125	0.999665	0.999479	0.999293	0.999107	0.998921	0.998735	0.998549	0.999851
Low Noise Amplifier (23 GHz)	0.31608	0.995028	0.992277	0.989533	0.986797	0.984069	0.981348	0.978634	0.997787
Low Noise Amplifier (32 GHz)	0.31608	0.995028	0.992277	0.989533	0.986797	0.984069	0.981348	0.978634	0.997787
Amplifier (23 GHz)	0.31608	0.995028	0.992277	0.989533	0.986797	0.984069	0.981348	0.978634	0.997787
Amplifier (32 GHz)	0.31608	0.995028	0.992277	0.989533	0.986797	0.984069	0.981348	0.978634	0.997787
Component	F/R x10-6	1	2	3	4	5	6	7	
Filter	0.03807	0.999400	0.999067	0.998734	0.998401	0.998068	0.997735	0.997402	0.999733
RF Detector	0.00259	0.999959	0.999936	0.999914	0.999891	0.999868	0.999846	0.999823	0.999982
Video Amplifier	0.0181	0.999715	0.999556	0.999398	0.999239	0.999081	0.998922	0.998764	0.999873
Signal Processing (Redundant)		0.995807	0.995119	0.994381	0.993592	0.992754	0.991867	0.990932	
Signal Processing (Single String)		0.979158	0.970348	0.961618	0.952966	0.944393	0.935896	0.927476	
Redundant Power Supplies		0.999889	0.999734	0.999513	0.999227	0.998878	0.998466	0.997994	0.999978
Group A		0.999708	0.999546	0.999384	0.999222	0.999060	0.998899	0.998737	
Group B		0.989165	0.983196	0.977263	0.971366	0.965505	0.959679	0.953888	
Channel 1 or 2		0.988767	0.982488	0.976185	0.969860	0.963515	0.957151	0.950771	
Ch.1&2 (Red. Signal Process.)		0.973952	0.961264	0.948629	0.936053	0.923538	0.911087	0.898706	
Ch.1&2 (SS Signal Process.)		0.957668	0.937335	0.917374	0.897780	0.878548	0.859674	0.841155	

** Equivalent ground time is the time that the instrument is in storage and undergoing tests. The 8 years is divided by 10, which is equivalent to dividing all failure rates by 10. This is the standard reduction in failure rate used under non-operating conditions.

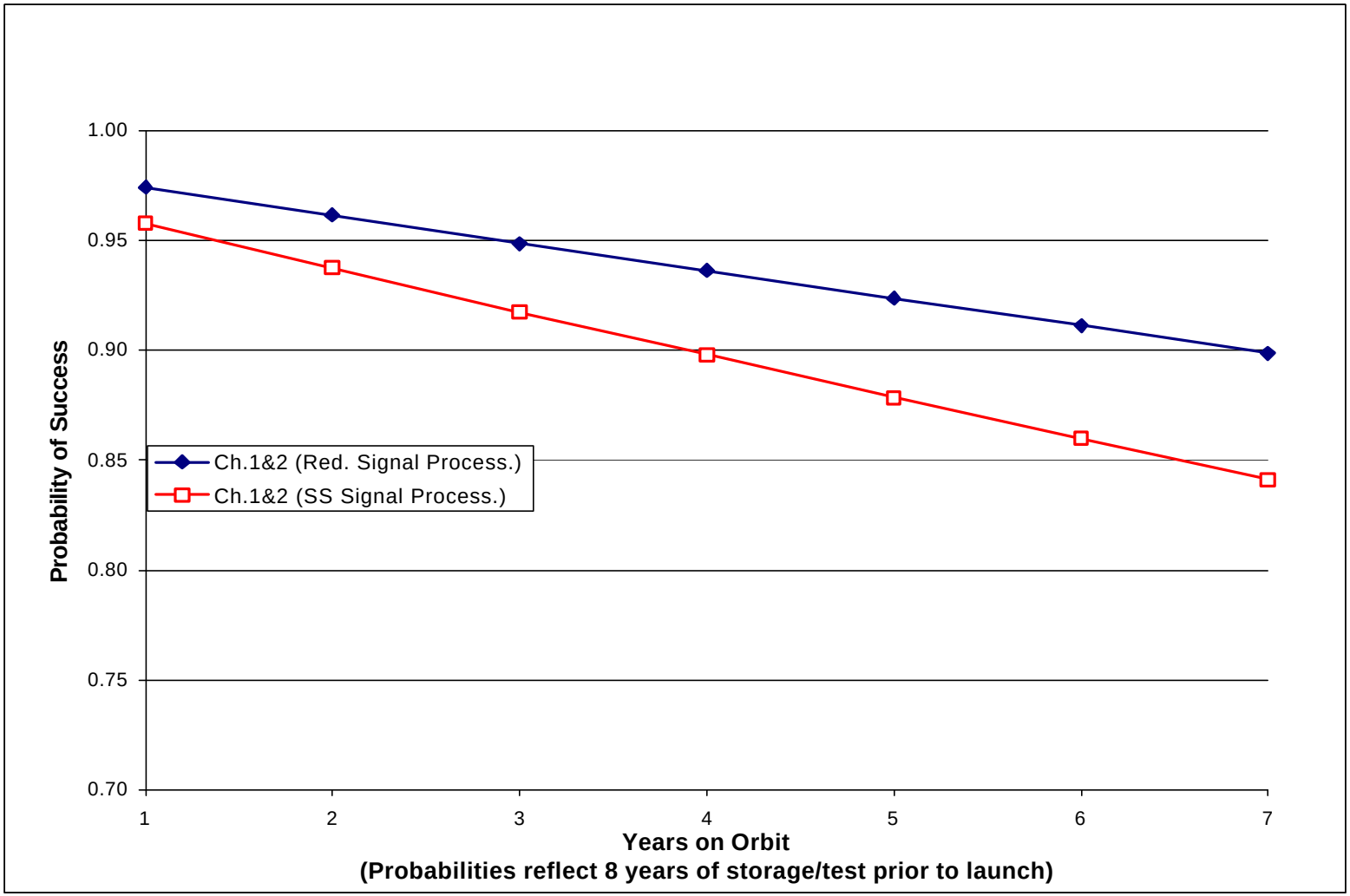

Figure 5–50. Channels 1 and 2 Reliability Plot with Single String and Redundant Signal Processing

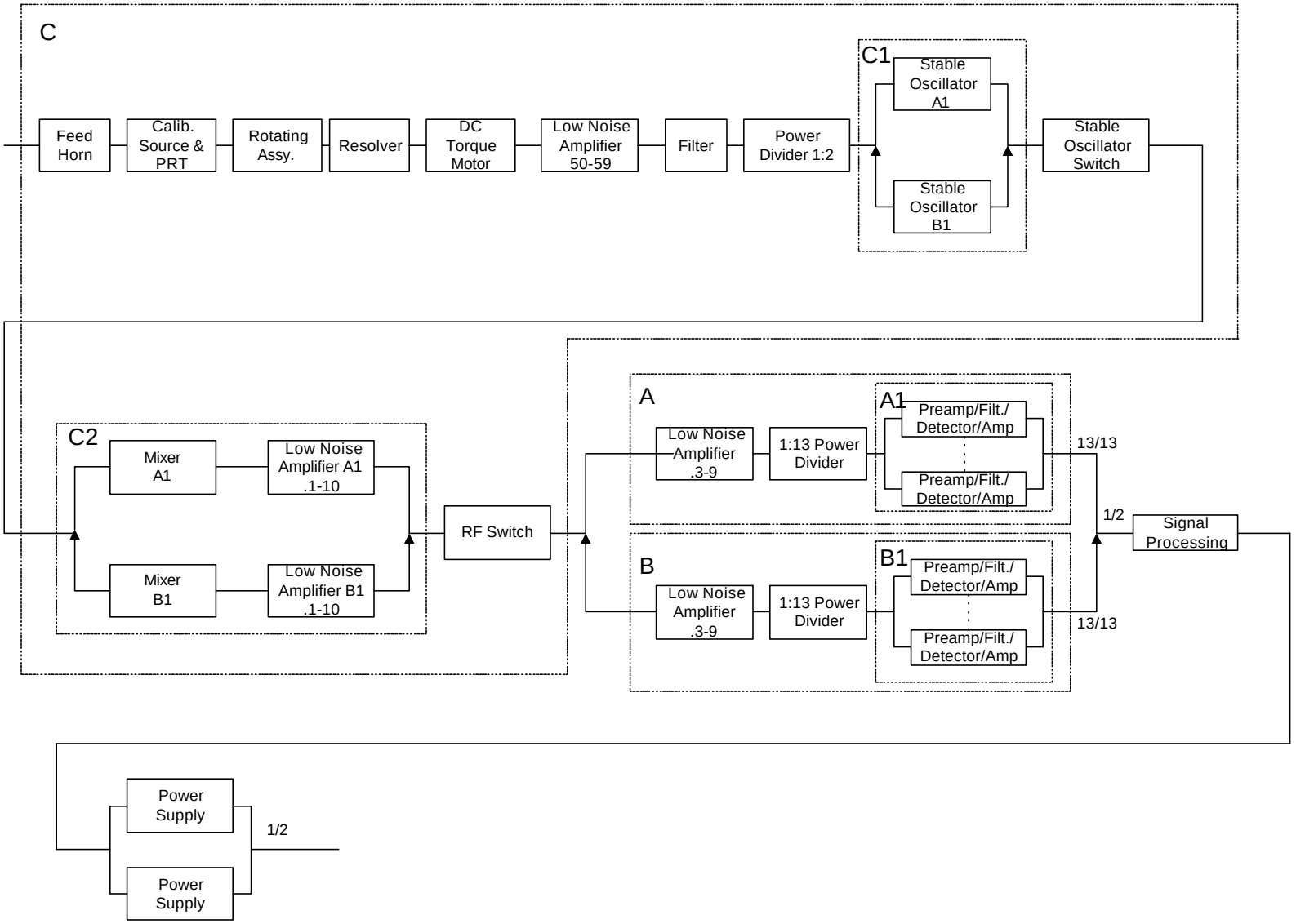

Figure 5-51. ATMS Channels 3 to 15 Reliability Block Diagram

Table 5-7. Channels 3-15 Failure Rates Data and Reliability Calculations

Component	F/R x10^{-6}	1	2	3	4	5	6	7	Ground
Feed Horn	0.001	0.999984	0.999975	0.999967	0.999958	0.999949	0.999940	0.999932	0.999993
Calibration Source & PRT	0.008	0.999874	0.999804	0.999734	0.999664	0.999594	0.999524	0.999454	0.999944
Rotating Assembly	0.15	0.997638	0.996328	0.995019	0.993713	0.992408	0.991105	0.989803	0.998949
Resolve	0.00713	0.999888	0.999825	0.999763	0.999700	0.999638	0.999575	0.999513	0.999950
Dual Winding DC Torque Motor	0.15735	0.997522	0.996148	0.994776	0.993406	0.992037	0.990671	0.989306	0.998898
Single Winding DC Torque Motor	0.2098	0.996697	0.994867	0.993041	0.991217	0.989397	0.987580	0.985767	0.998531
Power Divider	0.0175	0.999724	0.999571	0.999418	0.999264	0.999111	0.998958	0.998805	0.999877
Filter	0.03807	0.999400	0.999067	0.998734	0.998401	0.998068	0.997735	0.997402	0.999733
Mixer	0.02374	0.999626	0.999418	0.999210	0.999002	0.998795	0.998587	0.998379	0.999834
Low Noise Amplifier (50-59)	0.31608	0.995028	0.992277	0.989533	0.986797	0.984069	0.981348	0.978634	0.997787
Low Noise Amplifier (.1-10))	0.31608	0.995028	0.992277	0.989533	0.986797	0.984069	0.981348	0.978634	0.997787
Low Noise Amplifier (1-8)	0.31608	0.995028	0.992277	0.989533	0.986797	0.984069	0.981348	0.978634	0.997787
LNA Filter (0-250 mhz)	0.03807	0.999400	0.999067	0.998734	0.998401	0.998068	0.997735	0.997402	0.999733
DRO Oscillator (10)	0.026	0.999590	0.999362	0.999135	0.998907	0.998680	0.998452	0.998225	0.999818
Component	F/R x10^{-6}	1	2	3	4	5	6	7	
Stable Oscillator (50.1)	0.02600	0.999590	0.999362	0.999135	0.998907	0.998680	0.998452	0.998225	0.999818
Stable Oscillator Switch	0.02125	0.999665	0.999479	0.999293	0.999107	0.998921	0.998735	0.998549	0.999851
DRO Oscillator Switch	0.02125	0.999665	0.999479	0.999293	0.999107	0.998921	0.998735	0.998549	0.999851
RF Switch	0.02125	0.999665	0.999479	0.999293	0.999107	0.998921	0.998735	0.998549	0.999851
Preamplifier/Filter/Detector	0.12490	0.998033	0.996941	0.995851	0.994762	0.993674	0.992588	0.991502	0.999125
Redundant Signal Processing		0.995807	0.995119	0.994381	0.993592	0.992754	0.991867	0.990932	
Single String Signal Processing		0.979158	0.970348	0.961618	0.952966	0.944393	0.935896	0.927476	
Redundant Power Supplies		0.999889	0.999734	0.999513	0.999227	0.998878	0.998466	0.997994	
Standby Stab. Osc.Group C1		1.000000	1.000000	0.999999	0.999999	0.999998	0.999998	0.999997	
Standby Mixer/Amp Group C2		0.999971	0.999931	0.999873	0.999799	0.999707	0.999598	0.999473	
Single String Series Group C		0.987069	0.979957	0.972897	0.965887	0.958928	0.952019	0.945160	
Series Group C		0.988408	0.982002	0.975621	0.969264	0.962932	0.956626	0.950344	
Channels A3-A15 Group A1 (13)		13	0.974722	0.960957	0.947385	0.934005	0.920814	0.907810	0.894989
Channels B3-B15 Group B1 (13)		13	0.974722	0.960957	0.947385	0.934005	0.920814	0.907810	0.894989
	Group A		0.969609	0.953126	0.936923	0.920996	0.905339	0.889949	0.874820
	Group B		0.969609	0.953126	0.936923	0.920996	0.905339	0.889949	0.874820

Table 5-7. Channels 3-15 Failure Rates and Reliability Calculations (continued)

Component	Req'd Channels	1	2	3	4	5	6	7
Channels 3-15, 13 of 13		0.983246	0.974802	0.965807	0.956302	0.946326	0.935916	0.925110
Channels 3-15 SS, 13 of 13		0.937019	0.906086	0.876116	0.847083	0.818959	0.791720	0.765340
Channels 3-15 SS, 13 of 13, Red. Sig. Proc.		0.952952	0.929216	0.905966	0.883194	0.860898	0.839069	0.817704
Channels A3-A15 Group A1 (13)	11	0.999998	0.999992	0.999980	0.999960	0.999931	0.999890	0.999835
Channels B3-B15 Group B1 (13)	11	0.999998	0.999992	0.999980	0.999960	0.999931	0.999890	0.999835
Group A		0.994752	0.991843	0.988938	0.986033	0.983126	0.980217	0.977304
Group B		0.994752	0.991843	0.988938	0.986033	0.983126	0.980217	0.977304
Channels 3-15, 11 of 13		0.984128	0.976884	0.969547	0.962121	0.954610	0.947019	0.939353
Channels 3-15 SS, 11 of 13		0.961317	0.942892	0.924755	0.906900	0.889325	0.872025	0.854999
Channels 3-15 SS, 11 of 13, Red. Sig. Proc		0.977663	0.966963	0.956261	0.945562	0.934866	0.924177	0.913497
Channels A3-A15 Group A1 (13)	10	1.000000	1.000000	1.000000	0.999999	0.999999	0.999998	0.999996
Channels B3-B15 Group B1 (13)	10	1.000000	1.000000	1.000000	0.999999	0.999999	0.999998	0.999996
Group A		0.994754	0.991851	0.988957	0.986071	0.983193	0.980323	0.977462
Group B		0.994754	0.991851	0.988957	0.986071	0.983193	0.980323	0.977462
Channels 3-15, any 10 of 13		0.984128	0.976884	0.969547	0.962122	0.954612	0.947023	0.939360
Channels 3-15 SS, any 10 of 13		0.961319	0.942900	0.924773	0.906935	0.889385	0.872120	0.855136
Channels 3-15 SS, any 10 of 13, RSP		0.977665	0.966970	0.956280	0.945599	0.934930	0.924277	0.913644
Channels 3-15 SS, 10 of 13, with #6 & #7 OK		0.961061	0.942526	0.924290	0.906349	0.888702	0.871345	0.854276
Channels 3-15 SS, 10 of 13 with #6 & #7 OK,RSP		0.977403	0.966587	0.955781	0.944988	0.934212	0.923456	0.912725
Prob. that 2 failed channels are #6 & #7		0.000269	0.000397	0.000522	0.000646	0.000768	0.000888	0.001006

Note: Single string (SS) calculations include redundant power supplies dual winding motor, non-redundant oscillators, non-redundant channels, and non-redundant signal processing. RSP = Redundant Signal Processing

** Equivalent ground time is the time that the instrument is in storage and undergoing tests. The 8 years is divided by 10 which is equivalent to dividing all failure rates by 10. This is the standard reduction in failure rate used under non-operating conditions.

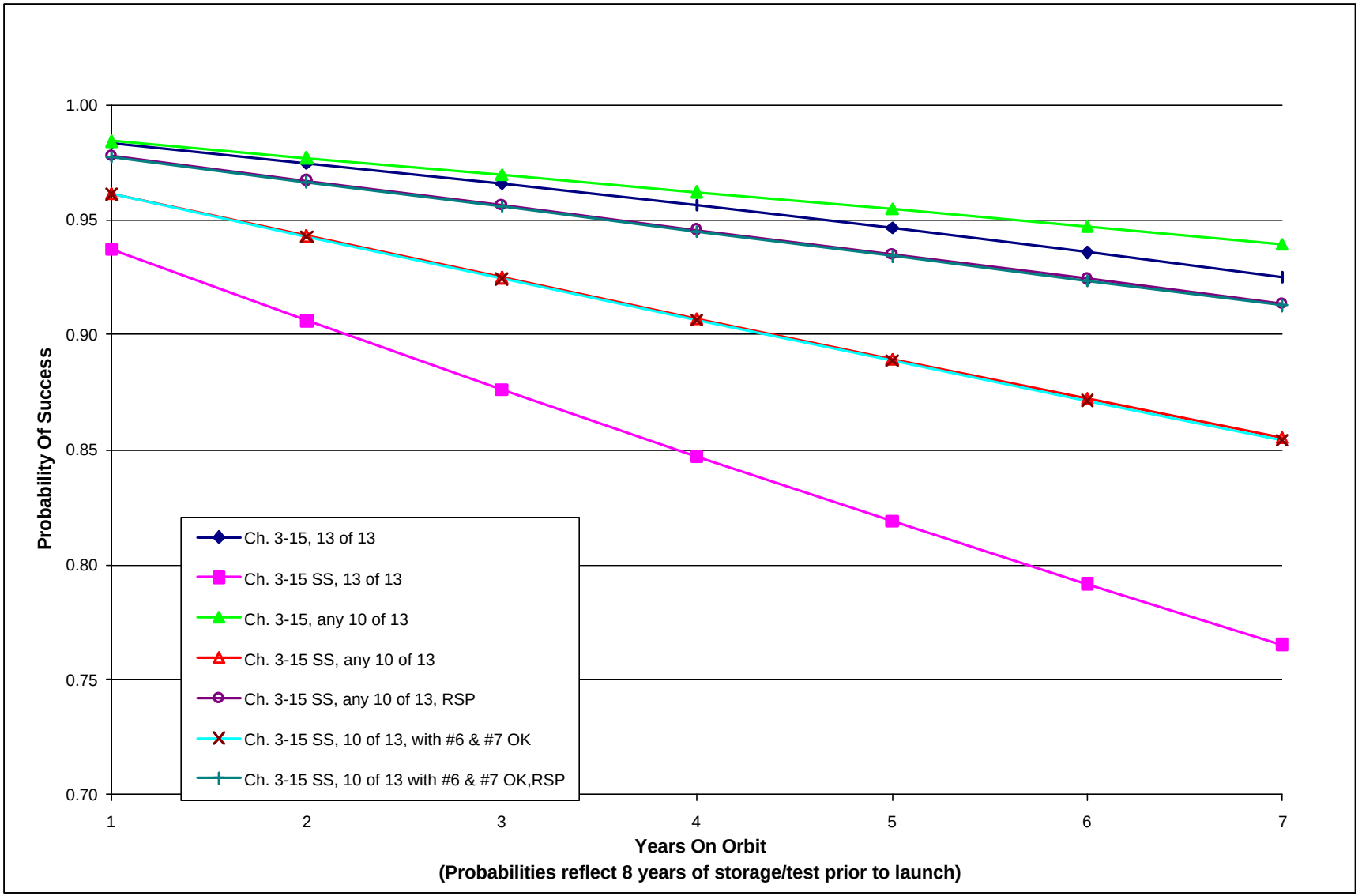

Figure 5-52. Channels 3-15 Reliability Plot With Single String and Redundant Channels

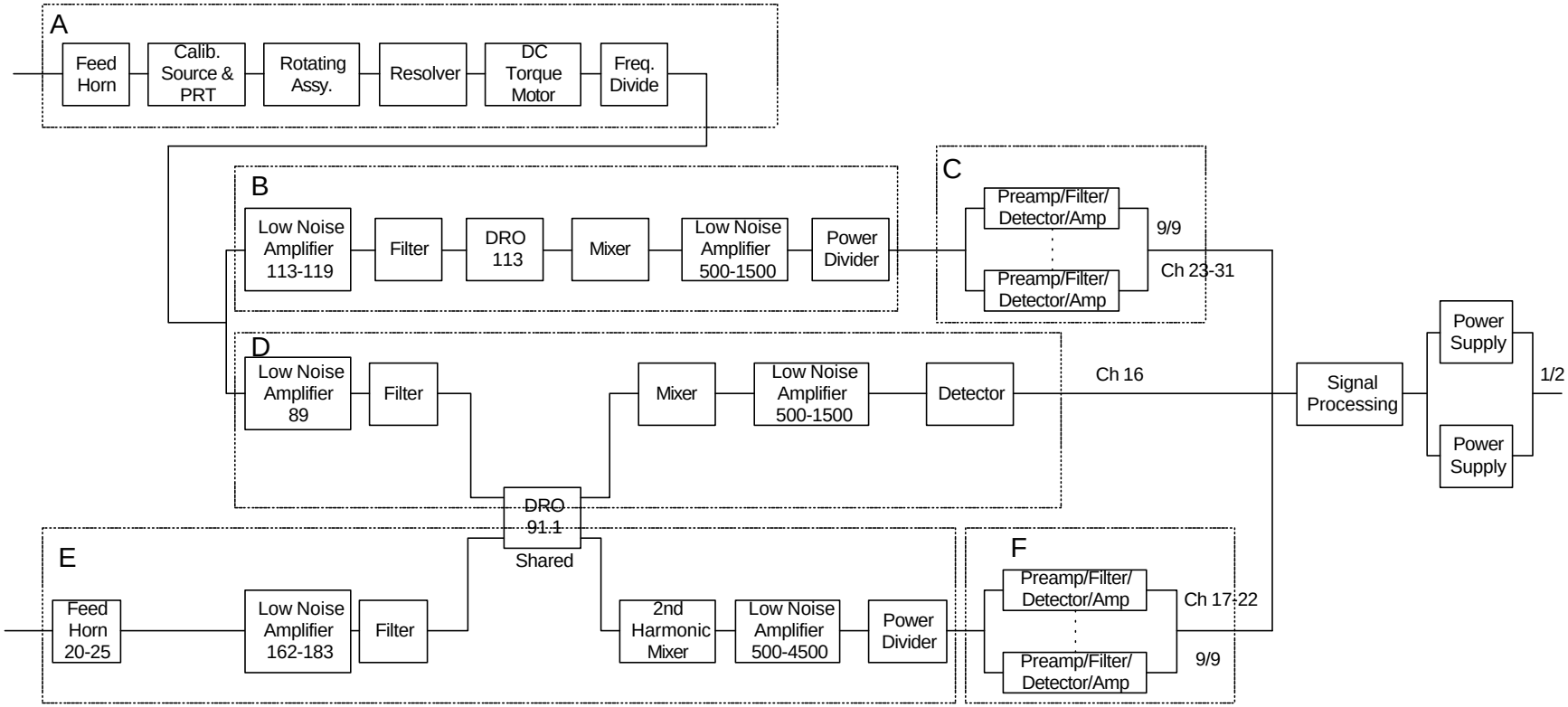

Figure 5-53. ATMS Channels 16, 17 to 22, and 23 to 31 Reliability Block Diagram

Table 5-8. Channels 16 – 22 and 23 – 31 Failure Rates and Reliability Calculations

Component	F/R x10^{-6}	1	2	3	4	5	6	7	Ground
Feed Horn	0.001	0.999984	0.999975	0.999967	0.999958	0.999949	0.999940	0.999932	0.999993
Calibration Source & PRT	0.008	0.999874	0.999804	0.999734	0.999664	0.999594	0.999524	0.999454	0.999944
Rotating Assembly	0.15	0.997638	0.996328	0.995019	0.993713	0.992408	0.991105	0.989803	0.998949
Resolver	0.00713	0.999888	0.999825	0.999763	0.999700	0.999638	0.999575	0.999513	0.999950
Dual Winding DC Torque Motor	0.15735	0.997522	0.996148	0.994776	0.993406	0.992037	0.990671	0.989306	0.998898
Single Winding DC Torque Motor	0.2098	0.996697	0.994867	0.993041	0.991217	0.989397	0.987580	0.985767	0.998531
Frequency Divider	0.0175	0.999724	0.999571	0.999418	0.999264	0.999111	0.998958	0.998805	0.999877
RF Switch	0.02125	0.999665	0.999479	0.999293	0.999107	0.998921	0.998735	0.998549	0.999851
Filter	0.35415	0.994431	0.991351	0.988280	0.985219	0.982167	0.979125	0.976092	0.997521
DRO Selector Switch	0.02125	0.999665	0.999479	0.999293	0.999107	0.998921	0.998735	0.998549	0.999851
1/2 DRO Selector Switch	0.010625	0.999832	0.999739	0.999646	0.999553	0.999460	0.999367	0.999274	0.999926
DRO Oscillator (113)	0.1213	0.998089	0.997029	0.995970	0.994913	0.993856	0.992800	0.991746	0.999150
DRO Oscillator (91.1)	0.1213	0.998089	0.997029	0.995970	0.994913	0.993856	0.992800	0.991746	0.999150
Redundant DRO Oscillators		0.999996	0.999991	0.999984	0.999974	0.999962	0.999948	0.999932	

Component	F/R x10^{-6}	1	2	3	4	5	6	7	
Low Noise Amplifier (89)	0.31608	0.995028	0.992277	0.989533	0.986797	0.984069	0.981348	0.978634	0.997787
Low Noise Amplifier (113-119)	0.31608	0.995028	0.992277	0.989533	0.986797	0.984069	0.981348	0.978634	0.997787
Low Noise Amplifier (162-183)	0.31608	0.995028	0.992277	0.989533	0.986797	0.984069	0.981348	0.978634	0.997787
Low Noise Amplifier (500-4500)	0.31608	0.995028	0.992277	0.989533	0.986797	0.984069	0.981348	0.978634	0.997787
2nd Harmonic Mixer	0.02374	0.999626	0.999418	0.999210	0.999002	0.998795	0.998587	0.998379	0.999834
Redundant 2nd Harmonic Mixers		1.000000	1.000000	0.999999	0.999999	0.999999	0.999998	0.999997	
Mixer	0.02374	0.999626	0.999418	0.999210	0.999002	0.998795	0.998587	0.998379	0.999834
RF Detector	0.00259	0.999959	0.999936	0.999914	0.999891	0.999868	0.999846	0.999823	0.999982
Preamplifier/Filter/Detector	0.1249	0.998033	0.996941	0.995851	0.994762	0.993674	0.992588	0.991502	0.999125
Signal Processing		0.995807	0.995119	0.994381	0.993592	0.992754	0.991867	0.990932	
Single String Signal Processing		0.979158	0.970348	0.961618	0.952966	0.944393	0.935896	0.927476	
Redundant Power Supplies		0.999889	0.999734	0.999513	0.999227	0.998878	0.998466	0.997994	

Table 5-8. Channels 16 – 22 and 23 – 31 Failure Rates and Reliability Calculations (continued)

Component	Req'd. Channels	1	2	3	4	5	6	7
Group A		0.994638	0.991671	0.988714	0.985765	0.982825	0.979893	0.976971
Group B		0.982048	0.972214	0.962479	0.952841	0.943300	0.933854	0.924503
Group C	9	0.982431	0.972805	0.963272	0.953833	0.944487	0.935232	0.926068
Group D		0.978160	0.967823	0.957546	0.947329	0.937175	0.927083	0.917054
Group E		0.982033	0.972190	0.962447	0.952801	0.943252	0.933799	0.924440
Group F	9	0.982431	0.972805	0.963272	0.953833	0.944487	0.935232	0.926068
Channels. 16 only		0.968728	0.954824	0.940960	0.927143	0.913378	0.899672	0.886030
Channels. 16 only, SS Sig Proc		0.952532	0.931056	0.909957	0.889234	0.868883	0.848903	0.829291
Ch.17-22 only		0.960628	0.940885	0.921440	0.902292	0.883442	0.864888	0.846630
Ch.17-22 only, SS Sig Proc		0.944567	0.917464	0.891080	0.865399	0.840405	0.816082	0.792414
Ch.23-31 only		0.955492	0.933072	0.911070	0.889485	0.868312	0.847548	0.827189
Ch.23-31 only, SS Sig Proc		0.939517	0.909845	0.881052	0.853116	0.826013	0.799721	0.774218

** Equivalent ground time is the time that the instrument is in storage and undergoing tests. The 8 years is divided by 10, which is equivalent to dividing all failure rates by 10. This is the standard reduction in failure rate used under non-operating conditions.

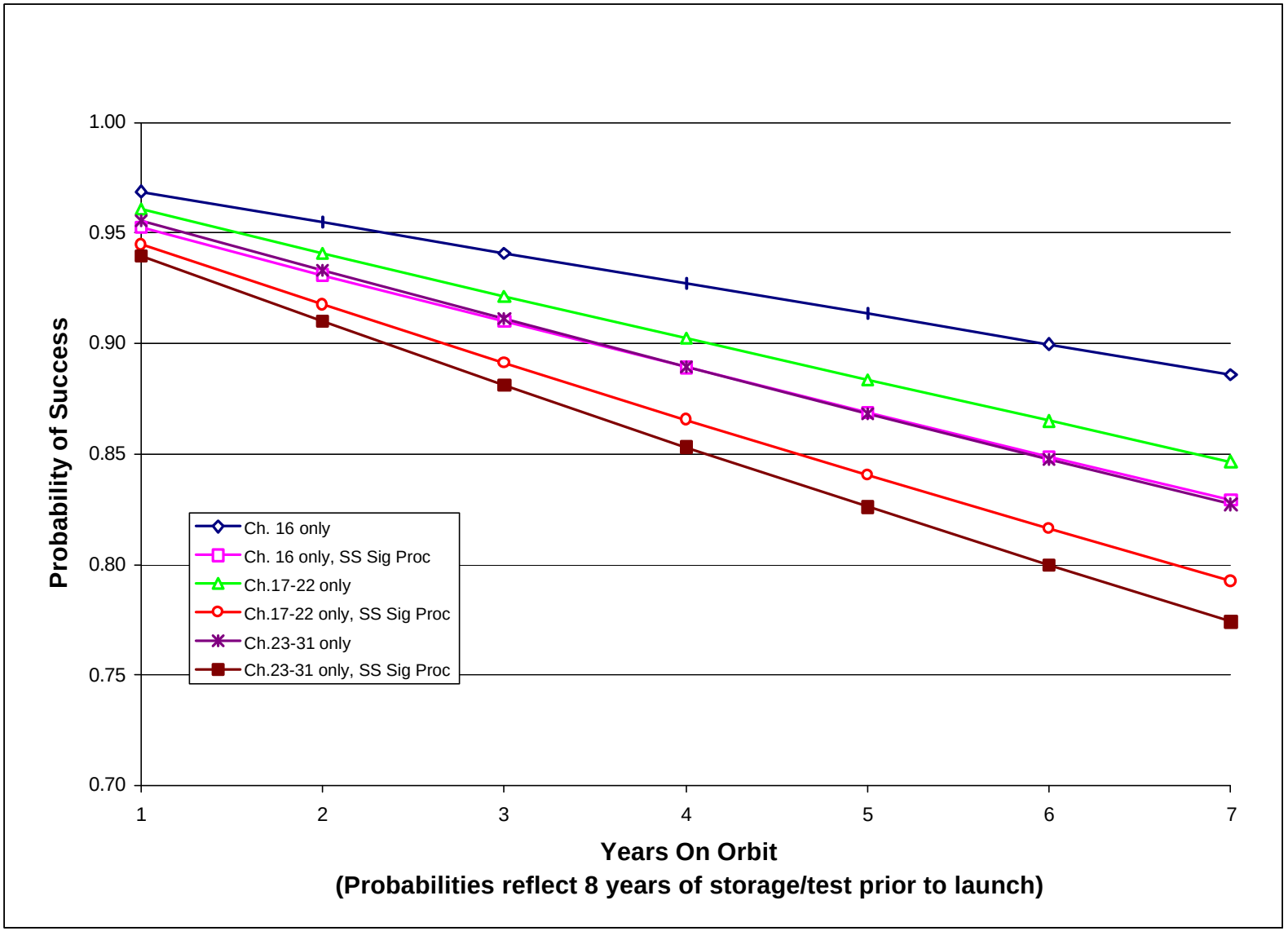

Figure 5-54. Channels 16 – 22 and 23 – 31 Reliability Plot with Single String and Redundant Signal Processing

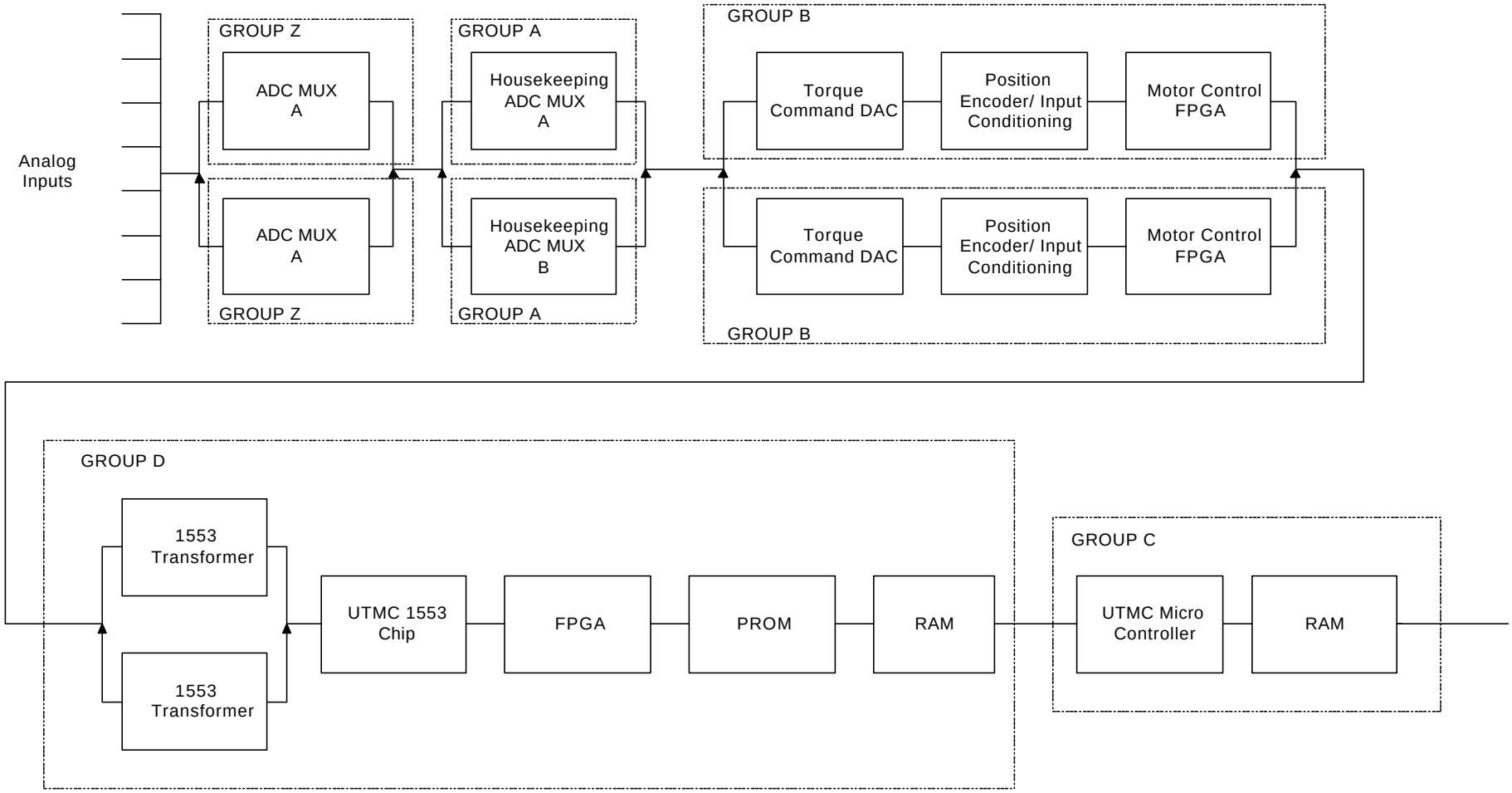

Figure 5-55. ATMS Signal Processing

Table 5-9. Signal Processing Failure Rates and Reliability Calculations

	F/R	Qty.	Tot. F/R	1	2	3	4	5	6	7
Temp. PRT ADC (Group A) SS			0.5046	0.992075	0.987699	0.983343	0.979006	0.974688	0.970389	0.966109
Redundant Groups A				0.999937	0.999849	0.999723	0.999559	0.999359	0.999123	0.998851
12 bit ADC	0.0046	1	0.0046							
Op. Amp	0.0095	2	0.019							
MUX Chips	0.017	18	0.306							
Resistors	0.0018	50	0.09							
Capacitors	0.0017	50	0.085							
Motor Controller Part of (Group B) SS			0.2266	0.994494	0.992522	0.990554	0.988589	0.986629	0.984672	0.98272
Redundant Groups B				0.99997	0.999944	0.999911	0.99987	0.999821	0.999765	0.999701
ACTEL FPGA	0.0046	1	0.0046							
12 Bit DAC	0.0046	1	0.0046							
Power FET	0.0069	6	0.0414							
Resistors	0.0018	60	0.108							
Diodes	0.0014	30	0.042							
Transformer	0.026	1	0.026							
Micro-controller (Group C)			0.0642	0.99591	0.99535	0.99479	0.994231	0.993672	0.993113	0.992555
UTMC Controller	0.0046	1	0.0046							
512K EEPROM	0.012	1	0.012							
1MB SRAM	0.043	1	0.043							
ACTEL FPGA	0.0046	1	0.0046							
1553 Interface (Group D)				0.999696	0.999393	0.999091	0.998789	0.998488	0.998186	0.997884
1554 Interface (Group D) SS				0.9997	0.999401	0.999102	0.998802	0.998503	0.998204	0.997905
Technitrol transformer	0.00031	1	0.00031	0.999995	0.999992	0.99999	0.999987	0.999984	0.999982	0.999979
Redundant Technitrol transformer	0.00031			1	1	1	1	1	1	1
UTMC Summit chip	0.0046	1	0.0046	0.999919	0.999839	0.999758	0.999678	0.999597	0.999517	0.999436
ACTEL FPGA	0.0046	1	0.0046	0.999919	0.999839	0.999758	0.999678	0.999597	0.999517	0.999436
16K SRAM	0.0079	2	0.0158	0.999862	0.999723	0.999585	0.999447	0.999308	0.99917	0.999032
Science Data ADC (Group Z) SS			0.2021	0.996818	0.995055	0.993295	0.991538	0.989784	0.988033	0.986286
Redundant Groups Z				0.99999	0.999976	0.999955	0.999928	0.999896	0.999857	0.999812
16 bit ADC	0.0046	1	0.0046							
Op Amp	0.0095	1	0.0095							

Table 5-9. Signal Processing Failure Rates and Reliability Calculations (continued)

MUX Chip	0.017	9	0.153							
Resistor	0.0018	10	0.018							
Capacitor	0.0017	10	0.017							
Signal Processing (Redundant)				0.995807	0.995119	0.994381	0.993592	0.992754	0.991867	0.990932
Signal Processing (Single String)				0.979158	0.970348	0.961618	0.952966	0.944393	0.935896	0.927476

6.0 INSTRUMENT RESOURCE DATABASE

6.1 TOTAL RESOURCES VERSUS OPTIONS

Table 6-1 presents the strawman resources as a function of the four configurations that were studied. Theses resources were used by NASA's Resource Analysis Office (RAO) as the basis of its cost estimate.

Table 6-1. Resource Requirements for the Four Strawman Configurations

	SCIENCE Channels	MASS kg	POWER watts	DATA kbps	L x H x W cm
Comparable AMSU Science	22	64	66	17	70 x 60 x 40
Descope Option #1	21	63	63	16	70 x 60 x 40
Descope Option #2	19	50	60	15	70 x 40 x 40
Enhanced Science	31	67	76	23	70 x 60 x 40

Revised 3/10/99:
- **New packaging concept allows the use of one scan motor for all configurations.**
- **RF shelf weights adjusted based on AMSU-A.**
- **Power for motors adjusted based on MHS and AMSU-A.**
- **DC/DC efficiency @ 75%**

6.2 DATA RATES

6.2.1 Data Rate Description

Science data from the ATMS is provided via a 1553 data bus. The bus data rate must be defined so the spacecraft data storage can be sized.

6.2.2 Calculation of Data Rates

Requirements for the calculation are based on derived requirements that evolved during the strawman instrument development. A scan is a period of 8/3 seconds or 2.67 seconds per revolution. The number of Earth-scan views is 96 at 1.1 degrees spatial resolution across a 106.5-degree Earth-look field-of-view. One scanner motor requires one encoder for position telemetry and each channel requires a minimum of two hot and two cold calibration looks per scan. The number of channels is dependent on the option. A 16-bit A/D is used as a worst case. Overhead for Consultative Committee for Space Data Systems (CCSDS) packaging of the data was quantified at 25%. Table 6-2 presents the requirements and resulting calculations for data rates of the four ATMS instrument options.

Table 6-2. Data Rates

	Enhanced Science	Comparable Science	Descope Option #1	Descope Option #2
Earth Looks/Scan	96	96	96	96
Cold Cal/Scan	2	2	2	2
Warm Cal/Scan	2	2	2	2
Total Data Samples/Scan	104	104	104	104
Time/Scan	2.67	2.67	2.67	2.67
Science Channels	31	22	21	19
Position Encoder Channels	1	1	1	1
Total Channels	32	23	22	20
Total Samples/Scan	3,328.0	2,392.0	2,288.0	2,080.0
A/D Bits	16	16	16	16
Total Bits/Scan	53,248	38,240	36,608	33,280
Bit/Sec	19,968	14,340	13,728	12,480
KBPS	20.0	14.3	13.7	12.5
CCSDS @ 15%	22.9	16.5	15.8	14.3
Rounded to Next Highest KBPS	23	17	16	15

6.3 RESOURCE DATABASE TABLES

This section presents the Excel database that was used to quantify instrument resources for the ATMS strawman configurations. In the interest of brevity only the databases for the **enhanced** and **comparable** science instrument options are presented.

6.3.1 Comparable Science

The three tables in this section delineate the resource requirements for the Comparable Science Strawman Option configuration. Table 6-3 details the major subsystem components with their corresponding mass, power, and volume requirements. Table 6-3 also tabulates the total instrument resource requirements by adding the individual requirements of all the subsystems including the LOW and HIGH-Frequency receivers that are detailed in Tables 6-4 and 6-5, respectively. Details in each table are self explanatory with the exception of the “r” in the left column. The “r” means that a component is redundant and, as such, is not powered on and, therefore, has no power requirement; but its mass and volume are added to the core requirements.

Table 6-3. Data Rate Description

	Summary of ALL Needed Resources								
COMPONENT	**Freq**	**Size**				Ribs	**Mass**	**PWR**	**VOL**
		L	W	H	Skin	Fill			
	GHz	cm	cm	cm	cm	%	gms	Watts	cm^3
23-50 Reflector		21	30Dia				500		14837
89-193 Reflector		15	21Dia				350		5193
Dual Motor Drive		6	18Dia				8190	5.0	1526
Compensator		6	18Dia				2000	5.0	1526
D/C Converter		20	10	5			2200	16.6	1000
D/C Converter		20	10	5			2200		1000
Electronics									
Digital		20	20	5			455	10.0	2000
Motor Drive		10	10	5			200	2.0	500
Harness							4550		
23-50 Warm Load			20.5Dia	6			3200		1979
Mount							350		
89-193 Warm Load			14.2Dia	5			1685		791
Mount							300		
Chasssis									
Baseplate		70	40	2	0.4	20%	0		5600
Outer Right		60	40	2	0.4	10%	0		4800
Outer Left		60	40	2	0.4	10%	0		4800
Top Right		40	25	2	0.4	10%	0		2000
Top Left		39	40	2	0.4	10%	0		3120
Front Right		24	40	1	0.4	10%	0		960
Middle Front		47	30	1	0.4	10%	0		1410
Left Front		38	40	1	0.4	10%	0		1520
Right Rear		24	40	1	0.4	10%	0		960
Middle Rear		47	30	1	0.4	10%	0		1410
Left Rear		38	40	1	0.4	10%	0		1520
1RF Shelf		70	40	0.5	0.2	10%	0		1400
1RF Shelf		70	40	0.5	0.2	10%	0		1400
Motor Mount							1100		300
Brackets							2275		3000
Conformal Coating							2275		
LOW Frequency Receiver Subtotals							0	0.0	0
HIGH Frequency Receiver Subtotals							0	0.0	0
TOTAL RESOURCES							**31830**	**38.6**	**64552**

FIGURE Of MERIT:

Packing Factor 0.38

Table 6-4. Comparable Science LOW-Frequency Receiver Requirements

	Channel 1					Channel 2					Channels 3-14				
COMPONENT	**Freq**	**Size**	**Mass**	**PWR**	**VOL**	**Freq**	**Size**	**Mass**	**PWR**	**VOL**	**Freq**	**Size**	**Mass**	**PWR**	**VOL**
	GHz	L W H cm cm cm	gms	Watts	cm^3	GHz	L W H cm cm cm	gms	Watts	cm^3	GHz	L W H cm cm cm	gms	Watts	cm^3
Beam Splitter 1.5		20 20 1	500		400		share CH 1					share CH 1			
FeedHorn		19 6Dia 2	150		537		Share CH 1					9 4Dia 2	150		113
Frequency Splitter		4 4 2	50		32		Share CH 1								
LNA	23	5 3 2	100	1	30	32	5 3 2	100	1	30					
Filter		8 4 2	200		128		8 4 2	200		128					
Filter		8 4 2	200		128		8 4 2	200		128					
LNA	23	5 3 2	50	0.5	30	32	5 3 2	50	0.5	30					
Filter	0.27	8 4 2	200		128	0.18	8 4 2	200		128					
Detector		5 2 2	20		20		5 2 2	20		20					
Video Amp	23	5 3 2	50	0.5	30	32	5 3 2	50	0.5	30					
LNA											50-59	10 5 2	200	2	100
Filter												8 4 2	100		64
r PWR Divider 2:1												4 3 2	50		24

Table 6-4. Comparable Science LOW-Frequency Receiver Requirements (continued)

	Channel 1						Channel 2						Channels 3-14					
COMPONENT	**Freq**	**Size**			**Mass**	**PWR**	**VOL**	**Freq**	**Size**			**Mass**	**PWR**	**VOL**	**Freq**	**Size**			**Mass**	**PWR**	**VOL**
	GHz	L cm	W cm	H cm	gms	Watts	cm^3	GHz	L cm	W cm	H cm	gms	Watts	cm^3	GHz	L cm	W cm	H cm	gms	Watts	cm^3
Mixer A-1																6	6	4	100	0.1	144
Stable Oscillator A-1															60	10	8	8	1,000	10	640
r Stable Oscillator B-1															60	18	8	8	1,000		1152
r Stable Osc. Switch																4	4	4	25		64
LNA A-1															.1-10	10	5	2	150	1	100
r RF Switch (A or B)																3	4	2	50		24
Frequency Splitter A																3	4	2	50		24
LNA A-2															.1-10	5	3	2	100	1	30
Power Divider A 1:13																10	4	5	200		200
Channel 3																					
Amplifer																4	4	2	50	0.2	32
Filter																8	4	2	100		64
Detector																5	2	2	50		20
Channel 4																					
Amplifer																4	4	2	50	0.2	32
Filter																8	4	2	100		64
Detector																5	2	2	50		20
Channel 4A																					
Amplifer																4	4	2	50	0.2	32
Filter																8	4	2	100		64
Detector																5	2	2	50		20

Table 6-4. Comparable Science LOW-Frequency Receiver Requirements (continued)

	Channel 1						Channel 2						Channels 3-14					
COMPONENT	**Freq**	**Size**			**Mass**	**PWR**	**VOL**	**Freq**	**Size**			**Mass**	**PWR**	**VOL**	**Freq**	**Size**			**Mass**	**PWR**	**VOL**
		L	W	H					L	W	H					L	W	H			
	GHz	cm	cm	cm	gms	Watts	cm^3	GHz	cm	cm	cm	gms	Watts	cm^3	GHz	cm	cm	cm	gms	Watts	cm^3
Channel 5																					
Amplifer																4	4	2	50	0.2	32
Filter																8	4	2	100		64
Detector																5	2	2	50		20
Channel 6																					
Amplifer																4	4	2	50	0.2	32
Filter																8	4	2	100		64
Detector																5	2	2	50		20
Channel 7																					
Amplifer																4	4	2	50	0.2	32
Filter																8	4	2	100		64
Detector																5	2	2	50		20
Channel 8																					
Amplifer																4	4	2	50	0.2	32
Filter																8	4	2	100		64
Detector																5	2	2	50		20
Channel 9																					
Amplifer																4	4	2	50	0.2	32
Filter																8	4	2	100		64
Detector																5	2	2	50		20
Channel 10																					
Amplifer																4	4	2	50	0.2	32
Filter																8	4	2	100		64
Detector																5	2	2	50		20
Channel 11																					
Amplifer																4	4	2	50	0.2	32
SAW Filter																8	4	2	100		64
Detector																5	2	2	50		20
Amplifer																4	4	2	50	0.2	32

Table 6-4. Comparable Science LOW-Frequency Receiver Requirements (continued)

	Channel 1						Channel 2						Channels 3-14					
COMPONENT	**Freq**	**Size**			**Mass**	**PWR**	**VOL**	**Freq**	**Size**			**Mass**	**PWR**	**VOL**	**Freq**	**Size**			**Mass**	**PWR**	**VOL**
	GHz	L cm	W cm	H cm	gms	Watts	cm^3	GHz	L cm	W cm	H cm	gms	Watts	cm^3	GHz	L cm	W cm	H cm	gms	Watts	cm^3
Channel 12																					
Amplifer																4	4	2	50	0.2	32
SAW Filter																8	4	2	100		64
Detector																5	2	2	50		20
Amplifer																4	4	2	50	0.2	32
Channel 13																					
Amplifer																4	4	2	50	0.2	32
SAW Filter																8	4	2	100		64
Detector																5	2	2	50		20
Amplifer																4	4	2	50	0.2	32
Channel 14																					
Amplifer																4	4	2	50	0.2	32
SAW Filter																8	4	2	100		64
Detector																5	2	2	50		20
Amplifer																4	4	2	50	0.2	32
r LNA B-2															.1-10	10	5	2	150		100
r Power Divider B 1:13																10	4	5	200		200
Channel 3																					
r Amplifer																4	4	2	50		32
r Filter																8	4	2	100		64
r Detector																5	2	2	50		20
Channel 4																					
r Amplifer																4	4	2	50		32
r Filter																8	4	2	100		64
r Detector																5	2	2	50		20
Channel 4A																					

Table 6-4. Comparable Science LOW-Frequency Receiver Requirements (continued)

	Channel 1						Channel 2						Channels 3-14					
COMPONENT	**Freq**	**Size**			**Mass**	**PWR**	**VOL**	**Freq**	**Size**			**Mass**	**PWR**	**VOL**	**Freq**	**Size**			**Mass**	**PWR**	**VOL**
		L	W	H					L	W	H					L	W	H			
	GHz	cm	cm	cm	gms	Watts	cm^3	GHz	cm	cm	cm	gms	Watts	cm^3	GHz	cm	cm	cm	gms	Watts	cm^3
r Amplifer																4	4	2	50		32
r Filter																8	4	2	100		64
r Detector																5	2	2	50		20
Channel 5																					
r Amplifer																4	4	2	50		32
r Filter																8	4	2	100		64
r Detector																5	2	2	50		20
Channel 6																					
r Amplifer																4	4	2	50		32
r Filter																8	4	2	100		64
r Detector																5	2	2	50		20
Channel 7																					
r Amplifer																4	4	2	50		32
r Filter																8	4	2	100		64
r Detector																5	2	2	50		20
Channel 8																					
r Amplifer																4	4	2	50		32
r Filter																8	4	2	100		64
r Detector																5	2	2	50		20
Channel 9																					
r Amplifer																4	4	2	50		32
r Filter																8	4	2	100		64
r Detector																5	2	2	50		20
Channel 10																					
r Amplifer																4	4	2	50		32
r Filter																8	4	2	100		64
r Detector																5	2	2	50		20
Channel 11																					
r Amplifer																4	4	2	50		32

Table 6-4. Comparable Science Low-Frequency Receiver Requirements (continued)

	Channel 1						Channel 2						Channels 3-14					
COMPONENT	**Freq**	**Size**			**Mass**	**PWR**	**VOL**	**Freq**	**Size**			**Mass**	**PWR**	**VOL**	**Freq**	**Size**			**Mass**	**PWR**	**VOL**
	GHz	L cm	W cm	H cm	gms	Watts	cm^3	GHz	L cm	W cm	H cm	gms	Watts	cm^3	GHz	L cm	W cm	H cm	gms	Watts	cm^3
r SAW Filter																8	4	2	100		64
r Detector																5	2	2	50		20
r Amplifer																4	4	2	50		32
Channel 12																					
r Amplifer																4	4	2	50		32
r SAW Filter																8	4	2	100		64
r Detector																5	2	2	50		20
r Amplifer																4	4	2	50		32
Channel 13																					
r Amplifer																4	4	2	50		32
r SAW Filter																8	4	2	100		64
r Detector																5	2	2	50		20
r Amplifer																4	4	2	50		32
Channel 14																					
r Amplifer																4	4	2	50		32
r SAW Filter																8	4	2	100		64
r Detector																5	2	2	50		20
r Amplifer																4	4	2	50		32
Mounting Plate																					
TOTAL					**1,520**	**2**	**1463**					**820**	**2**	**494**					**9,125**	**17.5**	**6251**
Subtotal LOW Frequency Receiver					**11,465**	**21.5**	**8207.98**														

Table 6-5. Comparable Science HIGH-Frequency Receiver Resource Requirements

	Channel 16							Channels 17-22						
COMPONENT	**Freq**	**Size**			**Mass**	**PWR**	**VOL**	**Freq**	**Size**			**Mass**	**PWR**	**VOL**
	GHz	L cm	W cm	H cm	gms	Watts	cm^3	GHz	L cm	W cm	H cm	gms	Watts	cm^3
Beam Splitter		14	14	1	500		196		14	14	1	500		196
FeedHorn		9	3Dia	1	150		64		4	2Dia	1	150		13
Frequency Divider		4	3	2	50		24							
LNA	89	5	3	2	100	0.6	30	162-183	5	3	2	100	0.6	60
Filter		8	4	2	200		128							
LNA A	500-1500	5	3	2	50	0.5		500-4500	5	3	2	50	0.5	60
Detector	CH-16A	5	2	2	50	0.1								
DRO A	91.1	8	5	5	80	3								
r DRO B	91.1	8	5	5	80									
r DRO Selector	91.1	4	4	4	25									
Power Divider A								1:6	10	4	5	200		400
Channel								17A						
Amplifer									4	4	2	50	0.2	64
Filter									8	4	2	100		128
Detector									5	2	2	50		40
Channel								18A						
Amplifer									4	4	2	50	0.2	64
Filter									8	4	2	100		128
Detector									5	2	2	50		40

Table 6-5. Comparable Science HIGH-Frequency Receiver Resource Requirements (continued)

	Channel 16						Channels 17-22						
COMPONENT	**Freq**	**Size**			**Mass**	**PWR**	**VOL**	**Freq**	**Size**			**Mass**	**PWR**	**VOL**
		L	W	H					L	W	H			
	GHz	cm	cm	cm	gms	Watts	cm^3	GHz	cm	cm	cm	gms	Watts	cm^3
Channel								19A						
Detector									5	2	2	50		40
Channel								20A						
Amplifer									4	4	2	50	0.2	64
Filter									8	4	2	100		128
Detector									5	2	2	50		40
Channel								21A						
Amplifer									4	4	2	50	0.2	64
Filter									8	4	2	100		128
Detector									5	2	2	50		40
Channel								22A						
Amplifer									4	4	2	50	0.2	64
Filter									8	4	2	100		128
Detector									5	2	2	50		40
Channel														
Amplifer														
Filter														
Detector														
Channel														
Amplifer														
Filter														
Detector														
Channel														
Amplifer														
Filter														
Detector														
Mounting Plate														
Subtotal Hi Frequency Receiver					**1,285**	**4.2**	**442**					**2050**	**2.1**	**1929**

6.3.2 Enhanced Science

The three tables in this section delineate the resource requirements for the Enhanced Science Strawman Option configuration. Table 6-6 details the major subsystem components with their corresponding mass, power, and volume requirements. Table 6-6 also tabulates the total instrument resource requirements by adding the individual requirements of all the subsystems including the LOW and HIGH-Frequency receivers that are detailed in Tables 6-7 and 6-8, respectively. Details in each table are self explanatory with the exception of the "r" in the left column. The "r" means that a component is redundant and, as such, is not powered on and, therefore, has no power requirement; but its mass and volume are added to the core requirements.

Table 6-6. Enhanced Science Total Resource Requirements

COMPONENT	Freq	Size				Ribs	Mass	PWR	VOL
		L	W	H	Skin	Fill			
	GHz	cm	cm	cm	cm	%	gms	Watts	cm^3
23-50 Reflector		21	30Dia				500		14837
89-193 Reflector		15	21Dia				350		5193
Dual Motor Drive		6	18Dia				8190	5.0	1526
Compensator		6	18Dia				2000	5.0	1526
D/C Converter		20	10	5			2200	18.9	1000
D/C Converter		20	10	5			2200		1000
Electronics									
Digital		20	20	5			455	10.0	2000
Motor Drive		10	10	5			200	2.0	500
Harness							4550		
23-50 Warm Load			20.5Dia	6			3200		1979
Mount							350		
89-193 Warm Load			14.2Dia	5			1685		791
Mount							300		
Chasssis									
Baseplate		70	40	2	0.4	20%	0		5600
Outer Right		60	40	2	0.4	10%	0		4800
Outer Left		60	40	2	0.4	10%	0		4800
Top Right		40	25	2	0.4	10%	0		2000
Top Left		39	40	2	0.4	10%	0		3120
Front Right		24	40	1	0.4	10%	0		960
Middle Front		47	30	1	0.4	10%	0		1410
Left Front		38	40	1	0.4	10%	0		1520
Right Rear		24	40	1	0.4	10%	0		960
Middle Rear		47	30	1	0.4	10%	0		1410
Left Rear		38	40	1	0.4	10%	0		1520
1RF Shelf		70	40	0.5	0.2	10%	0		1400
1RF Shelf		70	40	0.5	0.2	10%	0		1400
Motor Mount							1100		1400
Brackets							2275		1400
									300
Conformal Coating							2275		3000
LOW Frequency Receiver Subtotals							11,765	23	8,412
HIGH Frequency Receiver Subtotals							5,870	13	6,750
TOTAL RESOURCES							**66972**	**76.1**	**82514**

FIGURE Of MERIT:
Packing Factor 0.49

Table 6-7. Enhanced Science LOW-Frequency Receiver Resource Requirements

	Channel 1							Channel 2							Channels 3-15						
COMPONENT	**Freq**	**Size**			**Mass**	**PWR**	**VOL**	**Freq**	**Size**			**Mass**	**PWR**	**VOL**	**Freq**	**Size**			**Mass**	**PWR**	**VOL**
	GHz	L cm	W cm	H cm	gms	Watts	cm^3	GHz	L cm	W cm	H cm	gms	Watts	cm^3	GHz	L cm	W cm	H cm	gms	Watts	cm^3
Beam Splitter		20	20	1	500		400		share CH 1							share CH 1					
FeedHorn		19	6Dia	2	150		537		Share CH 1							9	4Dia	2	150		113
Frequency Splitter		4	4	2	50		32		Share CH 1												
LNA	23	5	3	2	100	1	30	32	5	3	2	100	1	30							
Filter		8	4	2	200		128		8	4	2	200		128							
LNA	23	5	3	2	100	0.5	30	32	5	3	2	100	0.5	30							
Filter		8	4	2	200		128		8	4	2	200		128							
LNA	23	5	3	2	50	0.5	30	32	5	3	2	50	0.5	30							
Filter	0.27	8	4	2	200		128	0.18	8	4	2	200		128							
Detector		5	2	2	20		20		5	2	2	20		20							
Video Amp	23	5	3	2	50	0.5	30	32	5	3	2	50	0.5	30							
LNA															50-59	10	5	2	200	2	100
Filter																8	4	2	100		64

Table 6-7. Enhanced Science LOW-Frequency Receiver Resource Requirements (continued)

	Channel 1						Channel 2						Channels 3-15					
COMPONENT	**Freq**	**Size**			**Mass**	**PWR**	**VOL**	**Freq**	**Size**			**Mass**	**PWR**	**VOL**	**Freq**	**Size**			**Mass**	**PWR**	**VOL**
	GHz	L cm	W cm	H cm	gms	Watts	cm^3	GHz	L cm	W cm	H cm	gms	Watts	cm^3	GHz	L cm	W cm	H cm	gms	Watts	cm^3
r PWR Divider 2:1																4	3	2	50		24
Mixer A-1																6	6	4	100	0.1	144
Stable Oscillator A-1															60	10	8	8	1,000	10	640
r Mixer B-1																6	6	4	100		144
r Stable Oscillator B-1															60	18	8	8	1,000		1152
r Stable Osc. Switch																4	4	4	25		64
LNA A-1															.1-10	10	5	2	150	1	100
r RF Switch (A or B)																3	4	2	50		24
Frequency Splitter A																3	4	2	50		24
LNA A-2															.1-10	5	3	2	100	1	30
Power Divider A 1:13																10	4	5	200		200
Channel 3																					
Amplifer																4	4	2	50	0.2	32
Filter																8	4	2	100		64
Detector																5	2	2	50		20
Channel 4																					
Amplifer																4	4	2	50	0.2	32
Filter																8	4	2	100		64

Table 6-7. Enhanced Science LOW-Frequency Receiver Resource Requirements (continued)

	Channel 1						Channel 2						Channels 3-15					
COMPONENT	**Freq**	**Size**			**Mass**	**PWR**	**VOL**	**Freq**	**Size**			**Mass**	**PWR**	**VOL**	**Freq**	**Size**			**Mass**	**PWR**	**VOL**
	GHz	L cm	W cm	H cm	gms	Watts	cm^3	GHz	L cm	W cm	H cm	gms	Watts	cm^3	GHz	L cm	W cm	H cm	gms	Watts	cm^3
Detector																5	2	2	50		20
Channel 5																					
Amplifer																4	4	2	50	0.2	32
Filter																8	4	2	100		64
Detector																5	2	2	50		20
Channel 5																					
Amplifer																4	4	2	50	0.2	32
Filter																8	4	2	100		64
Detector																5	2	2	50		20
Channel 6																					
Amplifer																4	4	2	50	0.2	32
Filter																8	4	2	100		64
Detector																5	2	2	50		20
Channel 7																					
Amplifer																4	4	2	50	0.2	32
Filter																8	4	2	100		64
Detector																5	2	2	50		20
Channel 8																					
Amplifer																4	4	2	50	0.2	32
Filter																8	4	2	100		64
Detector																5	2	2	50		20
Channel 9																					
Amplifer																4	4	2	50	0.2	32
Filter																8	4	2	100		64
Detector																5	2	2	50		20
Channel 10																					
Amplifer																4	4	2	50	0.2	32
Filter																8	4	2	100		64
Detector																5	2	2	50		20

Table 6-7. Enhanced Science LOW-Frequency Receiver Resource Requirements (continued)

	Channel 1						Channel 2						Channels 3-15					
COMPONENT	**Freq**	**Size**			**Mass**	**PWR**	**VOL**	**Freq**	**Size**			**Mass**	**PWR**	**VOL**	**Freq**	**Size**			**Mass**	**PWR**	**VOL**
	GHz	L cm	W cm	H cm	gms	Watts	cm^3	GHz	L cm	W cm	H cm	gms	Watts	cm^3	GHz	L cm	W cm	H cm	gms	Watts	cm^3
Channel 11																					
Amplifer																4	4	2	50	0.2	32
SAW Filter																8	4	2	100		64
Detector																5	2	2	50		20
Amplifer																4	4	2	50	0.2	32
Channel 12																					
Amplifer																4	4	2	50	0.2	32
SAW Filter																8	4	2	100		64
Detector																5	2	2	50		20
Amplifer																4	4	2	50	0.2	32
Channel 13																					
Amplifer																4	4	2	50	0.2	32
SAW Filter																8	4	2	100		64
Detector																5	2	2	50		20
Amplifer																4	4	2	50	0.2	32
Channel 14																					
Amplifer																4	4	2	50	0.2	32
SAW Filter																8	4	2	100		64
Detector																5	2	2	50		20
Amplifer																4	4	2	50	0.2	32
r LNA B-2															.1-10	10	5	2	150		100
r Power Divider B 1:13																10	4	5	200		200
Channel 3																					
r Amplifer																4	4	2	50		32
r Filter																8	4	2	100		64
r Detector																5	2	2	50		20

Table 6-7. Enhanced Science LOW-Frequency Receiver Resource Requirements (continued)

	Channel 1							Channel 2							Channels 3-15						
COMPONENT	**Freq**	**Size**			**Mass**	**PWR**	**VOL**	**Freq**	**Size**			**Mass**	**PWR**	**VOL**	**Freq**	**Size**			**Mass**	**PWR**	**VOL**
	GHz	L cm	W cm	H cm	gms	Watts	cm^3	GHz	L cm	W cm	H cm	gms	Watts	cm^3	GHz	L cm	W cm	H cm	gms	Watts	cm^3
r Filter																8	4	2	100		64
r Detector																5	2	2	50		20
Channel 7																					
r Amplifer																4	4	2	50		32
r Filter																8	4	2	100		64
r Detector																5	2	2	50		20
Channel 8																					
r Amplifer																4	4	2	50		32
r Filter																8	4	2	100		64
r Detector																5	2	2	50		20
Channel 9																					
r Amplifer																4	4	2	50		32
r Filter																8	4	2	100		64
r Detector																5	2	2	50		20
Channel 10																					
r Amplifer																4	4	2	50		32
r Filter																8	4	2	100		64
r Detector																5	2	2	50		20
Channel 11																					
r Amplifer																4	4	2	50		32
r SAW Filter																8	4	2	100		64
r Detector																5	2	2	50		20
r Amplifer																4	4	2	50		32
Channel 12																					
r Amplifer																4	4	2	50		32
r SAW Filter																8	4	2	100		64
r Detector																5	2	2	50		20
r Amplifer																4	4	2	50		32
Channel 13																					

Table 6-7. Enhanced Science LOW-Frequency Receiver Resource Requirements (continued)

	Channel 1							Channel 2							Channels 3-15						
COMPONENT	**Freq**	**Size**			**Mass**	**PWR**	**VOL**	**Freq**	**Size**			**Mass**	**PWR**	**VOL**	**Freq**	**Size**			**Mass**	**PWR**	**VOL**
	GHz	L cm	W cm	H cm	gms	Watts	cm^3	GHz	L cm	W cm	H cm	gms	Watts	cm^3	GHz	L cm	W cm	H cm	gms	Watts	cm^3
r Amplifer																4	4	2	50		32
r Filter																8	4	2	100		64
r Detector																5	2	2	50		20
Channel 11																					
r Amplifer																4	4	2	50		32
r SAW Filter																8	4	2	100		64
r Detector																5	2	2	50		20
r Amplifer																4	4	2	50		32
Channel 12																					
r Amplifer																4	4	2	50		32
r SAW Filter																8	4	2	100		64
r Detector																5	2	2	50		20
r Amplifer																4	4	2	50		32
Channel 13																					
r Amplifer																4	4	2	50		32
r SAW Filter																8	4	2	100		64
r Detector																5	2	2	50		20
r Amplifer																4	4	2	50		32
Channel 14																					
r Amplifer																4	4	2	50		32
r SAW Filter																8	4	2	100		64
r Detector																5	2	2	50		20
r Amplifer																4	4	2	50		32
Mounting Plate																					
TOTAL					**1,620**	**2.5**	**1493**					**920**	**2.5**	**524**					**9,225**	**17.5**	**6395**
Subtotal LOW Frequency Receiver					**11,765**	**22.5**	**8411.98**														

Table 6-8. Enhanced Science HIGH-Frequency Receiver Resource Requirements

	Channel 16						Channel 23-31						Channels 17-22					
COMPONENT	Freq	Size			Mass	PWR	VOL	Freq	Size			Mass	PWR	VOL	Freq	Size			Mass	PWR	VOL
	GHz	L cm	W cm	H cm	gms	Watts	cm^3	GHz	L cm	W cm	H cm	gms	Watts	cm^3	GHz	L cm	W cm	H cm	gms	Watts	cm^3
Beam Splitter		14	14	1	500		196		share CH 16							share CH 16					
FeedHorn		9	3Dia	1	150		64		Share CH 16							4	2Dia	1	150		13
Frequency Divider		4	3	2	50		24		Share CH 16												
LNA	89	5	3	2	100	0.6	30	113-119	5	3	2	100	0.6	60	162-183	5	3	2	100	0.6	60
Filter		8	4	2	200		128		8	4	2	200		128							
Mixer A		6	6	4	100	0.1	144		6	6	4	100	0.1	288		6	6	4	100	0.1	288
LNA A	500-1500	5	3	2	50	0.5		500-1500	5	3	2	100	0.5	60	500-4500	5	3	2	50	0.5	60
Detector	CH-A19	5	2	2	50	0.1															
DRO A	91.1	8	5	5	80	3		113	8	5	5	80	3	400							
r DRO B	91.1	8	5	5	80			113	8	5	5	80		400							
r DRO Selector	91.1	4	4	4	25			113	4	4	4	25		128							
Power Divider A								1:9	10	4	5	200		400	1:6	10	4	5	200		400
Channel								23A							17A						
Amplifer									4	4	2	50	0.2	64		4	4	2	50	0.2	64
Filter									8	4	2	100		128		8	4	2	100		128
Detector									5	2	2	50		40		5	2	2	50		40
Channel								245A							18A						
Amplifer									4	4	2	50	0.2	64		4	4	2	50	0.2	64
Filter									8	4	2	100		128		8	4	2	100		128
Detector									5	2	2	50		40		5	2	2	50		40
Channel								25A							19A						
Amplifer									4	4	2	50	0.2	64		4	4	2	50	0.2	64
Filter									8	4	2	100		128		8	4	2	100		128
Detector									5	2	2	50		40		5	2	2	50		40
Channel								26A							20A						
Amplifer									4	4	2	50	0.2	64		4	4	2	50	0.2	64
Filter									8	4	2	100		128		8	4	2	100		128
Detector									5	2	2	50		40		5	2	2	50		40
Channel								27A							21A						
Amplifer									4	4	2	50	0.2	64		4	4	2	50	0.2	64
Filter									8	4	2	100		128		8	4	2	100		128
Detector									5	2	2	50		40		5	2	2	50		40

Table 6-8. Enhanced Science HIGH-Frequency Receiver Resource Requirement (continued)

	Channel 16						Channel 23-31						Channels 17-22					
COMPONENT	**Freq**	**Size**			**Mass**	**PWR**	**VOL**	**Freq**	**Size**			**Mass**	**PWR**	**VOL**	**Freq**	**Size**			**Mass**	**PWR**	**VOL**
	GHz	L cm	W cm	H cm	gms	Watts	cm^3	GHz	L cm	W cm	H cm	gms	Watts	cm^3	GHz	L cm	W cm	H cm	gms	Watts	cm^3
Channel								28A							22A						
Amplifer									4	4	2	50	0.2	64		4	4	2	50	0.2	64
Filter									8	4	2	100		128		8	4	2	100		128
Detector									5	2	2	50		40		5	2	2	50		40
Channel								29A													
Amplifer									4	4	2	50	0.2	64							
Filter									8	4	2	100		128							
Detector									5	2	2	50		40							
Channel								30A													
Amplifer									4	4	2	50	0.2	64							
Filter									8	4	2	100		128							
Detector									5	2	2	50		40							
Channel								31A													
Amplifer									4	4	2	50	0.2	64							
Filter									8	4	2	100		128							
Detector									5	2	2	50		40							
Mounting Plate																					
Subtotal Hi Frequency Receiver					**1,385**	**4.3**	**586**					**2,685**	**6**	**3952**					**1800**	**2.4**	**2213**
Grand Totals (With Options)					**5,870**	**12.7**	**6750.145**														
Grand Totals with Options(this sheet)					**3,185**	**7**	**2,798**														
		OPTION DELTA			**2,685**	**6**	**3,952**														

7.0. COST ESTIMATION METHODS

Three independent methods were used to prepare the cost estimates for the implementation of the ATMS instrument configuration. This section describes the costing methods, but the cost estimates themselves are not included. The Feasibility Study Team prepared two of the cost estimates. The Chief Financial Office at GSFC generated the third type of cost estimate. A comparison of the three independent cost estimation methods is presented in Section 7.4.

Four different instrument configurations were costed: the baseline ATMS, with the same (**comparable)** science capability as the AMSU-A/MHS; two **descoped options** of the ATMS instrument; and one ATMS configuration with **enhanced science** capability compared to the AMSU-A/MHS. The baseline instrument configuration was costed using each method. The parametric cost model was run separately for each of the four configurations based on their weight, power, and data rate. In the other two costing methods, a complexity multiplier was applied to the baseline instrument cost estimate to derive the costs of the different configurations. For example, Descope Option #2 was costed as 0.85 of the baseline cost in the grassroots method.

All cost methods used the same ATMS development schedule. The key milestones include: the beginning of the Formulation Phase contracts in October 1999, the beginning of the Implementation Phase contract in February 2001, and the delivery of the protoflight unit to the NPP in June 2004.

7.1 AMSU-A ANALOGY

The costs of the AMSU-A development are fully known within the POES Project, which managed the development of the AMSU-A. This method of cost estimation compared the ATMS to the AMSU-A, which is the predecessor instrument to the ATMS and performs the same temperature measurements. Adjustments were made to account for the different number of instruments, the addition of the moisture channels, inflation, fee, technology, and development time. Contingency was applied.

7.2 PARAMETRIC MODELING

The GSFC Office of the Deputy Chief Financial Officer (Parametrics), formerly called the Resource Analysis Office (RAO), performed cost estimation for the ATMS implementation phase. This office maintains an instrument development cost estimation model that is continuously refined with historical instrument development cost data. Inputs to the model include instrument type, weight, power, data rate, and lifetime requirements. The model produces cost ranges for varying development times. The ATMS was modeled in the radiometer instrument family. A low-range estimate and a high-range estimate were prepared based on 36-month and 48-month development times, which encompassed the planned ATMS 40-month development time.

The RAO model accounted for the use of new technology in ATMS by applying a Technology Readiness Level (TRL). The TRLs for the four configurations varied from two (technology concept and/or application formulated) to three (analytical and experimental critical function and/or characteristic proof-of-concept). Weight and power margins were applied. Contingency was applied.

7.3 GRASSROOTS

The grassroots estimate is a "bottom up" cost estimation method that accounts for all labor and material needed to design, develop, and test an ATMS engineering unit and protoflight unit. A work breakdown structure was developed to identify all required engineering, manufacturing, business, and management elements. Costs were estimated in hours by labor category. An average, composite, fully burdened hourly labor rate, derived from potential ATMS vendors was applied. Material estimates were made based on current AMSU-A production cost of "build materials," adjusted as needed for ATMS. Travel costs were estimated assuming a U.S. West Coast contractor. Fee was applied. The costs were escalated by 3% annually for inflation. Contingency was applied.

7.4 RECONCILIATION

The results of the three cost estimates were compared. The analogy method is the coarsest of the estimates and merely constitutes a reasonableness check. The parametric modeling approach is heavily dependent on the historical database of instrument costs and the similarity of the instrument being costed to previous instruments. The technology aspects of the ATMS were addressed in the parametric modeling approach by applying a technology readiness factor. The grassroots estimate is the most accurate since it is a detailed, "bottom up" estimate based on the design developed during the study. The grassroots estimate was carried forward as the budget submittal.

8.0 CAD MODELS OF FINAL INSTRUMENT CONFIGURATIONS

The figures within this section present actual CAD models that the Study Team used to understand the effects of the optional configurations. The figures comprise a viewgraph presentation. It shows how the receiver circuits and their corresponding components change from the Enhanced Science version, to the Comparable Science version, to Descope Option #1 (deletion of the 89-GHz Channel), and concluding with Descope Option #2 (deletion of the 23- and 32-GHz Channels).

Figures 8-1 through 8-10 present the packaging and receiver circuits for the base strawman design that was the Enhanced Science Option.

Figures 8-11 and 8-12 depict the deletion of the 113- to 119-GHz channels, which converts the Enhanced Science strawman configuration into the Comparable Science configuration.

Figures 8-13 and 8-14 depict the deletion of the 89-GHz channel (Descope Option #1), which yields less science than the Comparable Science.

Figures 8-15 and 8-16 depict the deletion of the 23- and 32-GHz channels (Descope Option #2), which yields the least science of all the studied configurations.

The final Figure 8-17 shows the core 50- to 59-GHz component layout.

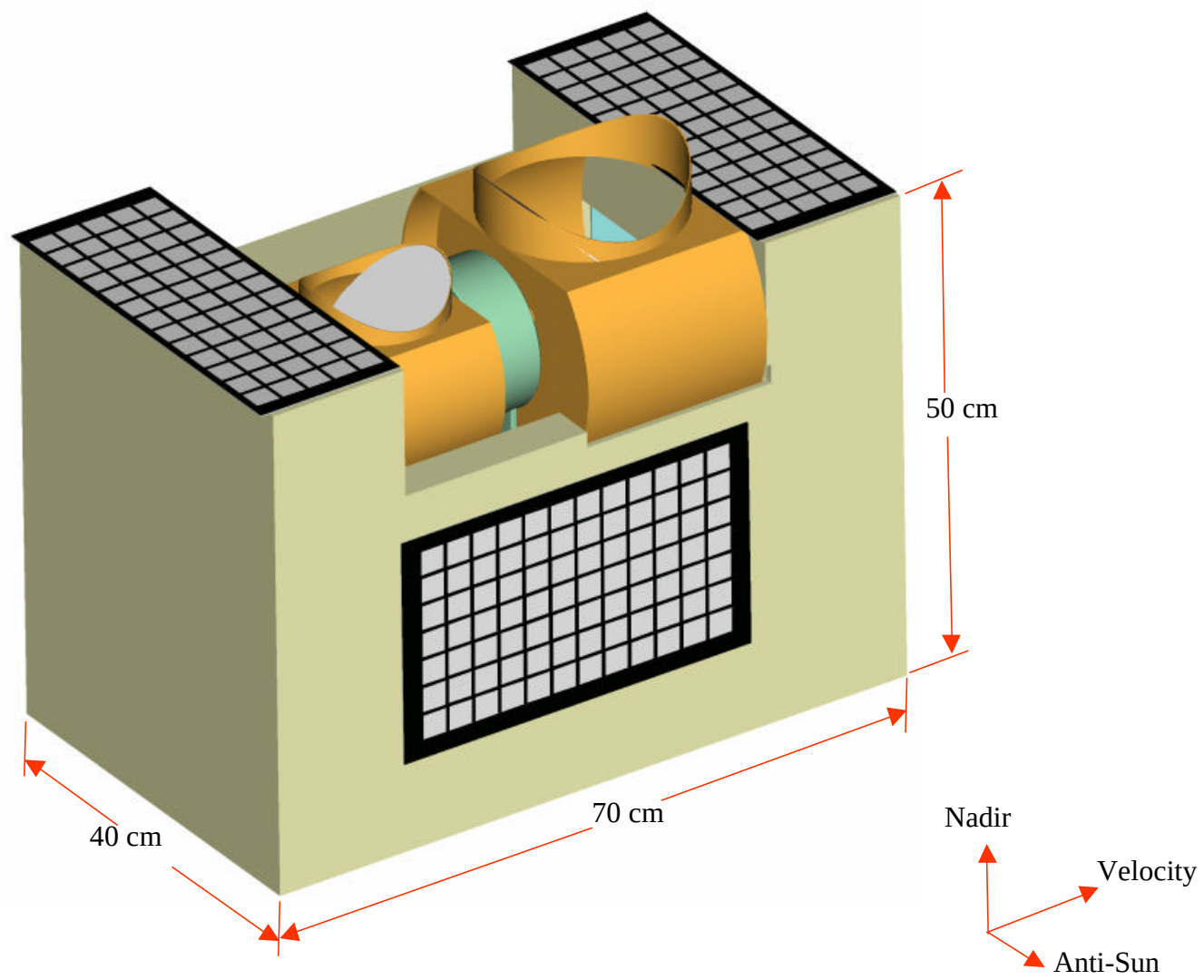

Figure 8-1. Enhanced Science Option Configuration

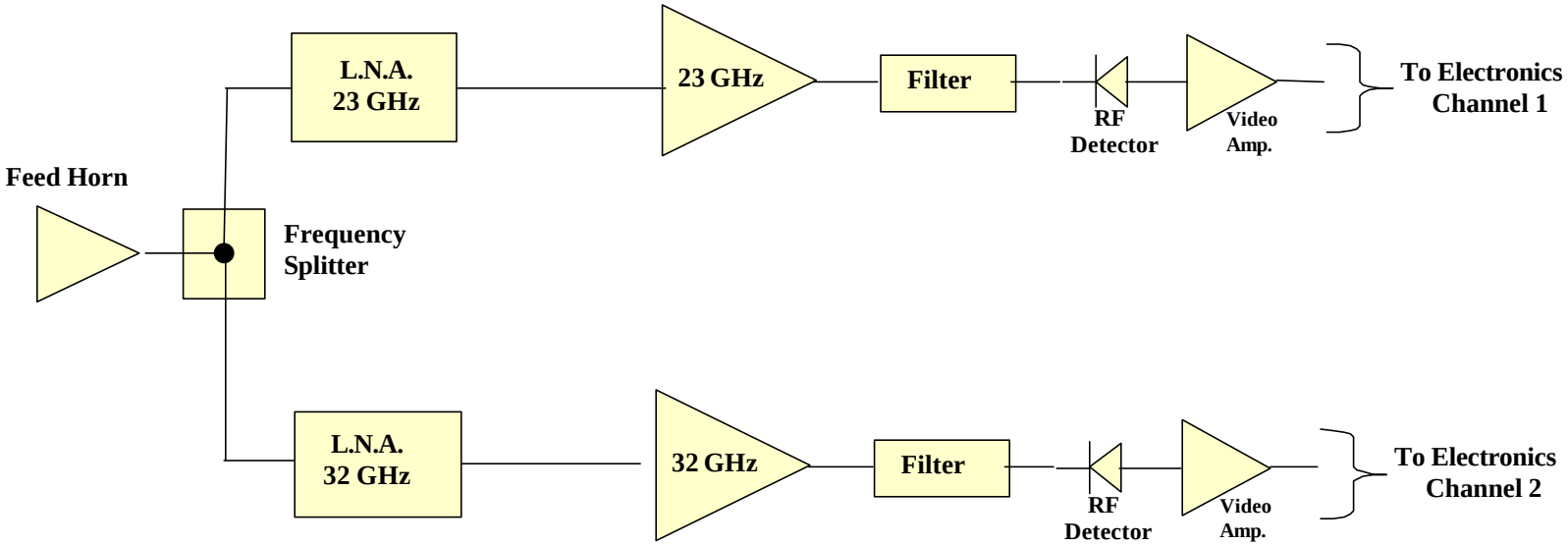

Figure 8-2. Enhanced Science Channel 1 and Channel 2 Receiver Details

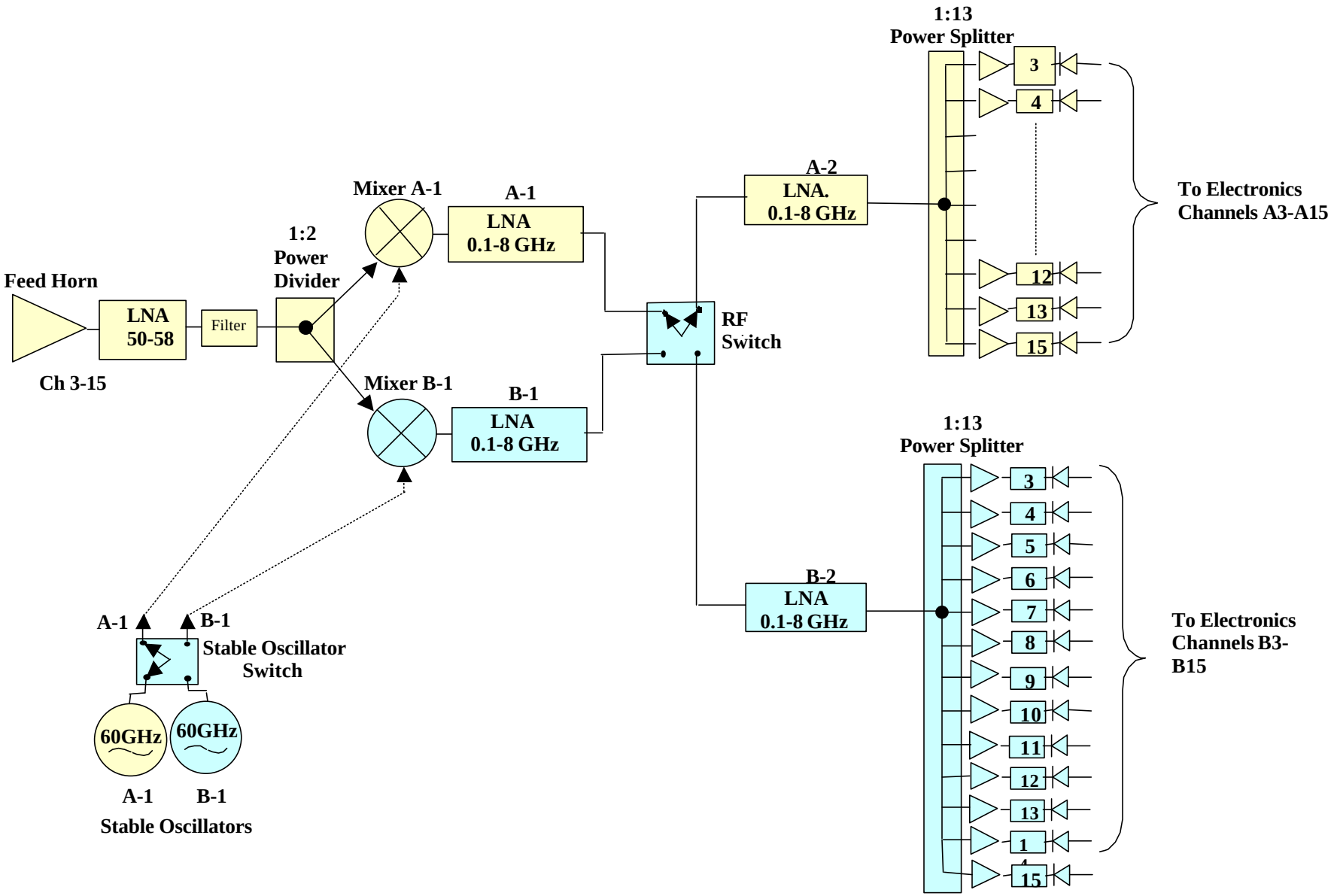

Figure 8-3. Enhanced Science Channels 3-15 Details

Note: redundant components are shown in blue.

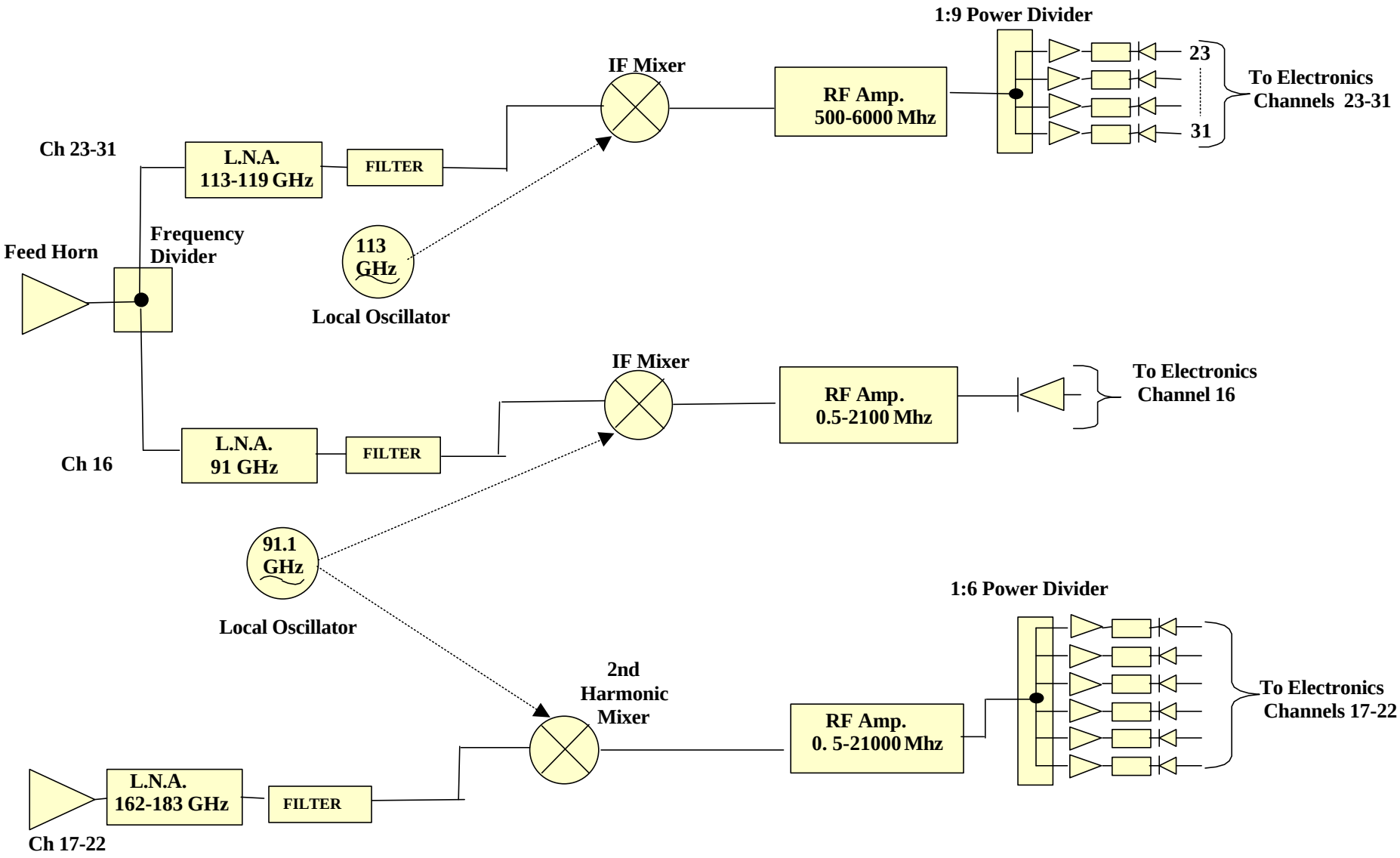

Figure 8-4. Enhanced Science Channels 16, 17-22, and, 23-31 Details

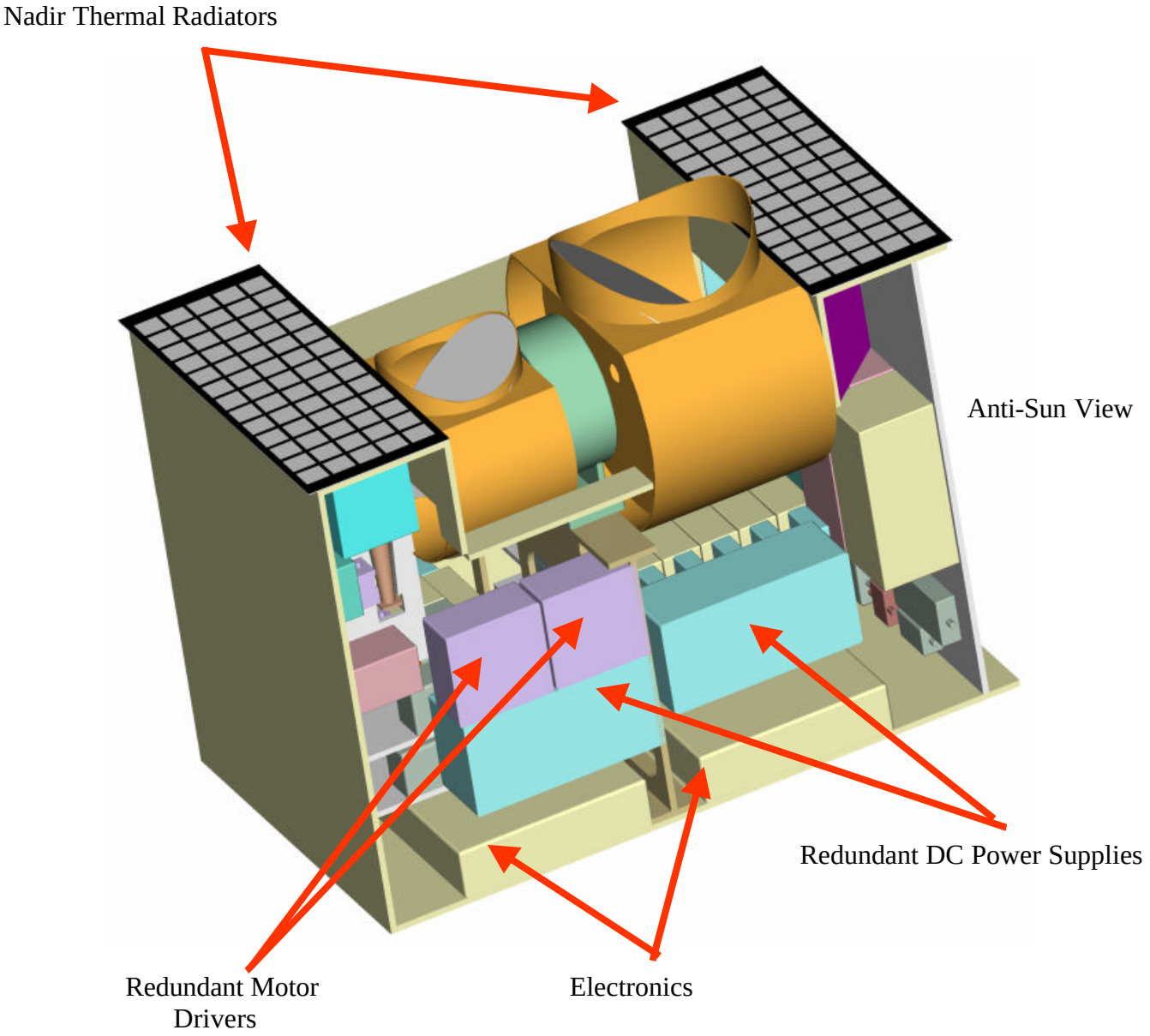

Figure 8-5. Enhanced Science Version Showing Anti-Sun View Internal Component Placement

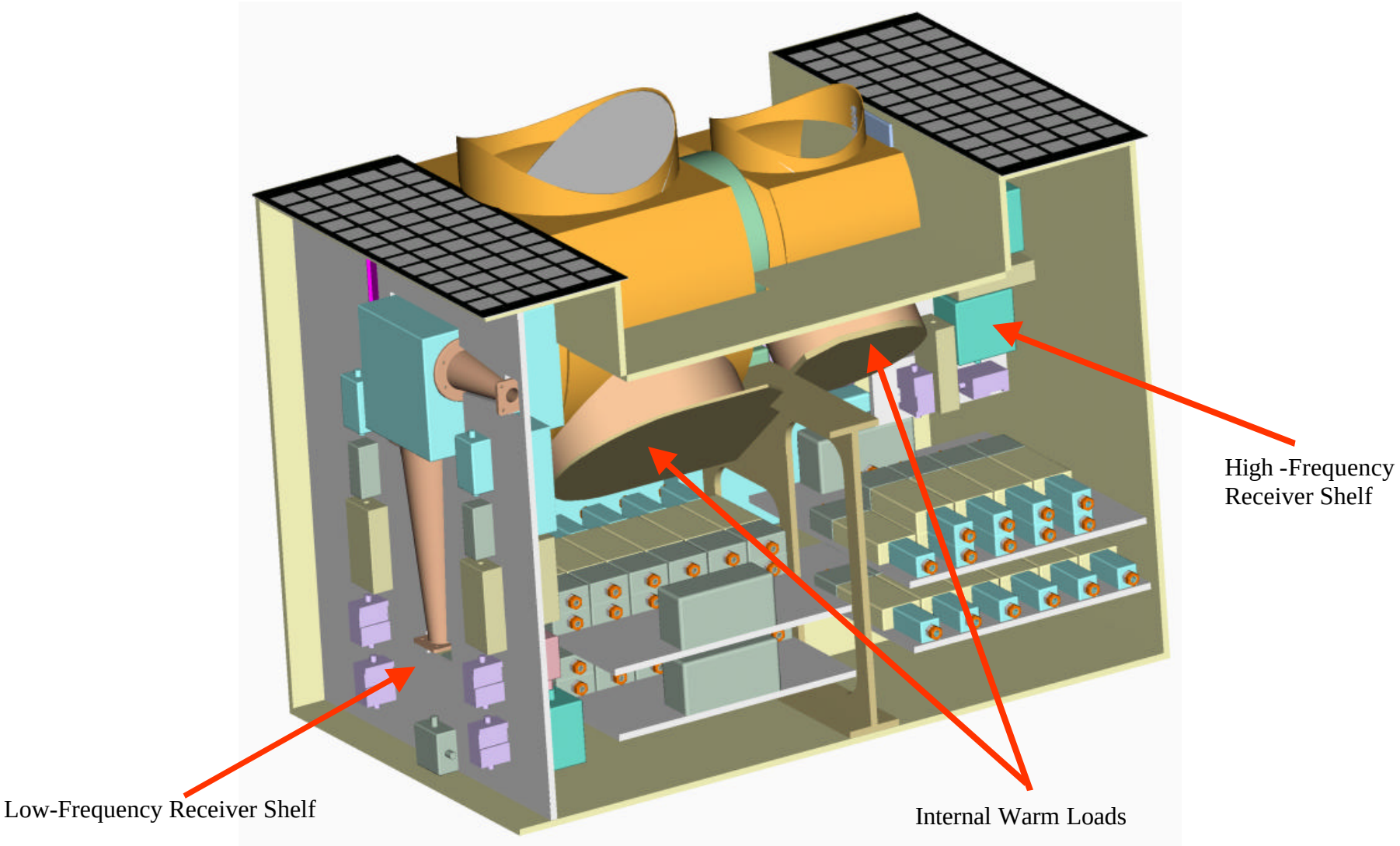

Figure 8-6. Enhanced Science Version Showing Sun View Internal Component Placement

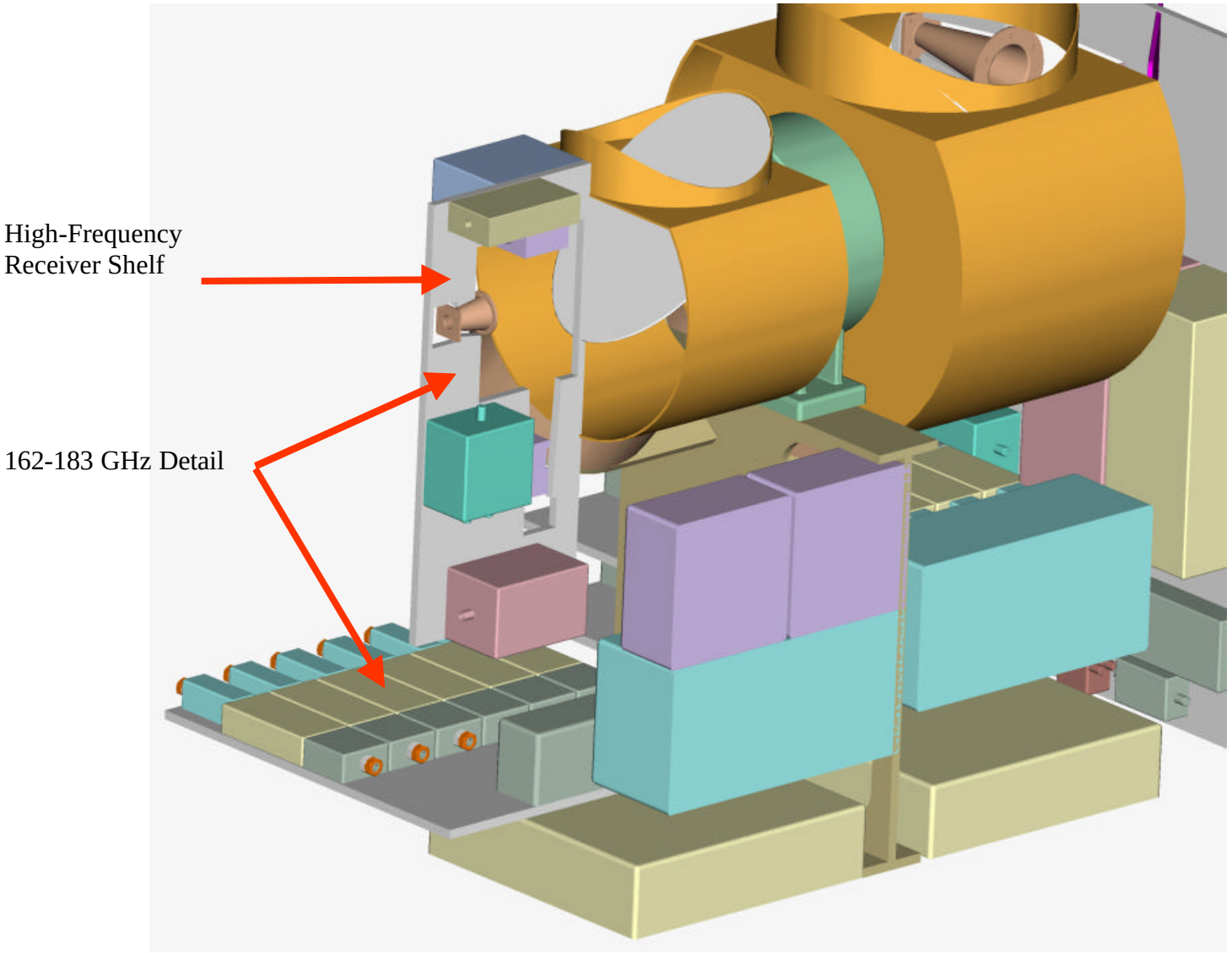

Figure 8-7 Enhanced Science Version Showing High-Frequency Receiver Components

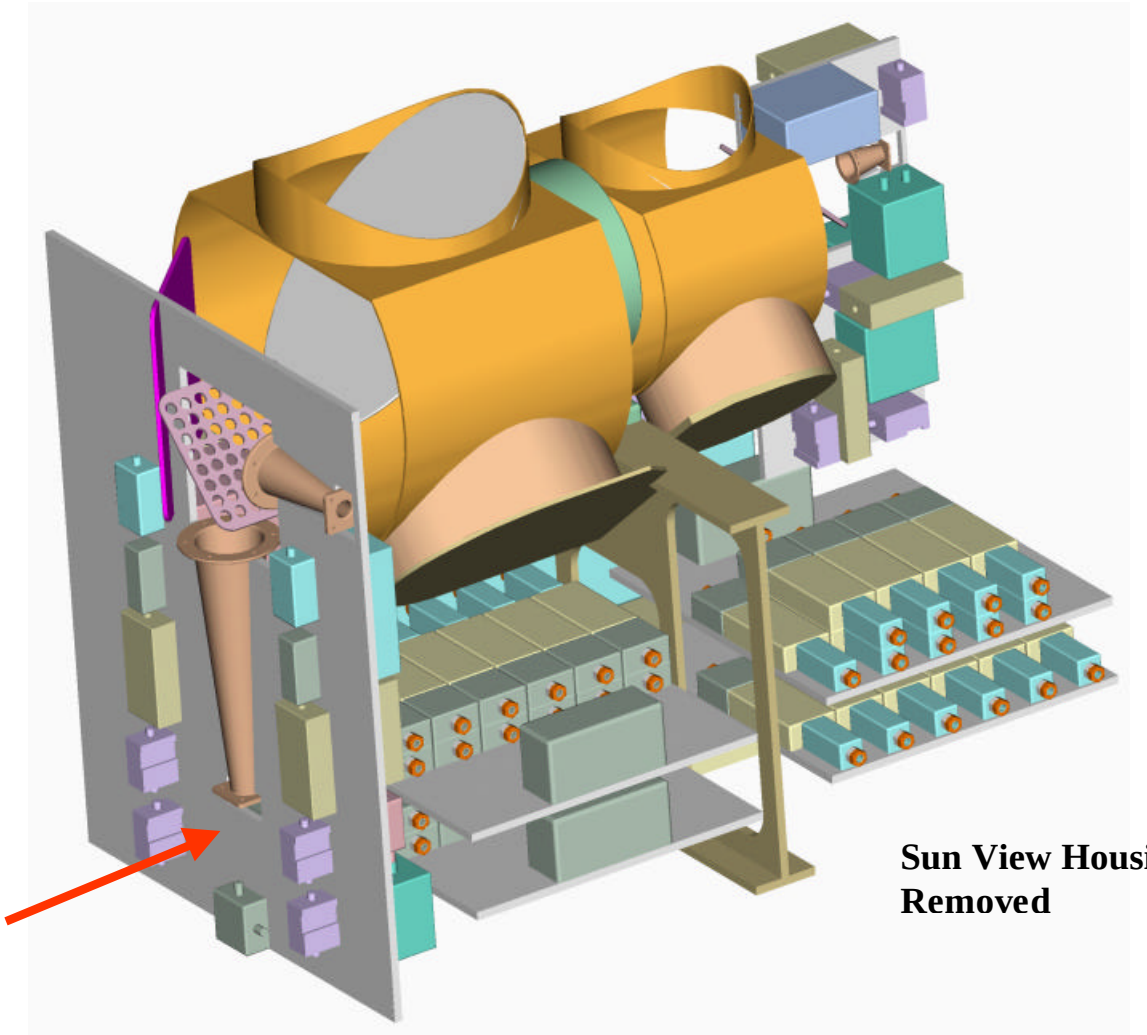

Figure 8-8. Enhanced Science Version Showing Low-Frequency Receiver Shelf Detail

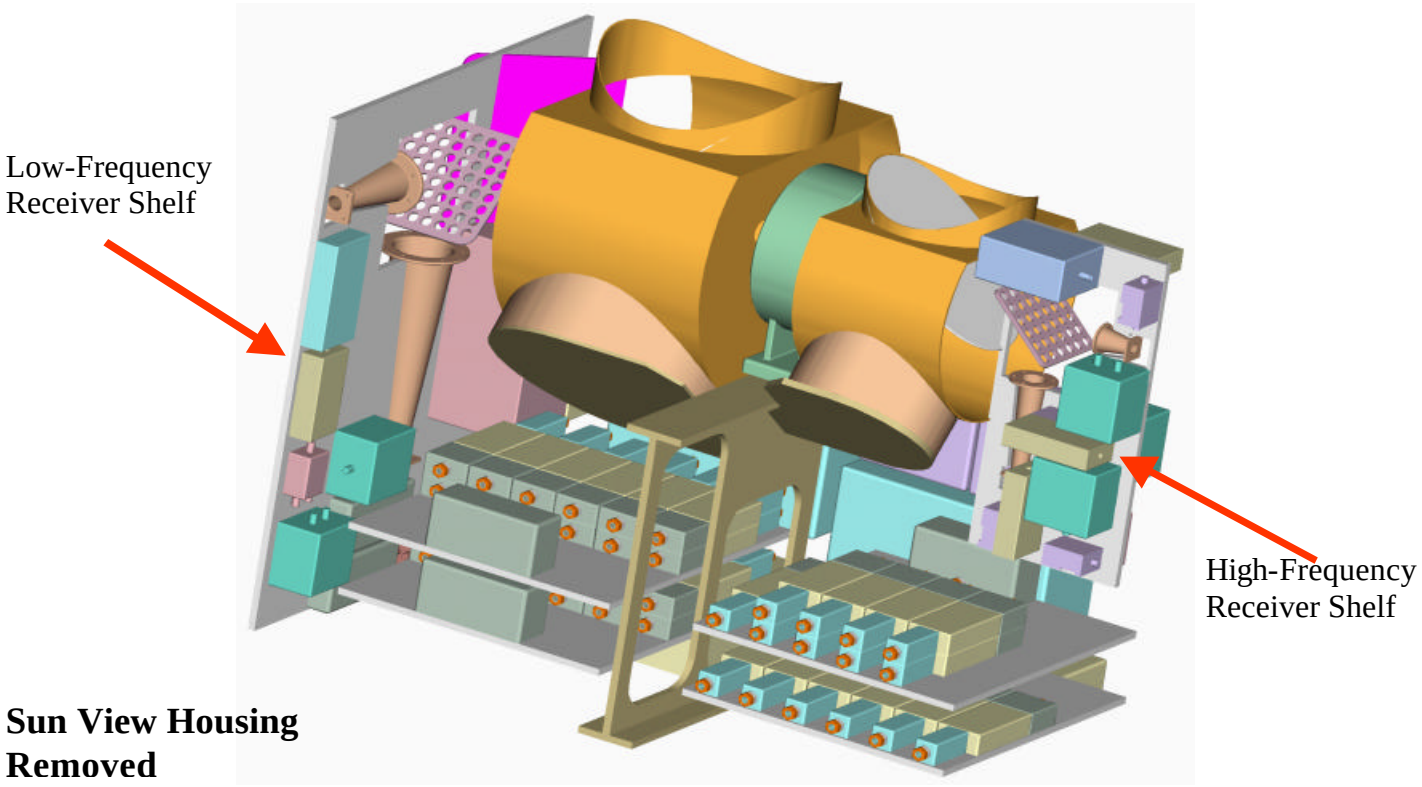

Figure 8-9. Enhanced Science Version Showing Receiver Shelf Placement

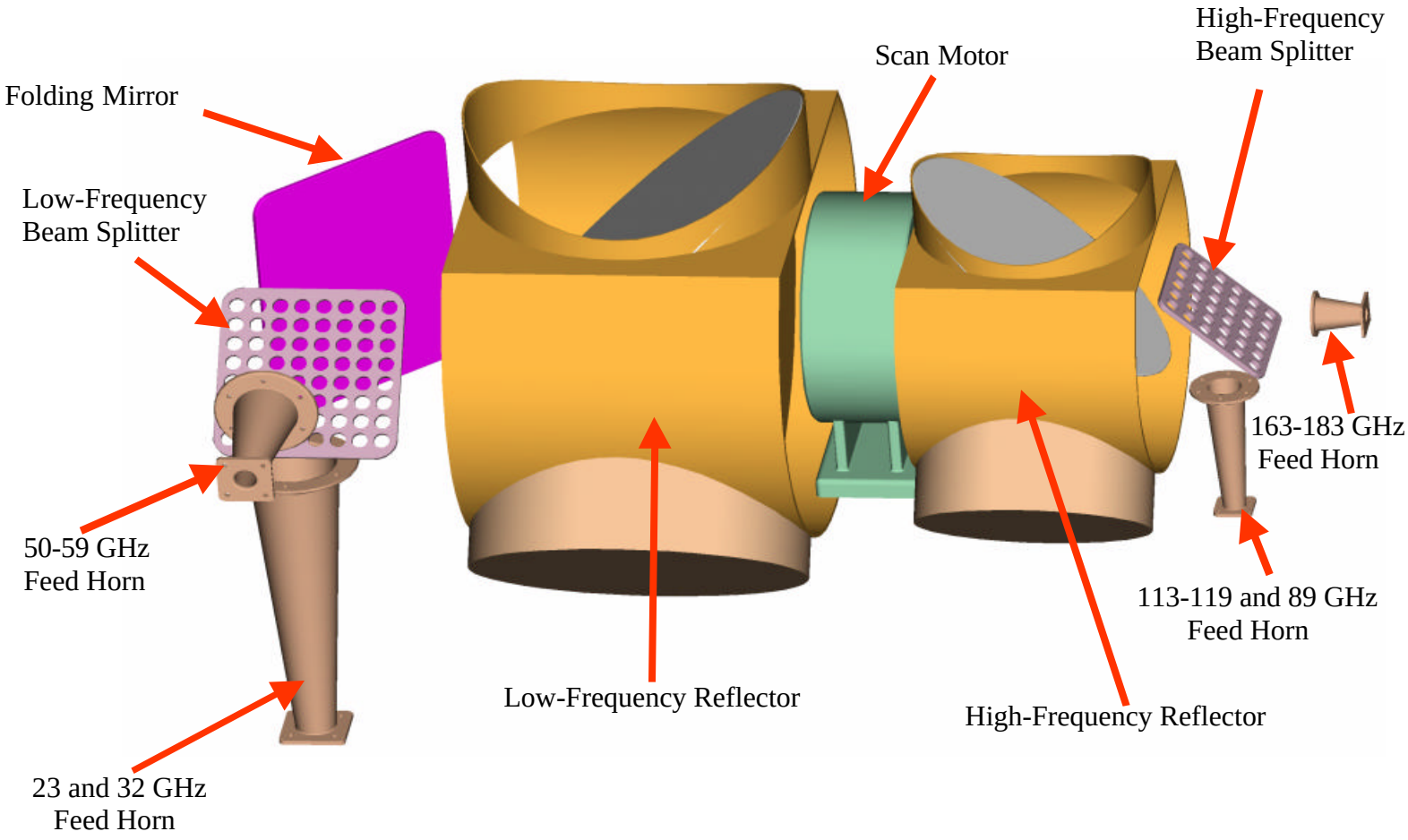

Figure 8-10. Enhanced Science Version Showing Optical Components Layout

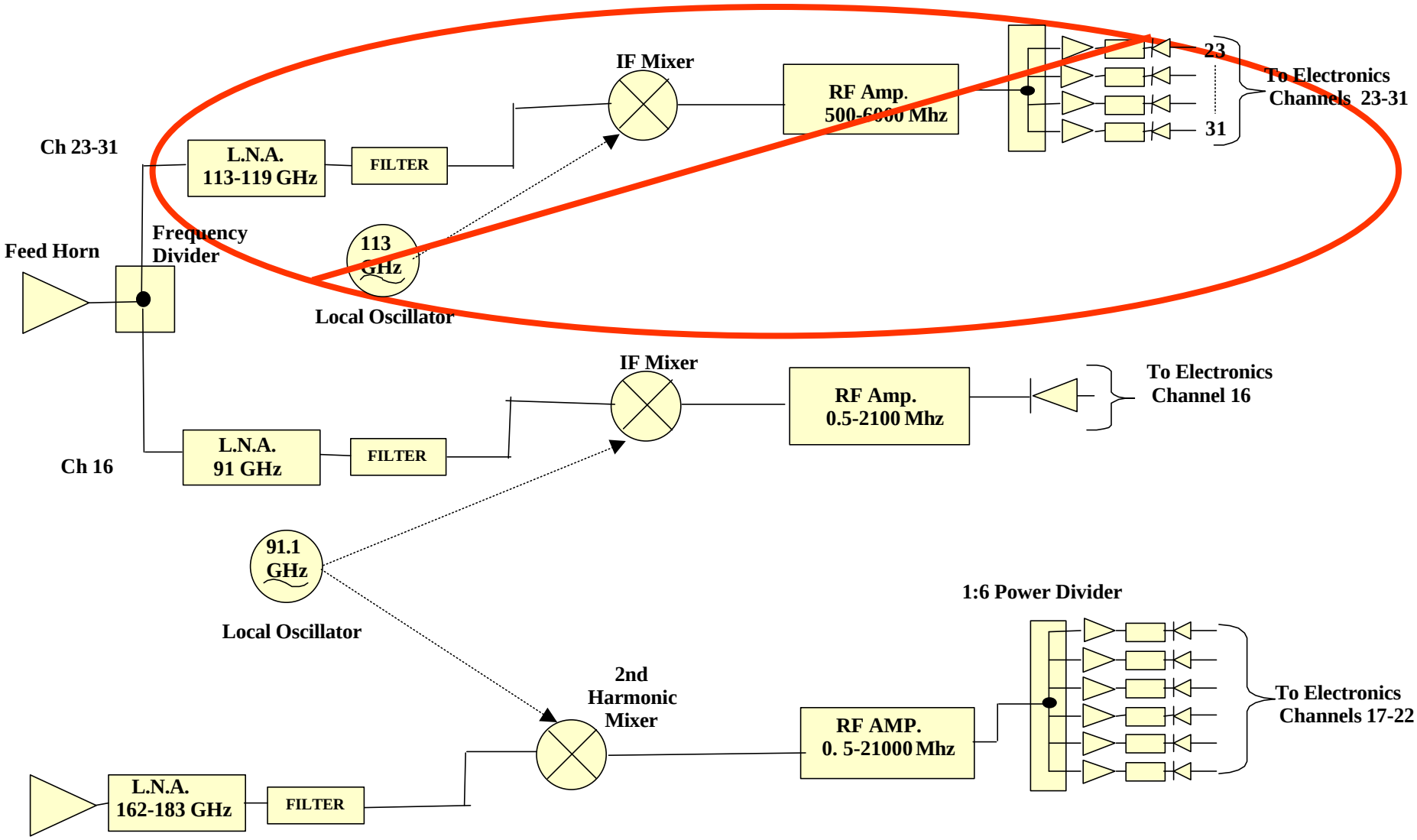

Figure 8-11. Receiver Deleted to Convert from Enhanced to Comparable Science

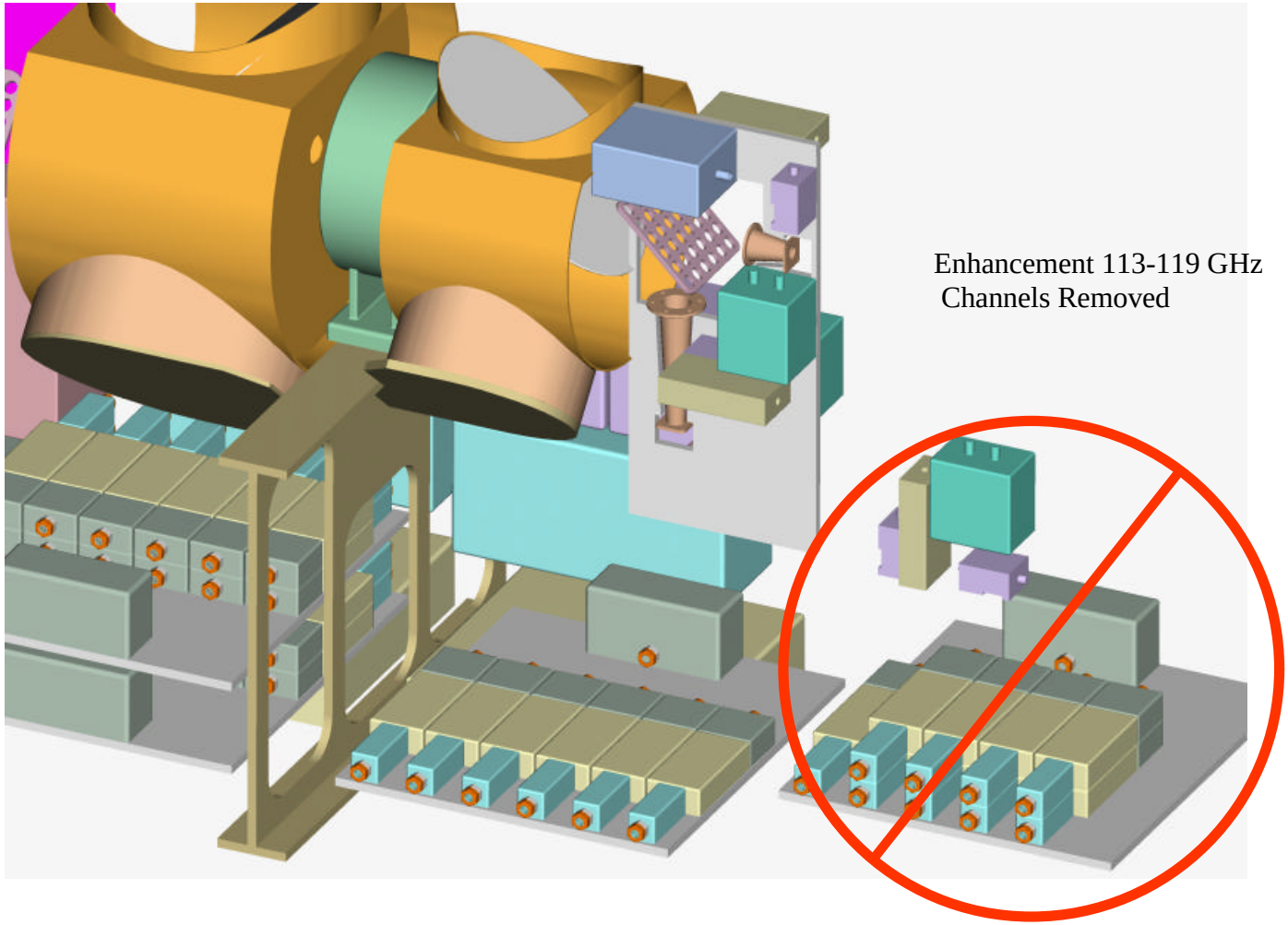

Figure 8-12. Components Deleted to Convert from Enhanced to Comparable Science

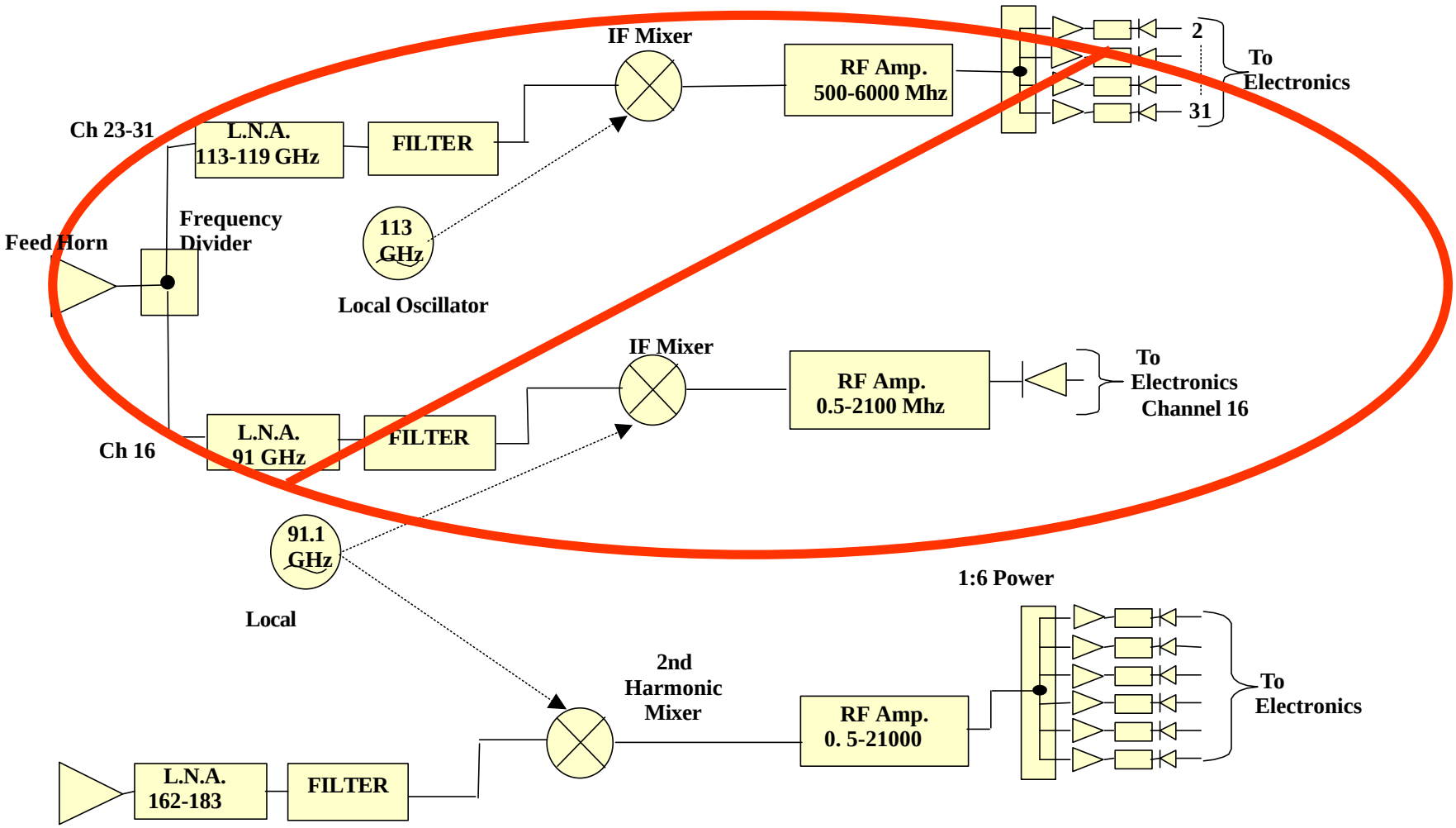

Figure 8-13. Descope Option # 1: Channel 16 Deleted

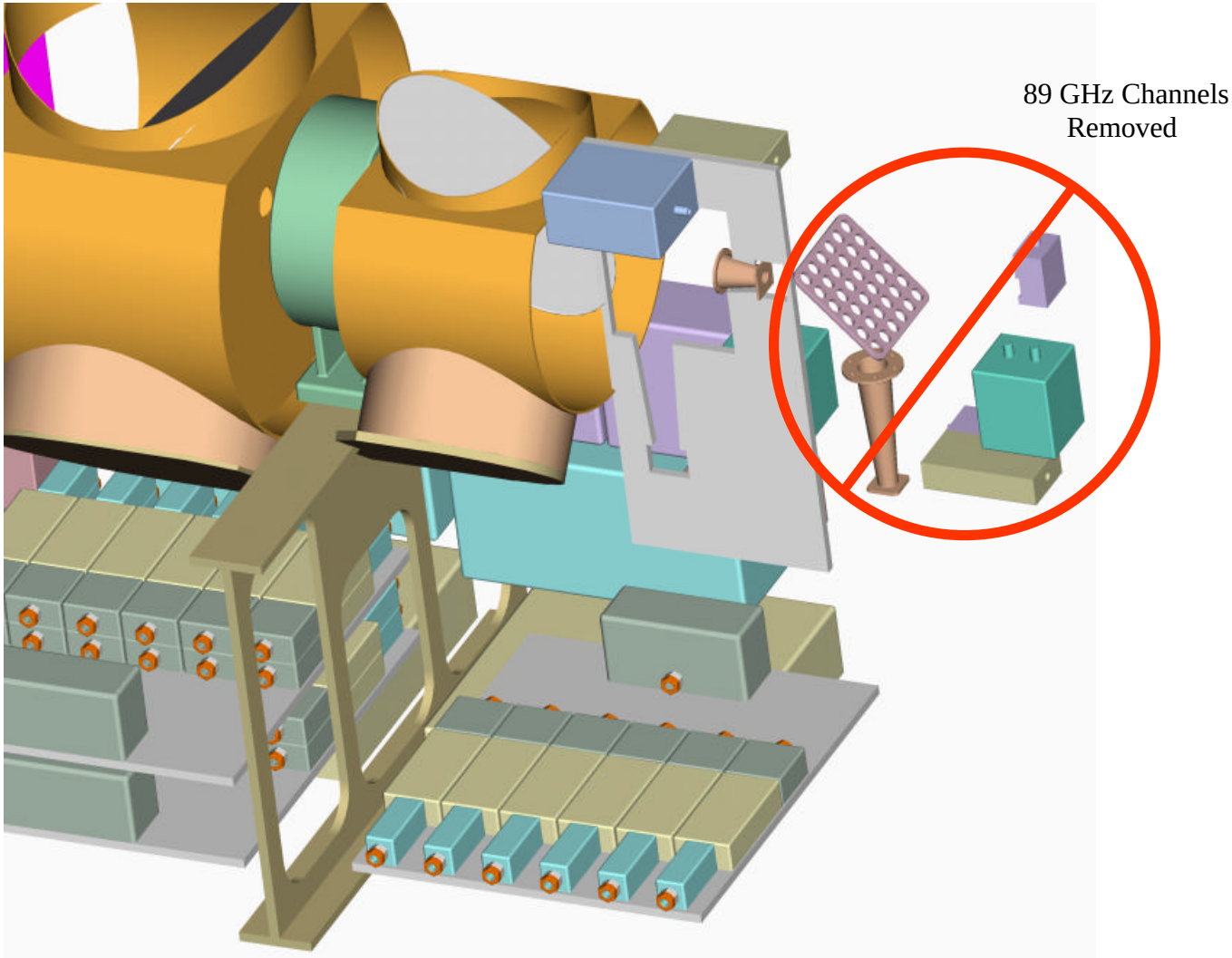

Figure 8-14. Descope Option # 1: Channel 16 Components Deleted

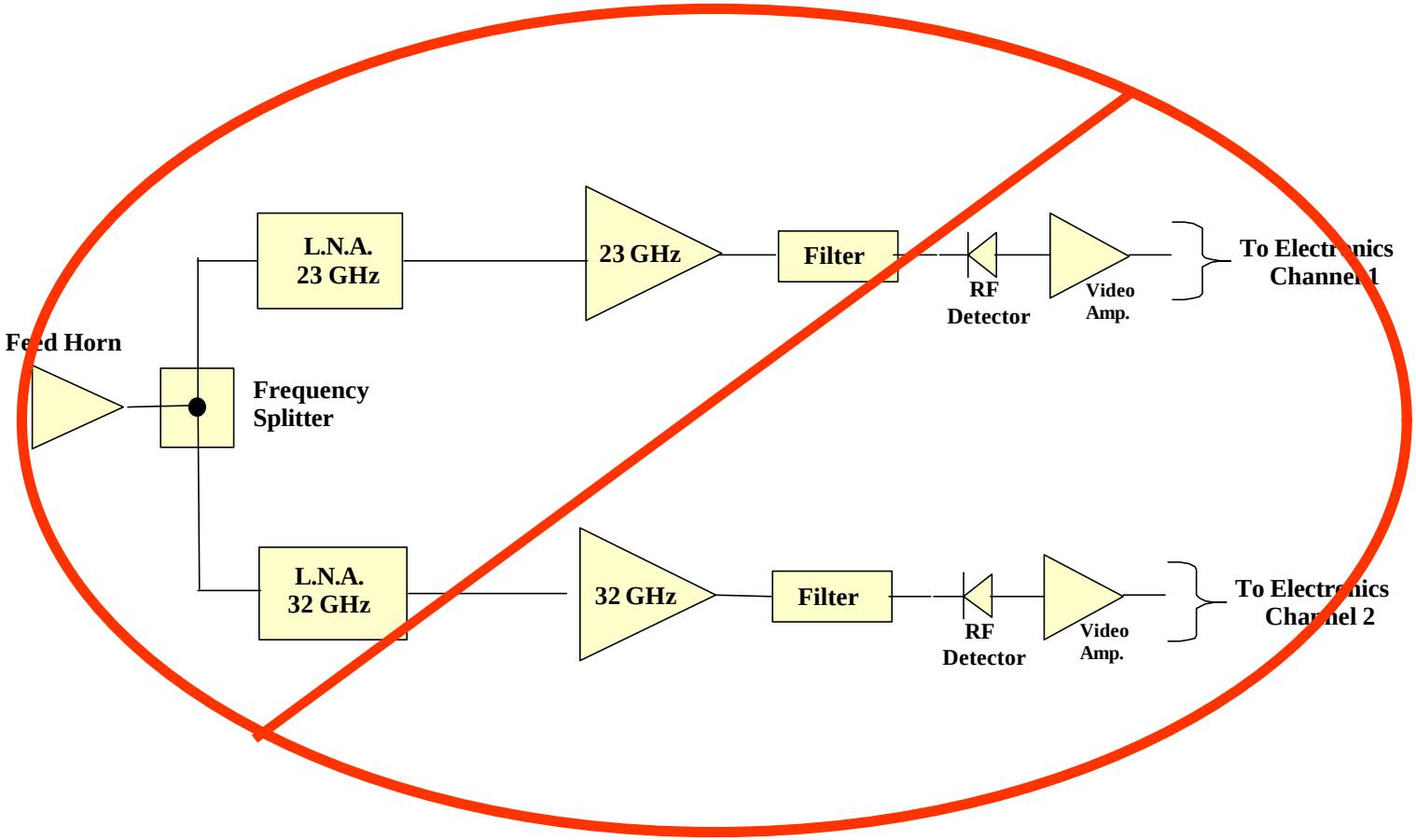

Figure 8-15. Descope Option # 2: Channels 1 and 2 Deleted

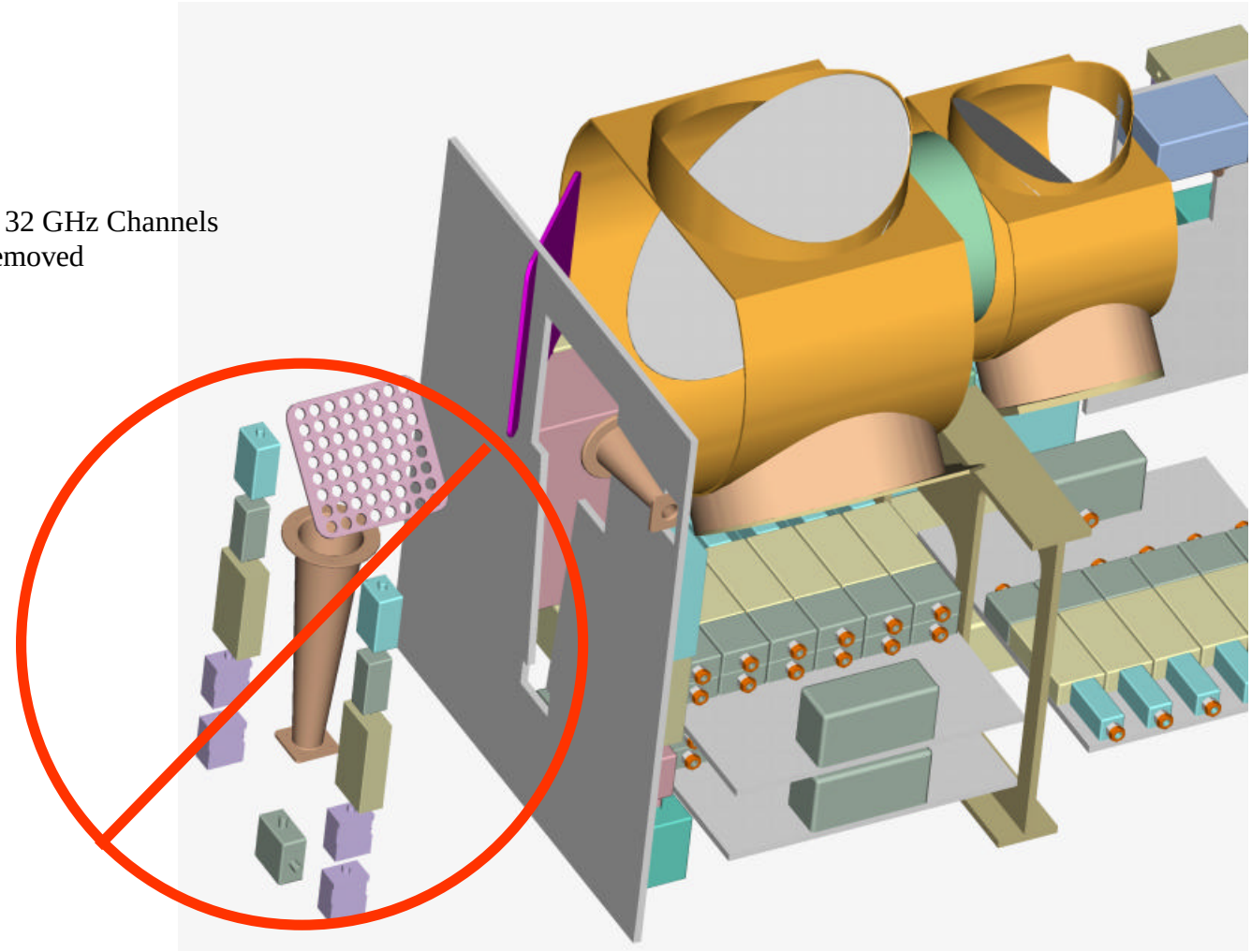

Figure 8-16. Descope Option # 2: Channels 1 and 2 Components Deleted

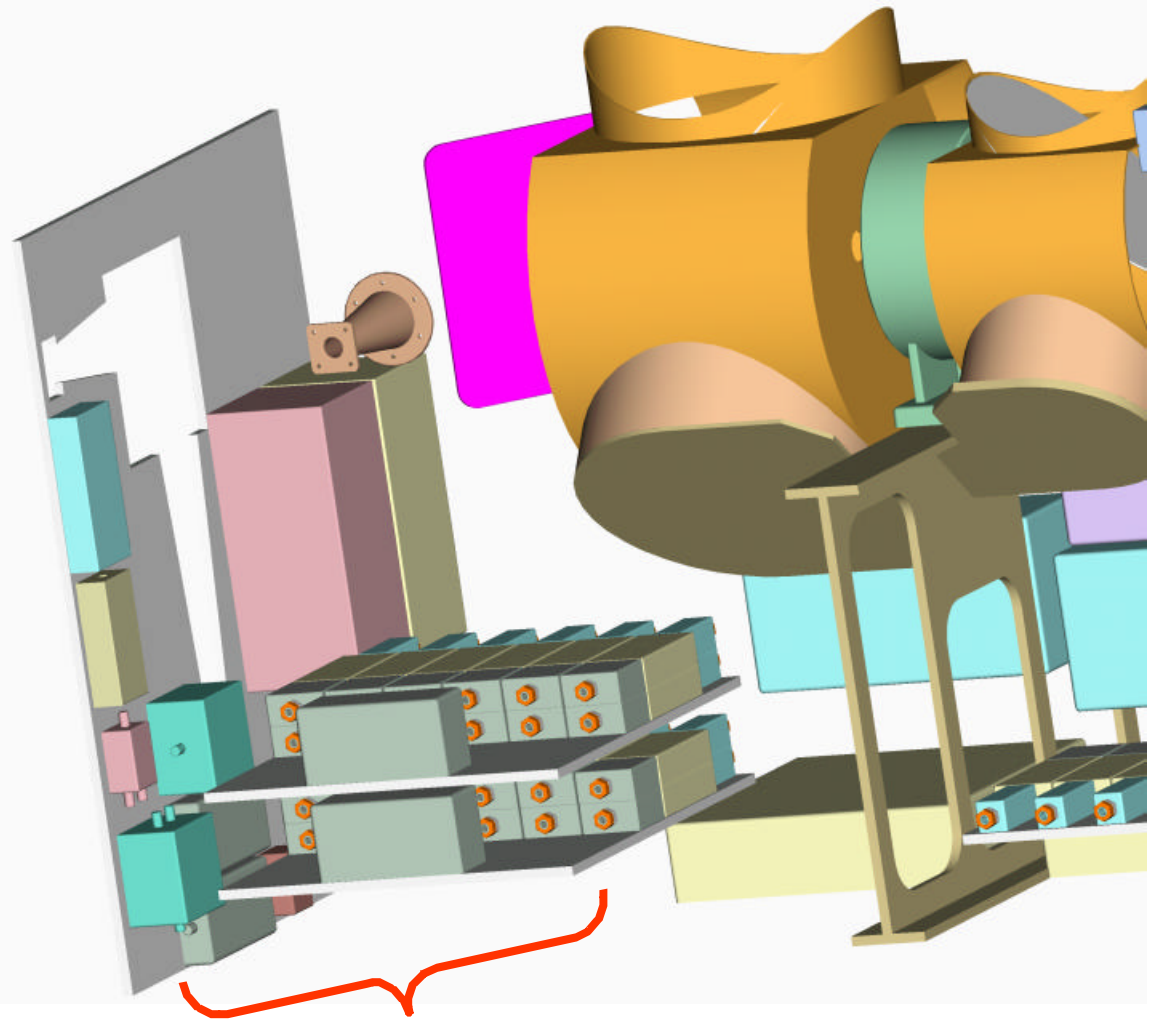

Figure 8-17. Core Science Channels 3-15 Component Layout

9.0 STUDY CONCLUSIONS

The POES ATMS Study Team concluded that the ATMS instrument is feasible and that it could be accomplished within the NPOESS resource requirements. The 31 channels of science that is provided is **enhanced** compared to 22 channels of **comparable** science that was provided by the heritage AMSU-A1, AMSU-A2 and AMSU-B/MHS instruments. The combined resources of the three heritage instruments required 188 watts of power, 159 kg of mass, a volume of 0.64 m^3, and a net data rate of 7.3 kbps. By comparison, the ATMS budgeted resources include 75 watts of power, 88 kg of mass, a volume of .25m^3, and a data rate to be less than 50 kbps. Additionally, if placed end-to-end, the three heritage instruments used 2.0 meters in length (velocity direction) while the ATMS was limited to 0.7 meters.

It is important to understand what enabling technology or unique circumstances make the ATMS feasible with what seems to be limited resources. The answer is found in three major areas:

- Antenna Beam Width

  The Science Team relaxed the beam width requirements for the 23- and 32-GHz channels so that they no longer fixed at 3.3 degrees; instead, they were allowed to be 5.2 degrees. This allowed the low-frequency reflector optics envelope to be reduced by almost 50%. Additionally, the 8/3-second-scan rate of the AMSU-B was adopted for all channels.

- LNAs

  Low-noise amplifiers replaced the heritage mixer/IF heterodyne amplifiers as the first stage of amplification in each channel. The LNAs had better noise figure performance compared to their mixer/ IF amplifier counterparts across all frequency bands except the 116- to 183-GHz bands. This better NF directly correlated to better channel noise equivalent temperature, because the first stage amplifier sets the noise figure for the whole channel. While enhanced noise NEΔT was not an ATMS requirement, the better LNA NFs permitted the use of less technically challenged components throughout the remainder of the channel electronics. The extensive use of LNAs also permitted a reduction of mixers/IF amplifier from 13 in the heritage instruments to just three in the ATMS strawman design. This reduction resulted in savings in power, volume, and circuit complexity; also, it permitted the use of many more standard off-the-shelf components.

- State-of-the-Art Electronics

  The electronic design of the heritage instruments used discrete components to build up individual circuits. The discrete components were soldered to PC boards that required large amounts of power and much “real estate.” This was typical of the 15-year-old electronic architecture used throughout the heritage instruments. The AMSU-A1 instrument required 23 (15 cm x 20 cm) electronic PC boards that were housed for operation in a 45-cm x 15-cm x 23-cm card cage within the instrument. By comparison, the ATMS state-of-the-art electronics makes extensive use of microprocessor and gate-array technology to gain substantial savings in size, mass, and power, together with

improved reliability. A Mil-STD-1553 interface will communicate with the spacecraft. By comparison the AMSU-A1 motor controllers required four PC cards (two for logic and two for driver control) and discrete power drivers. The ATMS motor controller will have a Digital-to-Analog Converter (DAC) for torque and Field Programmable Gate Array (FPGA) to interface to the micro-controller where torque commands are computed. The FPGA will also provide velocity loop closure. Overall the ATMS motor controller will all fit on a 10-cm x 10-cm board requiring 1/3 the "real estate" used by just one of the three heritage motor controllers. Use of Surface Mount Technology (SMT) further ensures quantum gains for reduction of size and also yields improvement in reliability.

Completing the comparison with the heritage instruments, we find the ATMS's total combined digital and motor electronics will fit comfortably within just 1/6 of the heritage AMSU-A1 electronics volume.

The ATMS Study Team incorporated a number of innovations and compromises. These incorporations allowed substantially equivalent AMSU science, as well as compatibility with three different IR sounders, to be packaged in the available volume, weight, and power. Among these are the use of the AMSU-B scan rate for Channels 1-15 to allow synthesis of temperature beams coincident with the possible IR sounder beams. The Study Team also allowed for the design of one scan drive for all antennas. Use of advanced millimeter technology such as low-noise amplifiers and advanced packaging yields further opportunities to achieve the volume, weight, and power goals.

Study results clearly demonstrate that the 31-channel enhanced science ATMS instrument is technically feasible and can be accomplished with the required resource requirements. The comparable science configuration and the two descoped configurations, which require fewer resources than the enhanced ATMS, were also demonstrated to be technically feasible.

APPENDIX A. SCAN OPTIONS

A-1 Introduction

This Appendix describes an investigation into the errors introduced when assigning a temperature from the microwave measurement to a considerably smaller IR measurement spot. This assignment may require interpolating between microwave measurements, should the desired IR spots and existing microwave measurements not align and the resulting error will depend on sampling density.

This investigation addressed three areas. First, it is shown that improving the resolution from the existing AMSU-A beam of 3.3° to 2.2° has a benefit in cases of high spatial structure. Second, the benefit of decreasing the spacing between samples is quantified and shown to be substantial under the same conditions of high spatial structure. Third, the deleterious effects of reducing integration time are almost completely mitigated when reproducing an AMSU-A beam.

In this investigation, the impact of improving resolution (decreasing beam size) of the microwave instrument was addressed first. Under the conditions of temperature variations within a beam width, as was the case of the NAST-M data employed in the analysis, a clear advantage is shown as the microwave beam size is reduced. This is easily explained as each measurement, IR or microwave, is an average of the temperatures subtended by the beam. As the microwave beam size is reduced toward the IR beam size, the difference between the microwave and IR measurement at the same location is reduced. In the case of a 0.8° IR beam compared to two candidate microwave beam widths, the rms error over the NAST-M data set was found to be 5.5 K for the 3.3° beam but only 1.8 K for the 2.2° beam.

Employing the better resolution (2.2°) beam to synthesize an AMSU-A measurement (3.3° beam width) was investigated in two steps. First, a simple addition of nine equally weighted measurements spaced by a half-beam width (1.1°) was shown to produce a good approximation of the desired AMSU-A beam. While the resulting beam was slightly square, the beam widths in the cardinal (scan- and along-track) planes was less than 10% larger than the desired 3.3° beam. In the diagonal planes, the beam width was larger than that in the cardinal planes, but still within 10% of the desired size.

The second, more detailed, beam synthesis technique employed a least-mean-squared error method with Gaussian beams to produce the desired 3.3° beam at a location between existing measurements with either 2.2° or 3.3° beams (interpolation / synthesis). This technique was exercised over a range of sample spacings between beams from 0.75° through 3.3° in both the scan and cross-scan planes. The error in interpolation was computed by multiplying the rms error between the synthesized beam and the desired (Gaussian) beam by the rms temperature variation in the synthesized beam. This error is shown to be minimal when the spacing between samples is 0.5 beam widths (1.1° for the 2.2° beam) or less. This error ranges from 1.8 K for a sample spacing of 3.3° (with a 2.2° beam width) to less than 0.05 K for a sample spacing of 1.1°. As is shown in the plot of the errors (Figure 11), using the existing AMSU-A system of 3.3° beams spaced by 3.3° can result in a 1.4 K estimation error when interpolating to a point between

measurements. This conclusion is valid under conditions of temperature variations on scales less than a beam width, as was the case in the NAST-M data used in the analysis.

Finally, as the spacing between samples is decreased, the time available for integration is correspondingly decreased. Assuming identical spacing between measurements in both the along-track and scan directions, the integration time is decreased by the square of the ratio of sample spacing to the current (3.3°) spacing. Thus, a variation in sample spacing from 1.1° to 3.3° implies the ratio of integration time to the current AMSU-A changes by as much as 1/9 ($1.1^2/3.3^2$). This results in an increase in instrument noise by factors as much as three because the instrument noise is proportional to the inverse of the square root of the integration time. Mitigating this increase is the use of several samples to realize an AMSU-A beam of 3.3°. For example, if nine beams of 2.2° width with a sample spacing of 1.1°, the increase in noise due to decreased integration time is exactly cancelled. It is shown below that the penalty of interpolating using the Gaussian beams is only 6%, or if the instrument noise of AMSU-A is 0.2 K, the resulting instrument noise from producing a 3.3° beam using 2.2° beams with samples spaced by 1.1° is only 0.21 K. Reproducing an "AMSU-A – like" measurement from an instrument with better resolution and more closely spaced samples will have a negligible impact on the instrument noise with the advantage that the individual measurements have better resolution and less aliasing noise with respect to CrIS and other IR sounders.

A-2. Resolution:

To determine the advantages of improving the resolution from the AMSU-A 3.3° beam width, data from NAST-M (N-POESS Airborne Sensor Testbed – Microwave) was used. This data has a resolution at nadir of approximately 2.6 km, more than sufficient to expose features, which would be missed with a larger beam.

Representative microwave brightness temperatures from the NAST-M instrument are shown in Figure A-1, which depicts the increasing spatial structure viewed by the lower atmospheric sounding channels at 54 GHz and the lower sounding channel at 118 GHz. In these images, the total flight distance (including turns) is represented in the horizontal axis and the sharp vertical striations occur when the aircraft banks, shifting the view angle and permitting the instrument a partial view of the colder upper atmosphere. These areas were not used in the subsequent calculations because they introduce strong discontinuities in the data.

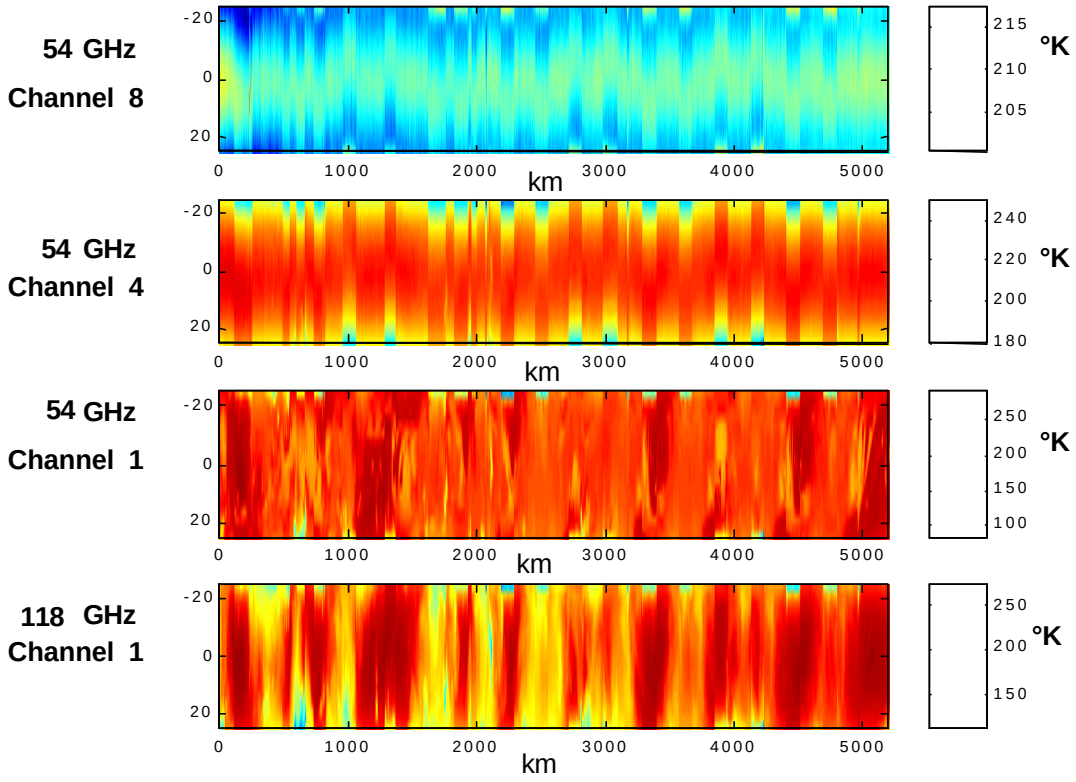

Figure A-1
Representative NAST-M Data

The lower altitude, 54-GHz channel (channel 1) was chosen to stress the interpolation method because of the large variations over all resolutions considered; the 32-km proposed beam width(nadir resolution at 2.2°), the 46-km existing AMSU beam width (nadir resolution at 3.3°) and the 11-km notional CrIS beam width (nadir resolution at 0.8°). Figure A-2 shows a representative region extracted from the total flight data to demonstrate the relative size of the three footprints. As seen in this figure, the larger beams will encompass more temperature variation in the scene, which can have up to 20 K temperature change over 50 km.

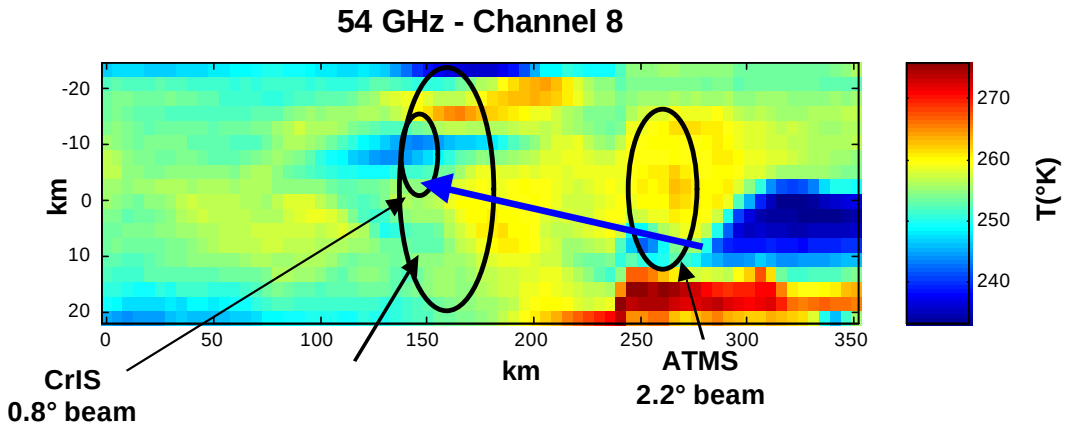

Figure A-2
NAST-M Data with AMSU, ATMS and CrIS Beams

The microwave measurement is an average, weighted by the beam shape, of the brightness temperatures inside a beam:

$$T_{meas} = \iint B(J, f) \cdot T(J, f) \cdot dJ \cdot df$$

Equation A1

where B is the beam shape function and T is the temperature field.

Ten regions were extracted from the NAST-M data and used to compute the measured temperature for the three beam sizes (3.3° AMSU, 2.2° ATMS and 0.8° infrared). Four of the regions are shown in Figure A-3. These measured temperatures for the two candidate microwave beams (2.2° and 3.3°) were then compared to the IR beam (0.8°) and the RMS error between the candidate beam and the IR beam was computed:

$$\Delta T_{RMS} = \frac{\sqrt{\sum_{scenes} \left| \overline{T}_{3.3° or 2.2°} - \overline{T}_{0.8°} \right|^2}}{\sqrt{N_{scenes}}}$$

Equation A2

As expected the larger (3.3°) beam had higher maximum and RMS errors to the IR beam than did the 2.2° beam because of the larger difference in beam size, Table A-1. These errors will be a function of the underlying temperature field. For highly varying conditions such as in this data, the error in ascribing the temperature from a large (2.2° or 3.3°) microwave beam to a smaller (0.8°) infrared measurement spot is considerably larger than produced by the microwave instrument noise (≈0.2 K). For all cases evaluated here, the rms errors relative to the IR data are reduced to less than half by using 2.2° beam widths on the ATMS instead of 3.3°.

Table A.1
RMS Temperature Estimation Error due to Beam width

Beam width	**$T_{microwave} - T_{IR}$ maximum**	**$T_{microwave} - T_{IR}$ rms**
2.2° (Candidate ATMS)	3.7 K	1.8 K
3.3° (AMSU –A1)	8.7 K	5.5 K

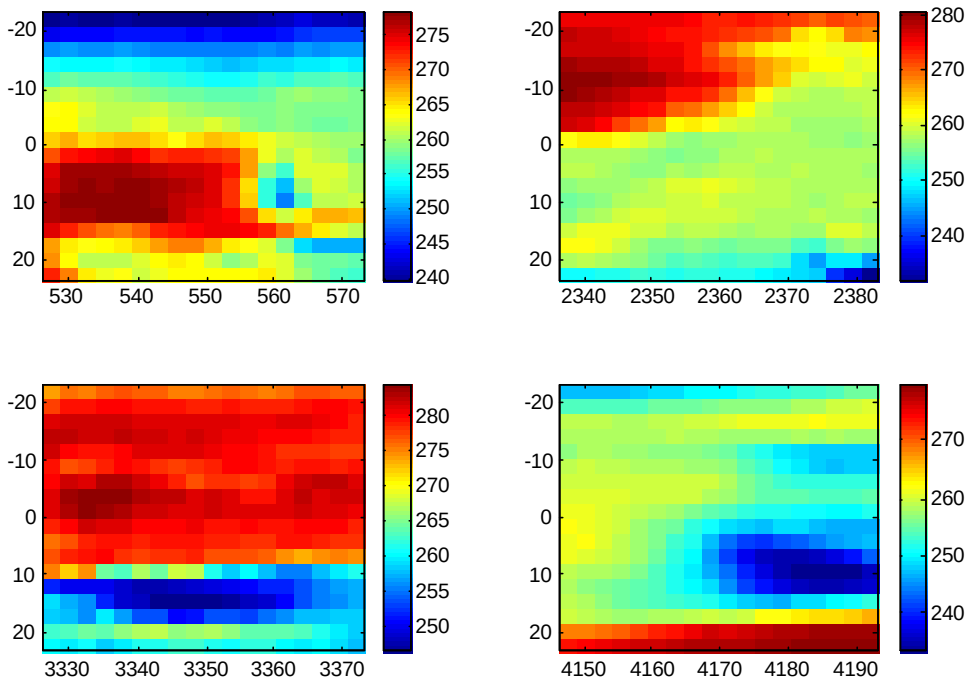

Figure A-3
Examples of Regions Examined

A-3. Simple Synthesis

The simplest method to synthesize the AMSU-A 3.3° beam from several beams of the proposed ATMS (2.2°) is to sum the power patterns. A simulation of this was done using patterns computed from a two-parameter aperture distribution:

$$A(r) = C + (1 - C) * [1 - (\frac{r}{a})^2]$$

Equation A3

where: ρ is the radius variable,
a is the aperture radius, and
C is related to the edge taper (ET in dB) by

$$C = 10^{ET/20}.$$

The radiation pattern was computed for nine beams of 2.2° spaced every 1.1° as shown in the Figure 4.1-4 A (-3 dB contours). These were summed (as power patterns) to produce an approximation of the AMSU-A 3.3° beam as shown in Figure A-5. The resulting beam has a beam width of very nearly 3.3° and is slightly wider than the desired beam (3.36° in the along- and cross-track dimensions and 3.54° diagonal to the satellite track) at the –3 dB level and slightly narrower at lower pattern levels. The contour of the synthetic beam is also slightly square at low pattern levels as was shown previously in figure 4.1-4 A.

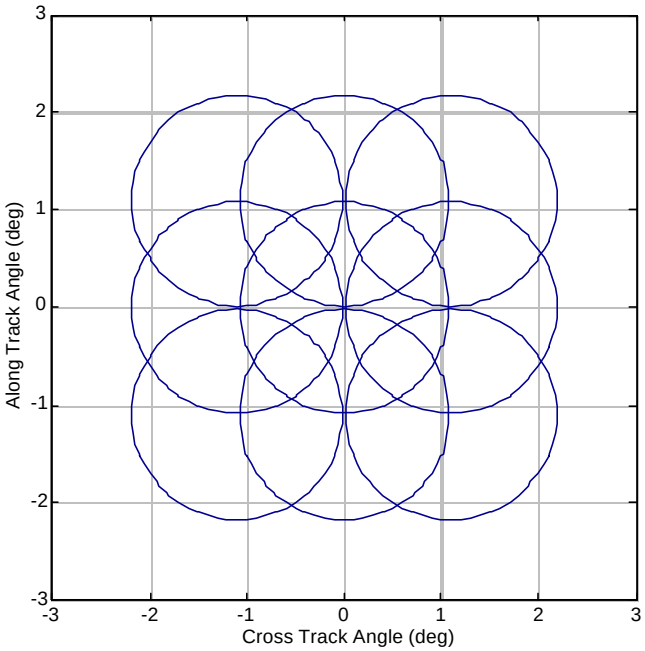

Figure A-4
Nine 2.2° Beams Used in Synthesis

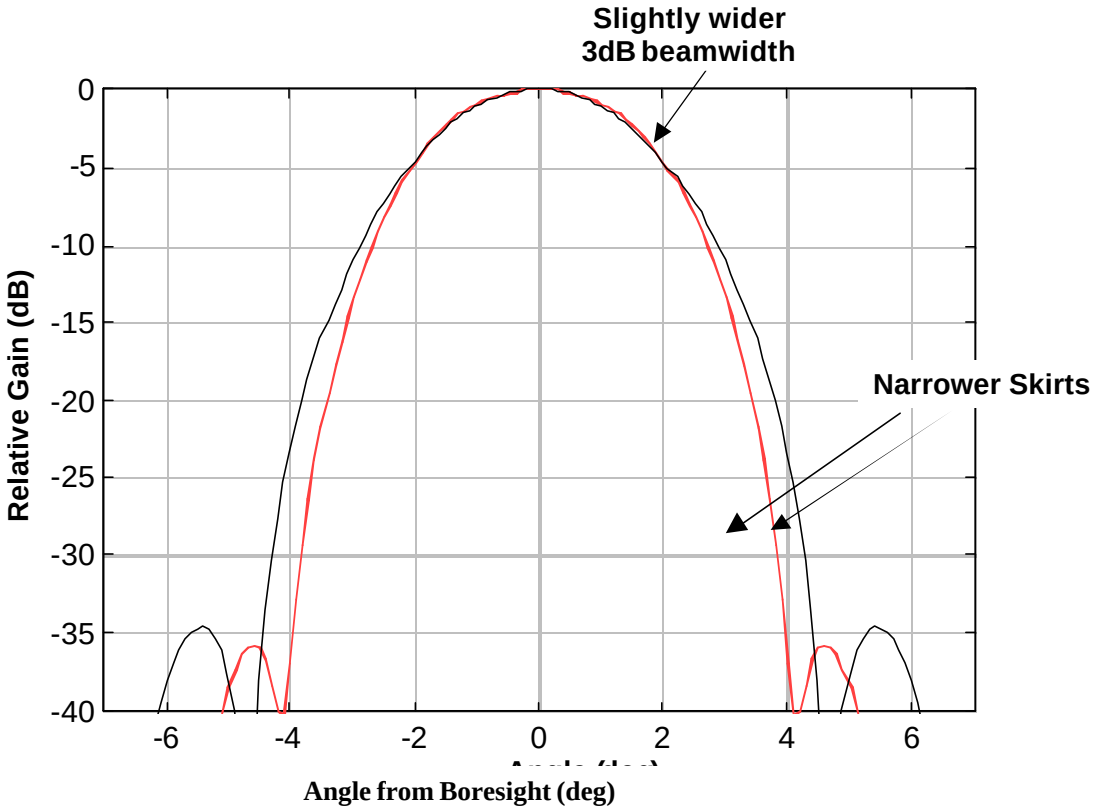

Figure A-5
Comparison of Synthetic and Real 3.3° Beams

A-4. Interpolation Between Microwave Measurements

The primary reason for increasing the spatial sampling of the microwave temperature and humidity field is to facilitate interpolation between measurement points. In the current AMSU instrument, the field is sampled at each beam width: 3.3° for AMSU-A and 1.1° for AMSU-B. The temperature and humidity information obtained from the microwave measurements will be used to initialize the retrieval process for the infrared instrument (for example, CrIS on the NPOESS satellite or IASI on the METOP satellite). The ground spot size of the infrared instrument is smaller than that of the microwave instrument, and any misalignment between the infrared and the microwave instruments, such as image rotation with scan in the infrared instrument, will make it difficult to assign a microwave measurement to an infrared spot. Figure A-6 shows a possible misalignment of the IR and microwave beams. This problem will be exacerbated by variations in temperature on scales of a beam width or less.

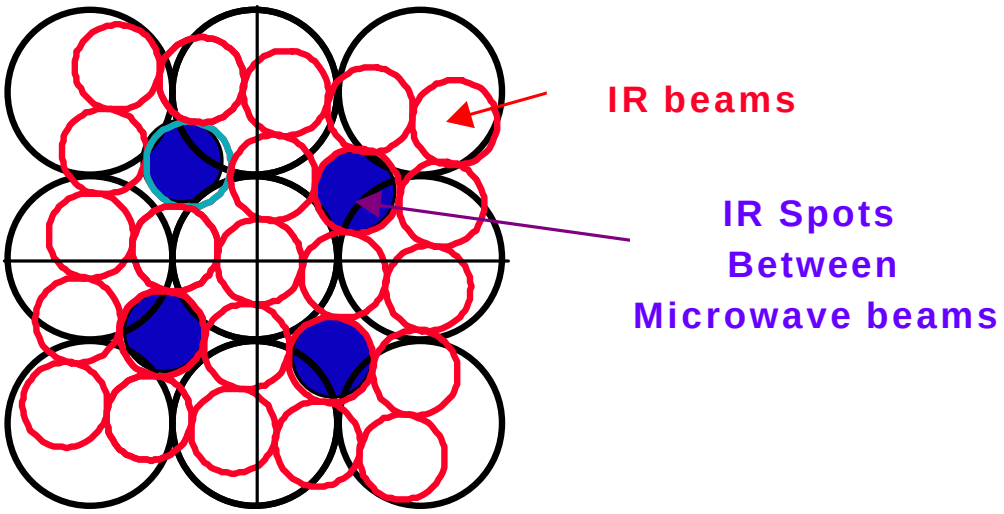

Figure A-6
Misalignment of Microwave and IR beams

To investigate potential difficulties in interpolation of the microwave data at locations between existing beams, a specific interpolation method was adopted and applied to data from one of the NAST-M surface sounding channels, where a high degree of spatial structure might be experienced. This situation stresses interpolation and occurs over regions of interesting weather phenomena.

The interpolation method assumed that Gaussian beams were used for the measurements (a reasonable approximation of the actual microwave beam) and used several of these beams to synthesize a Gaussian beam at a desired location. A desired location midway between existing measurements was the location chosen to evaluate the method, because it is the most stressing condition.

It is advantageous to use Gaussian beams in the analysis to simplify the derivation and computation. If a Gaussian beam is defined as:

$$B(\vec{r};s) = \frac{1}{ps^2}\exp(-\frac{|r|^2}{s^2}),$$

Equation A4

then its Fourier Transform is easily found:

$$Q(u) = \iint B(\vec{r};s)\exp(-ipru)dr^2 = \exp(-p^2s^2u^2).$$

Equation A5

The correlation of two Gaussian beams of differing widths and centers remains a Gaussian:

$$\iint B(\vec{r}-\vec{r}_1;s_1)B(\vec{r}-\vec{r}_2;s_2)dr^2 = B(r_1-r_2;\sqrt{s_1^2+s_2^2}).$$

Equation A6

How well a sparce set of measurements can be interpolated to a desired location and beam size depends on the sample spacing, and the scene spectum. For a uniform scene spectrum, the problem is reduces to the correlation between the measurement beams and desired beam.

The interpolated beam is a linear summation of measurement beams with weights given by w:

$$\hat{B}(r;\, s_2) = \sum w_n B(r - r_n; s_1)$$

Equation A7

where the weights are computed by:

$$w = C^{-1}V,$$

Equation A8

where C is the correlation matrix between all the measurement beams and V is the correlation beween all the measurements and the desired (interpolation) beam.

For gaussian beams the results can be expressed as:

$$C_{n,m} = \iint B(\vec{r} - \vec{r}_n; s_1) B(\vec{r} - \vec{r}_m; s_1) dr^2 = B(\vec{r}_n - \vec{r}_m; \sqrt{2}\, s_1)$$

Equation A9

$$V_n(\vec{d}) = \iint B(\vec{r} - \vec{r}_n; s_1) B(\vec{r} - \vec{d}; s_2) dr^2 = B(\vec{r}_n - \vec{d}; \sqrt{s_1^2 + s_2^2})$$

Equation A10

These equations were programmed in MATLAB to compute the weights for the beams at various interpolation points. The rms error between a true Gaussian beam at the desired point and the synthesized or interpolation beam at the same point was found as a function of beam widths and sample spacings.

A-5. Interpolation Results

A computer program was written in MATLAB to compute the weights to synthesize optimally, in a least-mean-square error sense, a Gaussian beam of a desired width from a set of Gaussian beams. The set of beams represents measurements by a microwave sensor with a fixed beam width and beam locations on a rectangular grid. The weights were computed to produce a beam located midway between the rows and columns of the measurement beams, Figure A-7, with a desired beam width. The grid spacing was varied to represent different spatial sample spacings, ranging from 1.1° to 3.3°. For a 2.2° beam width, these spacings varied from 0.5 beam widths (Nyquist's requirement) to 1.5 beam widths. The program synthesizes a Gaussian beam at the desired location and computes the rms error between the synthetic beam and true Gaussian beam at this location.

Figure A-8 shows a synthesized 3.3° beam located at the midpoint of the 1.1° x 1.1° measurement grid (spacing between 2.2° beams). This synthesized beam has small side-lobes which contribute to the rms error also shown in the figure. If the grid spacing is increased from 1.1° (0.5 beam widths) to 3.3° (1.5 beam widths), the difference between the desired and synthesized beam increases substantially from approximately 3.7% rms to 21.5% rms. Figure A-9 shows the difference between the desired 3.3° beam and the synthetic beam at the midpoint with the net rms error as 21.5%. The error in the synthetic beam is directly related to a temperature estimation error made by interpolating between existing measurements.

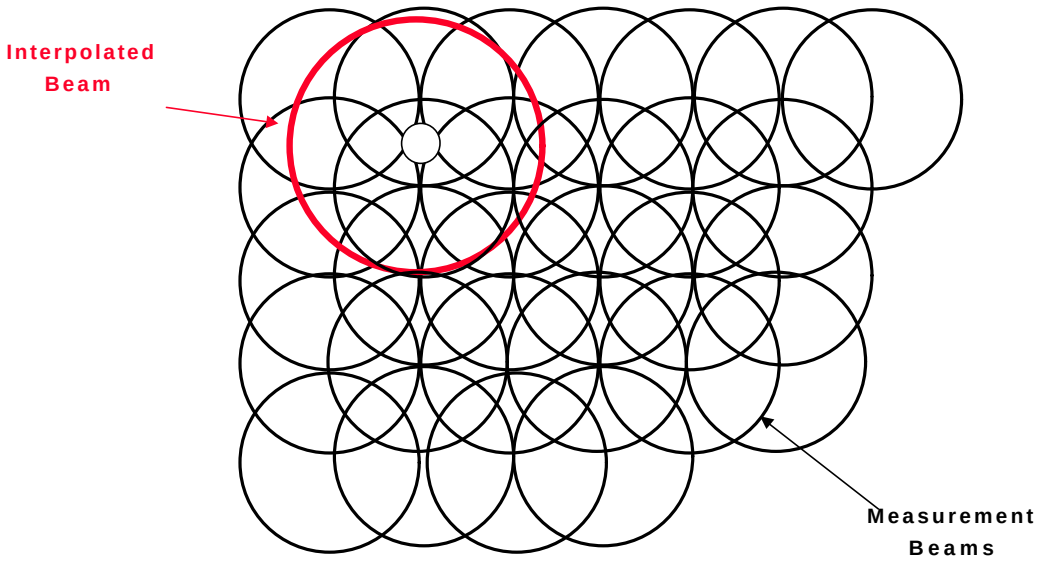

Figure A-7
Interpolated Beam at mid-point of Measurement Beams

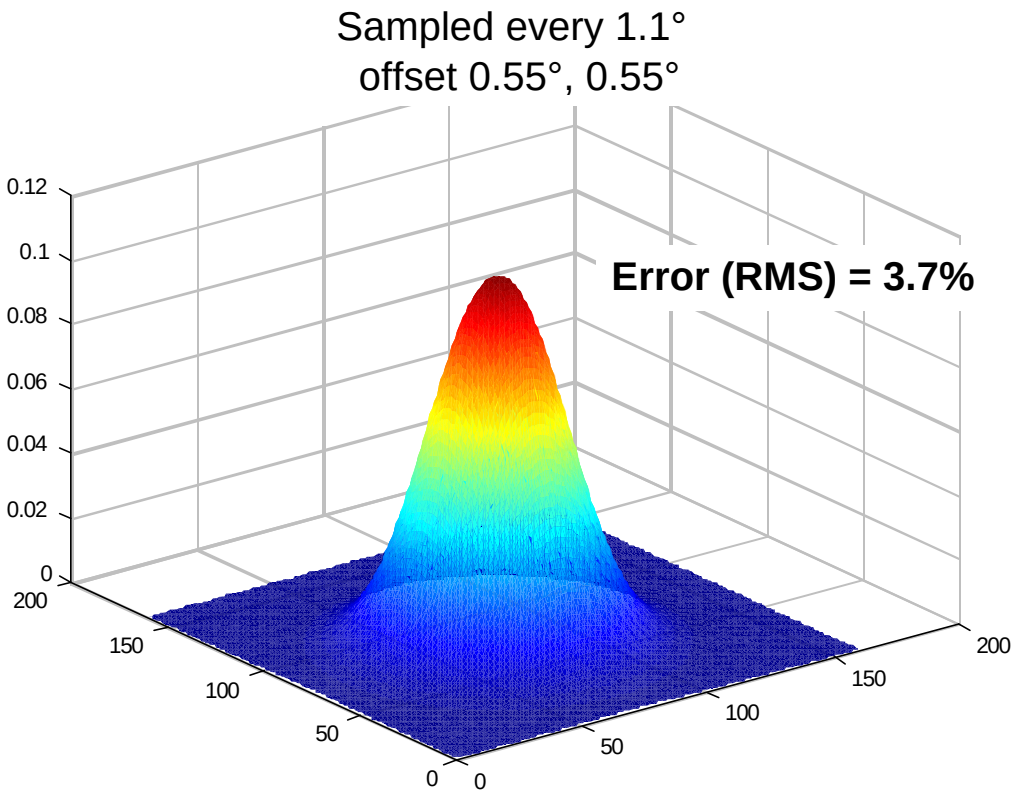

Figure A-8
Example Synthesized 3.3° Beam at mid-point of 1.1° x 1.1° Sampling with 2.2° beams

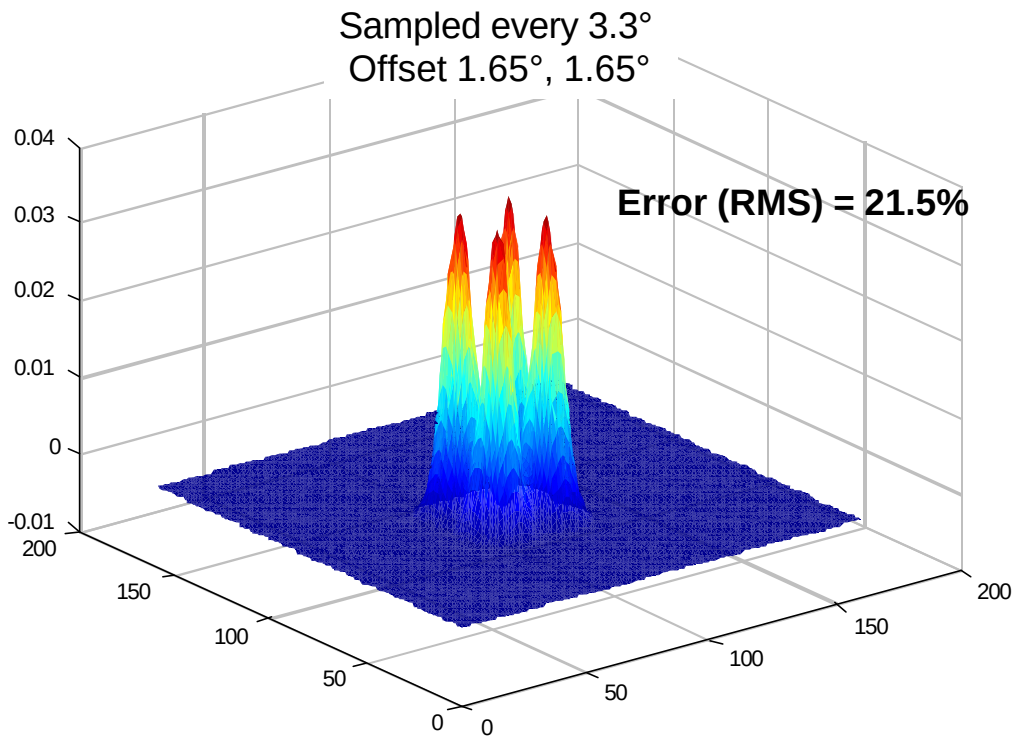

Figure A-9
Difference between Synthetic 3.3° Beam and True 3.3° Gaussian Beam

Two cases were investigated, 3.3° beams synthesized from either a grid of 2.2° beams, or a grid of 3.3° beams. Both cases reproduce an AMSU beam with either AMSU-A beam sizes (3.3°) or the proposed ATMS beam width (2.2°). The sample grid spacing was varied from 0.75° to 3.3° for both beam widths.

Interpolating measurements to a new position is also a function of the underlying temperature field as indicated by Figure A-10. Each measurement is the weighted (by the beam) average of the temperature field so the difference between the interpolated temperature and the temperature sampled by a real beam at that location is the error in the measurement. If the temperature (or humidity) field has low spatial structure, the interpolation error reduces to the beam synthesis error. It is also true if the spatial variation is random over dimensions much less than a beam width or, equivalently, has a uniform spatial spectrum at frequencies less than 1/beam width. In this case, the beam measures the average temperature and the error is proportional to the beam synthesis error multiplied by the standard deviation of the temperature within the beam. The analysis presented here employs this approximation: the interpolation error is the error in synthesizing the beam (rms error between the interpolated and desired beams) multiplied by the temperature fluctuations (standard deviation) within a beam.

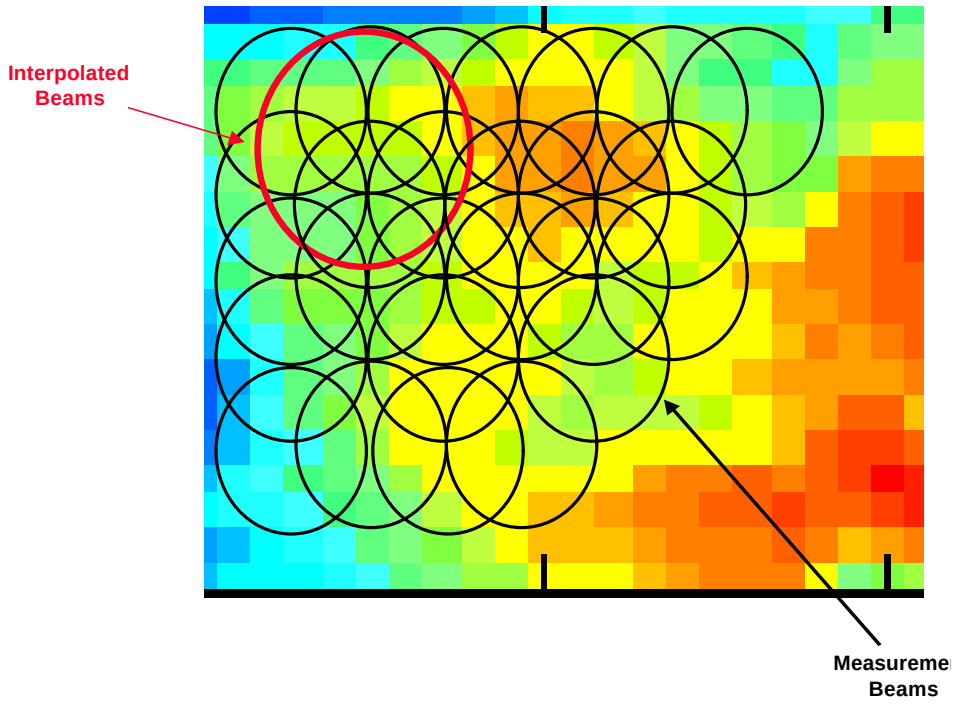

Figure A-10
Beams Overlaid on Temperature Field

To estimate the standard deviation, 10 regions were examined (four were shown in Figure A-3). The standard deviation of the temperature in each region was computed over the two beam widths: ≈32 km x 32 km for the 2.2° beam and ≈48 km x 48 km for the 3.3° beam. Averaging the results yields a standard deviation of 8.4K for the 3.3° beam and 6.2K for the 2.2° beam.

The previously mentioned MATLAB program was used to determine the beam synthesis error (rms) as a function of sample grid spacing and the resulting total error was the synthesis error multiplied by the temperature standard deviation for the 3.3° beam (only 3.3° beams were synthesized). For example, the estimation error of 21.5% from Figure A-9 (2.2° beams spaced 3.3°) is multiplied by the temperature standard deviation of 8.4° K to produce an interpolation error of 1.8° K.

Figure A-11 shows the expected temperature error for an interpolated measurement as a function of sample grid spacing. As already mentioned, two cases were addressed; first a 3.3° beam was synthesized from 3.3° beams to approximate interpolating with AMSU data. The second case used 2.2° beams to synthesize a 3.3° beam, representing a possible ATMS beam reproducing a synthetic AMSU beam at an interpolation point.

Synthesizing the larger beam from smaller beams has a higher noise for two reasons; a mismatch in beam sizes (3.3° beam is made from 2.2° beams), and a larger spacing in beam diameters, (a 3.3° spacing is 1.5 beam diameters for the 2.2° beam but only 1 beam diameter for the 3.3° beam). The interpolation noise is lower for the smaller beam synthesis at identical spacings in beam widths; i.e., <0.1° K noise for the 2.2° beams at the 1.1° spacing vs., 0.2K for the 3.3° beams at the 1.65° spacing. The figure shows the advantage of sampling the image at the Nyquist rate as defined by the beam diameter; the interpolation noise is very low when this rate is employed (1.1° for 2.2° beams and 1.65° for 3.3° beams).

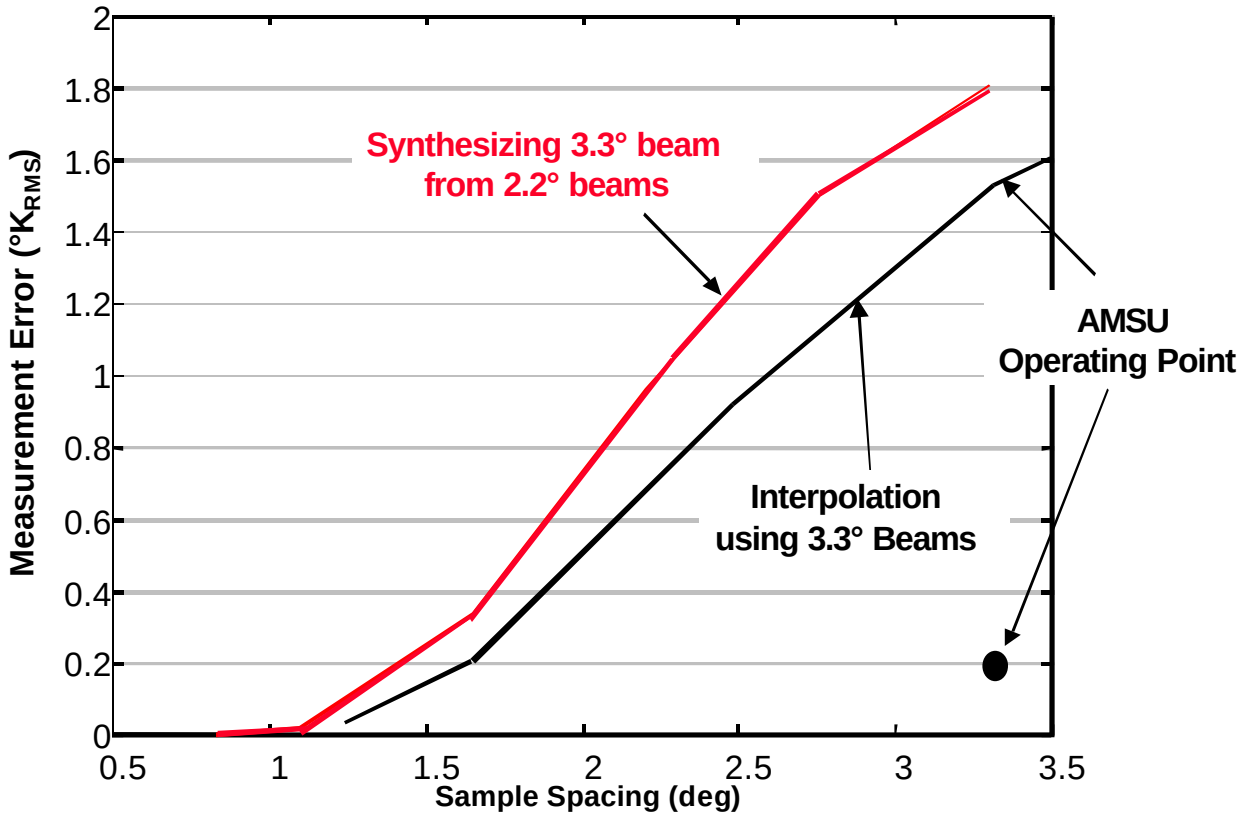

Figure A-11
Interpolation Noise (with Receiver Noise)

On the figure, the current AMSU receiver noise temperature requirement (0.2 K) is shown and compared to the potential interpolation noise of approximately 1.55K obtained when interpolating between the current 3.3° spaced samples. Under highly discontinuous temperature or humidity fields (e.g., severe weather or coastlines), the current AMSU-A sample spacing will result in a large temperature measurement error when interpolating to an IR sounding located between the microwave measurements.

A-6. Receiver Noise

The instrument noise of the current AMSU employing 3.3° beams spaced every 3.3° is approximately 0.2° K. As the sample spacing is decreased , the integration time also decreases, raising the instrument noise. However, if the measurements are used to synthesize a larger (3.3°) beam, the addition of several measurements is equivalent to longer integration and will reduce the noise. In the simplest case, adding 9 measurements together (three cross track measurements for three scan lines) will eliminate the penalty of sampling every 1.1° in both cross-track and along-track.

According to Kraus (1), the instrument noise in a radiometer is proportional to:

$$\Delta T = K \frac{T_{sys}}{\sqrt{B \cdot t \cdot n}}$$

Equation A11

where ΔT is the minimum detectable temperature (K),
K is a constant dependent on receiver type,
T_{sys} is the instrument system temperature (antenna and receiver)
B is the RF (predetection) bandwidth
t is the integration time, and
n is the number of samples integrated.

For the synthesized beam, the power received can be represented as:

$$\widehat{S}_{3.3} = \sum w_i \cdot \left[S_{2.2} + e_i \right].$$

Equation A12

To investigate the noise increase due to non-uniform weighting of the samples, the variance of the received power can be computed:

$$s^2_{\widehat{S}_{3.3}} = \overline{\left(\widehat{S}_{3.3} - \overline{\widehat{S}}_{3.3}\right)^2} = \overline{\left(\sum e_i w_i\right)^2} = s^2_{2.2}\left(\sum w_i^2\right)$$

Equation A13

where the e_i is the noise in the i_{th} measurement (2.2°) beam and $s_{2.2}$ is its standard deviation. Because the power received by a nearly diffraction limited radiometer is independent of beam width:

$$P_{rec} \propto A_e \cdot \Omega_A = Constant,$$

Equation A14

where A_e is the antenna area, and Ω_A is the area of the beam in square radians, the power received by the 3.3° beam is equal to the power received by the 2.2° beam (assuming the temperature field is constant over both beam widths). However, the instrument noise is a function of the integration time that decreases with the sample spacing but increases with the addition of measurements. In the interpolation case, the measurements are weighted before they are added, reducing the benefit of addition. This can be seen as follows; employing the relation between the signal power in the two beams (the synthesized 3.3° beam and the measurement 2.2° beam), the signal to noise in the synthesized beam is:

$$\frac{S_{synth}}{N_{synth}} = \frac{\widehat{S}_{3.3}}{s_{\widehat{S}_{3.3}}} = \frac{S_{2.2} \cdot \sum w_i}{s_{2.2} \cdot \sqrt{\sum w_i^2}}$$

Equation A15

Recalling that the signal in the two beams is the same and the noise in the smaller beam is related to the noise variance in the 3.3° beam by the ratio of the integration times, the ratio of signal to noise in the synthesized beam to that in the desired 3.3° beam is given by:

$$\frac{\frac{S_{synth}}{N_{synth}}}{\frac{S_{3.3}}{N_{3.3}}} = \sqrt{\frac{t_{3.3}}{t_{2.2}}} \cdot \frac{\sum w_i}{\sqrt{\sum w_i^2}} = \frac{N_{3.3}}{N_{synth}}, \text{ or}$$

Equation A16

$$N_{synth} = \sqrt{\frac{t_{2.2}}{t_{3.3}}} \cdot \frac{\sqrt{\sum w_i^2}}{\sum w_i} \cdot N_{3.3}$$

Equation A17

where $t_{3.3}$ is the integration time for the original 3.3° beam and $t_{2.2}$ is the integration time for each 2.2° beam. The first term on the right of equation A16 is equivalent to the ratio of 3.3° to the sample spacing. The noise in the synthetic beam, equation A17, is plotted in Figure A-12 as a function of the sample spacing (red curve). The noise in a single measurement, which increases with decreasing integration time (smaller sample spacing) is also plotted. The integration of many beams lowers the noise even at the 3.3° spacing, although by not as large a factor as the spacing is reduced. Summation of several weighted measurements reduces the noise by a factor less than the number of beams employed in the sum so that, at 1.1° spacing, the noise is approximately 6% higher than the original instrument noise (0.214° K). The effect can be viewed as an effective number of measurements integrated. Starting with equation A11, the ratio of the instrument noise of the synthesized beams ($n_{1.1}$ beams spaced every 1.1) to a 3.3° beam at that location can be shown to be:

$$\frac{\Delta T_{1.1}}{\Delta T_{3.3}} = \frac{\sqrt{t_{3,3} \cdot n_{3.3}}}{\sqrt{t_{1.1} \cdot n_{1.1}}},$$

Equation A17

where $n_{3.3}$ is 1. Noting that ΔT is proportional to the noise in equation A17, the effective number of integrated measurements can be shown to be:

$$n_{eff} = \frac{\left(\sum w\right)^2}{\sum w_i^2}$$

Equation A18

The equivalent number of samples is plotted as a function of sample spacing in Figure A-13. The values in this plot should be compared with the number of 1.1° beams contained within the 3.3° area. For example, approximately nine beams are within the 3.3° area if they are spaced 1.1° apart, and the plot indicates the effective number of samples is approximately eight. The receiver noise increase is proportional to the square root of the ratio of the effective number of samples to the number of beams available, or an increase of approximately 6%. At the 1.1° spacing, the extra receiver noise that results from this type of synthesis is minor.

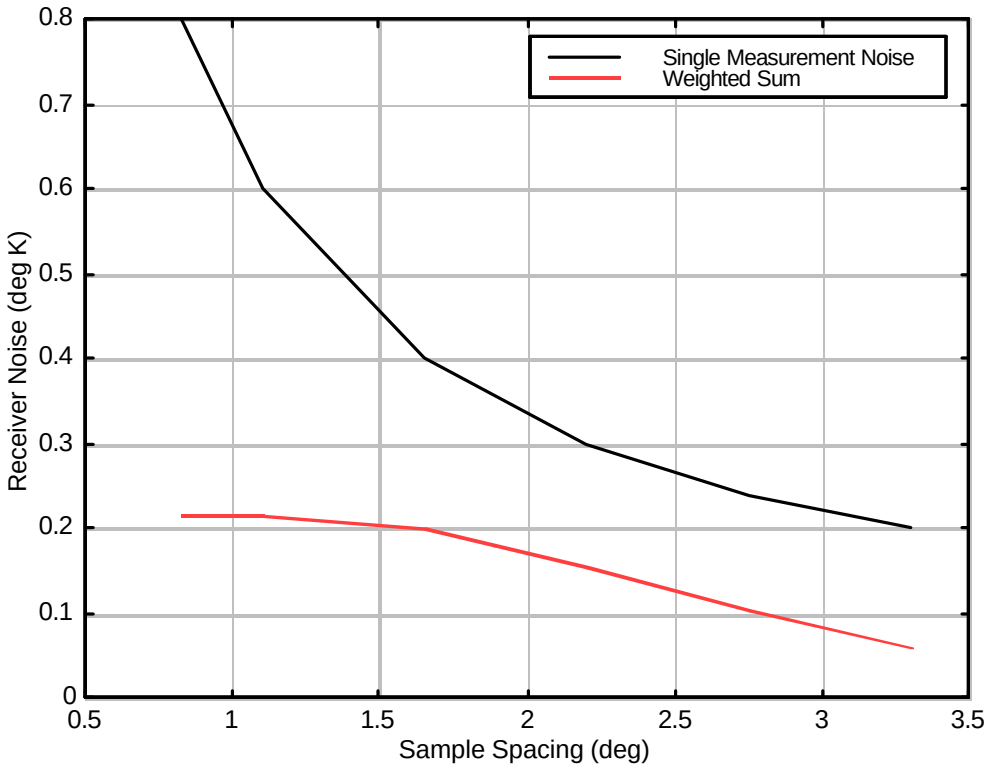

Figure A-12
Noise in Single Beam and Weighted Sum of Beams

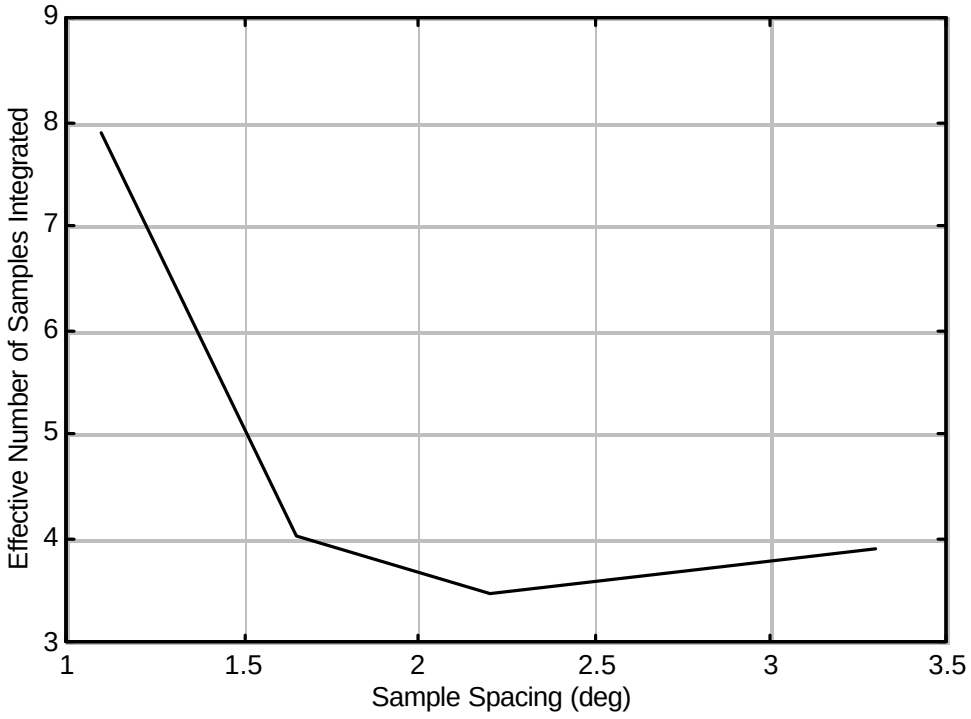

Figure A-13
Effective Number of Samples in Weighted Summation of Beams

A-7. Summary

An investigation of the effects of sample spacing was performed using data from NAST-M. The data have a better resolution than the proposed instrument and a high degree of spatial variation so to illuminate the effects of varying resolution and sample spacing. The data used were from a surface sounding channel at 54 GHz and were taken during over-flights of a hurricane. Although the NAST-M hurricane data represents conditions with extreme atmospheric variability, the IR/ATMS sounding data will be of most interest and importance for scenes approaching or including these cases.

A method of interpolating between measurements was presented and used with the data to quantify the effects of varying the spacing between measurements. The error in interpolating was calculated as a function of spacing between beams. Improved resolution is shown to be desirable to aid matching the measurements at the ATMS beam width with that of the CrIS which has a notional resolution of 0.8°. As the ATMS beam width is reduced from 3.3° currently used in AMSU to 2.2°, there is a clear benefit to reducing the spacing between measurements to a half beam width (1.1°). This benefit is lessened for regions that have low temperature spatial variation, but once the capability is included in the instrument, interpolation between measurements can be done for all possible temperature fields with low error.

The effect on the instrument noise due to the weighted sampling was also quantified and shown to be small. As the sample spacing is reduced, the effective number of samples included in the integration approaches the actual number, i.e., the increase in noise due to weighting the samples to achieve a better approximation of the desired beam shape is quite small.

The recommended specifications for ATMS improve performance at no increase in cost in the following areas. A smaller beam width and Nyquist sample spacing reduce errors due to the scene particularly when providing microwave data to a variety of IR sounders.

1. Kraus, J.D., Radio Astronomy, McGraw Hill, St. Louis, 1966, pg. 102

APPENDIX B. COMMUNIQUÉ FROM AEROJET CORPORATION

From: ISRAEL.GALIN@Aerojet.com (GALIN, ISRAEL)
To: "'John Maruschak"' <John.G.Maruschak.1@gsfc.nasa.gov
Cc: "Gould, Janette" <Janette.Gould@Aerojet.com,
"Scott, Steve" <Steve.Scott@Aerojet.com
Subject: RE: Mixer Technology for ATMS (from Aerojet)
Date: Fri, 26 Mar 1999 09:27:59 -0800

Dear John:
Thank you for your interest in Aerojet's MMW receiver technology, per your March 8, 1999 e-mail. I am delighted to assist in your study effort on the ATMS.

As you know, in the last 20 years, we have developed 183±8 GHz receivers for the SSMT-2, AMSU-B, and the SSMIS. In 1998, we completed a 32-element receiver array, the Passive Ultra-Compact Configuration Imager (PUCCI), operating at 200±18 GHz, under a NASA AITP contract. Just in the last month, we delivered a 177-207 GHz receiver to JPL for the MLS EM unit, and a 188±1.5 GHz receiver for the MIRO PFM unit. Experience gained from these accomplishments form the basis for my response to your inquiry.

Except for the SSMT-2, all these G-band receivers employ planar, whiskerless, GaAs Schottky diodes in sub-harmonic (x2) mixers (the SSMT-2 employs whisker diodes in similar mixers). Typically, a G-band mixer occupies a volume of approximately 1-inch cube. However, we developed for the PUCCI a super-compact mixer, measuring approximately 0.25 x 1.0 x 1.0 inch (in this volume the mixer includes an IF amplifier with 35 dB gain). All our G-band mixers require no DC bias, and their LO requirements are typically well under 10 mW. The best receiver noise-temperatures (from horn to detector, through mixer and amplifier) are just under 1000 K (NF=6.5 dB) DSB, measured with 8-15 GHz IF amplifiers. G-band receivers with narrower IF bandwidths (e.g., MIRO) yield receiver noise-temperature as low as 700 K (NF£5.5 dB) DSB.

Aerojet has subjected a prototype mixer, with the characteristics described here, to SSMIS-specific tests in a 183 GHz configuration (attachment enclosed in Appendix A). These tests demonstrate significant improvements, in practically all aspects, over the older technology 183 GHz mixers used in the current SSMIS.

The actual measured data that Aerojet is able to share with NASA compares favorably with the current state-of-the-art for receiver technology in this spectral region. Our experience in G-band mixer development, design, fabrication, test and qualification constitutes a unique in-house capability that can minimize cost, schedule, and technical risks.

A G-band receiver development program, of a one-year duration, should suffice to yield a breadboard G-band receiver for the ATMS. This effort should address specific ATMS requirements for a 166-192 GHz receiver with four IF outputs (three outputs DSB and the remaining IF output SSB). The NRE
cost of such effort is estimated as $300 K. As you know, cost of hardware for space-borne applications depends heavily on the particular requirements of a program. Assuming ATMS requirements are
"typical", and for fabrication of 5-10 mixers, the recurring cost would approximate $50K per mixer.

As for ATMS lower frequency bands (i.e., 23-32 GHz, 50-59 GHz, and 118 GHz) mixer technology is very well established and one can expect receiver noise temperature performance of about 600 K (NF»3-4 dB) DSB. We expect that a low-noise-amplifier front-end would be appropriate for bands below 60 GHz. In the 89 - 118 GHz band, LNA technology is fast maturing, but there may still be a cost advantage, and perhaps some performance advantages, in using a mixer front end.

I shared with you facts and observations about millimeter-wave (MMW) mixer technology at the various bands of the ATMS, on a "stand-alone" basis at each band. Perhaps equally important are the possibilities to simplify and improve ATMS (e.g., volume, mass, cost, reliability, and risk) with "truly" advanced system concepts which rely on Aerojet MMW mixer technology. Aerojet is looking forward to the opportunity to propose such exciting advanced possibilities in our ATMS proposal.

INTEROFFICE MEMO
To: Israel Galin
From: Shawn Gillespie
Date: March 25, 1999
Subject: Testing of MLS Prototype Mixer
Copies: C. Parry, C. Schnitzer

On June 30, a test was done on the MLS prototype mixer. The test was done to compare the performance of this mixer to the performance of the current SSMIS 183 GHz mixer. These tests are noise figure, stability, and thermal stability.

The first test was noise figure. The noise figure was measured with a LO frequency of 91.65 GHz and an input power level of 10 dBm. The performance was checked at 8 and 12 dBm but was optimum at 10 dBm. It is important to note that this mixer was previously tuned to operate at some other frequency significantly higher than 183 GHz but we did not do any re-tuning for this test. The measured noise figures were as follows:

7 GHz	3 GHz	1 GHz
6.0 dB	6.4 dB	5.9 dB

It is also important to note here that these numbers are measured without the RF diplexer normally used with the SSMIS mixers. The diplexer normally adds approximately 2 dB to each one of these numbers. Even with this, these numbers represent significant margin for the SSMIS performance. The worst case would be the 1Ghz channel, it is specified at 11.0 dB. This would show at least a 3-dB performance margin. Normally, on the mixers we build for SSMIS we are happy to get 1 to 1.5 dB margins. The next item measured is the noise power stability. This was measured under the same conditions as mentioned above. The measured performance is shown below:

7 GHz	3 GHz	1 GHz
0.24 deg K	0.18 deg K	0.16 deg K

In reference to the SSMIS requirements these numbers would appear to be quite good. Again the worst case would be the 1Ghz channel with a requirement of 1 degree K. However, it is not reasonable to make this comparison. As these numbers are measured without the diplexer and adding it would significantly increase these values. But, based on past measurement experience, there is a very good chance that this mixer would still have very good noise stability performance with the diplexer.

The last test made is the thermal stability test. This measurement test the mixer IF stability over temperature. The temperature range tested is -30 to +70 degrees C. The mixer is continuously monitored with a strip chart recorder for 5 cycles. The data of the chart recorder is then evaluated and analyzed to determine the mixer performance. There are two items that are looked for here. The first is to look for any erratic or non-uniform behavior in the second order of the output data. This would be something like the output taking a sudden change in direction and then maybe changing again to come back to where it started. The second item is how much IF change actually occurs over the temperature range, or the first order change in the data.

By using a calibration that is made for every test, both of these items are measured in terms of degrees K. For this mixer looking at the second order of the data, there was a small deviation that occurred that amounts to a 10 degree K step. This would be considered pretty small. SSMIS considers mixers with 75-degree steps to be problematic depending on the actual behavior of the step function. Most mixers can have any kind of behavior from 0 to hundreds of degrees.

For the total IF swing, the first order change, SSMIS has set a limit of 750 degrees K. SSMIS mixers can have any response less than that. A very good mixer would have 400 degrees K and a marginal mixer might have 650 degrees K. This MLS mixer had 272 degrees K.

Overall the MLS prototype mixer passed all the SSMIS requirements with very good margin. This could be considered very good but we must keep in mind that this is only a sample of one. However, this sample of one does test out quite well.

Shawn Gillespie
SSMIS Mixer Team Leader

-----Original Message-----
From: John Maruschak [mailto:John.G.Maruschak.1@gsfc.nasa.gov]
Sent: Monday, March 08, 1999 12:48 PM
To: israel.galin@aerojet.com
Cc: Caleb.principe@gsfc.nasa.gov; long@jazzman.gsfc.nasa.gov;
john.maruschak@gsfc.nasa.gov
Subject: estimates

Dear Israel:
Thank you for the technical information you conveyed during our telephone discussion of 5Mar99.

As I said at that time, we are interested in rough estimates of noise performance (double side band), and development time and costs, both non-recurring and recurring for our ATMS study. This information from Aerojet would allow us to compare your GaAs planar diode mixer solution to the InP MMIC solution and thereby determine the most efficient implementation at this time.

I believe that you are aware of our channels of interest, but, just to confirm, they are, in order of scientific importance, 50-59 GHz, 166-185 GHZ, 23-32 GHz, 89 GHz and 118 GHz.

Also, a rough estimate of mixer volume would be useful. As I will not be available from 9Mar99 through 17Mar99, please respond as soon as possible to my fellow team member Caleb Principe at caleb.principe@gsfc.nasa.gov.

Sincerely,
John Maruschak

APPENDIX C. DEFINITIONS AND CLARIFICATIONS

The definitions of some of the terms used are spelled out below to clarify the meaning of each term.

1. Beam Width

Beam Width is defined as Half-Power-Full-Width (HPFW) in degrees; it is commonly known as "3 dB" Beam Width in electrical engineering jargon. For simplicity sake, a circular beam is assumed. The term Instantaneous Field of View (IFOV) can also be used to mean HPBW. In addition, the IFOV, by convention, is used interchangeably to mean the footprint size of the IFOV. The footprint is the intersection of the IFOV on Earth Surface, and is either represented by a diameter, when the footprint is a circle, e.g., at nadir, or the footprint is represented by two diameters, a major diameter and a minor diameter, of the nearly elliptical-shaped footprint when off nadir.

2. Effective (Scanned) Field of View (EFOV) and IFOV

For the ATMS, we are assuming that the radiometer will use a slewing-scan mode (i.e., the antenna moves while the receiver integrates continuously to form a sample). This is a departure from the AMSU-A's stare-and-step scan mode, in which the antenna is parked at one beam position while the radiometer integrates for a fixed length of integration–time. The antenna is then moved to another beam position and repeats the integration. No integration takes place while the antenna is in transit.

One effect of the slewing-scan mode is that its EFOV along the scan direction (also known as "cross-track" direction) is slightly larger than that of the static IFOV values. However, for the ATMS requirements, we will ignore this effect. All the beam widths or are referred to the IFOVs.

3. Temperature Sensitivity NEDT

All the temperature sensitivity (NEΔT) values are defined on per-beam width basis. Since the temperature sensitivity is a function of the integration time length, in order to avoid ambiguity, this integration is taken to be "the time it takes for the scanning beam to move one beam width along the scan direction."

APPENDIX D. ACRONYMS AND ABBREVIATIONS

ADC	Analog-to-Digital Converter
A/D	Analog to Digital
AIRS	Atmospheric Infrared Sounder
AMSU	Advanced Microwave Sounding Unit
ATMS	Advanced Technology Microwave Sounder
BP	Bandpass
BW	Bandwidth(s)
C	Celsius
CAD	Computer Aided Design
CCSDS	Consultative Committee for Space Data Systems
COMS	Complimentary Metal Oxide Semiconductor
COTS	Commercial off-the-Shelf
CrIMSS	Cross-track Infrared Microwave Sounding Suite
CrIS	Cross-track Infrared Sounder(s)
DAC	Digital to Analog Converter(s)
dB	Decibel(s)
dBm	Decibels related to 1 mW (microwave work standard unit of power)
DC	Direct Current
DMSP	Defense Meteorological Satellite Program
EEPROM	Electrically Erasable Programmable Read Only Memory
EMI	Electromagnetic Interference
EOS	Earth Observing System
FET	Field Effect Transistor
FFT	Fast Fourier Transform
FIR	Finite Impulse Response
FOV	Field of View
FPGA	Field Programmable Gate Array(s)
FSS	Frequency Selective Surface
GaAs	Gallium Arsenide
GHz	Gigahertz
GSFC	Goddard Space Flight Center
HIRS/MSU	High Resolution Infrared Sounder/Microwave Sounder Unit
HPFW	Half-Power-Full-Width
HSB	Humidity Sounder Brazil
Hz	Hertz
IASI	Infrared Atmospheric Sounding Interferometer
IC	Integrated Circuit/Circuitry
IF	Intermediate Frequency
IFA	IF Amplifier(s)
IIA	Initial Implementation Agreement
InP	Indium Phosphide
IPO	Integrated Program Office
IR	Infrared
JPL	Jet Propulsion Laboratory
K	Kelvin
Kbps	Kilobits per second
kg	Kilogram(s)
km	Kilometer(s)
KRAD	Kilo-RAD
LCC	Leadless Chip Carriers
LNA	Low Noise Amplifier(s)
LO	Local Oscillator
LSB	Least Significant Bit

LVPS	Low Voltage Power Supply
MAP	Microwave Anisotropy Probe
MEMS	Micro Electro Mechanical Systems
METOP	Meteorological Operation
MHS	Microwave Humidity Sounder
mhz	Megahertz
MIC	Microwave Integrated Circuitry
MIDEX MAP	Medium Explorer Microwave Anisotropy Mission
MIL-STD	Military Standard
MIPS	Million Instructions Per-Second
MIT	Massachusetts Institute of Technology
MMIC	Microwave Monolithic Integrated Circuitry
ms	Millisecond
msps	million samples per second
mW	Milliwatt
MUX	Multiplexer
N/A	Not Applicable
NASA	National Aeronautics and Space Administration
NE T	Noise Equivalent Temperature Difference
NPOESS	National Polar-orbiting Operational Environmental Satellite System
NPP	NPOESS Preparatory Program
NRAO	National Radio Astronomy Observatory
PECL	Positive Emitter Coupled Logic
PLLO	Phase Lock Loop Oscillator
PLO	Phase Lock Oscillator
POES	Polar-Orbiting Operational Environmental Satellite
PRT	Platinum Resistance Temperature
PWB	Printed Wiring Board
PWM	Pulse Width Modulator
QFP	Quad Flat Pack
RAM	Random Access Memory
RAO	Resource Analysis Office
RBD	Reliability Block Diagram
RF	Radio Frequency
ROM	Read Only Memory
SMEX	Small Explorer Program
SMEX-Lite	SMEX technology project name
SOAT	Sounder Operational Algorithm Team
SUMMIT	United Technology Microelectronics' Registered Trade Mark for Mil-std-1553 protocol chip
SRAM	Static RAM
TBD	To Be Determined
TBS	To Be Supplied
TIROS	Television Infrared Operational Satellite
TRL	Technology Readiness Level
ULP	Ultra Low Power
UTMC	United Technology Microelectronics Center
VSWR	Voltage Standing Wave Ratio